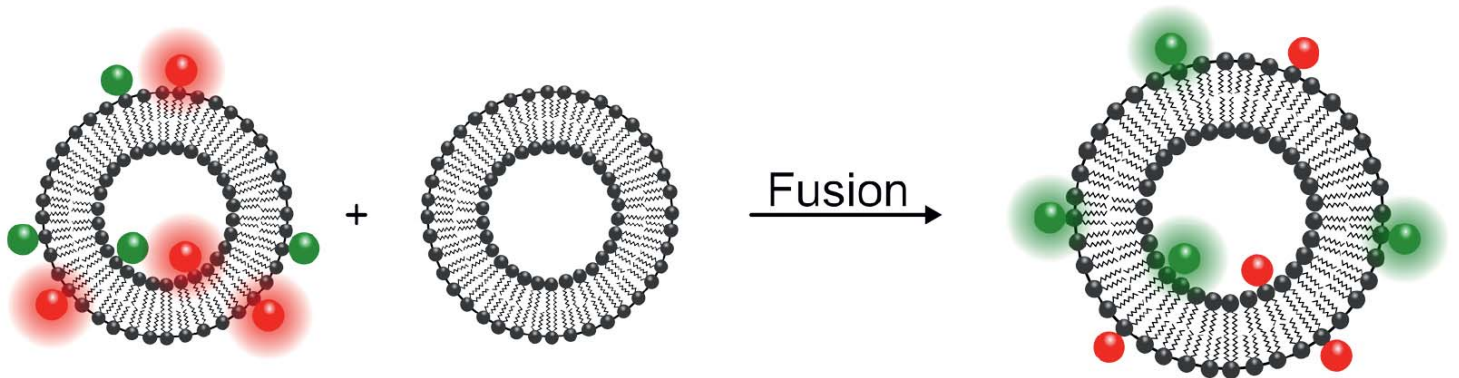


Barbara Elisabeth Hubrich

Synthesis of Model Systems for SNARE Mediated Membrane Fusion Based on PNA/PNA Base Pair Recognition



Cuvillier Verlag Göttingen
Internationaler wissenschaftlicher Fachverlag



Barbara Elisabeth Hubrich

Synthesis of Model Systems for SNARE Mediated Membrane Fusion Based on PNA/PNA Base Pair Recognition



Cuvillier Verlag Göttingen
Internationaler wissenschaftlicher Fachverlag



Bibliografische Information der Deutschen Nationalbibliothek

Die Deutsche Nationalbibliothek verzeichnet diese Publikation in der Deutschen Nationalbibliografie; detaillierte bibliografische Daten sind im Internet über <http://dnb.d-nb.de> abrufbar.

1. Aufl. - Göttingen: Cuvillier, 2018

Zugl.: Göttingen, Univ., Diss., 2017

© CUVILLIER VERLAG, Göttingen 2018

Nonnenstieg 8, 37075 Göttingen

Telefon: 0551-54724-0

Telefax: 0551-54724-21

www.cuvillier.de

Alle Rechte vorbehalten. Ohne ausdrückliche Genehmigung des Verlages ist es nicht gestattet, das Buch oder Teile daraus auf fotomechanischem Weg (Fotokopie, Mikrokopie) zu vervielfältigen.

1. Auflage, 2018

Gedruckt auf umweltfreundlichem, säurefreiem Papier aus nachhaltiger Forstwirtschaft.

ISBN 978-3-7369-9761-5

eISBN 978-3-7369-8761-6



Synthesis of Model Systems for SNARE Mediated Membrane Fusion Based on PNA/PNA Base Pair Recognition

Dissertation

for the award of the degree
“Doctor rerum naturalium”
of the Georg-August-Universität Göttingen

within the doctoral program
Physics of Biological and Complex Systems
of the Georg-August University School of Science (GAUSS)

submitted by
Barbara Elisabeth Hubrich
from Bonn

Göttingen 2017



Thesis Committee

Prof. Dr. Ulf Diederichsen
Institute of Organic and Biomolecular Chemistry, University of Göttingen

Prof. Dr. Reinhard Jahn
Department of Neurobiology, Max Planck Institute for Biophysical Chemistry, Göttingen

Prof. Dr. Claudia Steinem
Institute of Organic and Biomolecular Chemistry, University of Göttingen

Members of the Examination Board

Referee:
Prof. Dr. Ulf Diederichsen
Institute of Organic and Biomolecular Chemistry, University of Göttingen

2nd Referee:
Prof. Dr. Reinhard Jahn
Department of Neurobiology, Max Planck Institute for Biophysical Chemistry, Göttingen

Further Members of the Examination Board

Prof. Dr. Claudia Steinem
Institute of Organic and Biomolecular Chemistry, University of Göttingen

Prof. Dr. Kai Tittmann
Department of Molecular Enzymology, University of Göttingen

Prof. Dr. Silvio Rizzoli
Department of Neuro- and Sensory Physiology, University Medical Center Göttingen

Dr. Sebastian Kruss
Institute of Physical Chemistry, University of Göttingen

Date of oral examination: February 1, 2018



The work described in this thesis was carried out under the supervision of Prof. Dr. Ulf Diederichsen at the Institute of Organic and Biomolecular Chemistry of the Georg-August University of Göttingen between January 2014 and December 2017.

It was supported by the *Deutsche Forschungsgemeinschaft* within the Collaborative Research Center 803 (SFB 803) “Functionality controlled by organization in and between membranes”.





Abstract

SNARE proteins are regarded as key players in membrane fusion. They reside on both sides of opposite membranes and specifically interact via their characteristic SNARE motifs. The interaction leads to the formation of a stable SNARE complex which pulls the membranes together and eventually results in membrane merger. The exact mechanism of SNARE mediated membrane fusion, however, is still of a matter of debate. Therefore, the development of SNARE model systems is a valuable tool to study membrane fusion by mimicking the action of SNARE proteins *in vitro*. Model systems contain fusogenic peptides that exhibit a less complex structure compared with that of the native models. This allows easy modifications of the structure. In this way, the influence of essential SNARE domains on distinct steps of the fusion pathway can be examined.

In this thesis, model peptides are developed that exhibit artificial peptide nucleic acid (PNA) hybrid recognition units. These are made of *N*-(2-aminoethyl)glycine-PNA and alanyl-PNA, which feature different duplex formation rates due to different topologies. With this, it is intended to achieve a directed duplex formation of the PNA hybrid recognition units so that the model peptides mimic the assumed SNARE zippering.

The model peptides are synthesized by means of solid-phase peptide synthesis. The transmembrane domains of two neuronal SNAREs are taken to anchor the peptides into the membrane of large unilamellar liposomes. The fusion behavior of the model peptides is then comprehensively analyzed via fluorescence spectroscopy in bulk lipid mixing assays, via fluorescence cross-correlation spectroscopy, and via dynamic light scattering. The strengths and weaknesses of these experimental techniques are examined and discussed. Only the combination of all of them enables to obtain a detailed picture of the fusogenicity of the model peptides. It is shown that a directed duplex formation does not occur between the SNARE analogues. Instead, additional alanyl-PNA in the recognition unit reduces the extent of fusion. By studying a variety of peptides it is found that model peptides with a recognition unit made of pentameric aeg-PNA strands exhibit the highest fusogenicity. With that, they represent useful and easily accessible alternatives to previously reported model peptides with a decameric aeg-PNA recognition unit.





Contents

1. Introduction	1
2. Membranes and Membrane Fusion	5
2.1. The Structure of Biological Membranes	5
2.2. Concepts of Membrane Fusion	7
2.3. Neuronal Exocytosis	9
2.4. Fusion Proteins	11
2.4.1. Overview	11
2.4.2. The Structure of SNARE Proteins	13
2.4.3. The Presumed Functioning of SNARE Proteins	15
2.5. Model Systems for the SNARE Mediated Membrane Fusion	24
2.6. How to Monitor Liposome Fusion <i>In Vitro</i>	29
2.6.1. Bulk Lipid Mixing Assays	30
2.6.2. Fluorescence Cross-Correlation Spectroscopy	33
2.6.3. Dynamic Light Scattering	36
3. Design and Synthesis of the Model Peptides	37
3.1. Principles and Rational Design of the Peptides	37
3.2. Synthesis of Alanyl-PNA Monomers	42
3.3. Coupling Behavior of the Alanyl-PNA Monomers	45
3.4. Synthesis of PNA/Peptide Hybrid Sequences	47
4. Fusion Assays	55
4.1. Preparation of Liposomes	55
4.2. Description of the Employed Lipid Mixing Assays	57
4.3. Total Lipid Mixing Assays	62
4.3.1. The Influence of Peptide and Lipid Concentration	62
4.3.2. The Influence of DOPS	64
4.3.3. The Influence of the Peptide Structure	65



4.3.4.	TLM Assays at High Concentrations of Peptides 11 + 12	72
4.3.5.	Control Experiments	73
4.3.6.	Comparison of Quenching and Dequenching Assays	75
4.3.7.	Estimated Stoichiometry of Liposome Interactions	77
4.4.	Inner Lipid Mixing Assays	80
4.5.	Fusion Monitored with Fluorescence Cross-Correlation Spectroscopy	85
4.6.	Fusion Monitored with Dynamic Light Scattering	91
5.	Conclusions	97
6.	Experimental Section	101
6.1.	General Equipment and Methods	101
6.2.	Chromatographic Methods	103
6.3.	Spectroscopic Methods	104
6.4.	Synthesis of the Alanyl-PNA Building Blocks	107
6.4.1.	Determination of Enantiomeric Purity	107
6.4.2.	Detailed Synthetic Procedures	108
6.5.	Peptide Synthesis	114
6.5.1.	Loading of First Amino Acid	114
6.5.2.	Determination of Resin Loading	115
6.5.3.	Automated Solid-Phase Peptide Synthesis	116
6.5.4.	Manual SPPS for Attachment of PNA Monomers	117
6.5.5.	Cleavage from Resin and Work-Up	118
6.5.6.	Attempts for Purification of Model Peptides	118
6.5.7.	Synthesized Model Peptide Sequences	119
6.6.	Fusion Assays	144
6.6.1.	General Remarks	144
6.6.2.	Preparation of Lipid Films via Direct Mixing	144
6.6.3.	Preparation of Lipid Films via Detergent Removal	145
6.6.4.	Preparation of Liposomes via Extrusion	146
6.6.5.	Phosphate Test for Quantification of Phospholipids	146
6.6.6.	Examination of Liposome Fusion with TLM Assays	147
6.6.7.	Examination of Liposome Fusion with ILM Assays	148
6.6.8.	Examination of Liposome Fusion with FCCS	149
6.6.9.	Examination of Liposome Fusion with DLS	150



A. Appendix	151
A.1. Additional Chromatograms Obtained From HPLC and SEC	151
A.2. Individual Fusion Curves From TLM Dequenching Assays	153
A.3. Additional DLS Data	154
A.4. Estimating the Number of Lipids and Model Peptides per Liposome . . .	155
List of Abbreviations	157
Bibliography	160





1. Introduction

motifs,^[15,16] deoxyribonucleic acid (DNA)^[17,18] and peptide nucleic acid (PNA)^[19,20] strands and even small molecules^[21-23]. The achievement of full fusion or at least hemifusion has been reported in all cases. The SNARE zippering, however, has not yet been specifically addressed in artificial model systems. One possibility to do so is to equip SNARE model peptides with a recognition unit that is made of two parts. If these parts differ for example in the rate of dimerization, a directionality in complex formation ought to be achieved.

The intention of this work was to design and analyze SNARE model peptides containing recognition units that are made of two different types of PNA. PNA is a DNA analogue, in which the nucleobases are attached to a backbone based on peptide bonds.^[24] This makes PNA neutral and resistant towards enzymatic cleavage. By using PNA, the recognition unit can be designed in a highly predictable fashion concerning the stability and orientation of the strands. The two PNA types are *N*-(2-aminoethyl)glycine (aeg)-PNA and alanyl (ala)-PNA, which differ in their backbone structure. This results in different topologies of the double strands and different dimerization kinetics. The assembly of helical aeg-PNA duplexes is fast,^[25] whereas the complex formation of linear ala-PNA oligomers is kinetically hindered and thus slow.^[26] Combining aeg-PNA and ala-PNA within one recognition unit thus aims at achieving a directionality in duplex formation, which starts with fast aeg-PNA dimerization followed by ala-PNA interaction. With this, the minimal structural requirements for mimicking the presumed SNARE zippering are probed.

This thesis targets at the following two main points: First, implementation of the synthesis of model peptides with a PNA hybrid recognition unit. This is accomplished by using Fmoc-based solid-phase peptide synthesis (SPPS). The PNA monomers for the recognition unit are assembled stepwise in a continuous fashion on the resin containing the native SNARE transmembrane domain sequences. Making use of these does not only ensure a stable anchorage in the membrane but also takes account of the assumed active role of the TMDs during fusion.^[27] Purification of these kinds of peptides is challenging. Therefore, different strategies based on high performance liquid chromatography (HPLC) and size exclusion chromatography (SEC) are tested elaborately.

Second, analysis of the model peptides regarding their fusogenicity, which is the capability to fuse membranes. Are the peptides with a PNA hybrid recognition unit in general capable of liposome fusion? Does the PNA hybrid recognition unit constitute the minimal structural requirement for mimicking the SNARE zippering? How is the extent of liposome fusion compared to other model systems? To obtain results that are as differentiated



as possible, various fusion assays are applied, which are based on two different principles. The first principle is detecting liposome fusion by making use of fluorophore-labeled liposomes. Depending on the position of the fluorophores—they are either located on one liposome population or are separated on two different liposome populations—the change in their distance is expressed by either a decrease in Förster resonance energy transfer (FRET) or an increase in FRET. This is monitored in bulk lipid mixing assays, of which two options are applied, total lipid mixing (TLM) and inner lipid mixing (ILM) assays. Whereas with TLM assays it is possible to detect lipid mixing in general, ILM assays allow the specific detection of the mixing of the inner leaflets.^[28] Therefore, they indicate whether the liposome fusion process proceeds completely or is arrested in the hemifusion stage, a step in the fusion process in which only the outer leaflets of the liposomes have merged.^[29,30] In addition, fluorescence cross-correlation spectroscopy (FCCS) is employed. With this technique the interaction of fluorophore-labeled liposomes can be determined in more detail as it allows distinguishing between docking and fusion of liposomes. The second principle is detecting liposome fusion by applying dynamic light scattering (DLS). DLS gives quantitative information on the size distribution of particles. Therefore, it is a valuable supplement to the fluorophore-based assays as it provides the size of interacting liposomes, a quantity that is not accessible by lipid mixing assays.



2. Membranes and Membrane Fusion

2.1. The Structure of Biological Membranes

Biological membranes constitute the boundaries of cells and cell organelles and ensure the spatial separation of cellular processes.^[31,32] Apart from that they are a place where a multitude of reactions occurs, made possible by various attached proteins. The essential components of biological membranes are lipids.^[33] They shape the basic membrane framework by being ordered into a lipid bilayer. Their polar headgroups point to the outside whereas their unipolar alkyl chains are oriented inward (see Figure 2.1). Due to their amphipathic character, the lipid bilayer is formed spontaneously in an aqueous environment driven by non-covalent interactions among the hydrophobic alkyl chains.

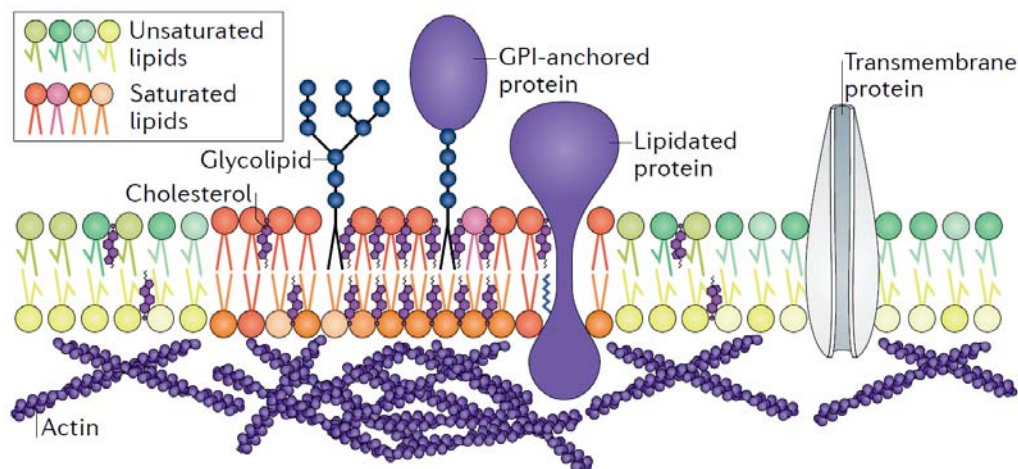


Figure 2.1. Schematic view of the composition of biological membranes. Usually, the membrane components are not evenly distributed but form membrane patches (often denoted as “lipid rafts”), in which saturated phospholipids, glycolipids, sphingolipids, lipidated proteins and glycosylphosphatidylinositol (GPI)-anchored proteins segregate from areas with unsaturated phospholipids and other membrane components. Lipid rafts likely participate in various physiological functions. Cortical actin is thought to mediate the lateral distribution and to support domain formation. Reprinted by permission from Macmillan Publishers Ltd: NATURE REVIEWS MOLECULAR CELL BIOLOGY (Ref. [34]), copyright (2017).



2. Membranes and Membrane Fusion

In addition to lipids, biological membranes host a wealth of proteins fulfilling various tasks, thus providing different types of membranes with different functional properties. Accordingly, the membrane composition is organelle-specific and can differ wildly.^[35] Membrane proteins are involved in processes such as transport of particles across the membrane, signal transduction via receptors, enzymatic activities for membrane-associated reactions or intercellular recognition.^[36] Proteins are often classified as integral or peripheral membrane proteins, depending on how they are associated with the lipid bilayer. Integral proteins exhibit segments that are inserted into the lipid bilayer. Transmembrane proteins, for example, span the entire membrane via single or multiple helices or as β -barrels.^[37,38] Proteins can also be embedded in the membrane via a lipid anchor or the glycosylphosphatidylinositol anchor, which is an oligosaccharide linker (see also Figure 2.1). Peripheral proteins are bound to one side of the membrane without being embedded in the hydrophobic core of the lipid bilayer. Instead, they interact with the membrane via binding to integral proteins or via association with the polar lipid headgroups.

In the early 1970s, Singer and Nicolson developed the fluid mosaic model, which made an essential contribution to understanding the structure of membranes.^[39] It describes membranes as a two-dimensional sea of lipids in which proteins are evenly distributed in a low concentration. Proteins and lipids rapidly diffuse within the membrane which is referred to as lateral diffusion. Up to now, however, a huge amount of investigations suggests that the fluid mosaic model is not as generally applicable as it seemed to be at the time it was proposed. Over the past decades, the concept of lipid rafts emerged, ensuing from various observations that cell membranes are highly heterogeneous and can be separated into different fractions (see Figure 2.1).^[34] According to this concept, sterols and sphingolipids self-ensemble into microdomains (“rafts”) which are separated from the other membrane components.^[40] Rafts are commonly described as small dynamic assemblies being about 10–200 nm in size and containing lipids and proteins.^[41] The formation of rafts is based on the liquid-liquid immiscibility of different lipid species, and proteins associate with rafts according to their affinity for these lipid patches. Proceeding from the first hypothesis that rafts play an important role in membrane-associated signalling processes,^[42] there is growing evidence that rafts are relevant for physiological functions.^[34] Proper detection of lipid rafts, however, is difficult, especially in living cells. From the very beginning of its postulation, the lipid raft model has therefore been discussed controversially.^[43] Though hints that lipid rafts do exist increase,^[40] alternative models explaining how the plasma membrane is organized are discussed as well.^[44] For example, the segregation of lipids and proteins into distinct domains can also be medi-

ated by charge.^[45] The concept of lipid shells hypothesizes that proteins are surrounded by lipids, conceptually analogously to the hydration shell of molecules in water. Lipid shells are assumed to be the smallest entity of domains in the lipid bilayer and formed by specific lipid–protein interactions.^[46] On top, heterogeneity in the membrane composition is achieved by the actin cytoskeleton. Cortical actin is supposed to modulate the lateral distribution of lipids and proteins in the membrane by anchoring proteins via an actin cytoskeleton “fence” which hinders other proteins and lipids from diffusing by.^[47]

2.2. Concepts of Membrane Fusion

Membrane fusion is the merger of two opposing lipid bilayers to form one continuous lipid bilayer. Already in 1968, Palade and Bruns studied vascular tissues with electron microscopy and described fusion of membranes and intermediates therein.^[48] Remarkably, this was done even before basics of the structure of membranes were known. The fluid mosaic model by Singer and Nicolson, for example, did not come up until 14 years later (see Section 2.1).

Today, mainly two mechanisms regarding membrane fusion are distinguished, depending on whether proteins (“direct fusion”) or lipids (“fusion-through-hemifusion”) form the fusion pore.^[49,50] In the direct fusion pathway, proteins from both membranes assemble and a proteinaceous fusion pore is formed upon a conformational change of the protein complex. The fusion pore is believed to be surrounded by a ring of proteins. In a second step, the fusion pore widens when lipids replace the proteins.^[51] This mechanism implies that content mixing takes place before lipid mixing. Details, however, are unknown to date.^[50] A more often discussed pathway of membrane fusion is the mechanism of fusion-through-hemifusion, in which lipids shape the fusion pore (see Figure 2.2).^[49] Proteins may ensure that the membranes are located closely next to each other, but the pore formation is thought to be brought about solely by lipids. It is assumed that if the opposing membranes are in close proximity (Figure 2.2, step i) a point-like protrusion of several lipids reduces the hydration repulsion (ii) so that a hemifusion stalk (iii) can form. In the hemifusion stage, the outer leaflets of the lipid bilayer have merged, but the inner leaflets are still separated. From this stalk, the formation of the fusion pore (v) can take place, possibly via an extended hemifusion diaphragm (iv). The fusion pore establishes an aqueous connection between the formerly separated bilayers so that contents can be exchanged. Contrary to the proteinaceous pore formation, lipid mixing precedes content mixing here.



2. Membranes and Membrane Fusion

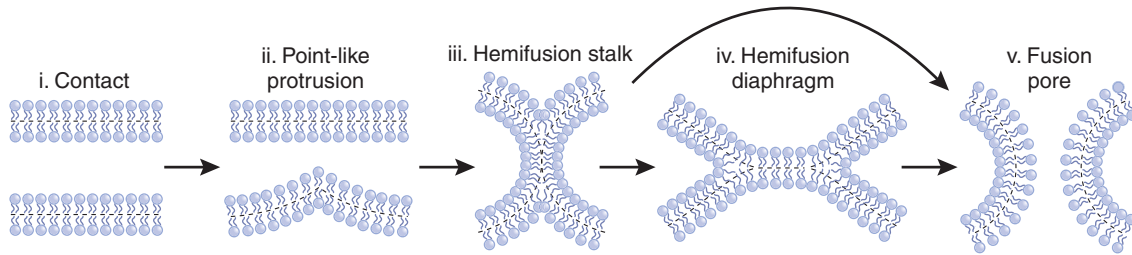


Figure 2.2. Schematic view of steps in the fusion-through-hemifusion pathway of membrane fusion. The details are explained in the text. Reprinted by permission from Macmillan Publishers Ltd: NATURE STRUCTURAL & MOLECULAR BIOLOGY (Ref. [30]), copyright (2008).

The stalk model was originally described by Kozlov and Markin in 1983.^[52] They theoretically studied the formation of the stalk by implying mathematical calculations of the transition states during membrane fusion. Although it became apparent that the elastic energy was overestimated due to an incorrect assumption of the curvature of the stalk—a refinement of the model was done in 2002,^[53,54] the stalk model profoundly contributed to the understanding of membrane fusion.

Hemifusion diaphragms have been observed directly^[29,55] and there are studies that consider the hemifusion diaphragm a dead-end state in membrane fusion.^[56] Calculations showed that it is an unusually stable intermediate and that its formation as well as the subsequent dilation into the fusion pore are energetically costly.^[57] Especially if the length of the hemifusion diaphragm increases, it is very unlikely that the formation of a fusion pore occurs spontaneously due to a decreasing lateral tension.^[57,58] Consequently, only a small frame remains in which the hemifusion diaphragm is short enough for a fusion pore to efficiently increase in size.^[56] It is thought that proteins prevent the extension of the hemifusion diaphragm and thus ensure fast membrane fusion.^[58] This was also shown by experiments in which protein-free and protein-containing liposomes were examined.^[29] The extent of observable extended hemifusion diaphragms was significantly higher in the case of protein-free liposomes indicating that proteins suppress the formation of elongated hemifusion diaphragms.

The tendency of membranes to fuse is crucially influenced by their lipid composition. Depending on the ratio of the area required by headgroups and alkyl chains, lipids adopt different shapes (see Figure 2.3a). For example, lipids are cone-shaped if the mean diameter of the headgroup is smaller than that of the area occupied by the alkyl chains, like in unsaturated phosphoethanolamine (PE). The shape determines the spontaneous curva-

ture of the monolayers. The curvature is defined as positive if the monolayer's surface is bent into the direction of the lipid headgroups. Respectively, it is defined as negative in the opposite case.^[59] As the stalk has a negative curvature, cone-shaped lipids like PE promote its formation. Inverted-cone-shaped lipids like lysophosphatidylcholine (LPC), on the contrary, inhibit stalk formation.^[30] Figure 2.3 illustrates these relationships. In contrast to that, adding LPC to the distal leaflets supports fusion pore formation whereas PE inhibits it. This confirms that the rims of the fusion pore are positively curved.^[30]

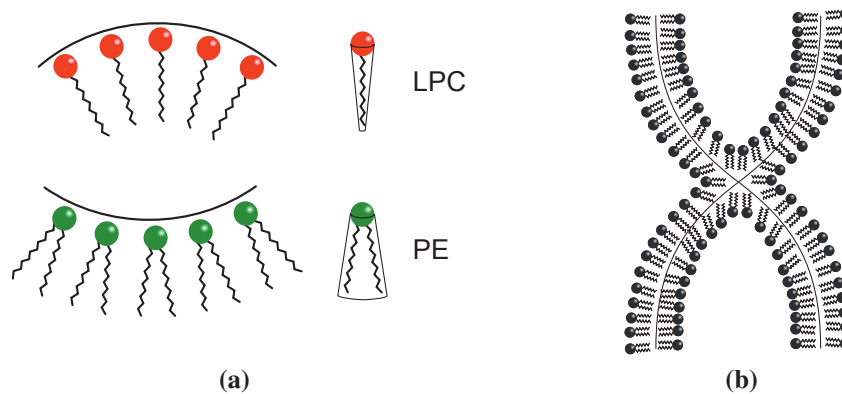


Figure 2.3. Illustration of lipid shapes. (a) Inverted-cone-shaped lipids like LPC (red) form a positively curved monolayer, whereas cone-shaped lipids like PE (green) lead to a negatively curved monolayer. (b) The distal leaflets in the stalk intermediate are negatively curved, which is why cone-shaped lipids promote stalk formation. Inverted-cone shaped lipids would disturb the arrangement and thus inhibit stalk formation.

The extent of curvature is relevant as well. Highly curved membranes fuse more readily than less curved membranes.^[30] Accordingly, the smaller the liposomes the more fusogenic they are. This is because a high curvature implies a high tension and thus a high readiness to fuse.

2.3. Neuronal Exocytosis

Since the seminal work by Katz and Miledi, who discovered the fundamental pathways of synaptic transmission,^[60] neuronal exocytosis is one of the best studied membrane fusion processes in nature. Neuronal exocytosis happens at the conjunction sites of two nerve cells. Briefly, nerve cells consist of the soma, *i.e.* the cell body that contains nucleus and cell organelles and ramifies into dendrites (see Figure 2.4a). The axon is an elongated appendix of the soma along which an electrical pulse is transmitted. The termini of the

2. Membranes and Membrane Fusion

axon are called synapses and constitute the connection sites to other cells, for example other neurons.

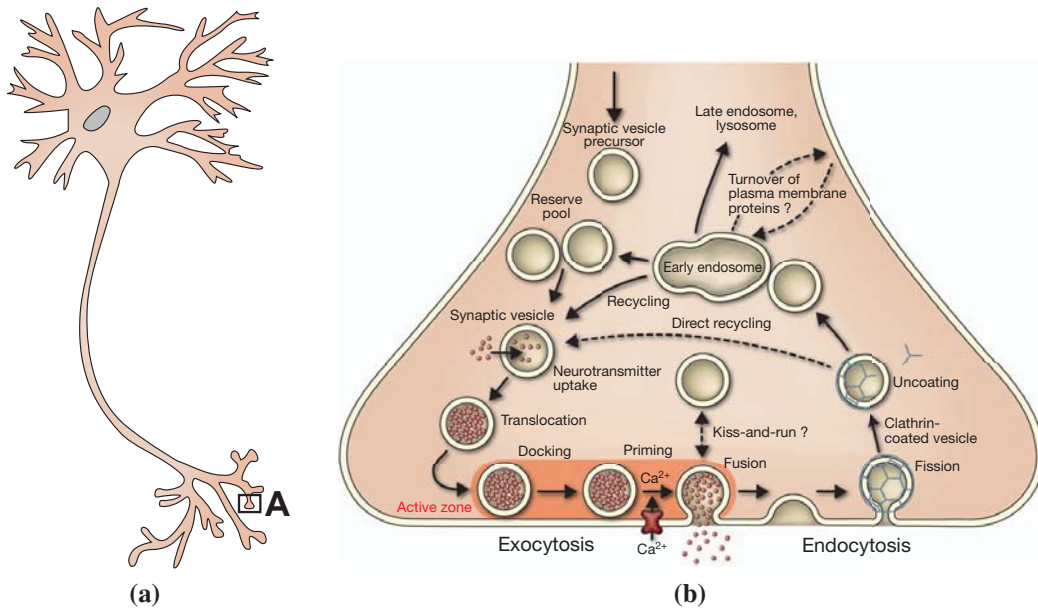


Figure 2.4. Synaptic transmission. (a) Schematic illustration of a neuron. (b) Enlargement of a synaptic bouton region (marked with “A”): The trafficking cycle of vesicles in the synapse is shown. Details are explained in the text. Figure 2.4a is modified from a picture provided by Q. Jarosz at English Wikipedia, published under the Creative Commons (CC BY-SA 3.0) license (Ref. [61]); Figure 2.4b is reprinted by permission from Macmillan Publishers Ltd: NATURE (Ref. [3]), copyright (2012).

The ion composition inside and outside nerve cells is different, which results in a voltage difference and thus a potential across the membrane. This potential is maintained by ion pumps. Due to a multitude of voltage-gated ion channels located along the axon, the potential can rapidly change when Na^+ and K^+ ions are exchanged with the exterior of the cell. Through characteristic increase and decrease in the potential an electrical signal can be transmitted along the axon in the form of a so-called action potential. It is generated at the axon hillock and then travels along the axon until it reaches the nerve terminal. There, the incoming action potential results in the opening of voltage-gated Ca^{2+} channels. In order to transfer the signal to the next nerve cell, the incoming electrical signal needs to be converted into a chemical signal. This is done in the form of neurotransmitters, which are released from synaptic vesicles into the neural interstice and activate receptors on the next neuron. These in turn set off processes to generate the next action potential. How this conversion is accomplished remained illusive for a long time. During the last decades, a

more and more distinct picture has evolved and it still is part of ongoing research to find out how exactly Ca^{2+} ions trigger synaptic vesicle fusion.^[1] The process from Ca^{2+} influx to the completed synaptic vesicle fusion is finished in less than a millisecond.¹ It thus needs to be tightly regulated, also in terms of colocalization of the different components. The cycle of synaptic vesicle trafficking in the synapse is thought to proceed as follows (see also Figure 2.4b).^[3,63] Synaptic vesicles filled with neurotransmitters are stored in the synapse and a part of them is recruited to the active zone close to the presynaptic membrane. In the active zone, docking and priming of the vesicles occur, transferring them into a ready-to-fuse state. Primed vesicles constitute the so-called readily releasable pool. Upon the Ca^{2+} trigger, they are ready to immediately fuse with the presynaptic membrane. The readily releasable pool is a dynamic construct where fused vesicles can be rapidly replaced by new ones.^[64] After fusion, the synaptic vesicles are assumed to be endocytosed by clathrin-coated proteins. Concerning recycling, different pathways are discussed.^[65] Eventually, they make the vesicles available for a next round of fusion.

2.4. Fusion Proteins

2.4.1. Overview

The fusion of biological membranes is a tightly regulated process and is usually accomplished by proteins. During evolution, different types of fusion proteins have developed. They differ in their structure as well as in the way how and between which membranes they mediate fusion.

Viruses, for example, make use of specific viral fusion proteins to enter host cells and infect them. Viral fusion proteins from enveloped viruses share transmembrane segments that anchor the proteins into the viral membrane and a special hydrophobic domain called “fusion peptide” that is able to interact with the target membrane. There are different classes of viral fusion proteins but they are thought to act based on the same principle. One of the best studied class I viral membrane fusion processes is that of influenza viruses, in which hemagglutinin interacts with the host cell membrane. In short, upon a trigger the viral fusion protein being in an active trimeric state changes into an expanded conformation so that it bridges both membranes. Thereby, the fusion peptide is inserted into

¹ This is true for synchronous release, which constitutes the majority of neurotransmitter release events. In case of asynchronous release, the process can also take several seconds.^[62]



2. Membranes and Membrane Fusion

the target lipid bilayer. Next, the fusion peptide folds back to the trimer forming a hairpin structure. This distorts the membrane and finally leads to fusion pore formation.^[66]

Contrary to viral fusion machineries, those of intracellular fusion events require fusion proteins located on both sides of the opposing membranes. Two families of fusion proteins have been identified: dynamin-like atlastins and SNAREs. Atlastins are frequently found on the endoplasmic reticulum (ER). They are thought to be key factors in maintaining the dynamic structure and function of the ER as they are involved in homotypic ER fusion.^[67] They are multidomain membrane-bound GTPases and can interact with their counterpart on the second membrane. Hydrolysis of guanosine triphosphate (GTP) brings about a conformational change that finally leads to fusion of the ER membranes.^[68] The family of SNARE proteins is found in the secretory pathway. They are much smaller than atlastins but also accomplish membrane fusion by assembling proteins in opposing membranes. The required energy, however, is provided from the assembly itself and not via nucleotide hydrolysis.^[69]

The fusion of mitochondria is managed by another set of fusion proteins, which were found only recently.^[70] It is an even more complex procedure because mitochondria exhibit two membranes which means that during fusion four membranes need to merge. Up to now, two core components are known that likely constitute the mitochondrial fusion machinery in mammals: MFN1 (mitofusin 1) and its isoform MFN2 are located on the outer mitochondrial membrane and OPA1 (optic atrophy protein 1) is located on the inner mitochondrial membrane.^[71] Like the atlastins, they belong to the dynamin protein family and exhibit an intrinsic GTPase function. Fusion of the outer membranes is linked to that of the inner membranes and there are hints that the fusion proteins are needed on both sides of the opposing membranes. However, the mechanism of mitochondrial fusion is far from being well understood.^[72]

Another type of fusion is the fusion between cells, an essential process involved in fertilization or syncytia formation, for example. The participating fusion proteins and the underlying mechanisms in these extracellular cell–cell fusion processes are, however, mostly unknown. Several proteins related to cell–cell fusion have been identified in mice and nematodes.^[73] Due to common characteristics, such as a transmembrane anchor, a glycosylated extracellular domain with a specific disulfide bond pattern and an unstructured cytosolic C-terminal part, they have been ranked among the fusion family (FF) proteins. Recently, a model has been proposed suggesting proteins of opposite membranes to assemble in trimers. Subsequent conformational changes and zipper-like interactions of the transmembrane domains then leads to the formation of a fusion pore.^[74]

The following sections go into the details of SNARE proteins, in particular those mediating neuronal exocytosis, as they constitute the models of the mimetics examined in the present work.

2.4.2. The Structure of SNARE Proteins

The neuronal exocytosis machinery consists of the SNARE proteins Syntaxin-1A, SNAP-25 (25 kDa synaptosome-associated protein) and Synaptobrevin-2 (also known as VAMP, vesicle-associated membrane protein). The latter is located at the surface of the synaptic vesicles, whereas the two proteins mentioned first are located in the presynaptic membrane. The structure of the neuronal SNAREs is schematically depicted in Figure 2.5a.

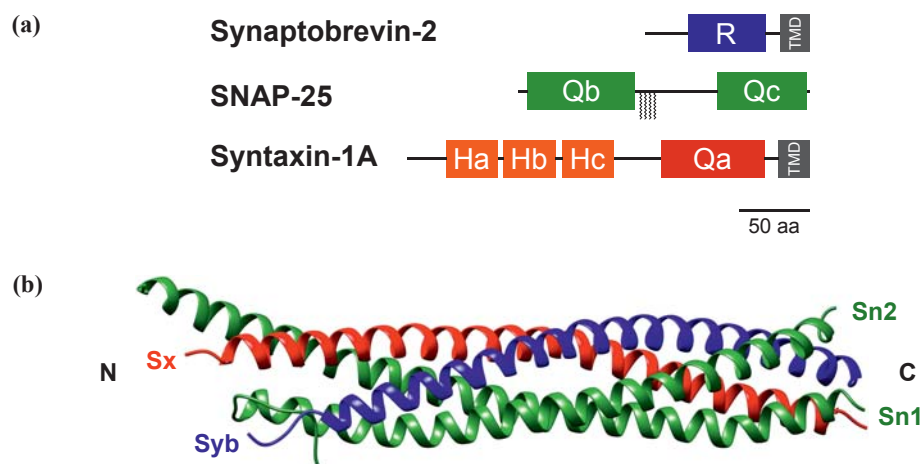


Figure 2.5. (a) Schematic structure of the three neuronal SNARE proteins. Their characteristic domains are highlighted in color. The scheme is drawn to scale regarding the number of amino acids (see scale bar). Data on number of amino acids was taken from Ref. [75] (H_{abc} domain), Ref. [76] (N-peptide) and Ref. [77] (all the others). (b) Ribbon diagram of the synaptic fusion complex consisting of the SNARE motifs of Syntaxin-1A (Sx, red), Synaptobrevin-2 (Syb, blue) and SNAP-25 (Sn1+Sn2, green). The diagram was created with the *UCSF Chimera* package.^[78]

Syntaxin-1A and Synaptobrevin-2 are anchored in the membrane via a transmembrane domain (TMD), which is a common characteristic of many SNARE proteins. However, anchoring in the membrane is also possible via palmitoyl chains attached to the side chains of cysteine residues, as in SNAP-25, for example. The TMDs predominantly exhibit an α -helical structure and are made of ≈ 20 amino acids with mainly hydrophobic side chains.^[79,80] Their role during membrane fusion is not conclusively clarified but there is strong evidence that it is a significant one. This is discussed in more detail in Section 2.4.3.



2. Membranes and Membrane Fusion

All SNARE proteins exhibit the so-called SNARE motif, which is attached N-terminally to the TMD via a short linker region. The SNARE motif enables SNARE proteins to interact and thus to form the specific SNARE complex which is thought of as the crucial step in SNARE mediated membrane fusion (see Section 2.4.3). Some proteins such as SNAP-25 consist of two SNARE motifs, which are connected via a loop. The SNARE motif has a length of around 60–70 amino acids and can adopt an α -helical structure. The amino acids are arranged in heptad repeats. Each position in the heptad is occupied specifically with polar or unpolar amino acids. This results in the formation of a tight coiled-coil structure upon interaction of four individual α -helices (see Figure 2.5b). In this complex, the α -helices are arranged in parallel. Interacting amino acid side chains form characteristic layers. The layers are perpendicular to the longitudinal axis of the complex and consist of four amino acids, each contributed by one of the four intertwined α -helical SNARE motifs. The layers are mainly hydrophobic except for the central “zero layer”, which displays amino acids with polar side chains. While the sequence of amino acids varies among SNAREs of different organisms, the amino acid in the very middle of a SNARE motif is evolutionarily highly conserved. With only very few exceptions, it either is an arginine (R) or a glutamine (Q), and on the basis of this amino acid the SNAREs are classified as R-SNAREs and Q-SNAREs.^[81] It has been shown that three Q-SNAREs and one R-SNARE are needed to constitute a fully functional SNARE complex. The SNARE complex is exceptionally stable.^[82] In fact, several molecules of adenosine triphosphate (ATP) and a whole protein machinery are necessary to disassemble the SNARE complex into single SNARE proteins.^[83]

N-terminally to the SNARE motif, some SNARE proteins exhibit an additional N-terminal domain. These domains vary in structure and their exact role during membrane fusion is highly discussed.^[84] For example, Qa-SNAREs such as Syntaxin-1A feature an antiparallel three-helix bundle at their N-terminus (see Figure 2.5a). This so-called H_{abc} domain is independently folded. It can fold back on the SNARE motif holding Syntaxin-1A in an inactive state.^[85] There is also evidence that it functions as a binding site for regulatory proteins.^[2] The same is assumed for the N-peptide, a short stretch of around 30 amino acids located N-terminally of the H_{abc} domain.^[76,86] This segment is mainly unstructured. However, it contains an evolutionarily conserved Asp-Arg-Thr (DRT) motif to which SM (Sec1/Munc18-like) proteins bind.^[76]

2.4.3. The Presumed Functioning of SNARE Proteins

Formation of the SNARE Complex

In 1998, Sutton *et al.* determined a high-resolution crystal structure of the neuronal SNARE complex for the first time.^[79] As can be seen in Figure 2.5b, it shows an ordered coiled-coil complex in which the α -helices are oriented in parallel. The crystal structure was made from the *cis*-SNARE complex and thus represents the final outcome of the interaction of the SNAREs. It was long assumed that, before interaction, the monomeric SNAREs, especially SNAP-25 and Synaptobrevin-2 exist in a rather random structure.^[87] However, recent nuclear magnetic resonance (NMR) studies in solutions showed that monomeric micelle-bound Synaptobrevin-2^[88] as well as monomeric micelle-bound Syntaxin-1A^[89] exhibit an intrinsic helical structure suggesting that the helical domains may serve as a nucleation site for SNARE complex formation.

The crucial question is: What does happen in between, *i.e.* how exactly does the assembly of the SNARE motifs proceed? This question is anything but easily answered. Plenty of research has been conducted during the last few years to unravel the SNARE assembly mechanism.^[3,4,12,58,90] The topic is still much debated and mechanistic details are far from being fully understood. It is difficult to detect the interaction of SNAREs because many factors play a role during the native SNARE mediated membrane fusion. This might also be the reason why so many different approaches exist trying to unveil the SNARE assembly mechanism and why they sometimes appear to be inconsistent with one another. The way how SNAREs behave is influenced by their environment, so different methods of reconstitution, performing the assay and the way of detection might provide contrasting outcomes. Studying the SNARE interaction in simplified settings such as in cell-free assays, however, is necessary because the natively given condition is way too complex to be analyzed in its entirety.

A widely spread hypothesis comprises the so-called “zippering” of the SNARE motifs, meaning that the interaction of the SNARE motifs starts at the N-termini and then proceeds towards the C-termini in a zipper-like fashion.^[8] Up to now, it is unclear whether the assembly of the SNAREs proceeds stepwise or rather in an all-or-nothing manner.

On the one hand, several research groups succeeded in capturing and measuring partially zippered SNARE complexes, suggesting that multiple steps are involved during interaction of the SNARE motifs. Gao *et al.*, for example, studied the SNARE assembly on the basis of single reconstituted SNARE complexes with the help of optical tweezers.^[6] They concluded that the assembly proceeds in three distinct steps rather than in



2. Membranes and Membrane Fusion

a continuous fashion. By using fluorescence anisotropy measurements and lipid mixing assays Li *et al.* suggested a rate-limiting assembly of the N-terminal half of the SNARE motifs, which is required for the subsequent fast assembly of the C-terminal half. The second step then provides the energy needed for membrane fusion.^[7] They also pointed out that it is rather the middle layers that are crucial for interaction than the layer at the very N-terminal end as it is proposed by the conventional N to C zippering model. Shin *et al.* did structural investigations by applying electron paramagnetic resonance spectroscopy and single molecule FRET studies with SNARE proteins embedded in nanodiscs so that SNARE assembly was possible but membrane fusion was not.^[91] They detected the N-terminal half of the SNARE complex up to the ionic layer to be in a defined coiled-coil like structure while the structure of the C-terminal half varied between fully structured, an unknown intermediated state, and unstructured. On the basis of these results, they proposed a three-step SNARE assembly.

Generally, the picture that emerges on the basis of the recent studies that suggest a stepwise zippering is the following: The zippering of the SNARE motifs is initiated in the N-terminal domain. This association is slow and probably paused partway in the middle around the central ionic layer.^[92] Afterwards, zippering of the C-terminal domain takes place. This assembly is fast and it is thought that the C-terminal half of the Synaptobrevin-2 SNARE motif zippers along a pre-organized template of the Syntaxin-1A and SNAP-25 motifs. Zippering is possibly continued on the linker region.^[77] The assembly of the C-terminal domain provides the main energy for membrane fusion as shown by theoretical calculations.^[93] The two-step zippering process was also found for other than neuronal SNAREs,^[93] suggesting that it is a conserved pathway.

In contrast to that, Jahn *et al.* propose that zippering might rather happen in an all-or-none fashion meaning that once the SNAREs interact, zippering proceeds straightaway to the C-terminal ends.^[3,94] They explain it with the steep gradient in energy that arises from the highly exergonic SNARE complex formation. For example, Synaptobrevin-2 is able to rapidly replace the C-terminal fragment from the Δ N-complex resulting in membrane fusion.^[8] The Δ N-complex is a construct made of Syntaxin-1A, SNAP-25 and a soluble fragment of Synaptobrevin-2 (see Section 2.5 for more details). Thus, it might be difficult for regulating proteins to successfully intervene the zippering reaction.^[3]

Regulation of the SNARE Assembly

The fusion of a synaptic vesicle with the presynaptic membrane is not accomplished by the SNARE proteins alone. A variety of additional proteins is involved in neuronal ex-

ocytosis as well. Though SNARE proteins are seen as the key players in this process, which are likely responsible for summoning the energy to yield lipid rearrangement and fusion pore formation, they rely on additional help. In the last few years, a more and more distinct picture arose concerning the structure and function of these additional proteins. As with the function of the SNAREs themselves, the detailed mechanisms of the actions of the regulating proteins are not fully understood and they are a highly discussed topic up to now.^[2,3,95–97] Figure 2.6 illustrates today's idea about the interaction between SNAREs and their regulating proteins. These proteins and their proposed function are explained in the following.

Munc18-1 (mammalian uncoordinated-18-1, also called neuronal Sec1) is an arch-shaped protein, which belongs to the SM protein family. As seen from crystal structures, it exhibits three domains that form cavities and thus provide different binding sites for SNAREs.^[99] For example, Munc18-1 has been found to bind tightly to the folded Syntaxin-1A as well as to the N-terminal regions (N-peptide and H_{abc} domain) of Syntaxin-1A. Its exact role during membrane fusion including the specific binding site is still controversially discussed.^[100] Deletion of Munc18-1 in experiments with knockout mice, however, led to a loss of neurotransmitter release,^[101] implying a crucial role during membrane fusion. It seems to gain wide acceptance that Munc18-1 holds Syntaxin-1A in a closed conformation, thereby inhibiting premature SNARE complex formation. Accordingly, the Syntaxin-1A-Munc18-1 complex rather than the Syntaxin-1A-SNAP-25 complex (previously termed “acceptor complex”) is currently discussed as the actual starting point for neuronal exocytosis.^[102]

The opening of the conformation of Syntaxin-1A is thought to be orchestrated in collaboration with Munc13,^[103] which is a large multidomain protein that ranks among the group of CATCHR (complex associated with tethering containing helical rods) proteins and is regulated by RIMs.² There is evidence that it plays a crucial if not necessarily fully clarified role during neuronal exocytosis. For example, Yang *et al.* showed that mutations in characteristic regions of the MUN domain of Munc13 lead to the inability of keeping Syntaxin-1A in a closed state and SNARE assembly was not possible anymore.^[104] Thus, Munc13 probably alters the structure of Munc18-1, thereby allowing Syntaxin-1A to switch to an open conformation. As the structure of Munc13 resembles various tethering factors it might also play a universal role during fusion.^[105] It is thought that these

² RIM is the abbreviation for *Rab3-interacting molecule*. Rab3 is a GTPase involved in the sorting process of synaptic vesicles and belongs to the Rab (*Ras*-related in *brain*) protein family. Rab proteins belong to the group of the Ras superfamily. The eponym Ras codes for the Ras protein and is a gene that was originally identified in viruses in rats (*rat sarcoma*). Hence the name “RIM”.

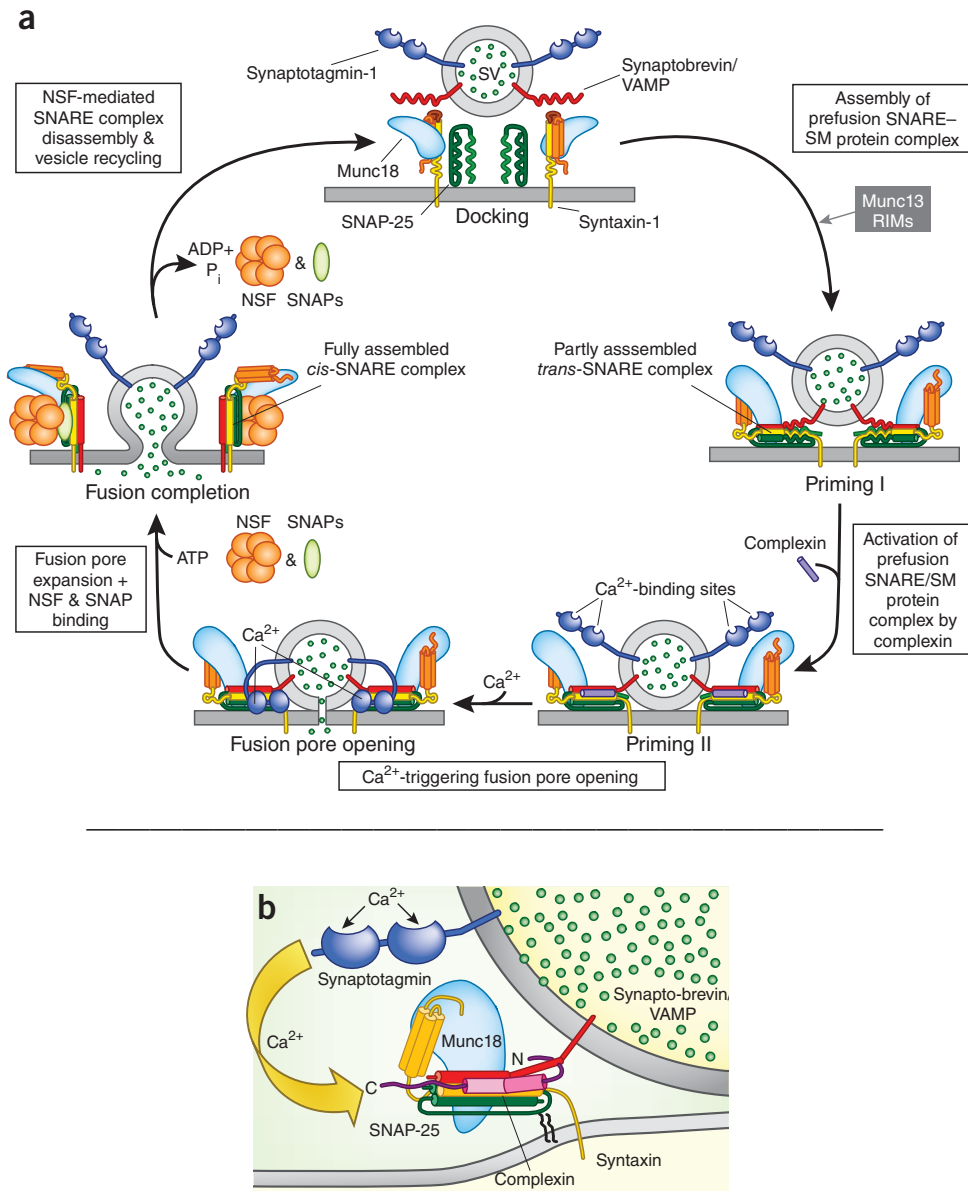


Figure 2.6. Today’s idea of how the interaction between SNAREs and further proteins leads to the fusion of a synaptic vesicle with the presynaptic membrane. (a) Schematic representation of the “SNARE cycle” starting with the “Docking” step (at top). See text for a detailed description. (b) Detailed view of the primed fusion complex ready to initiate fusion upon the influx of Ca²⁺. Adapted by permission from Macmillan Publishers Ltd: NATURE MEDICINE (Ref. [98]), copyright (2013).

proteins together ensure the assembly of the SNAREs to form the probably partially zippered *trans*-SNARE complex (see first step in Figure 2.6a, Docking → Priming I). The zippering process of the SNAREs has been discussed in more detail in the previous section.

A process such as neuronal exocytosis that is triggered by the influx of Ca^{2+} needs to be equipped with specialized Ca^{2+} sensors that transfer information of the trigger to the fusion initiating SNARE proteins. This task is taken on by synaptotagmins. Synaptotagmin-1 is a transmembrane protein located on the side of the synaptic vesicles. It exhibits two Ca^{2+} binding domains termed C2A and C2B. Up to date, it is unclear how synaptotagmins function upon Ca^{2+} binding and different scenarios have been proposed. Recent NMR and crystallographic studies, for example, showed multiple interaction sites between Synaptotagmin-1 and the SNARE complex, suggesting the formation of a super-complex around the docking site.^[2] However, there is also evidence that Synaptotagmin-1 does not assemble with the SNARE complex at all but only binds to phosphatidylinositol 4,5-bisphosphate (PIP_2)-containing membrane domains via electrostatic interactions.^[106]

Synaptotagmin-1 likely works in cooperation with complexins.^[107] Complexins are small proteins, which are only able to bind to the SNARE complex and not to individual SNAREs alone.^[108] For binding, the SNAREs thus have to be at least in a partially zippered state. NMR and crystallography studies revealed that complexins exhibit a central α -helix that is connected to an accessory α -helix.^[109,110] The role of complexins is highly discussed and not conclusively untangled. Complexins were shown to have an activating as well as an inhibitory influence on membrane fusion. They bind to the SNARE complex via their central helix, which is thought to stabilize the zippered complex and keeping it in a ready-to-fuse state, thus acting facilitatingly.^[109] A facilitatory role is also ascribed to the unstructured amino terminus of complexins.^[110] The negatively charged accessory helix, however, inhibits neurotransmitter release probably due to electrostatic repulsion^[110] and/or due to directly competing with Synaptobrevin-2.^[3] In this way, Complexin clamps the SNARE complex and prevents progression of zippering unless Ca^{2+} flows in and binds to Synaptotagmin-1, which then releases the blockage. Different possibilities for this release are currently discussed, among them is the suggestion that Synaptotagmin-1 binds to the SNARE complex and replaces Complexin or that it destabilizes the adjacent lipid bilayer by binding to it.^[3] In contrast, there is evidence that complexins are rather located between the vesicle and plasma membrane instead of directly binding to the SNARE complex.^[111] In the outcome of a very recent study both suggestions are combined. It was proposed that Complexin binds both to the prefusion SNARE complex (via the α -helices) and to the membrane (via its C- and N-terminal regions).^[112]

In the scheme depicted in Figure 2.6a, Complexin is designated to activate the prefusion SNARE/Munc protein complex by binding to it (see Step 2, Priming I \rightarrow Priming II). The inflowing Ca^{2+} ions bind to Synaptotagmin-1 causing it to bind to the SNARE complex



2. Membranes and Membrane Fusion

and to replace Complexin (see detailed view in Figure 2.6b). This allows the SNAREs to fully assemble. A complex interplay among the involved proteins eventually leads to the opening of the fusion pore (see Step 3, Priming II → Fusion pore opening). When the SNARE complex is fully assembled and membranes have merged, all SNARE proteins reside on the same membrane side, and the SNARE complex is called *cis*-SNARE complex (see Step 4, Fusion pore opening → Fusion completion). Upon expansion of the fusion pore, neurotransmitters are released from the synaptic vesicle into the synaptic cleft. They diffuse through the synaptic cleft and activate receptors in the postsynaptic membrane. The receptors evoke a cascade of further reactions ensuring signal transmission from neuron to neuron (see Section 2.3).

Once membrane fusion is completed, the SNARE complex is separated into single SNAREs. This disassembly is an ATP-dependent process mediated by NSF (*N*-ethylmaleimide-sensitive factor) and SNAPs (soluble NSF attachment proteins) (see Step 5, Fusion completion → Docking). NSF belongs to a group of ATPases that change their conformation when catalyzing the hydrolysis of ATP.^[113] It is thought that up to four SNAP molecules bind to the *cis*-SNARE complex followed by binding of NSF. Recent cryo electron microscopy studies revealed important insight into structural details of this so-called 20S supercomplex.^[114] Ryu *et al.* performed single-molecule fluorescence spectroscopy and proposed that SNARE disassembly can be likely described by a “spring-loaded” model.^[115] It implies that ATP is completely consumed first and afterwards the energy resulting from ATP hydrolysis is released onto the SNARE complex leading to its disassembly. The exact mechanism, however, still remains a debated topic.^[83]

The Role of the Transmembrane Domains

There is general belief that by means of their interaction SNAREs exert mechanical force onto the membranes to overcome the energy barrier and to open the fusion pore. The crucial question is: How is this accomplished? Many studies suggest an essential role of the TMDs not least because the X-ray structure of the neuronal SNARE complex reported by Stein *et al.* implied a continuous helix from the N-termini up to the very C-termini of each of the SNAREs.^[77] On the opposite side it is argued that SNARE assembly alone serves to bring the membranes into close proximity and that this proximity is then sufficient for the lipid leaflets to eventually merge.^[116] In this way of thinking, the TMDs just function as an anchor to hold the SNAREs within the membrane.

Most widely, there is consensus that the length of the anchoring part is important and that it needs to span both lipid leaflets to effectively induce membrane fusion.^[12] For

example, SNAREs with a truncated TMD were investigated and it was shown that they are no longer capable of fusing membranes.^[117,118] There is a vast amount of studies that report detrimental effects on membrane fusion when the TMDs of fusion proteins are modified.^[27] In contrast, a recent study by Zhou *et al.* suggests that SNAREs with an artificial lipid anchor actually can induce fusion.^[119] Herein, neuronal SNAREs featuring the lipid anchor of Syntaxin-19 were able to rescue the release of neurotransmitters in cultivated neurons lacking the wild-type SNARE. Several other investigations also indicated that SNAREs with an artificial lipid anchor can lead to fusion of membranes as long as their length is sufficient to span the entire lipid bilayer.^[120] This is supported by a study, which proposed that any TMD can serve as an anchor and that TMDs do not specifically interact.^[121] In contrast, experiments by Lygina *et al.* with SNARE model peptides showed that an identical TMD on both sides of the membranes leads to significantly less fusion efficiency, thus suggesting the opposite case.^[19]

Ngatchou *et al.* added amino acids with charged side chains to the C-terminus of SNAREs, which was found to prevent fusion.^[122] On the basis of this finding, they proposed a mechanism that supports the idea of an active role of the TMDs (see Figure 2.7).

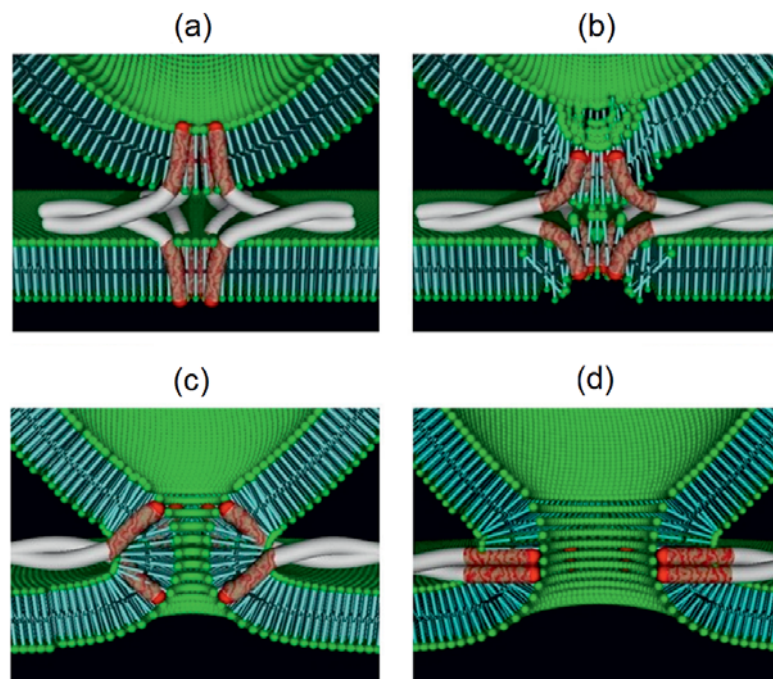


Figure 2.7. Schematic view of the fusion pore opening as proposed by Ngatchou *et al.*^[122] The TMDs of Syntaxin-1A and Synaptobrevin-2 (a) are pulled towards the hydrophobic core of the lipid bilayer as a result of SNARE zippering (b). The membrane structure is disrupted, which leads to pore formation (c) with the TMDs finally arranged in parallel (d). Reproduced from Ref. [122] with permission.



2. Membranes and Membrane Fusion

They suggested that in course of the fusion process a movement of the TMDs takes place meaning that the TMDs are pulled inward into the hydrophobic core. This disturbs the order of the lipids, causes a rearrangement, and finally leads to the formation of the fusion pore. A study by Wehland *et al.* systematically investigated the influence of different amino acids at the C-terminus of the TMDs of Syntaxin-1A and Synaptobrevin-2.^[117] The results indicate that the C-termini likely are involved in the fusion process and thus support the proposed mechanism by Ngatchou *et al.* In addition to the penetration of the C-termini into the center of the lipid bilayer, TMDs may also exert forces leading to highly localized deformations of lipids located on the inner leaflet in proximity to the TMDs. This was suggested by recent molecular dynamics simulations and experiments with SNAREs from yeast vacuoles.^[123,124]

Summarizing, the question whether a simple lipid anchor in the membrane is sufficient or whether the TMD has in addition a more complex function within the fusion process remains controversially discussed. There is strong evidence coming from many studies, though, that the role of the TMD during membrane fusion is an active one.

Interaction With Lipids

There is growing evidence that not only accessory proteins but also lipids present in the involved membranes regulate membrane fusion. For example, it was shown that the hydrophobic mismatch, *i.e.* the difference between the length of the SNAREs' trans-membrane domains and the lipid bilayer thickness, contributes to the lateral organization of SNAREs in the membrane.^[125]

Especially, negatively charged lipids have been in the focus of research in the past years. It was postulated that Ca^{2+} ions interact with lipids and thus lower the electrostatic repulsion between both membranes as well as bridge opposite membranes, thereby facilitating membrane fusion.^[126] Phosphatidylinositol 4,5-bisphosphate (PIP_2) is a polyanionic lipid and crucial in neuronal exocytosis. Its normal abundance in the plasma membrane is about 1 mol%, but it was found to be locally enriched up to 5 mol% at the site of docked vesicles.^[127,128] PIP_2 was shown to interact with more than a dozen of proteins potentially related to regulated exocytosis.^[129] Due to its negative charges it readily interacts with the polybasic $^{260}\text{KARRKK}^{265}$ motif in the linker region of Syntaxin-1A, for example. PIP_2 clusters with Syntaxin-1A into non-raft microdomains,^[128] thus recruiting Syntaxin-1A to the fusion site. Recently, Ca^{2+} ions were found to act as a bridge between anionic PIP_2 molecules leading to large Syntaxin-1A/ PIP_2 domains.^[130] PIP_2 also binds to the polybasic stretch in the C2B domain of Synaptotagmin-1.^[131] Due to this binding, the affinity



of Synaptotagmin-1 for Ca^{2+} is significantly enhanced, which emphasizes the key role of PIP_2 during membrane fusion. A regulatory role is also ascribed to the negatively charged lipids phosphatidylserine and phosphatidic acid.^[12]

On top, cholesterol is an important regulating lipid in membranes. Due to its unique structure, it alters the lipid bilayer in different ways, for example regarding thickness, fluidity, curvature and the overall lipid organization.^[132] Cholesterol induces a negative curvature of monolayers and thus should favor the highly bent membrane structure during fusion (see also Section 2.2). Indeed, it was shown to accelerate fusion rates by decreasing the energy needed for membrane bending and by recruiting SNAREs to the fusion pore.^[133] Summarizing, membrane lipids have an important role in all steps of membrane fusion.

2.5. Model Systems for the SNARE Mediated Membrane Fusion

A multitude of model systems has been developed to unravel the mechanisms underlying the complex SNARE mediated membrane fusion process.^[13,14,90] Model systems allow the study of membrane fusion in a simplified setting (see Figure 2.8). Thus, it is possible to focus on certain aspects of the complex process and to decipher it piece by piece.

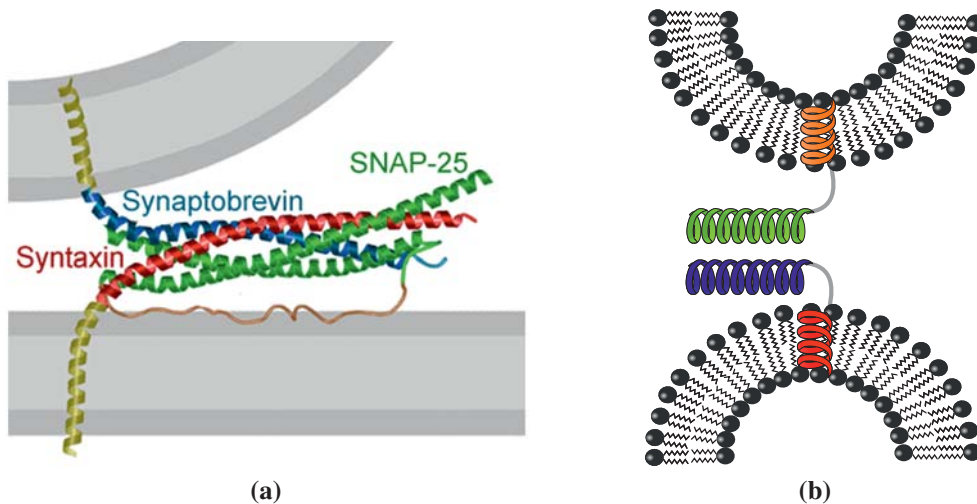


Figure 2.8. Concept of SNARE model systems (“bottom-up approach”). Their design is inspired by the native SNAREs (a). Model systems exhibit a less complex structure as the number of interacting units is reduced from four to two (b, schematic depiction). The interacting units share the ability for specific molecular recognition but their structure can differ wildly. As membranes, usually liposomes with a defined lipid composition are applied. Figure 2.8a is reprinted and modified by permission from Macmillan Publishers Ltd: NATURE (Ref. [79]), copyright (1998).

Commonly, model systems include fusogens that are incorporated in liposomes. The fusogens can differ widely in their structure but they share the ability to induce membrane fusion upon specific interaction to mimic the highly specific native SNARE interplay.³ As a model for the native membranes, liposomes of a defined lipid composition are used. The capability of membrane fusion can then be investigated by different assays (see Section 2.6). Two *in vitro* strategies have been followed to find out how SNARE proteins work—applying the native SNAREs in a cell-free environment or designing artificial SNARE analogues.

³ In contrast to these so-called targeted model systems, non-targeted model systems exist as well. They are typically based on the interaction of a fusogen with the lipid bilayer, see Ref. [14] for a review.



2.5. Model Systems for the SNARE Mediated Membrane Fusion

One of the first *in vitro* experiments was presented by Weber *et al.* in 1998.^[134] They reconstituted native neuronal SNAREs in proteoliposomes and observed lipid mixing. It made them conclude that the SNAREs constitute the “minimal fusion machinery” for membrane fusion. A lot of experiments followed and did not always lead to consistent results. One reason might be differing experimental procedures. Chen *et al.* for example prepared the liposomes in different ways and noted that the fusogenicity of the very same SNAREs depended on the physical state of the liposomes.^[135] The fact that it took hours to complete the fusion with isolated native SNAREs was especially considered problematic. Native neuronal exocytosis, however, proceeds in less than a millisecond.^[136] A major contribution to this discussion was given by Pobbati *et al.* in 2006.^[8] They created a stabilized acceptor complex referred to as ΔN -complex. It consists of Syntaxin-1A, SNAP-25 and a C-terminal fragment of Synaptobrevin-2 (49-96). This fragment prevents the formation of the inactive 2:1 complex, in which a second Syntaxin-1A molecule is attached to the 1:1 complex of Syntaxin-1A and SNAP-25. During fusion, the full-length Synaptobrevin-2 located on the opposite membrane is able to rapidly replace the fragment. This results in a delayed onset of lipid mixing but an overall dramatically increased speed of liposome fusion compared to experiments in which the 1:1 complex is used.

Recently, single-vesicle fusion assays gained in importance as they allow the study of single fusion events and thus provide information on the dynamics of SNARE interaction. With these assays it is possible to observe fusion rates occurring at a time scale of milliseconds which is only one magnitude away from the native time scale.^[94,137,138]

Despite the progress made with purified native SNARE proteins it is still beneficial to follow a second strategy to elucidate fusion mechanisms at the molecular level. This strategy is a “bottom-up approach”, in which artificial SNAREs are designed that mimic the native proteins.^[14] These SNARE mimetics are usually characterized by the replacement of an essential domain of the SNAREs—recognition motif, linker region, or transmembrane domain—by an artificial moiety. Synthetic SNARE analogues offer the advantage of a reduced structural complexity. It is easily possible to systematically vary their structural elements. This allows elucidating how relevant those elements are in the membrane fusion process. Thus, fundamental questions of liposome–liposome fusion can be addressed and mechanistic details of membrane fusion can be better understood on the molecular level.

Membrane fusion can be induced by small molecule recognition as various assays show. For example, it is possible to apply molecules as small as melamine and cyanuric acid, each attached to a lipid anchor, to achieve liposome fusion.^[23] Here, formation of hydro-

2. Membranes and Membrane Fusion

gen bonds between the molecules allows specific melamine–cyanuric acid pairing. Also, the interaction of boronic acid with molecules containing *cis*-diols, as for example *myo*-inositol, has been described to fuse liposomes. However, this was only possible when a polyethylene glycol (PEG) spacer kept the boronic acid from being embedded in the hydration layer.^[139] Very recently, it has been reported that the strain-promoted azide-alkyne cycloaddition using lipids functionalized with either cyclooctene or an azide moiety can induce liposome fusion.^[21] Certainly, these systems cannot be seen as true structural SNARE mimics anymore but they provide an interesting alternative of fusogens inducing membrane fusion especially due to their bioorthogonal properties.

In most of the SNARE analogues that can be found in literature the characteristic SNARE motif has been replaced by an artificial recognition unit. For example, Chan *et al.* introduced a model system in which the fusogens consist of DNA strands attached to a phospholipid anchor.^[17] Recognition between complementary DNA strands through specific Watson–Crick base pairing brings opposing membranes into close proximity so that they can fuse. The model system of Stengel *et al.* uses double stranded DNA recognition units with sticky ends (see Figure 2.9).^[18] Two cholesterol moieties ensure a stable membrane anchoring and guarantee efficient liposome fusion. In the case of one cholesterol anchor only mixing of the outer leaflets and lipid instabilities were recognized.^[140] Elongating the DNA recognition units did not result in a higher amount of lipid mixing.

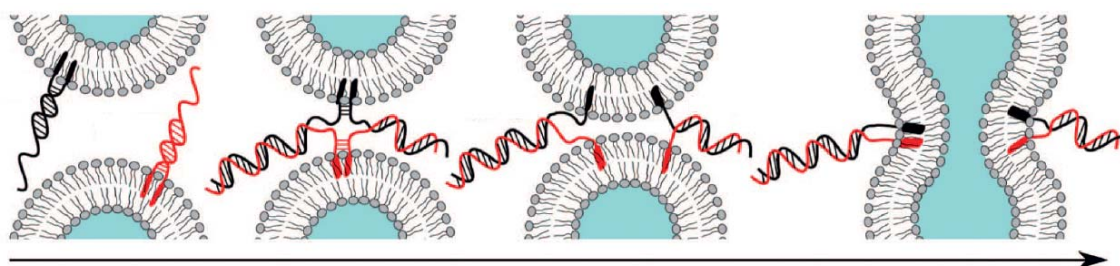


Figure 2.9. Schematic view of the DNA model system introduced by Stengel *et al.*^[140] in which DNA strands with sticky ends are anchored via two cholesterol moieties in the membrane of large unilamellar vesicles (LUVs). From left to right: Upon recognition, the DNA strands sequentially hybridize which finally leads to liposome fusion. Reprinted with permission from G. Stengel *et al.*, *J. Phys. Chem. B* **2008**, *112*, 8264. Copyright (2008) American Chemical Society.

Peptidic recognition units have been tested as well. For example, the specific recognition between vancomycin and a D-Ala-D-Ala dipeptide, which is based on the formation of hydrogen bonds, leads to the fusion of liposomes.^[141] Often used SNARE model systems are those that are based on coiled-coil interactions between α -helical peptides as

2.5. Model Systems for the SNARE Mediated Membrane Fusion

introduced by Marsden *et al.*^[16] They designed SNARE-mimicking peptides containing either a K3 (KIAALKE)₃ or an E3 (EIAALEK)₃ sequence, which is attached via a PEG-linker to a phospholipid anchor. E3 and K3 are α -helical sequences designed such that they form stable coiled-coils upon interaction.^[142] With this, they mimic native SNAREs, which also form a coiled-coil complex upon interaction (see Section 2.4.2 for more details). Fluorescence-based lipid mixing and content mixing assays with liposomes showed that full fusion is possible with these peptides. In a follow-up study, it was shown that the length of the coiled-coil is important and is directly related to the fusogenicity of the peptides. Extending the coiled-coil by one heptad unit (thus leading to sequences E4 and K4) increased the extent of lipid mixing while shortening the recognition unit by one heptad (thus leading to E2 and K2) decreased the amount of lipid mixing (see Figure 2.10).^[143]

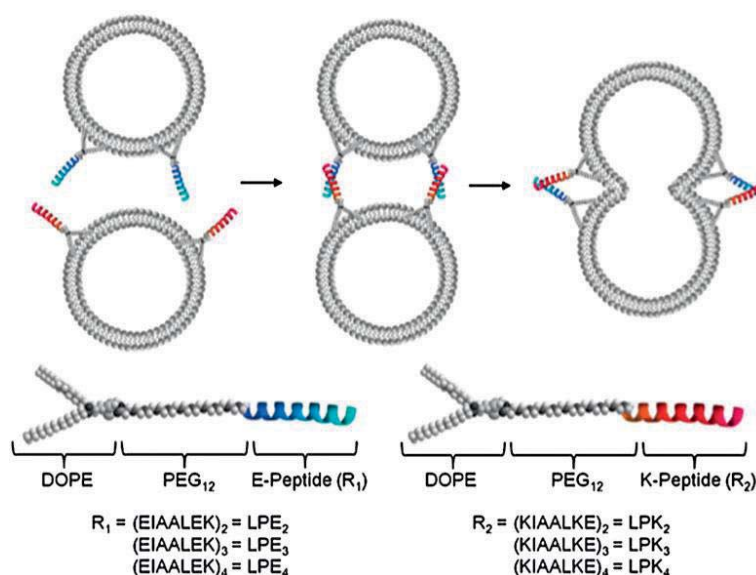


Figure 2.10. Schematic view of the model system introduced by Marsden *et al.*^[16] The coiled-coil forming peptide sequences (E-peptides (blue) and K-peptides (red)) are attached to DOPE via a PEG₁₂ linker. The length of the peptide is varied between 2 and 4 heptad units. Incorporation of the lipopeptides into LUVs leads to liposome fusion due to coiled-coil formation between E- and K-peptides. Reproduced from Ref. [143] with permission of The Royal Society of Chemistry.

The question of the helices' orientation within the duplex has also been addressed in several assays. With the lipopeptides described above, a parallel orientation—as in the native SNARE complex—was achieved. Instead of attaching the lipid anchor C-terminally to both the E3 and K3 sequence, it was attached N-terminally to one of the sequences to obtain an antiparallel orientation.^[144] The extent of lipid mixing, however, was similar in



2. Membranes and Membrane Fusion

both cases suggesting that in these SNARE models the coiled-coil interaction itself rather than the orientation of the interacting units is crucial. The experiment was repeated with a “true” antiparallel coiled-coil interaction by reversing the amino acid sequence of E3 and leaving the lipid anchor attached C-terminally in both peptides.^[145] Again, no significant difference between both orientations in terms of lipid mixing could be detected. Contrary to that is an independently performed study by Pähler *et al.*, in which real lipid mixing was observed with the parallel orientation while the antiparallel orientation only lead to docked liposomes.^[146] The differences in both studies were two things: the lipid anchor (phospholipids vs. cholesterol) and the spacer between coiled-coil sequence and anchor (PEG₁₂ vs. glycin tetramer). There are hints that the type of the lipid anchor influences the extent of lipid mixing.^[147,148] Antiparallel orientation has also been achieved by using recognition units made of β -PNA.^[149] Peptides with these recognition units were capable to induce liposome fusion, suggesting the fusion mechanism being alternative to that of native SNAREs.

As discussed in Section 2.4.3, many studies indicate an essential role of the SNAREs’ transmembrane domains during membrane fusion. To account for this important influence, SNARE mimicking hybrid peptides that contain the transmembrane domain of native SNAREs were developed. This allows a deeper insight into how the TMDs function as membrane anchors as well as how they influence the fusion process. Meyenberg *et al.* developed peptides containing the E3/K3 recognition motif attached to the native TMD sequences of Syntaxin-1A and Synaptobrevin-2.^[15] With these constructs, which well resemble the native SNAREs as they feature a continuous strand of α -amino acids, full fusion was possible as shown by lipid mixing and content mixing experiments. The kinetics were even comparable to those of the native SNAREs as a similar behavior to the Δ N-complex was detected. This suggests that the artificial SNARE analogues are well suited to mimic the SNARE action *in vitro*.

SNARE model peptides with an artificial recognition unit made of PNA have been developed as well. In a recently reported study, PNA was attached to a lipid anchor.^[20] On the contrary, Lygina *et al.* proposed PNA/peptide hybrids in which the native TMDs were used as membrane anchors (see Figure 2.11).^[19] In complementary PNA strands, interaction is possible via Watson–Crick base pairing of opposing nucleobases.^[24]

PNA offers the advantage that parameters such as stability, strand orientation and recognition can be easily set by simply adjusting the nucleobase sequence. It was shown that these PNA/peptide hybrids are capable to induce membrane fusion as well. The PNA recognition units, which were originally developed by Nielsen *et al.*,^[25] were chosen

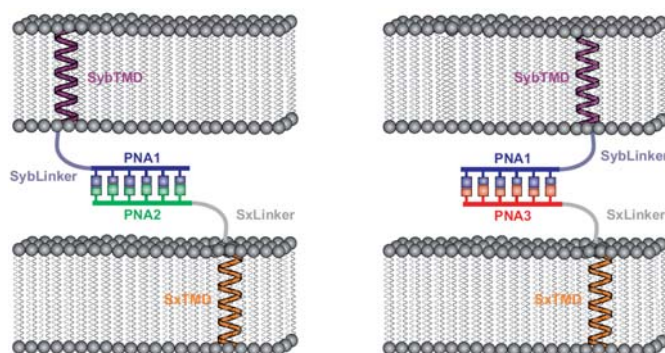


Figure 2.11. Schematic view of the PNA model system introduced by Lygina *et al.*^[19] Complementary PNA strands (PNA1, PNA2 or PNA3) are attached to the native sequences of linker and transmembrane domain of Syntaxin-1A (Sx) or Synaptobrevin-2 (Syb), which anchor the model peptides in the membrane of LUVs. Depending on the PNA sequence, antiparallel (PNA1/PNA2, left) or parallel (PNA1/PNA3, right) strand assembly is possible. © 2011 Wiley-VCH Verlag GmbH & Co. KGaA, Weinheim. Reproduced from Ref. [19] with permission.

such that they form duplexes in either a parallel or antiparallel fashion. The interaction of hybrids assembled in parallel leads to a higher extent of lipid mixing. While outer as well as inner leaflet mixing was observed, the intermixing of the liposomes' content was not verified. On the basis of these results, it was proposed that the PNA/peptide hybrids arrest the fusion process to a large extent at the hemifusion stage. On top, it was also shown that the fusogenicity is significantly reduced when equal TMDs are used, *i.e.* two Syntaxin-1A TMDs instead of the TMDs of Syntaxin-1A and Synaptobrevin-2. The PNA/peptide hybrids were further investigated regarding the role of the TMDs by systematically modifying the amino acids at the C-terminus.^[117] It was shown that introducing amino acids with a net neutral charge, such as lysine, significantly enhances lipid mixing. Modifications with doubly charged amino acids, however, considerably decrease lipid mixing. Also, changing the native carboxylic acid terminus to a neutral amide terminus leads to increased lipid mixing. This confirms the active role of the C-terminus during fusion which is assumed to move into the lipid bilayer upon zippering of the recognition unit (see Section 2.4.3 for more details).

2.6. How to Monitor Liposome Fusion *In Vitro*

There are different techniques to study the fusion of liposomes *in vitro*. Very often, fluorescence-based methods are applied. They range from the traditional bulk fusion assays to the more recent single-molecule studies.^[90] Liposomes are labeled with appro-

2. Membranes and Membrane Fusion

appropriate fluorophores and fusion is expressed for example by a change in the emission intensity of the fluorophores which can be monitored using a spectrometer or a microscope. Depending on the chosen setup, it is possible to distinguish between different intermediate fusion states, like docking, hemifusion or full fusion. In addition, it is possible to follow the fusion process by dynamic light scattering (DLS).^[150] This technique is applied to derive the size distribution of the liposomes during the fusion process. However, DLS cannot distinguish between fusion and aggregation. On top of that, the technique of electron microscopy offers the possibility to directly visualize the liposomes. Especially, cryo-transmission electron microscopy has been applied to study liposome fusion and the morphology of fusion intermediates.^[151] It is a powerful technique because fusion structures are straightly observable. However, as the samples need to be fixed on a substrate and stained, the preparation process may influence the outcome. On top, it only allows capturing snapshots of the fusion process. A continuous time-resolved monitoring, as with DLS or fluorescence-based methods, is not possible. In the following, the assays that are applied in this work are explained in detail.

2.6.1. Bulk Lipid Mixing Assays

Lipid mixing assays were first reported by Struck *et al.* in 1981.^[151] They detected lipid mixing via Förster resonance energy transfer (FRET) between fluorophores bound to the headgroup of lipids.

FRET is a nonradiative energy transfer between a donor molecule and an acceptor molecule.^[152] It can take place if the luminescence energy of the donor matches the absorption energy of the acceptor. Thus, the emission spectrum of the donor needs to overlap with the absorptivity spectrum of the acceptor (see Figure 2.12a). The FRET efficiency η_{FRET} depends on the distance r between donor and acceptor in an r^{-6} manner as can be seen in the following Equation 2.1.

$$\eta_{\text{FRET}} = \frac{1}{1 + \left(\frac{r}{R_0}\right)^6} \quad (2.1)$$

The Förster radius R_0 , a commonly tabulated value for FRET pairs, is the distance between donor and acceptor at which the FRET efficiency is 50%. Most R_0 values range from 1.5 to 6 nm. Consequently, FRET is most sensitive in a range between approximately 1 and 10 nm or, in other words, between $0.5R_0$ and $2R_0$ (see Figure 2.12b).^[153]

In FRET-based lipid mixing assays, liposomes are labeled with two fluorophores that constitute a FRET pair (“dequenching assays”, see Figure 2.13a). The fluorophores are

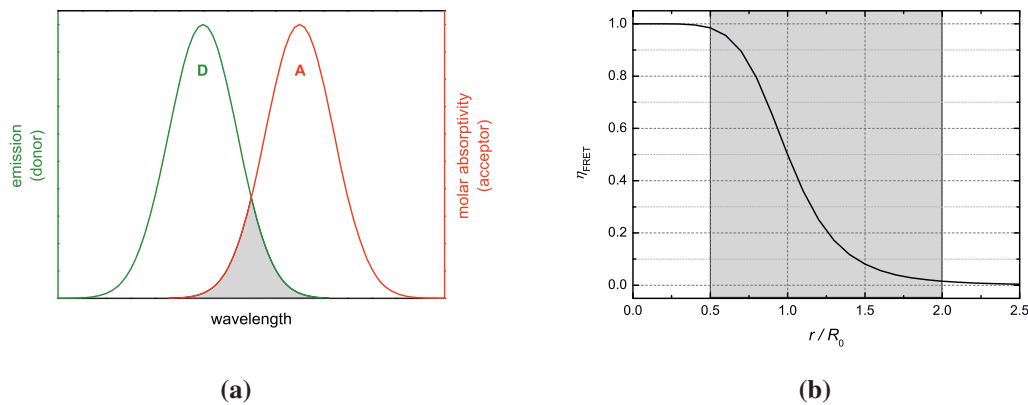


Figure 2.12. (a) For FRET to take place, the emission spectrum of the donor (D) and the absorption spectrum of the acceptor (A) need to overlap. The overlap integral (grey area) is directly proportional to the FRET rate. (b) The FRET efficiency η_{FRET} is shown as a function of the donor–acceptor distance r . Due to the r^{-6} dependence (see Equation 2.1) the sensitivity of η_{FRET} is limited to $0.5R_0$ – $2R_0$ (area shaded in grey, R_0 is the Förster radius).

attached to the lipid headgroups. The usage of various FRET pairs has been reported. Among those, for example, are 7-nitro-2-1,3-benzoxadiazole (NBD) and Lissamine Rhodamine B (Rh),^[134,151] Oregon Green 488 (OG) and Texas Red (TR),^[154] or OG and 1,1'-dioctadecyl-3,3,3',3'-tetramethylindodicarbocyanine (DiD)^[15].

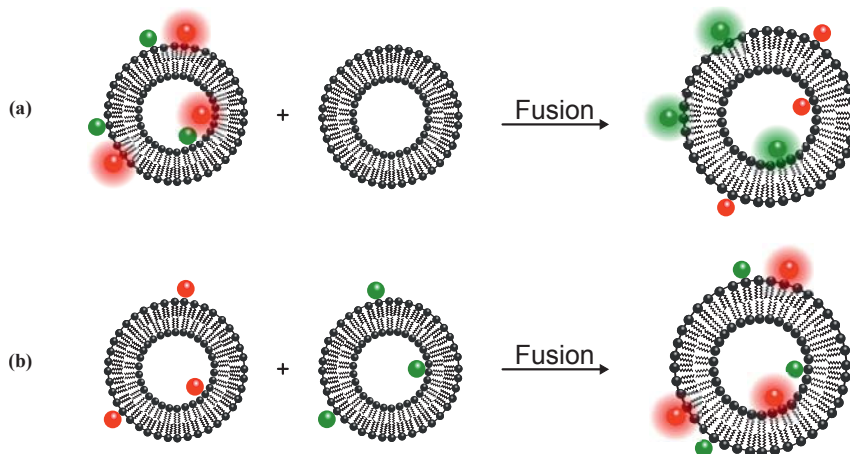


Figure 2.13. Principle of total lipid mixing (TLM) assays. Donor (green) and acceptor (red) fluorophores can either be in one liposome population ((a), dequenching assay) or in a different populations ((b), quenching assay). In both cases, the donor fluorophore is excited. Typically, the raising donor emission is recorded in a dequenching assay, whereas in a quenching assay, the increase in acceptor emission is monitored.



2. Membranes and Membrane Fusion

The sample is irradiated with light of a wavelength suitable for excitation of the donor. Due to the close distance between donor and acceptor in the liposome, efficient FRET is possible, and the acceptor emission can be detected. When the liposomes are mixed with unlabeled liposomes and fusion, *i.e.* lipid mixing, takes place, the FRET efficiency decreases due to the increased donor–acceptor distance upon dilution with unlabeled lipids. This is expressed by a decrease in the acceptor emission or, conversely, by an increase in the donor emission.

Besides labeling liposomes with a FRET pair, other types of labeling have been described for lipid mixing assays using other principles than FRET. For example, liposomes contained lipids labeled with octadecyl rhodamine B in a concentration that is high enough for self-quenching of this fluorophore.^[155] Successful lipid mixing with unlabeled liposomes increases the dye–dye distance and self-quenching is stopped, so that an increase in fluorescence was observed. Other assays made use of pyrene excimer formation between pyrene moieties that were attached to the lipid alkyl chains.^[156] Lipid mixing with unlabeled liposomes leads to an increase in the pyrene–pyrene distance and a decrease in excimer fluorescence was monitored.

Alternatively to the FRET-based dequenching assays, it is possible to label one liposome population with the donor fluorophore and the other population with the acceptor fluorophore (see Figure 2.13b). Lipid mixing is then indicated by an increase in the acceptor emission due to increasing FRET (“quenching assay”).

The mentioned assays, which are commonly known as total lipid mixing (TLM) assays, provide information on general lipid mixing. They cannot distinguish between mixing of outer and inner leaflets, thus between hemifusion and full fusion. In contrast, inner lipid mixing (ILM) assays provide information about mixing of inner leaflets (see Figure 2.14). Therefore, they are often used in combination with TLM assays. ILM assays were first described by McIntyre and Sleight who used liposomes labeled with NBD and Rh as the FRET pair fluorophores.^[28] The labeled liposomes were treated with a sodium dithionite solution. In water, the $S_2O_4^{2-}$ ion quickly decomposes to the radical ion SO_2^- which reduces NBD to the 7-amine-2,1,3-benzoxadiazol-4-yl (ABD) derivative.^[157] As dithionite does not cross intact membranes, the NBD molecules located on the inner leaflet are not affected by dithionite. ABD is non-fluorescent at the excitation wavelength typically used in the experiments. Thus, mixing of the inner leaflets can be easily monitored.

Another method to detect full liposome fusion is performing content mixing assays. The idea is to fill two liposome populations with different compounds that specifically react when they meet, thereby proving that the contents of liposomes have been ex-

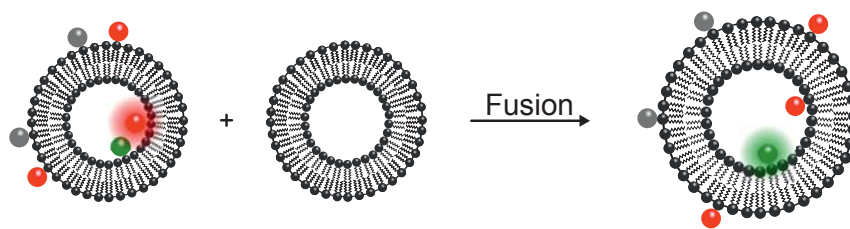


Figure 2.14. Principle of inner lipid mixing (ILM) assays. Prior to the experiment, NBD fluorophores on the outer leaflet (grey balls) are reduced and thus made non-fluorescent by dithionite. Rhodamine fluorophores (red balls) as well as NBD fluorophores on the inner leaflet (green balls) are not affected. Increase in donor fluorescence after subsequent lipid mixing with unlabeled liposomes can then be assigned to mixing of the inner leaflets.

changed. For example, TbCl_3 was included in one liposome population and dipicolinic acid molecules in the other. Upon successful content mixing, a significant increase in fluorescence can be detected arising from Tb^{3+} /dipicolinic acid complex formation.^[158] Content mixing assays based on self-quenched fluorophores have also been described. Here, a soluble fluorophore, such as calcein or sulforhodamine, is encapsulated in a high concentration into one population.^[15] Content mixing with empty liposomes leads to dilution of the fluorophores and stops self-quenching so that fluorescence can be measured. A big disadvantage of content mixing assays is that they are highly prone to leakage. This is mainly due to a mismatch in osmotic pressure, especially when soluble content markers are encapsulated in a high concentration. Leakage due to a general instability of the liposomes is problematic and falsifies the experimental outcome because it also occurs during the fusion process itself, for example near the fusion stalk.^[159] Adding external inhibitors to quench leaking markers may help to detect leakage but cannot solve the general leakage problem.^[90]

2.6.2. Fluorescence Cross-Correlation Spectroscopy

Fluorescence cross-correlation spectroscopy (FCCS), also known as dual-color fluorescence correlation spectroscopy (dual-color FCS) offers the possibility to sensitively detect molecular interactions between binding partners labeled with fluorophores. It is especially interesting for the study of liposome fusion as it allows the discrimination between docked and fused liposomes.^[160]

For this, the liposomes are labeled such that one liposome population contains the donor (“green”) dye and the other population contains the acceptor (“red”) dye. Usually, the fluorophores are covalently bound to the lipid headgroups. Two-photon excitation via an ultra fast pulsing laser can be used to excite the fluorophores. Due to these focussing

2. Membranes and Membrane Fusion

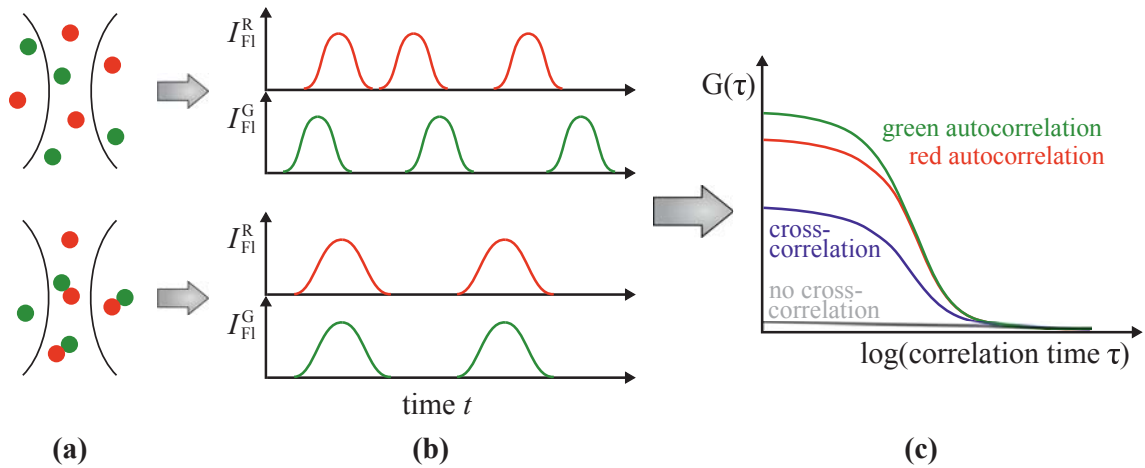


Figure 2.15. Principle of FCCS with two colors. Green- and red-labeled particles diffuse in and out of the focal volume (a) and the resulting intensity fluctuations are recorded for each channel (b). In case of no correlation, the signals appear randomly and independently in both channels (top row). If particles co-diffuse, however, the signals in both channels appear at the same time (bottom row). From the intensity fluctuations, correlation curves are calculated (c). The amplitude of the cross-correlation curves is proportional to the amount of colocalized particles. Autocorrelation curves are calculated for each channel separately.

conditions, the focal volume is very small (typically ≤ 1 fL). This allows the detection of only several particles at a time. The two dyes are excited simultaneously and detected separately. The separation of the emitted photons is accomplished via a dichroic mirror which splits the beam into a red and a green channel. Avalanche photodiode detectors collect the emitted photons of each of both channels and the intensity fluctuations arising from fluorophore-labeled particles diffusing in and out of the focal volume are statistically analyzed (see Figure 2.15).^[161] This is done by calculating autocorrelation curves from the intensity fluctuations according to the following Equation 2.2:^[162]

$$G(\tau) = \frac{\langle I_{Fl}(t) \cdot I_{Fl}(t + \tau) \rangle}{\langle I_{Fl}(t) \rangle^2} - 1 \quad (2.2)$$

Here, $I_{Fl}(t)$ describes the fluorescence intensity observed at the time t , $\langle I_{Fl}(t) \rangle$ is the mean fluorescence intensity and τ is the correlation time. The brackets denote that all products $I_{Fl}(t) \cdot I_{Fl}(t + \tau)$ are averaged. In short, autocorrelation compares a measured value of a quantity at time t with the value of the quantity at the time $t + \tau$. The autocorrelation curve is fitted with an appropriate autocorrelation function. Given that the diffusion of the liposomes is a free three-dimensional diffusion, the following equation can be used for the fit (see Equation 2.3).

$$G(\tau) = \frac{1}{N} \cdot \left(\left(1 + \frac{\tau}{\tau_D} \right) \cdot \sqrt{1 + \frac{w \cdot \tau}{\tau_D}} \right)^{-1} \quad (2.3)$$

In this equation, N is the average number of particles in the focal volume, τ is the correlation time, τ_D is the diffusion time and w is a parameter that describes the geometry of the focal volume.

In addition, the signals from both channels are cross-correlated resulting in a cross-correlation curve. The cross-correlation curve is calculated according to the following Equation 2.4:

$$G_X(\tau) = \frac{\langle I_{Fl}^G(t) \cdot I_{Fl}^R(t + \tau) \rangle}{\langle I_{Fl}^G(t) \rangle \cdot \langle I_{Fl}^R(t) \rangle} - 1 \quad (2.4)$$

In this equation, $I_{Fl}^G(t)$ and $I_{Fl}^R(t)$ are the intensities detected in the green (G) and the red (R) channel at the time t , τ is the correlation time and the brackets denote that the average is taken.

The autocorrelation curves are calculated separately and individually for each channel. In case of no correlation, *i.e.* if no binding takes place, the cross-correlation G_X is zero for all τ (see Figure 2.15c). In case the liposomes colocalize and move together, the calculation of the cross-correlation according to Equation 2.4 yields positive values for G_X . The amplitude of the cross-correlation is directly proportional to the concentration of colocalized (*i.e.* doubly labeled) particles and can maximally reach the level of the autocorrelation amplitudes. Thus, the cross-correlation provides quantitative information on the interaction of liposomes. It yields robust data on binding of molecules, regardless of their size or at which site they have been labeled.^[162]

If single photon count modules are used in the FCCS setup, it is possible to determine the fluorescence lifetime of the fluorophores. This is useful in order to examine whether FRET takes place because FRET goes along with a decrease in the fluorescence lifetime of the donor.^[160] Due to the fact that lipid mixing only takes place in case of fusion, FRET largely occurs in fused liposomes. Thus, a high amplitude in the cross-correlation together with a decrease in the donor lifetime indicates fusion whereas a high amplitude in the cross-correlation without a significant change in the lifetime indicates docking. Therefore, FCCS is a powerful technique to determine whether interacting liposomes are in the docking state or have fused.

2.6.3. Dynamic Light Scattering

With dynamic light scattering (DLS) it is possible to examine the size of particles. Therefore, DLS is a valuable technique to study the size increase of liposomes during fusion.^[150,163,164] However, DLS can not distinguish between different states of fusion or aggregation which is why further examination methods should be used in addition. An advantage of DLS is that it is not necessary to attach fluorophores to the liposomes. Thus, possible effects of the fluorophores on the fusion process can be excluded.

In a DLS experiment, the sample is irradiated with an IR laser and the scattered light is detected.^[165] The intensity of the light fluctuates due to interference of overlapping signals stemming from particles that move due to Brownian motion. Small particles move faster than large particles do, causing the signals to change more rapidly. The DLS signal analysis follows the same principle as in FCS (see Section 2.6.2): The fluctuations are quantified in an autocorrelation analysis. This analysis yields decay rates which are proportional to the diffusion coefficient. The diffusion coefficient D , in turn, is inversely proportional to the size of the particle, *i.e.* the hydrodynamic radius r_h , according to the following Stokes–Einstein relationship

$$r_h = \frac{k_B T}{6\pi\eta D}, \quad (2.5)$$

where k_B is the Boltzmann constant, T is the absolute temperature and η is the viscosity of the solvent. At a given temperature and viscosity of the solvent, the size of the particles can be determined. Note that the Stokes–Einstein relationship is only valid for spherical particles. The hydrodynamic radius includes the actual radius of the particle plus the solvent shell that surrounds particles. To convert the correlation function obtained by the autocorrelation analysis into information about the particles' sizes, special algorithms are used. In the commonly applied cumulants analysis, for example, a polynomial is used to fit the logarithm of the correlation function.^[166] The first and the second term (“cumulant”) of the equation of this fit then provide the mean size and the extent of homogeneity of the sample, respectively.

3. Design and Synthesis of the Model Peptides

In this chapter, the construction of the novel model peptides with recognition units that combine two types of PNA is illustrated. The model peptides are based on PNA/peptide hybrids that have been developed earlier.^[19] These contained aeg-PNA decamers as recognition units. This chapter illuminates how the peptides are designed (Section 3.1) and how the ala-PNA monomers that are needed for the ala-PNA recognition part are synthesized (Section 3.2). The examination of the coupling behavior of the ala-PNA monomers is described in Section 3.3. The last section delineates how the model peptides are synthesized including a description of the efforts that have been made to purify the target peptides (Section 3.4).

3.1. Principles and Rational Design of the Peptides

The SNARE mimicking model systems presented here are inspired by the SNARE proteins Syntaxin-1A, SNAP-25, and Synaptobrevin-2 that form the SNARE complex during neuronal exocytosis. To decrease the level of complexity in the model systems, the number of participating SNARE motifs is reduced from four to two. The native transmembrane domain sequences of Synaptobrevin-2 (85-116) and Syntaxin-1A (256-288), identical to those found in *Rattus norvegicus*, are chosen as membrane anchors (see Figure 3.1). Note that the chosen sequences also comprise the linker region (grey letters in Figure 3.1). For reasons of simplification, the term “transmembrane domain” will generally include both the linker and transmembrane domain region when used in this thesis. In particular, “SxTMD” is used as the abbreviation for Syntaxin-1A (256-288) and “SybTMD” is used to abbreviate Synaptobrevin-2 (85-116). The TMDs are linked to artificial recognition units, which replace the original SNARE motifs. The recognition units are made of PNA and are complementary to each other, *i.e.* they can interact specifically to form a characteristic duplex. The N-terminal domains of Syntaxin-1A are omitted.

3. Design and Synthesis of the Model Peptides

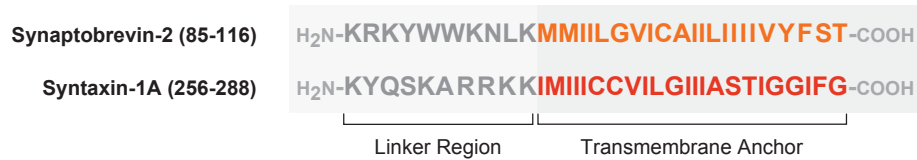


Figure 3.1. The sequences of the TMDs in the model peptides are adapted from the native sequences of the neuronal SNARE proteins Synaptobrevin-2 and Syntaxin-1A. For simplification, linker region and transmembrane anchor are summarized by the term “TMD” throughout this study.

The model peptides thus represent a shorter and much less complex structure than the native SNARE proteins. This allows studying the role of the interacting recognition units more closely. Figure 3.2 shows a schematic overview of the architecture of the model peptides which will explicitly be explained in the following.

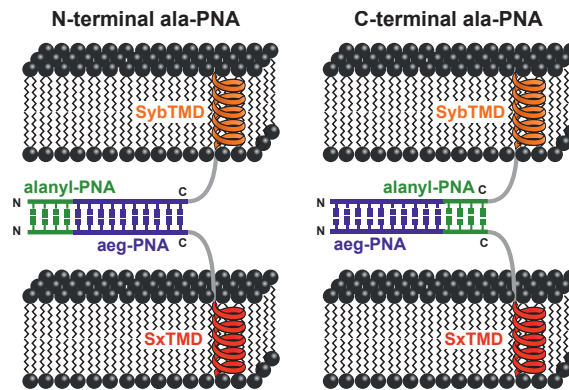


Figure 3.2. Schematic depiction of the novel SNARE model systems. An artificial recognition unit consisting of two different types of PNA (aeg-PNA, blue and alanyl-PNA, green) is attached to the native TMDs of Synaptobrevin-2 (SybTMD, orange) and Syntaxin-1A (SxTMD, red). Within the recognition unit, the alanyl-PNA part is attached either N-terminally (left) or C-terminally (right) to the aeg-PNA part.

The native transmembrane sequences are chosen in order to use a stable membrane anchor and to achieve a closer resemblance of the model peptides with their native examples. This is done since there is significant evidence that the TMDs play a key role during membrane fusion (see Section 2.4.3). SNARE mimics consisting of a lipid anchor are also commonly investigated,^[16–18] but do not allow for studying the substantial influence of the native TMDs. Two different TMDs are chosen because it has previously been shown that the use of identical TMDs leads to a significant loss in fusion activity.^[167]

The recognition unit consists of PNA. PNA offers the benefit of forming well-defined duplexes via specific nucleobase pairing. Depending on the sequence of the nucleobases, key parameters such as stability, strand orientation, and recognition are very well ad-

justable.^[24,25,168] The PNA recognition units of the model peptides used in this thesis are designed such that they form parallel duplexes. This behavior closely mimics the native system as the SNARE motifs are likewise known to assemble in parallel.^[79] On top of that, model peptides bearing the parallel orientation of the PNA duplexes turned out to be more fusogenic than model peptides with recognition units that form the duplex in an antiparallel way.^[167] Two different types of PNA are chosen for the recognition unit: aeg-PNA and ala-PNA. aeg-PNA consists of an *N*-(2-aminoethyl)glycine backbone to which the nucleobases are attached via methylene carbonyl linkages.^[24] The second part of the recognition unit comprises alanyl-PNA (ala-PNA).^[26,169] Each ala-PNA monomer consists of a backbone based on the amino acid alanine to which a nucleobase is attached via the alanyl side chain. Both types of PNA show different duplex formation rates resulting from different topologies of ala-PNA and aeg-PNA. While complementary strands of aeg-PNA form a helical duplex, a duplex of ala-PNA strands is linear. This becomes obvious when looking at the structure of both PNA types and focusing on the different backbones (see Figure 3.3).

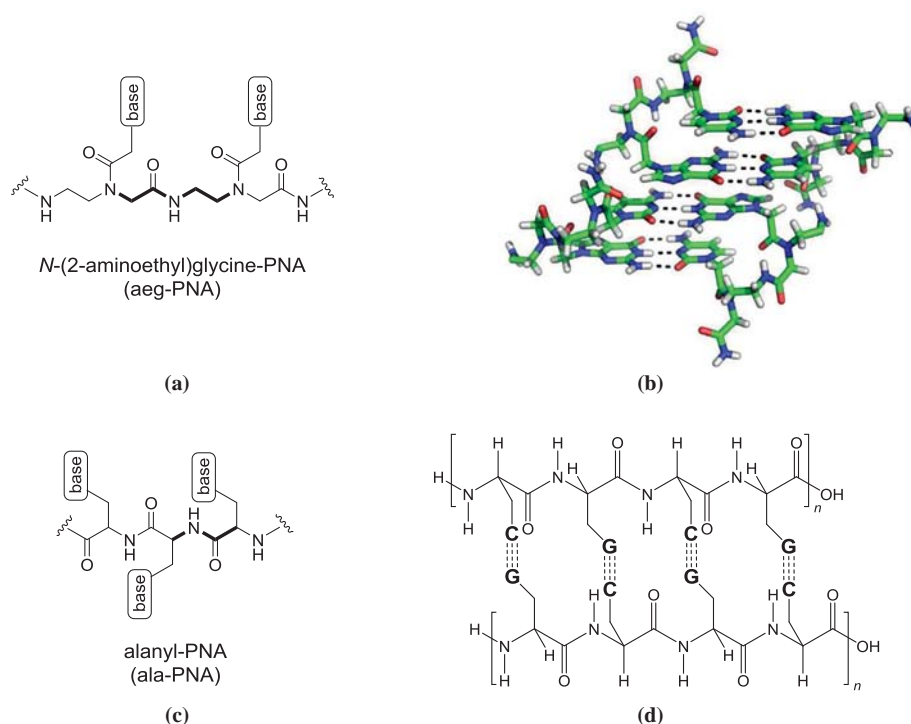


Figure 3.3. Structures of aeg-PNA and ala-PNA in comparison. Left: Structural formulae with highlighted backbone of aeg-PNA (a) and ala-PNA (c). Right: 3D view of the helical aeg-PNA (b) and the linear ala-PNA duplex (d). The different topology is a result of the different backbone structures. Figure 3.3b is reprinted by permission from Macmillan Publishers Ltd: NATURE NANOTECHNOLOGY (Ref. [170]), copyright (2015).



3. Design and Synthesis of the Model Peptides

In aeg-PNA strands, each repetition unit contributes six bonds to the backbone, meaning that the nucleobases are six backbone bonds apart from each other. Contrarily, in ala-PNA, each repetition unit contributes three bonds to the backbone, so the nucleobases are only three backbone bonds apart from each other. This is reflected in the measured nucleobase–nucleobase distances: In an ala-PNA strand, the distance between two nucleobases is around 3.6 Å, which is close to the ideal distance of 3.4 Å yielding the strongest possible interaction between two nucleobases.^[171] Thus, a linear topology of the duplex results as conformational changes in the backbone do not lead to a more stable configuration.^[169,172] In contrast, the distance of the nucleobases in aeg-PNA would be 8.3 Å in case of a linear duplex,^[173] so aeg-PNA duplexes show a helical structure in order to maximize nucleobase pair interactions. The linear topology of ala-PNA causes a sterical rigidity, due to which the duplex formation of ala-PNA is kinetically hindered. For example, an incubation period of 3 h at 0 °C was necessary for ala-PNA oligomers to reach duplex formation.^[174,175] In contrast, aeg-PNA duplexes form spontaneously at ambient temperature.^[25] By combining both PNA types in one recognition unit, a directed duplex formation is intended starting with the fast duplex formation of the aeg-PNA part, followed by the slower duplex formation of the ala-PNA part. According to the zipper hypothesis, there is a direction in the formation of the SNARE complex as well. The model systems presented here thus aim at mimicking the zippering of the SNARE motifs, a process that is assumed to start N-terminally and to then proceed towards the C-termini of the interacting units (see Section 2.4.3 for details). The aeg-PNA decamers PNA1 and PNA3 are used, which have originally been designed by Wittung *et al.*^[25] They are non-self complementary strands, which form stable duplexes ($T_m = 45.5$ °C^[25]) in a parallel fashion featuring Watson–Crick base pairing. The alanyl-PNA part of the recognition unit is made of a tetramer of alternating guanine and cytosine building blocks. In order to achieve a parallel orientation of complementary alanyl-PNA strands, the configuration of the chiral alanyl-PNA monomers in a single strand needs to be altered. On top of that, opposite nucleobases in the duplex need to have a different configuration to achieve a Watson–Crick base pairing mode.^[169] Therefore, the ala-PNA building blocks Fmoc-D-AlaG-OH and Fmoc-L-AlaC(Z)-OH are applied (see Sections 3.2–3.4). In the preceding master thesis,^[176] various aeg-PNA/ala-PNA hybrid oligomers were tested to examine their behavior in complex formation and to identify suitable candidates for the recognition units of the SNARE model peptides. Ultraviolet absorption (UV) melting curve analyses confirmed a duplex formation that was independent of an incubation period at 0 °C. Circular dichroism spectroscopy showed that both PNA parts contribute to the du-

plex formation. Thus, the sequences depicted in Figure 3.4a are chosen as recognition units, in which an alanyl-PNA tetramer is attached either N-terminally or C-terminally to a decameric aeg-PNA sequence.

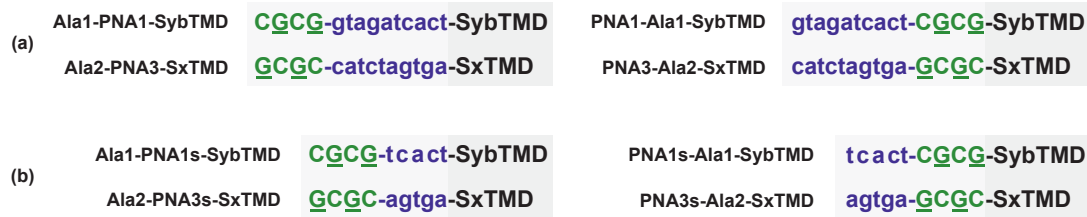


Figure 3.4. The sequences of the PNA hybrid recognition units consist of an aeg-PNA part (blue) and an ala-PNA part (green). (a) First generation of model peptides with a decameric aeg-PNA sequence; (b) second generation of model peptides with a pentameric aeg-PNA sequence; D-configured monomers are underlined.

During the course of this work it was found that PNA/peptide hybrids with an aeg-PNA recognition unit comprising five monomers are capable of liposome fusion as well. They even show a higher fusion efficiency than their analogues with ten monomers (see Section 4.3.3 for a detailed description). It was thus decided to study the fusion behavior particularly based on these shortened analogues. This implies a huge simplification concerning the synthesis of the PNA/peptide hybrids resulting in a greater purity of the peptides which makes the shorter versions even more attractive (see Section 3.4). Consequently, shorter recognition units made of the aeg-PNA pentamers PNA1s and PNA3s are used in addition to the recognition units of the first generation presented in Figure 3.4a (see Figure 3.4b). Those comprise the C-terminal half (*i.e.* the first five monomers starting from the C-terminus, s = short) of PNA1 and PNA3, respectively.

In the full-length SNARE model peptides, each PNA hybrid recognition unit is then attached to the N-terminus of the respective TMD sequence via its C-terminus. Following the design reported by Lygina *et al.*,^[19] recognition units containing PNA1 are attached to the TMD of Synaptobrevin-2 and those containing PNA3 are linked to the TMD of Syntaxin-1A.

The synthesis of the SNARE model peptides is carried out in three steps and is described detailedly in the following sections. First, the ala-PNA building blocks are synthesized as described in Section 3.2. The aeg-PNA monomers are commercially available and are used as received. Next, the transmembrane domains are synthesized and in the end, the PNA monomers are attached to the TMDs as described in Section 3.4. This is done in a continuous fashion, so the monomers are coupled in the respective order to the TMDs on resin.

3.2. Synthesis of Alanyl-PNA Monomers

A defined stereochemistry of the monomers is required to achieve the desired mode of duplex formation in the ala-PNA part of the recognition units. To this end, two different ala-PNA building blocks were synthesized in a parallel synthesis route. The first route starts from Boc-L-serine and yields Fmoc-L-AlaC(Z)-OH (**3**), whereas the second route starts from the enantiomeric Boc-D-serine and yields Fmoc-D-AlaG-OH (**6**). As the main part of the monomer synthesis has already been described in detail in the preceding master thesis,^[176] the following section focuses on the improvements and changes that have been made during this thesis.

The first step was the conversion of the respective Boc-serine into the Boc-serine β -lactone **1** or *ent*-**1** via a Mitsunobu-like reaction (see Figure 3.5).^[177,178]

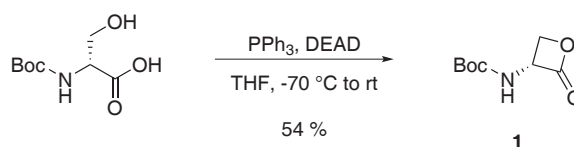


Figure 3.5. The first step in the synthesis of the alanyl-PNA building blocks. Boc-L-serine β -lactone (*ent*-**1**) was obtained analogously in 35 % yield; PPh₃ = triphenylphosphine, DEAD = diethyl azodicarboxylate, THF = tetrahydrofuran, rt = room temperature.

In the next step, the β -lactones were converted into the Boc-protected alanyl nucleobase amino acids through a nucleophilic attack of the respective nucleobase (see Figure 3.6).^[26] Cytosine needs to be applied as the protected *N*4-Z-cytosine (Z = benzyl oxycarbonyl protection group). The protection at the reactive exocyclic NH₂ site of cytosine can be achieved via a reaction of deprotonated cytosine and benzyl chloroformate.^[179] The Z-protecting group is not removed until the final cleavage of the complete peptide from the resin. This prevents complications in the subsequent solid-phase peptide synthesis. In place of the guanine nucleobase, the guanine precursor 2-amino-6-chloropurine was used because pure guanine is too unreactive in the β -lactone ring opening step.^[26]

In the reaction of Boc-L-AlaC(Z)-OH (**2**), *N*4-Z-cytosine was applied in 1.5-fold excess. When non-reacted *N*4-Z-cytosine was removed prior to purification via flash column chromatography, the amount of purified product could significantly be increased. Nevertheless, a maximum yield of 85 % could only be obtained when column chromatography was performed twice instead of once. The yield in the synthesis of Boc-D-AlaG-OH (**4**) was always lower. This is mainly due to the fact that the nucleophilic attack of the guanine precursor does not only proceed via the N9 atom, though this is the preferred site,

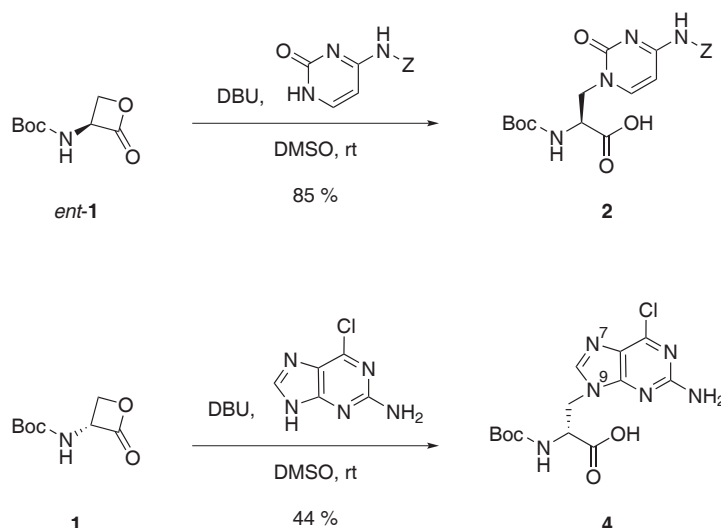


Figure 3.6. Nucleophilic addition of the respective nucleobases to the Boc-serine β -lactones *ent-1* and **1** yields the Boc-protected alanyl nucleo amino acids **2** and **4**, respectively. The positions of the N9 and N7 atom in the guanine ring are labeled; DBU = 1,8-diazabicyclo[5.4.0]undec-7-ene, DMSO = dimethylsulfoxide, Z = carboxybenzyl protection group.

but also via the N7 atom.^[180] The positions of the N7 and the N9 atom in the guanine ring are marked in Figure 3.6. It is very important to separate these species during purification as the N7-alkylated product would not lead to the desired duplex structure when interacting with the complementary sequence after being incorporated into the recognition unit. NMR helps to distinguish between both species, as a heteronuclear multiple bond correlation (HMBC) spectrum makes an assignment of the different couplings between methylene protons and C4/C5 of the guanine ring possible.^[176] In addition, the retention time of the N7 species on unmodified silica gel is slightly higher than that of the N9 species so a categorization about the N9 or N7 product could be made on the basis of the spots in thin layer chromatography (TLC). To verify this, a fraction that had been classified as an N7/N9 mixture on the basis of TLC spot monitoring was analyzed via HPLC and compared to a fraction that was supposed to contain the pure N9 product. Small amounts of both fractions were converted with enantiomerically pure Boc-L-Ala-OSu to the respective dipeptides to increase the structural difference and to achieve distinguishable retention times (see Figure 3.7).

The chromatograms show a major peak assignable to the dipeptide of the N9 species; the minor peak belonging to the dipeptide of the N7 species has a slightly higher retention time. Comparing the peak integrals yielded an N9:N7 ratio of roughly 10:1 in the case of the mixed fraction and a ratio of 100:1 in the case of the pure N9 fraction. Thus, the

3. Design and Synthesis of the Model Peptides

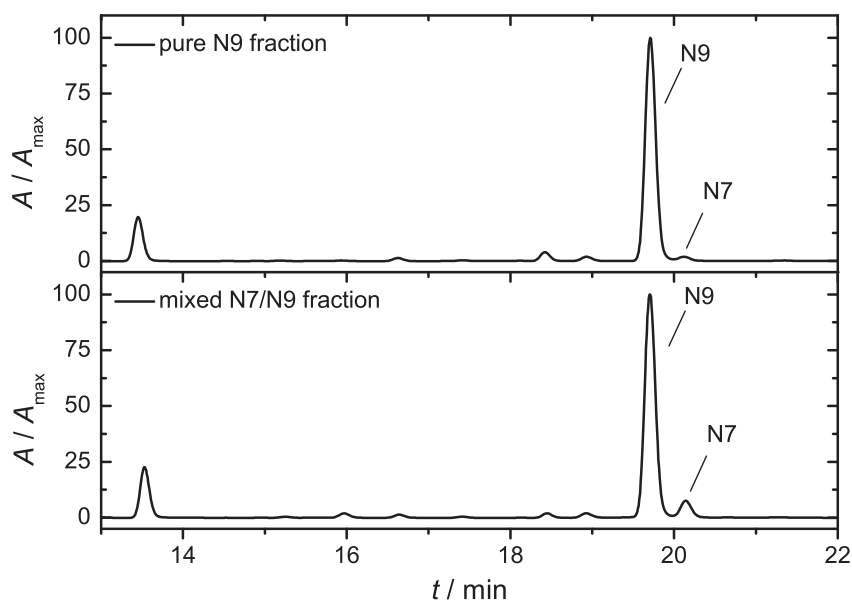


Figure 3.7. HPLC chromatograms of Boc-Ala-D-AlaG-OH dipeptides to analyze the amount of N7 by-products in the synthesis of **4**. Top: pure N9 fraction, bottom: mixed N7/N9 fraction. The absorption was recorded at 254 nm.

amount of the N7 species is less than 1 % in the pure N9 fraction and TLC can be used as a convenient and reliable method to evaluate the purity of the fractions.

In order to ensure that the conversion into the Boc-protected alanyl nucleo amino acids proceeded enantioselectively, the enantiomeric excess (ee) of each compound was determined. For this, a small portion of the compound was reacted with stereochemically pure Boc-L-Ala-OSu, and the ratio of the generated diastereomers was analyzed via HPLC. Figure A.1 in the appendix shows the resulting chromatograms. Values of $ee \geq 99\%$ and $ee \geq 96\%$ were obtained for Boc-L-AlaC(Z)-OH (**2**) and Boc-D-Ala(2-amino-6-chloropurin-9-yl)-OH (**4**), respectively, indicating a highly enantioselective nucleophilic addition in this step.

In the next step, the Boc-protected alanyl nucleo amino acids were converted into their Fmoc-protected analogues in order to be compatible with the subsequent Fmoc-based SPPS of the PNA/peptide hybrids (see Figure 3.8).

Therefore, the Boc protecting group was removed under acidic conditions. Boc-L-AlaC(Z)-OH (**2**) was deprotected quantitatively as confirmed by electrospray ionization mass spectrometry (ESI-MS). In case of the guanine variant, treatment with acid was extended to a reaction time of 48 h as the oxidation from Ala-(2-amino-6-chloro-9H-purin-9-yl)-OH to Ala-(2-amino-6-oxo-1,6-dihydro-9H-purin-9-yl)-OH had to take place in addition. Here, complete conversion was confirmed with ESI-MS as well. This step

3.3. Coupling Behavior of the Alanyl-PNA Monomers

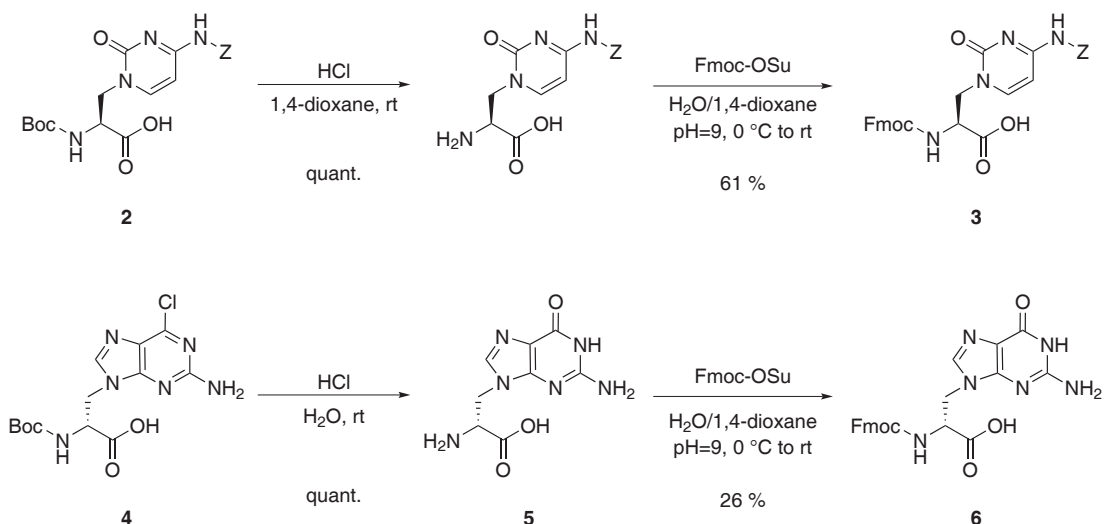


Figure 3.8. In the last two steps of monomer synthesis the amino protection groups are exchanged from Boc to Fmoc. At the same time, the guanine precursor is converted into the guanine nucleobase yielding Fmoc-alanyl amino acids **3** and **6**.

was also very well possible using an aqueous HCl solution, which has the additional advantage of directly generating the reactive hydrochloric salt of the building block. In contrast to the use of trifluoroacetic acid (TFA), due to which the resulting unreactive TFA salt has to be converted into the HCl salt by repeated treatment with HCl, this represents a reasonable and time-saving alternative.

The last step in the synthesis of the ala-PNA monomers was the attachment of the Fmoc protecting group.^[181] Here, the same conditions could be employed for both types of alanyl nucleo amino acids. Fmoc-OSu was applied in 0.89 equivalents in order to suppress the undesired side reaction with unprotected amino functionalities of the nucleobases. The enantiomeric purity of the purified products was tested with the procedure described above. The ee was always $\geq 99\%$ for Fmoc-L-AlaC(Z)-OH (**3**) and $\geq 93\%$ for Fmoc-D-AlaG-OH (**6**) showing that the stereochemical information was retained (see Figure A.1 in the appendix).

3.3. Coupling Behavior of the Alanyl-PNA Monomers

To ensure well-defined coupling in the synthesis of the model peptides, the prepared alanyl nucleo amino acids were tested as described in the following. It was checked whether the enantiomeric purity of the alanyl-PNA building blocks is maintained during coupling to a peptide sequence. For this, a test tripeptide was synthesized. As an exam-



3. Design and Synthesis of the Model Peptides

ple, Fmoc-D-AlaG-OH (**6**) was reacted under the normal coupling conditions with a Wang resin preloaded with Gly. After that, Boc-L-Ala-OSu was attached as well, so that the following tripeptide resulted: Boc-L-Ala-D-AlaG-Gly-OH. The test peptide was analyzed with HPLC. The chromatogram showed one main peak, indicating that the configuration of Fmoc-D-AlaG-OH barely changes during coupling (see Figure A.2a in the appendix).

In further test reactions, the alanyl nucleo amino acids were coupled to the transmembrane domain of either Syntaxin-1A or Synaptobrevin-2, employing the conditions that are necessary for the synthesis of the PNA/peptide hybrids later on. Coupling of Fmoc-L-AlaC(Z)-OH always produced the desired product in a high yield and the peptide educt could not be detected with ESI-MS anymore. Some Fmoc-D-AlaG-OH samples showed a very low reactivity in the coupling step as high amounts of the peptide educt were detected with ESI-MS. There were no detectable differences in the NMR spectra or HPLC chromatograms compared to those Fmoc-D-AlaG-OH samples that showed a high reactivity in the coupling reaction. Different parameters were changed in order to find a reason for the high variance in the reactivity among the sample batches.

The first hypothesis was that possible impurities not observable in NMR prevented the building block from proper coupling. Therefore, the building block was purified applying HPLC. However, the coupling efficacy could not be improved. The same is true for an Fmoc-D-AlaG-OH sample that was lyophilized after flash column chromatography purification. The coupling time was shortened from 2 h to down to 45 min in order to prevent possible detachment or any other detrimental side reactions during elongated coupling periods. However, the amount of desired product was not increased in this case either. Measures such as raising the equivalents of the activator HATU (4.9 eq instead of 4.5 eq) or of the building block (7.6 eq instead of 5.0 eq), changing the coupling solvent (DMSO instead of NMP) or the cleavage mixture, likewise did not lead to an improvement in the reactivity. Changing the entire activator system from HATU/HOAt to PyBOP resulted in a slightly higher yield, but still a lot of educt was present. The low reactivity of these Fmoc-D-AlaG-OH samples was independent of the transmembrane used (SxTMD or SybTMD). To exclude any possible interactions with the N-terminal lysine of the TMD, an additional glycine was introduced serving as a spacer between the TMD and the first alanyl-PNA building block. However, an improvement in the reactivity resulting in a higher amount of the product peptide was not detected. Coupling ala-PNA was also performed with microwave irradiation. Here, successful coupling of the alanyl nucleo amino acids was achieved within 2 x 3 min reaction time. However, with progressing attachment of monomers, the formation of side products increased more pronouncedly

than without microwave irradiation being employed. This method can thus be useful for attaching the first monomer to the peptide chain, but further monomers should be coupled at room temperature for the sake of the peptide's purity. It should be noted that microwave irradiation did not improve the coupling efficiency of those Fmoc-D-AlaG-OH samples that did not react at room temperature.

All in all, the different reactivities for different batches of Fmoc-D-AlaG-OH in the coupling reaction cannot be attributed to specific impurities in the sample or be overcome by changing the reaction conditions. In the end, only those batches of Fmoc-D-AlaG-OH building blocks were used for the synthesis of the PNA/peptide hybrids that showed a high reactivity in the coupling reaction.

3.4. Synthesis of PNA/Peptide Hybrid Sequences

The native transmembrane sequences of Syntaxin-1A and Synaptobrevin-2 were synthesized automatically on a peptide synthesizer by employing solid-phase peptide synthesis (SPPS). The resin was a Wang-type resin to generate the native carboxy functionalized C-terminus. It has a low loading density to prevent pronounced aggregation of the growing peptide chains. Standard Fmoc-chemistry was used with *N,N'*-diisopropylcarbodiimide (DIC) and ethyl cyanohydroxyiminoacetate (Oxyma) as activator and activator base, respectively. Due to these efficient coupling reagents and an elevated temperature of 90 °C provided by microwave irradiation, it took less than 6 hours for each TMD to be completely assembled (see Section 6.5.3 for synthetic details). According to ESI-MS, the reactions proceeded without considerable formation of deletion sequences or by-products.

For the coupling of the PNA monomers Fmoc-chemistry was employed as well. In principle, SPPS of PNA building blocks follows the same rules as SPPS of amino acid building blocks. However, a few adaptations are needed for successful coupling. In Figure 3.9 the PNA-SPPS cycle is shown using the example of coupling ala-PNA.

The resin containing the respective transmembrane domain was swollen for at least 2 h in NMP to allow for proper expansion of the resin beads and the long peptide chains, followed by deprotection of the N-terminal Fmoc group with piperidine (20 % in NMP). aeg-PNA monomers were coupled for 2 x 1 h; for ala-PNA monomers the coupling time was elongated to 2 x 2 h. Following a protocol described by Casale *et al.*,^[182] 1-hydroxy-7-azabenzotriazole (HOAt) and 1-(bis(dimethylamino)methylene)-1*H*-1,2,3-triazolo[4,5-*b*]pyridinium 3-oxide hexafluorophosphate (HATU) were used as activators together with a mixture of *N,N*-diisopropylethylamine (DIPEA) and 2,6-lutidine as ac-

3. Design and Synthesis of the Model Peptides

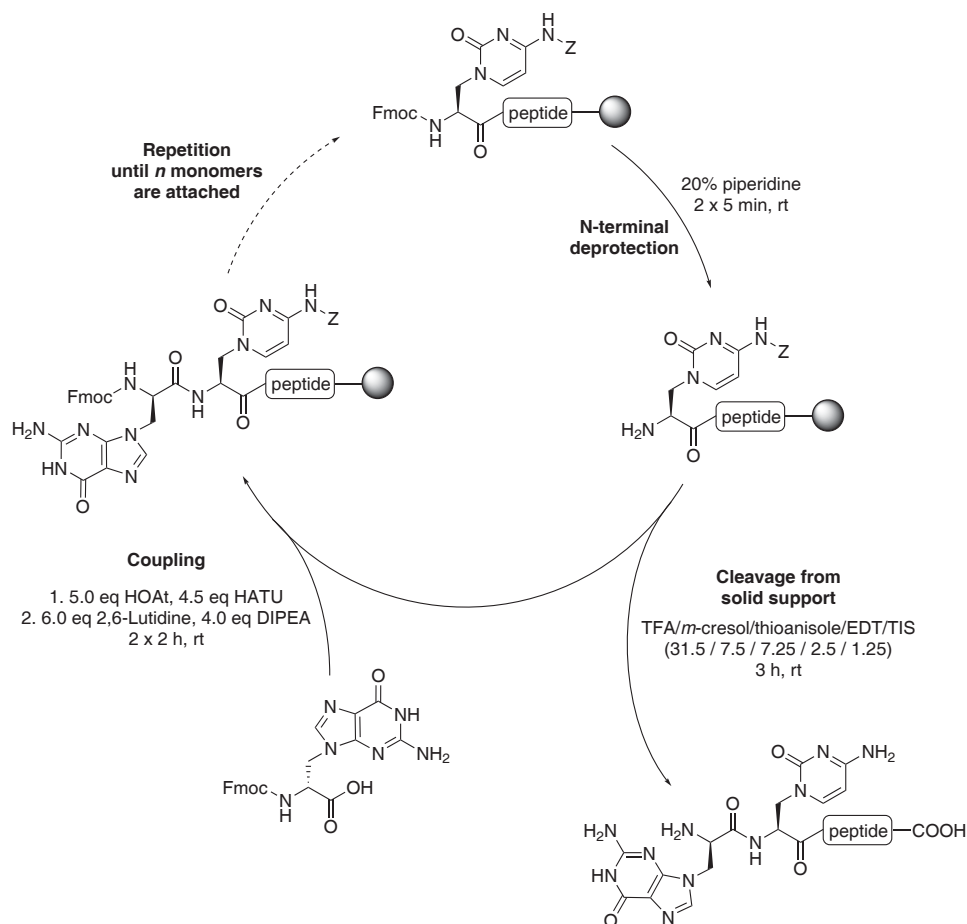


Figure 3.9. The cycle of PNA-SPPS using the example of coupling ala-PNA monomers to the peptide sequence on resin (grey spheres). A cycle started with the removal of the N-terminal Fmoc protection group under basic conditions (“deprotection”), followed by the attachment of the next building block (“coupling”). The building block was applied as an active ester. To generate the active ester, the building block was pretreated with activators (HATU and HOAt) and activator bases (DIPEA and 2,6-lutidine). Capping was omitted during ala-PNA coupling but was commonly performed after the aeg-PNA coupling step using acetic anhydride to acetylate non-reacted otherwise free amino groups at the N-terminus. The cycle was repeated until the target sequence was assembled. Then, a final deprotection step took place and the peptide was separated from the solid support under strongly acidic conditions (“cleavage”).

tivator bases. HATU was applied as 0.9 equivalents with regard to the monomer. This was done in order to avoid tetramethyl guanidine capping due to HATU directly reacting with the free N-terminal amino group. When aeg-PNA was coupled, a capping step was performed after the second coupling step. It was followed by the recommended thorough washing step with 5 % DIPEA in order to deprotect possibly temporarily acetylated nucleobase amines. When coupling the ala-PNA part, only those Fmoc-D-AlaG-OH building



3.4. Synthesis of PNA/Peptide Hybrid Sequences

blocks with a high reactivity in the prior test reaction were used (see Section 3.3). Also, the capping step was omitted to prevent acetylation with non-protected exocyclic amino groups. The coupling cycle was repeated until the desired sequence was reached.

Assembling the PNA recognition unit unfortunately produced a multitude of side products that increased notably after the attachment of the sixth aeg-PNA building block and during the attachment of the ala-PNA monomers. The crude peptides were detectable via ESI-MS but the amount of side products was high, especially when the recognition unit contained the additional ala-PNA part. In particular, it was difficult to obtain the SybTMD-based analogues in a satisfying quality. This is probably due to aggregation processes among the growing PNA/peptide chains. To improve the quality of the PNA/peptide hybrids, several measures were taken. For example, the resin was changed to a hydrophilic polyethylene glycol (PEG) based resin. Compared with the hydrophobic cross-linked polystyrene beads of the commonly used Wang resin, the PEG-based resin is known to diminish or even prevent aggregation.^[183] The loading density of the PEG-based resin was set to a very low value (0.1–0.2 mmol/g) to further minimize interactions among the hydrophobic chains. Also, the addition of chaotropic salts such as KSCN and LiCl prior to each coupling step was tested. However, the mentioned measures against possible aggregation only slightly increased the yield of the desired products.

The synthesis of the recognition unit was also tested using microwave irradiation. By applying microwave irradiation, the reaction time for each coupling step can be reduced, so the overall time for synthesis of the PNA/peptide hybrids would be significantly shortened. The best conditions for aeg-PNA coupling were achieved with a double coupling of the monomer using the same reagents as described above for the manual coupling at room temperature. However, the ESI mass spectrum of the target peptide showed a larger amount of side products than the spectrum for the conventionally coupled peptide. The same was true for coupling ala-PNA monomers, which has been described in the previous section (see Section 3.3). In the end, all PNA/peptide hybrids were coupled using manual SPPS at room temperature as this procedure yielded the most reliable results. Their successful synthesis was confirmed by ESI-MS. The amount of impurities, however, was high. In Section 6.5.7, ESI mass spectra for selected target peptides are shown. The model peptides of the first generation containing a decameric aeg-PNA sequence are listed in Table 3.1.

Model peptides of the second generation contain a pentameric aeg-PNA sequence attached to the tetrameric ala-PNA stretch. The purity of the resulting PNA/peptide hybrids as estimated from ESI mass spectra is remarkably higher than that of the model peptides of

3. Design and Synthesis of the Model Peptides

Table 3.1. PNA/peptide hybrids of the first generation, which exhibit a decameric aeg-PNA sequence and a tetrameric ala-PNA sequence in the recognition units. Ala-PNA building blocks and amino acids are denoted in capital letters, and aeg-PNA building blocks in small letters; D-configured units are underlined.

Peptide	Sequence
PNA3-SxTMD PNA1-SybTMD	catctagtga-KYQSKARRKKIMIII CCVILGIII ASTIGGIFG-OH (7) gtagatcact-KRKYWWKNL KMMIILGVICAILLIII VYFST-OH (8)
Ala2-PNA3-SxTMD Ala1-PNA1-SybTMD	<u>GCGC</u> -catctagtga-KYQSKARRKKIMIII CCVILGIII ASTIGGIFG-OH (9) <u>CGCG</u> -gtagatcact-KRKYWWKNL KMMIILGVICAILLIII VYFST-OH (10)
Ala2-SxTMD Ala1-SybTMD	<u>GCGC</u> -KYQSKARRKKIMIII CCVILGIII ASTIGGIFG-OH (11) <u>CGCG</u> -KRKYWWKNL KMMIILGVICAILLIII VYFST-OH (12)
PNA3-Ala2-SxTMD PNA1-Ala1-SybTMD	catctagtga- <u>GCGC</u> -KYQSKARRKKIMIII CCVILGIII ASTIGGIFG-OH (13) gtagatcact- <u>CGCG</u> -KRKYWWKNL KMMIILGVICAILLIII VYFST-OH (14)

the first generation. The synthesis proceeded with fewer by-products because the deletion sequences especially occurred during synthesis of the second half of the aeg-PNA unit. Still, the attachment of the four ala-PNA monomers did not proceed quantitatively in each step. The overall purity of the target PNA/peptide hybrids, however, was enhanced considerably (see ESI mass spectra in Section 6.5.7).

The following Table 3.2 provides an overview of all synthesized PNA/peptide hybrids of the second generation relevant for the work described in this thesis.

Cleavage from the resin was achieved with various TFA containing mixtures depending on the type of the sequence (see Section 6.5.5 for details). For example, it was important to include *m*-cresol when aeg-PNA building blocks were present in order to scavenge the highly reactive benzhydryl cation originating from the benzhydryloxycarbonyl (Bhoc) protection groups.^[182]

Purification of the synthesized PNA/peptide hybrids turned out to be challenging. HPLC was applied as the method of choice since it provides a convenient and easily adjustable method for purification. Various parameters such as different column materials, different solvent mixtures, temperatures, and gradient programs were tested for both SxTMD- and SybTMD-based peptides (see Table 6.3 in Section 6.5.6 for details). Among them was the use of reversed phase (RP)-C18, RP-C8 and RP-C4 columns with pore sizes between 100 Å and 300 Å. Besides the solvents methanol (MeOH) and acetonitrile (MeCN), a solvent mixture composed of formic acid, 1-propanol, and trifluoroethanol (TFE) recently proposed by Hara *et al.*^[184] was tested as well. The authors emphasized the beneficial addition of TFE which significantly improved the separation of transmembrane peptides

Table 3.2. PNA/peptide hybrids of the second generation, in which—compared to the first generation—the decameric aeg-PNA sequence is replaced by a pentameric sequence. Ala-PNA building blocks and amino acids are denoted in capital letters, and aeg-PNA building blocks in small letters; D-configured units are underlined.

Peptide	Sequence
PNA3s-SxTMD	agtga-KYQSKARRKKIMIII CCVILGIII ASTIGGIFG-OH (15)
PNA1s-SybTMD	tcact-KRKYWWK NLKMMIILGVICAILLIIII VYFST-OH (16)
PNA1s-SxTMD	tcact-KRKYWWK NLKMMIILGVICAILLIIII VYFST-OH (17)
PNA3s-SxTMD-NH ₂	agtga-KYQSKARRKKIMIII CCVILGIII ASTIGGIFG-NH ₂ (18)
PNA1s-SybTMD-NH ₂	tcact-KRKYWWK NLKMMIILGVICAILLIIII VYFST-NH ₂ (19)
Ala2-SxTMD	<u>GCGC</u> -KYQSKARRKKIMIII CCVILGIII ASTIGGIFG-OH (11)
Ala1-SybTMD	<u>CGCG</u> -KRKYWWK NLKMMIILGVICAILLIIII VYFST-OH (12)
Ala1-SxTMD	<u>CGCG</u> -KYQSKARRKKIMIII CCVILGIII ASTIGGIFG-OH (20)
Ala2-PNA3s-SxTMD	<u>GCGC</u> -agtga-KYQSKARRKKIMIII CCVILGIII ASTIGGIFG-OH (21)
Ala1-PNA1s-SybTMD	<u>CGCG</u> -tcact-KRKYWWK NLKMMIILGVICAILLIIII VYFST-OH (22)
Ala1-PNA1s-SxTMD	<u>CGCG</u> -tcact-KYQSKARRKKIMIII CCVILGIII ASTIGGIFG-OH (23)
PNA3s-Ala2-SxTMD	agtga- <u>GCGC</u> -KYQSKARRKKIMIII CCVILGIII ASTIGGIFG-OH (24)
PNA1s-Ala1-SybTMD	tcact- <u>CGCG</u> -KRKYWWK NLKMMIILGVICAILLIIII VYFST-OH (25)
PNA1s-Ala1-SxTMD	tcact- <u>CGCG</u> -KYQSKARRKKIMIII CCVILGIII ASTIGGIFG-OH (26)

that are typically difficult to purify. In addition, HPLC was performed at elevated temperatures which generally favors the de-aggregation of aggregated species. None of the applied conditions, however, led to a satisfying purification in terms of sharp and separable peaks in the chromatogram. To give an impression of how the best obtainable peak resolution looks like, one of the chromatograms with the best resolved peaks obtained from Ala1-PNA1-SybTMD (10) is shown in Figure A.2b in the appendix. Likely, the PNA/peptide hybrids tend to aggregate due to the highly hydrophobic transmembrane domain. At the same time, they have a rather hydrophilic recognition unit due to which HPLC methods specially designed for hydrophobic sequences failed. In addition, the peptides tend to stick to the column material which was identifiable when subsequent runs were performed on an RP-C4 column without injecting the peptide sample again. Even after three of these “blank” runs, the resulting chromatograms were remarkably similar to the original peptide chromatogram (data not shown).

Therefore, size exclusion chromatography (SEC) was used as an alternative strategy. A Superose column, which has a matrix of cross-linked agarose, was applied. For this column, aqueous conditions are required. In order to make the peptides soluble, a phosphate buffer containing 2% sodium dodecylsulfate (SDS) was used. SDS was found to be the

3. Design and Synthesis of the Model Peptides

only detergent that dissolves the PNA/peptide hybrids to a satisfying extent. Figure 3.10 shows the chromatogram that was obtained after SEC of a raw sample of PNA3-Ala2-SxTMD (**13**).

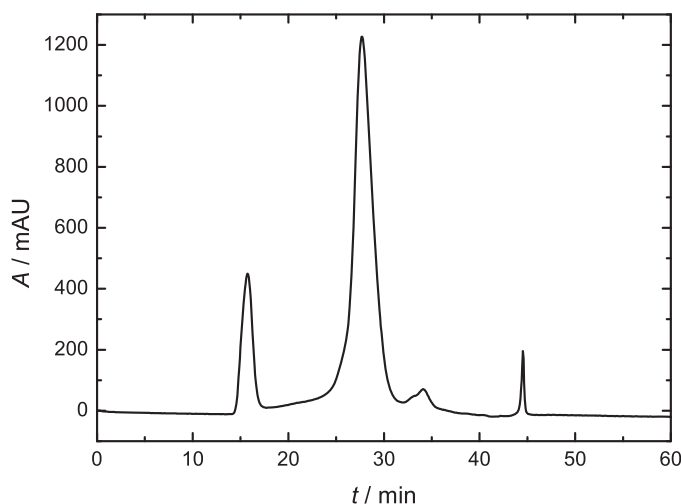


Figure 3.10. Chromatogram of the raw peptide **13** obtained from SEC in phosphate buffer containing 2% SDS. The absorption was recorded at 254 nm.

Considering the high amount of deletion sequences with a mass around 3000 Da that had occurred during the synthesis of **13** (see Section 6.5.7 for an ESI mass spectrum of the raw peptide) and the fact that the desired peptide has a mass around 7000 Da, the shown chromatogram gives a first hint that a separation of these two groups of species can be possible. The peaks are still rather broad, but compared with those in the best chromatograms obtained from **10** on an HPLC RP-C4 column they are sharper and more defined. It is important to note that the interpretation of the SEC chromatogram was made only on the basis of the ESI mass spectra of the raw peptide as it was not possible to further analyze the peaks. For a proper analysis of the peaks via ESI-MS, it was necessary to remove the salts from the buffer beforehand. This was accomplished following the protocol of the chloroform/methanol/water extraction by Puchades *et al.*^[185] However, it was impossible to detect the peptides in the ESI mass spectrum afterwards. It is likely that due to their bad solubility the peptides are removed together with SDS instead of staying in aqueous solution. In addition, CHAPS was tested as a detergent, which can more easily be removed than SDS due to its high critical micelle concentration. Unfortunately, the peptides were only to a very little extent soluble in buffer containing CHAPS. As an alternative, a phosphate buffer with addition of MeCN (30%) was used, in which the peptides were tolerably soluble and which is the highest organic solvent content that is compatible with the SEC column. However, the peak resolution in the chromatogram

3.4. Synthesis of PNA/Peptide Hybrid Sequences

was not as good as with the use of SDS buffer and on top of that it was not possible to sufficiently remove the buffer salts from the peptides for analysis via mass spectrometry.

Thus, separation based on size rather than on hydrophobic interaction with the stationary phase as in reversed-phase HPLC can be an alternative purification strategy. SEC is particularly interesting for peptides like PNA3-Ala2-SxTMD (**13**) and PNA1-Ala1-SybTMD (**14**), which feature a high amount of deletion sequences resulting from the synthesis of the ala-PNA part. Those deletion sequences are sufficiently different in size compared with the target peptides to be separable via SEC. Indeed, the chromatogram obtained from SEC of PNA1-SybTMD (**8**) exhibited just one main broad peak in spite of the many by-products observed in the ESI mass spectrum of the raw peptide. Likewise, the peaks in the chromatogram of Ala1-PNA1-SybTMD (**10**) are poorly separated. As the raw samples of these peptides contained by-products with molecular masses that lie close together, a separation with the applied SEC column was not possible (see Figure A.3 in the appendix for the chromatograms and Section 6.5.7 for the ESI mass spectra). However, a reliable method for work up and subsequent peptide analysis still needs to be established.

Generally, there were not many solvents in which the synthesized PNA/peptide hybrids were very well soluble. A variety of solvents was tested and the solubility was best in fluorinated compounds like TFE and hexafluoro-2-isopropanol. This is why TFE was the solvent of choice for peptide stock solutions required for the preparation of lipid films (see Section 6.6.1). Also, acetonitrile with addition of formic acid was a suitable solvent in most cases, as well as the mentioned phosphate buffer with 2 % SDS. In water, the peptide hybrids were completely insoluble. If they once had completely been dissolved in an appropriate solvent, however, water could be added to a large extent without precipitation of the peptide. This was useful for HPLC applications.

For further applications in fusion assays, the peptides are used as crude products because none of the attempted purification strategies was successful. However, crude peptides are only used if ESI-MS has confirmed that the desired peptide was the main product and if high resolution mass spectrometry yielded reasonable results.



4. Fusion Assays

The fusogenicity of the novel SNARE model peptides was extensively studied in various fusion assays. Initially, the preparation of the vesicles as well as the way of performing the fusion assays were improved in order to obtain reliable results. The measures and refinements that were introduced are described and explained in the first two sections (Sections 4.1 and 4.2). Following this, the outcomes of the fusion assays are presented. Fusion was studied via FRET in classic bulk lipid mixing assays (Section 4.3 and Section 4.4) and using the technique of fluorescence cross-correlation spectroscopy (FCCS, Section 4.5). On top of that, dynamic light scattering (DLS, Section 4.6) was employed and yielded valuable information about the size change during liposome fusion.

4.1. Preparation of Liposomes

Liposomes were prepared by mixing appropriate amounts of lipid and peptide stock solutions in glass test tubes (see Section 6.6.2 for a detailed description). The test tubes were thoroughly vortexed at room temperature in order to ensure a complete mixing of the TFE and chloroform solutions, which are immiscible at 0 °C. Working at 0 °C, however, is necessary in order to prevent solvent loss from the stock solutions due to evaporation. The concentrations of the lipid stock solutions stayed stable over a period of several months if the vials were only opened on ice for the moment of liquid removal. This was confirmed by phosphate tests, in which phospholipids are converted into inorganic phosphate and reacted with ammonium molybdate. The amount of resulting molybdenum blue complexes could then be quantified spectroscopically (see Section 6.6.5 for details). The solvents could be easily removed from the test tubes in a nitrogen stream which left over a clear lipid film on the inner glass wall. After drying, the lipid film was rehydrated in filtrated buffer at an elevated temperature of around 40 °C to yield a mixture of multilamellar vesicles (MLVs). When the rehydration process took at least 2 hours, detachment of the lipid film from the glass wall was easier and the subsequent homogenization in the sonicator was completed faster. After homogenization, which typically took less than 10 s,

4. Fusion Assays

the MLV mixture was immediately extruded through a polycarbonate membrane. Lipid loss during extrusion was determined via phosphate tests and was shown to vary between 8 % and 59 % with the mean value being 31 %. A reason for this variation could not be determined. It did not depend on the incorporated peptides, and a broad variation of the loss was also observed for the same compositions of the MLV mixtures.

Dynamic light scattering (DLS) experiments were performed on a spot-check basis and confirmed a uniform size distribution of the extruded vesicles. The weighted average of the hydrodynamic radius of all spot-checked liposomes varied between 146 nm and 169 nm, with the mean value being (155 ± 7) nm. A dependence on the type of the incorporated peptide type or the fluorophores was not generally observable. For a better comparability, the liposomes were examined with DLS shortly after extrusion. Figure 4.1 exemplarily shows an intensity size distribution of liposomes containing PNA1s-SybTMD (**16**) in a peptide-to-lipid (P/L) ratio of 1:1000, which exhibit a mean diameter of 147 nm.

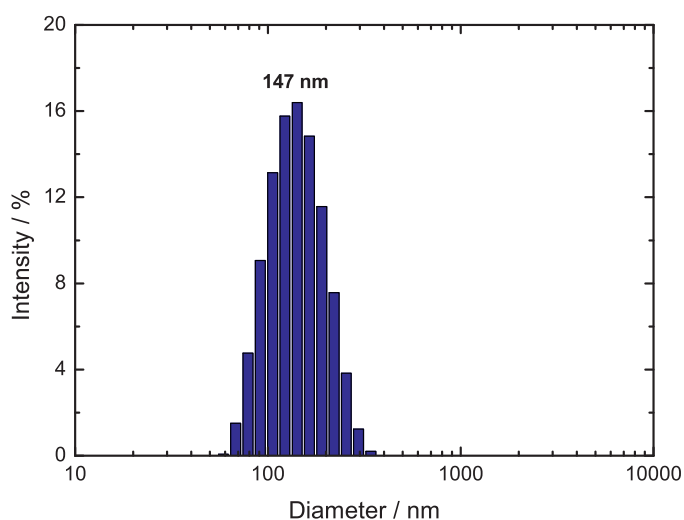


Figure 4.1. Mean intensity size distribution of the prepared liposomes using the example of liposomes containing **16** (total amount of lipids in lipid film: $0.625 \mu\text{mol}$, P/L ratio: 1:1000). The sample was measured three times and the mean distribution was calculated. The resulting mean diameter (mean weighted average of the size distribution) is 147 nm.

The stock solutions of the extruded vesicles were stored at room temperature during the course of measurements. This ensures an equal temperature of both vesicles and buffer in the cuvette and prevents artifacts or false results due to possible temperature gradients in the first seconds of the measurements.

Besides the described direct mixing of lipid and peptide solutions to yield a lipid film, a detergent-assisted lipid film preparation was tested as well. Here, the detergent *n*-octyl- β -D-glucoside was applied during mixing of peptide and lipids which should support the in-

corporation of the hydrophobic peptides^[186] and ensure uniformly shaped liposomes^[187] (see Section 6.6.3 for experimental details). The fusogenicity of peptides incorporated in liposomes that had been prepared by both of the described methods was compared but a significant difference was not detected. There is also the possibility that residual amounts of detergent might remain in the lipid film and thus have an additional unspecific influence on the liposome fusion. For these reasons, liposomes were prepared without the addition of detergent to exclude any possible side effects attributable to the detergent.

4.2. Description of the Employed Lipid Mixing Assays

Fusion experiments were performed at 25 °C in a HEPES (4-(2-hydroxyethyl)-1-piperazineethanesulfonic acid) buffer. This is in accordance with previous experiments^[19,149] and should ensure a better comparability with these experiments. The buffer contained ethylenediaminetetraacetic acid (EDTA) to catch any present divalent cations like Ca²⁺, and dithiothreitol (DTT) to prevent the cysteine moieties in the TMDs from being oxidized to disulfide bridges.

Lipid mixing was monitored by using either a quenching assay or a dequenching assay with the latter being mainly employed. Common features and differences between these assays have been described in Section 2.6.1. Quenching assays were generally performed with the donor fluorophores incorporated into liposomes containing SxTMD-based peptides and the acceptor fluorophores incorporated into liposomes containing SybTMD-based peptides. In typical dequenching assays, liposomes with peptides containing a Syb-TMD were labeled with the FRET fluorophores whereas liposomes containing SxTMD-based peptides stayed unlabeled. Usually, the combination of peptides and fluorophores did not influence the results of the fusion experiments. In Figure 4.2, this is exemplarily shown for the peptide combination Ala2-PNA3s-SxTMD (**21**) and Ala1-PNA1s-SybTMD (**22**). An exception of this case is presented in Section 4.3.4.

The liposomes differed in their stability depending on the type of peptide incorporated. It could not be ruled out that the stability is partially influenced by the presence of labeled lipids. For example, labeled liposomes containing SxTMD-based peptides seemed to be a few hours longer stable than unlabeled liposomes with SxTMD-based peptides. Conversely, also liposomes containing SybTMD-based peptides that were not labeled tended to precipitate a bit faster than labeled liposomes. However, these were minor differences. Generally, in stock solutions of liposomes with SxTMD-based peptides a cloudy white precipitate was formed faster than in stock solutions of liposomes with SybTMD-based

4. Fusion Assays

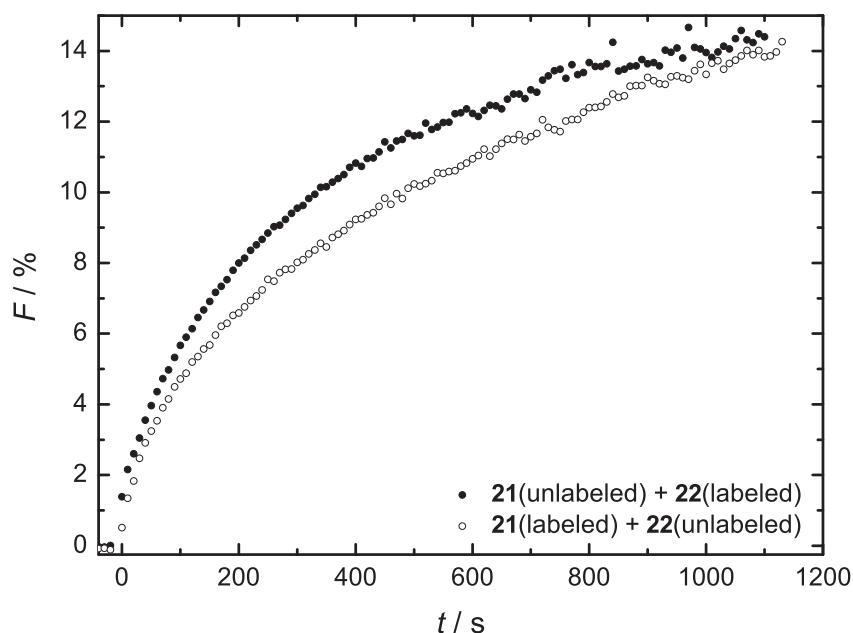


Figure 4.2. Obtained fusion curves when changing the order of labeling. The relative fluorescence intensity F normalized according to Equation 6.5 is plotted against the time t . Either labeled liposomes contain the SybTMD-based peptide **22** and unlabeled liposomes contain the SxTMD-based peptide **21** (●) or labeled liposomes contain the SxTMD-based peptide **21** and unlabeled liposomes contain the SybTMD-based peptide **22** (○). In both cases, the ratio of labeled to unlabeled liposomes in the cuvette was 1:4. The lipid films used for the preparation of the liposomes contained 2.5 μmol lipids and the P/L ratio was 1:200.

peptides. For this reason, liposomes with SybTMD-based peptides were always prepared first. Subsequently, liposomes containing peptides with a SxTMD were extruded and the measurement was started immediately afterwards. This seemed to be necessary to adequately compare different fusion curves, as the fusion efficiency decreased significantly in the time after extrusion (see Figure 4.3). Accordingly, the recorded fusion curves could not be reproduced with vesicles from the same batch at a later time.

This decrease in fusion efficiency over time cannot be explained by a pre-fusion and thus inactivation of liposomes within one population. DLS measurements showed that the size did not significantly change within one liposome population (see Section 4.6). As the liposome stock solutions stayed clear, precipitation could be ruled out as a reason as well. It is rather conceivable that aging processes of the liposomes or interactions among the peptides lead to early aggregation of the liposomes, which are then less capable to undergo fusion. Also possible are interactions of the peptides with the membrane that prevent complementary recognition units from proper interaction.

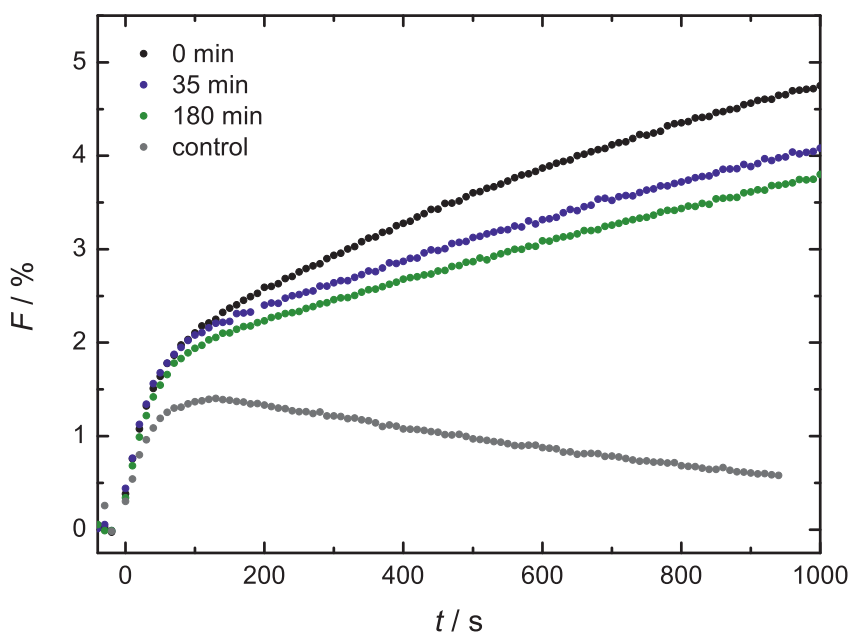


Figure 4.3. Fusion curves recorded at different points in time after extrusion. The indicated times refer to the age of the liposomes after the second population had been extruded. All curves were measured on the same day with the same liposomes, which contained PNA3s-SxTMD (**15**) and PNA1s-SybTMD (**16**) in a P/L ratio of 1:1000. In the control measurement only labeled liposomes contained peptides.

In dequenching assays, the ratio of labeled to unlabeled liposomes in the cuvette was always 1:4. This ratio was adopted from previous assays by Lygina *et al.* in order to better compare the obtained results to the previously reported results.^[19] Lygina examined different ratios between 1:1 and 1:4 and found that the ratio of 1:4 exhibits the most pronounced increase in donor emission.^[167] On the contrary, in quenching assays a 1:1 ratio of donor-labeled to acceptor-labeled liposomes was generally applied. In Section 4.3.7, a closer look is taken on the topic of different liposome ratios and their implications for the stoichiometry of interacting liposomes.

The vesicle population labeled with the donor fluorophore was filled into the cuvette first and, in case of dequenching assays, an emission spectrum was measured to check for FRET between the fluorophores. Then, the change of the fluorescence emission of either the donor (in dequenching assays) or acceptor fluorophore (in quenching assays) was monitored over time. For this, the second vesicle population was added when the fluorescence signal was nearly constant. It was never possible to reach a horizontal baseline here, instead a slight and continuous decrease in the donor emission was always recorded, likely due to processes like photobleaching and sticking of vesicles to the wall of the cuvette.

4. Fusion Assays

As the FRET pair, either 7-nitro-2-1,3-benzoxadiazole (NBD) and Lissamine Rhodamine B (Rh) or Oregon Green 488 (OG) and Texas Red (TR) were used. For excitation and emission, wavelengths were applied at which the intensity ratio of donor to acceptor excitation as well as the ratio of fluorophore of interest to other fluorophore were close to maximal (see also Section 6.3). This means that excitation of the donor involves minimal simultaneous excitation of the acceptor fluorophore, and that the recorded emission of the donor fluorophore, for example, involves as few acceptor emission as possible. In Figure 4.4, the measured spectra of the different FRET fluorophores are shown.

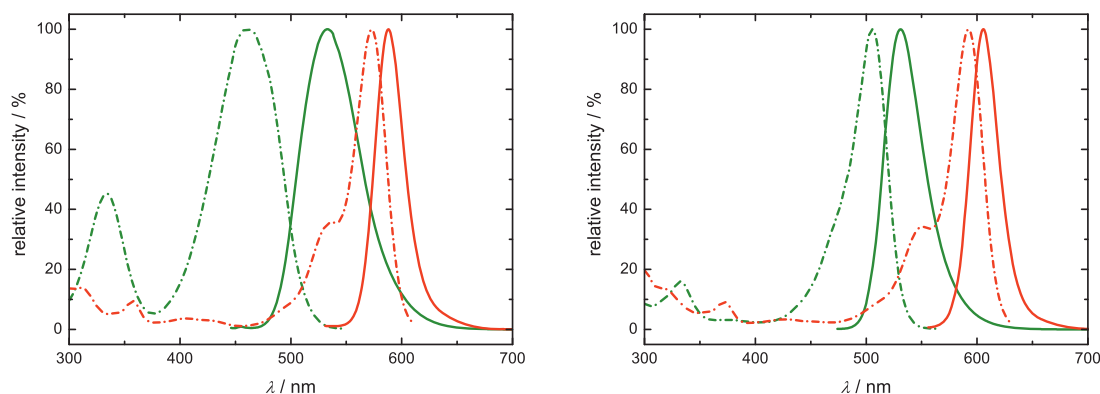


Figure 4.4. Measured excitation (dashed lines) and emission spectra (solid lines) of the different FRET fluorophores used in this thesis. The relative intensity is shown. Left: NBD and Rh; right: OG and TR. The donor fluorophore is depicted in green and the acceptor fluorophore is depicted in red. The fluorophores were bound to the membrane of liposomes into which peptides had been incorporated. OG- and TR-labeled liposomes contained **18** and **19**, respectively; NBD- and Rh-labeled liposomes contained **15** and **16**, respectively. The P/L ratio was 1:1000 in NBD-labeled liposomes and 1:200 in the other three cases.

Measurements were performed with liposomes that contained 1.5 mol% of the respective labeled lipid (in case of TR: 1.0 mol%) in the presence of peptides. This was done in order to reflect the setup of the lipid mixing assays as closely as possible because the spectral properties of fluorophores can be strongly influenced by the environment.^[188] The presence of peptides did not have an influence on the location of the maxima, however, the emission intensity was affected. For example, the donor emission was quenched in case peptides were present with the quenching being stronger for OG than for NBD (data not shown). It is likely that the nucleobases in the recognition sequences cause the quenching. Especially OG has an extended delocalized π -electron system, which might readily interact with aromatic nucleobases. In contrast, NBD is a small molecule with a less extended π -system and thus possibly has a lower tendency to interact with nucleobases.

4.2. Description of the Employed Lipid Mixing Assays

Fusion curves are always shown as normalized curves (see Equation 6.5 in Section 6.6.6). Values for the normalizing procedure were always mean values of at least 30 data points. The maximally achievable donor fluorescence was determined by measuring the fluorescence after the addition of the detergent Triton X-100 (TX-100), which destroyed the liposomes. It has to be noted that the addition of TX-100 notably influences the donor fluorescence. The fluorescence of NBD, for example, was quenched by TX-100. After the addition of TX-100 to NBD-labeled liposomes, the NBD fluorescence was decreased by a factor of 1.45 on average. This is in good agreement with values reported in literature.^[189] As a result, the normalized fusion curves have higher values than they in fact should have because the obtained value for F_{\max} is lower due to the fluorescence-quenching influence of TX-100 (see also Equation 6.5 in Section 6.6.6, which was used to calculate the normalized fusion curves). In contrast to NBD, the fluorescence of OG was enhanced by TX-100 by a factor of ca. 1.36, so that the obtained fusion curves showed smaller values than they actually should. Alternative detergents were also tested. Among them were reduced Triton X-100 (RTX-100) and *n*-dodecyl- β -D-maltoside (DDM), which are used in lipid mixing experiments as well.^[190,191] In contrast to TX-100, these detergents do not show any fluorescence upon excitation. Their addition only led to a slight increase in the NBD fluorescence. The capability to destroy the liposomes was high for RTX-100 just as for TX-100. However, it was insufficient for DDM. Even increasing the concentration of DDM to a value three times higher than the value used in the experiments with TX-100 and RTX-100, a large amount of liposomes stayed intact as derivable from the high persistent acceptor fluorescence.

The idea of adding a detergent is that thereby donor and acceptor fluorophore are separated so that FRET is no longer possible and the maximally achievable donor fluorescence can be determined. However, the donor fluorescence achievable in this way is higher than the donor fluorescence that is achieved when all liposomes in the cuvette have fused completely. In this case, the fluorophores are located on intact liposomes in a smaller distance than if being solubilized by detergent molecules. To respond to this, so-called mock-fused liposomes can be used to determine F_{\max} , which contain the fluorophores in a lower concentration, but still are intact liposomes, thus yielding a more realistic value for F_{\max} .^[192,193] A drawback of mock-fused liposomes is that they are an independently prepared liposome population. Experiments in this work showed that the loss of lipid material during extrusion varies between 8 % and 59 % even when equal lipid compositions were used. This is why consistent concentrations cannot be expected in each case. For this reason, addition of detergent was preferred over applying mock-fused liposomes.



4. Fusion Assays

For quenching assays, detergent was not added. Instead, the obtained fusion curves were corrected for the background and were then scaled arbitrarily to compare the shape of the fusion curves with those from dequenching assays. A comparison between the results of the different approaches is made in Section 4.3.6.

4.3. Total Lipid Mixing Assays

Total lipid mixing (TLM) assays were applied to study the fusogenicity of the model peptides. First, the influence of the peptide and lipid concentration on the extent of lipid mixing was tested, which is described in Section 4.3.1. The effect of the lipid composition on the lipid mixing efficiency is delineated in the succeeding Section 4.3.2. On the basis of these results, TLM assays were performed at optimized conditions for a variety of model peptide combinations to examine the influence of different structures of the recognition unit (see Section 4.3.3). Various control experiments are explained in Section 4.3.5. The main focus of TLM assays was on dequenching assays. However, quenching assays were performed as well and the results are compared to those of dequenching assays (see Section 4.3.6). On top, the experimental outcomes of the TLM assays are used to estimate the stoichiometry of interacting liposomes (see Section 4.3.7).

4.3.1. The Influence of Peptide and Lipid Concentration

As a starting point, concentrations were adjusted to values used earlier for liposomes containing SNARE model peptides with aeg-PNA strands as recognition units.^[19] This included a lipid composition of 1,2-dioleoyl-*sn*-glycero-3-phosphocholine (DOPC), 1,2-dioleoyl-*sn*-glycero-3-phosphoethanolamine (DOPE) and cholesterol (Chol) of DOPC/DOPE/Chol = 50:25:25 mol%, an amount of lipids in each lipid film of 2.5 μmol , and a peptide-to-lipid ratio of 1:200. When following these conditions, however, the prepared liposomes were not very stable. In most cases, a cloudy precipitate started to form several minutes after extrusion. On top of that, the lipid film did not easily detach from the glass wall so that only prolonged treatment in the sonicator could yield a homogeneous yet only shortly stable emulsion. However, long-term treatment with ultrasound should be avoided as it promotes the formation of small unilamellar vesicles^[194] instead of the desired LUVs. The detachment of the lipid film from the glass wall could be facilitated by the addition of glass beads but still a long-lived homogeneous emulsion was not achieved.



For these reasons, the overall lipid content was reduced. Instead of 2.5 μmol lipids per 500 μL , 0.625 μmol per 500 μL were used. The stability of the liposomes increased significantly. The emulsion after sonication was quite stable and the extruded liposome solution stayed clear for at least several hours. Surprisingly, reducing the concentration of vesicles led to an increase in fusion efficiency as can be seen when comparing the normalized fusion curves (see Figure 4.5).

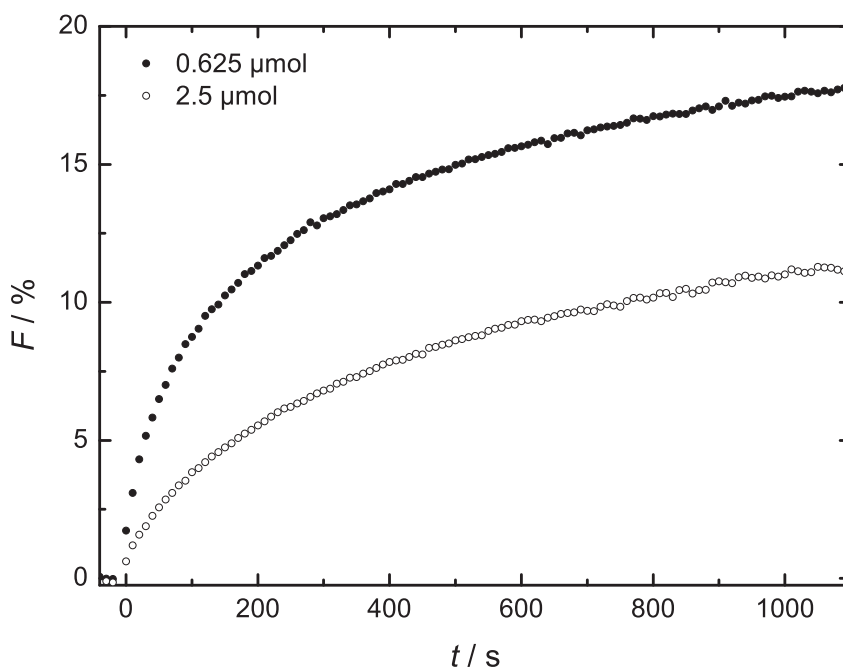


Figure 4.5. Difference in fusogenicity of liposomes containing **15** and **16** when changing the amount of lipids in the liposome stock solution from 2.5 μmol (\circ) to 0.625 μmol (\bullet). The P/L ratio was 1:200 in both cases.

It has to be noted that the final volumes of liposome stock solutions added to the cuvette were equal in both cases so that the liposomes prepared as 0.625 μmol stock solutions are more efficient even at a lower total concentration in the cuvette. The effect can be explained with an increase in the quality of the vesicles. Possibly, even the incorporation of peptides is more efficient.

The described problems with the precipitation only arise if peptides were present in the lipid films. Purely lipidic films without peptides were stable for a very long time. The peptides had a different influence on the liposome stability. Liposomes containing peptides with a SybTMD tended to be more stable than those containing peptides with a SxTMD. Possibly, the polybasic linker region of Syntaxin-1A interacts with the lipid headgroups, thereby bringing about aggregation or impeding proper insertion of the peptide into the membrane causing it to be rather peripherally bound.

4. Fusion Assays

Decreasing the peptide-to-lipid ratio from 1:200 to 1:1000 increased the stability of the liposomes further such that problems with precipitation were mostly avoided.¹ The stock solutions of the liposomes did not show any precipitation for several days (if containing SxTMD-based peptides) or even weeks to months (if containing SybTMD-based peptides). In this way, the reproducibility of the fusion assays could be largely improved. The decrease of the peptide-to-lipid ratio also meant a decrease in the fusion efficiency as it is exemplarily shown in Figure 4.6. However, this was acceptable in return for the advantages described above.

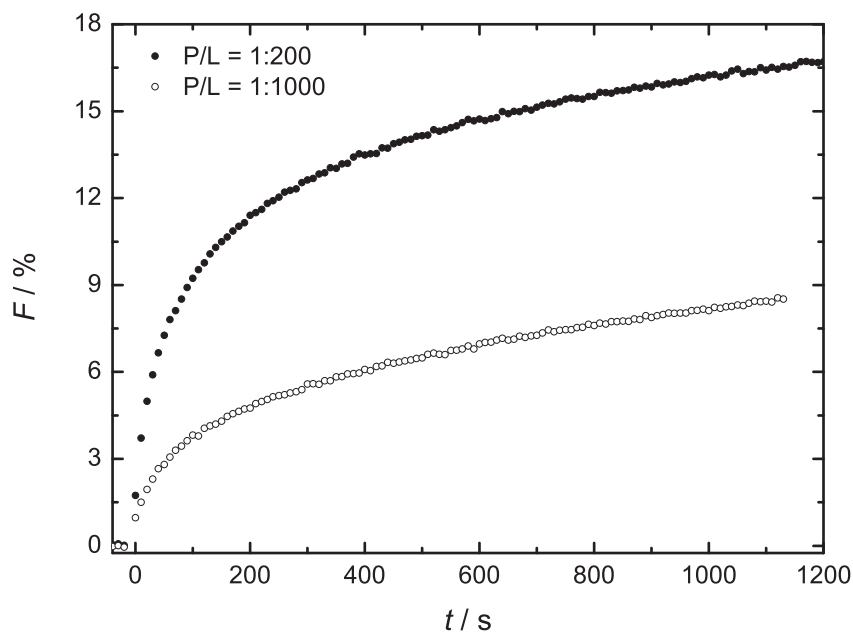


Figure 4.6. Difference in fusogenicity of liposomes containing **15** and **16** when reducing the P/L ratio from 1:200 (●) to 1:1000 (○). The amount of lipids in the lipid stock solutions was 0.625 μmol in both cases.

4.3.2. The Influence of DOPS

Besides the typically applied lipid composition of DOPC/DOPE/Chol = 50:25:25 mol%, another lipid composition was tested comprising additional 1,2-dioleoyl-*sn*-glycero-3-phospho-L-serine (DOPS) in a ratio of DOPC/DOPE/DOPS/Chol = 50:20:20:10 mol%. This mixture reflects the native composition of a synaptic vesicle more closely, which contains about 12 mol% DOPS.^[195]

¹ The number of PNA/peptide hybrids located on one liposome was roughly estimated to be 275 at a peptide-to-lipid ratio of 1:1000. See Section A.4 in the appendix for details.



In Figure 4.7, the fusion curve obtained with the lipid mixture containing DOPS is compared to a fusion curve obtained with the standard lipid mixture.

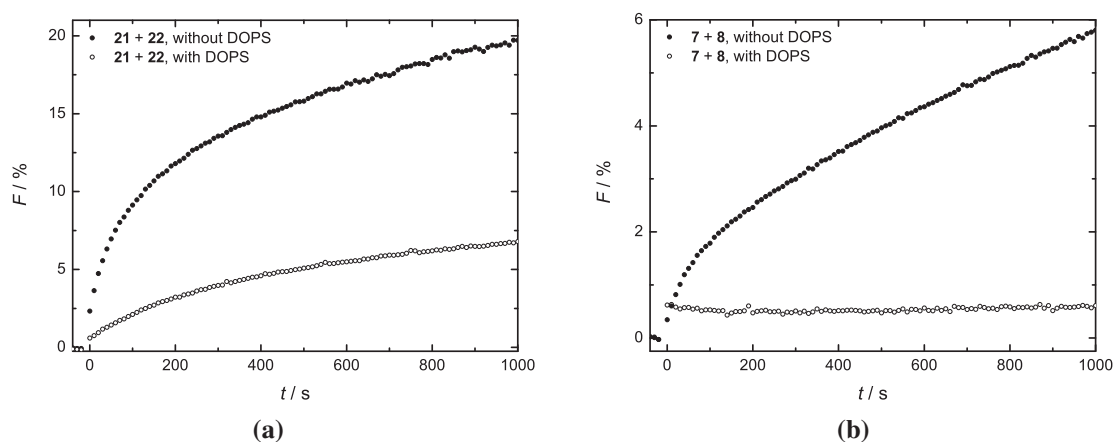


Figure 4.7. Fusion curves obtained in assays with liposomes containing DOPS (\circ) or without DOPS (\bullet). The liposomes either contained **21** and **22** in a P/L ratio of 1:200 (a) or **7** and **8** in a P/L ratio of 1:1000 (b). The amount of lipids in each lipid film was 2.5 μmol .

It is clearly visible that the presence of DOPS decreases the fusion efficiency dramatically. As expected, the fusion efficiency is higher if a higher peptide-to-lipid ratio is used (see Figure 4.7a vs. b).

The finding that the addition of DOPS decreases liposome fusion agrees with observations made with assays reported previously that showed the fusion inhibiting effect of DOPS.^[196,197] The observed decrease can be explained by the negative charge that is introduced with DOPS. Due to this charge, membranes are electrostatically more repulsive and it seems as if the SNARE model peptides are not capable of completely overcoming these additional repulsive forces. It is worth mentioning that the stability of the vesicles is also greatly enhanced. Even liposomes containing SxTMD-based peptides in a high peptide-to-lipid ratio of 1:200 showed a clear solution for many days which was not possible to achieve with the standardly used lipid mixture. This suggests that the observed precipitation is due to aggregation of the liposomes which can be prevented if DOPS is present.

4.3.3. The Influence of the Peptide Structure

For the systematic investigation of the influence of the different model peptides on the fusion process, optimized conditions based on the findings from the experiments described in Sections 4.1–4.3.2 were applied. This includes the usage of liposomes without DOPS

4. Fusion Assays

made from lipid films with an overall lipid amount of 0.625 μmol and a peptide-to-lipid ratio of 1:1000.

Initially, fusion assays were performed with model peptides of the first generation, which exhibit a decameric aeg-PNA sequence in the recognition unit (see Table 3.1 in Section 3.4). As the purity of the peptides was not as good as desired for obtaining reliable results, though (see Section 3.4), model peptides with a shorter recognition unit were examined. A comparison of the fusion efficiency of model peptides with aeg-PNA recognition units differing in their length yielded astonishing results. The results of TLM dequenching assays with liposomes containing PNA3-SxTMD (**7**) and PNA1-SybTMD (**8**) as well as with liposomes containing PNA3s-SxTMD (**15**) and PNA1s-SybTMD (**16**) are depicted in Figure 4.8. Omitting the N-terminal half of the aeg-PNA decamer resulted in a distinct increase in fusogenicity of the liposomes decorated with peptides **15** and **16**. These contain a pentameric aeg-PNA sequence and thus only five base pairs contribute to duplex formation. Though fewer base pairs are available, this is sufficient and even more efficient to induce lipid mixing.

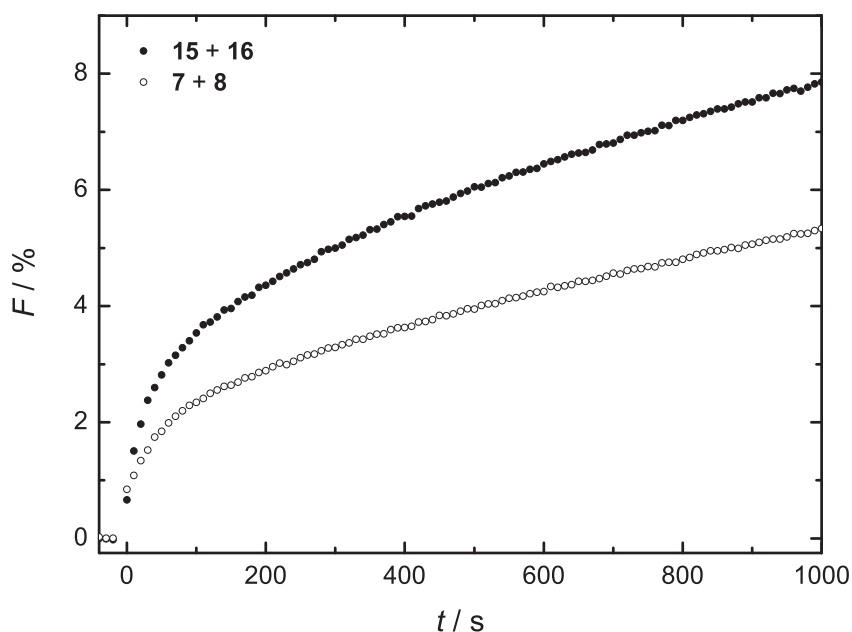


Figure 4.8. Fusion curves from assays with liposomes containing peptides either with a decameric aeg-PNA sequence (**7** + **8**, ○) or with a pentameric aeg-PNA sequence (**15** + **16**, ●). The P/L ratio was 1:1000 in both cases.

This effect was first observed by Pawan Kumar² and could have different reasons. On the one hand, it might be a matter of peptide purity. The synthesis of the PNA/peptide hy-

² Pawan Kumar, AK Diederichsen, personal communication.

brids with five PNA monomers attached proceeded with fewer by-products than the synthesis of the sequence with ten PNA monomers (see also Section 3.4). If the PNA/peptide hybrid is purer, the determination of the concentration of the stock solution via UV absorption is more accurate and hence the applied amount of peptides with the correct sequence is higher. This implies that the amount of deletion sequences, which do not contribute to the specific peptide interaction but may have an influence on the liposomes' stability, is lower. Another point is that the incorporation of peptides with a pentameric recognition unit might be better than that of peptides bearing a decameric recognition unit. The TMD sequences are the same for both peptide types. Hence, the effect has to be attributed to the recognition unit. It might be possible that a longer recognition unit interacts with the membrane and disturb the correct incorporation of the entire peptide. On top of that, also the recognition itself might be more efficient if only five monomers are present. The probability that mismatched duplexes form, *i.e.* duplexes in which the overlap of the strands is less than 100 %, is higher in the case of ten monomers. Mismatched duplexes are likely less tightly bound so that liposome fusion is less or even not possible at all. Even if the formation of mismatched duplexes is reversible, it will still contribute to the overall speed of liposome fusion. Therefore, the pentameric PNA strands are more efficient in inducing fusion. Thus, model peptides of the second generation (see Table 3.2), in which the decameric aeg-PNA sequence is replaced by a pentameric aeg-PNA sequence, were used for detailed liposome fusion studies.

Figure 4.9 depicts the fusion curves that were obtained from TLM dequenching assays with PNA/peptide hybrids containing alanyl-PNA and aeg-PNA sequences connected in four different ways. The presented curves are the mean curves that were obtained by averaging the data of at least 4 measurements. Each one of the measurements was performed with independently prepared samples.³

The upper two curves (black and blue) belong to the peptide combinations PNA3s-SxTMD (**15**) and PNA1s-SybTMD (**16**) as well as Ala2-PNA3s-SxTMD (**21**) and Ala1-PNA1s-SybTMD (**22**). These PNA/peptide hybrids have an aeg-PNA sequence attached to the TMD and differ in the absence (**15** + **16**) or presence (**21** + **22**) of an additional N-terminal ala-PNA sequence. With both of the peptide combinations a similar fusion behavior is achieved. It was systematically observed, however, that liposomes with peptides containing the additional ala-PNA sequence in the recognition unit show a less extent of lipid mixing. The lower two curves (green and red) belong to the peptide combina-

³ In the appendix, plots of all single measurements that were used for the mean fusion curves are listed (see Figure A.4). Error bars shown in the plots of this thesis were calculated from the standard deviation of the mean including the respective values from Student's *t*-distribution (see Section 6.1 for details).

4. Fusion Assays

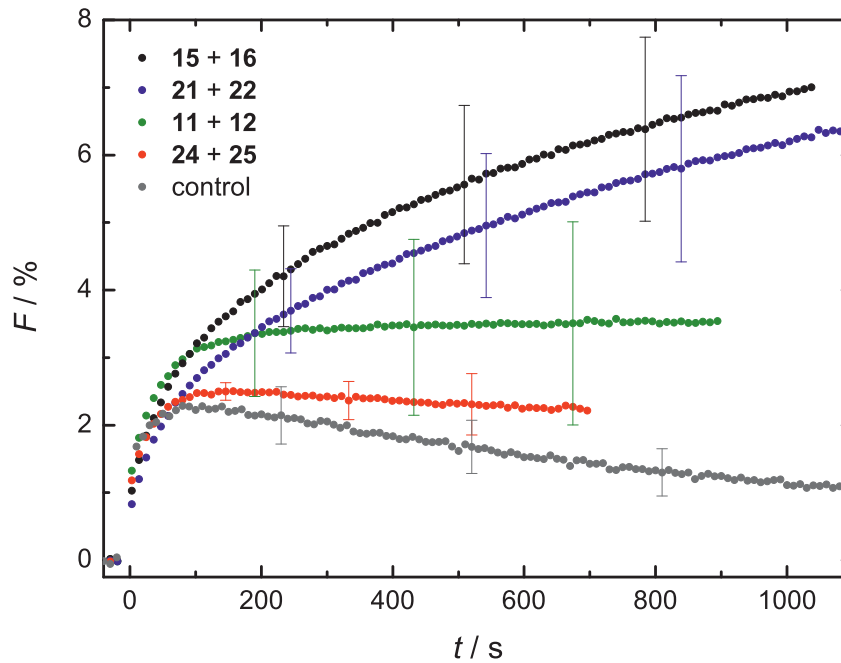


Figure 4.9. Mean fusion curves from TLM dequenching assays. Liposomes contained the peptide combinations **15 + 16** (black), **21 + 22** (blue), **11 + 12** (green) or **24 + 25** (red). Control measurements (grey) were performed with liposomes lacking peptides. The P/L ratio was 1:1000 in all cases.

tions Ala2-SxTMD (**11**) and Ala1-SybTMD (**12**) as well as PNA3s-Ala2-SxTMD (**24**) and PNA1s-Ala1-SybTMD (**25**). In these peptides, the alanyl-PNA sequence is directly attached to the TMD, with PNA/peptide hybrids **24** and **25** featuring an extra aeg-PNA sequence added N-terminally. Compared with the upper two curves the initial slope is slightly higher and the maximum NBD fluorescence is reached faster. To better assess the shape of the different fusion curves, the mean fusion curve of the control measurements with liposomes lacking peptides is shown as well (grey). A detailed look on the various control measurements that were performed in this work will be given in Section 4.3.5.

The comparison of the fusion curves shown in Figure 4.9 leads to two general statements: First, the fusion efficiency depends on via which type of PNA the recognition unit is attached to the transmembrane domain. Whereas peptides with a C-terminal aeg-PNA part in the recognition unit lead to a significant extent of lipid mixing, peptides with a C-terminal ala-PNA in the recognition unit show a reduced fusogenicity. Second, the addition of another PNA type at the N-terminus of the recognition unit reduces the fusogenicity. This is even the case when it is the same PNA type, as it was shown in Figure 4.8. Peptides with a pentameric aeg-PNA sequence were superior in lipid mixing compared



with peptides with a decameric aeg-PNA recognition unit. When aeg-PNA is connected N-terminally to the ala-PNA recognition unit, a very low lipid mixing efficiency was detected which practically does not differ from that of the control measurement. Thus, peptides **24** and **25** are not capable of fusing liposomes. This becomes further apparent when control measurements with non-complementary peptides were performed (see Section 4.3.5).

The finding that five aeg-PNA monomers in the recognition unit were sufficient and most efficient in inducing liposome fusion is also supported by an experiment in which liposomes containing peptides PNA3s-SxTMD (**15**) and Ala1-PNA1s-SybTMD (**22**) were mixed. The fusion curves are depicted in Figure 4.10a.

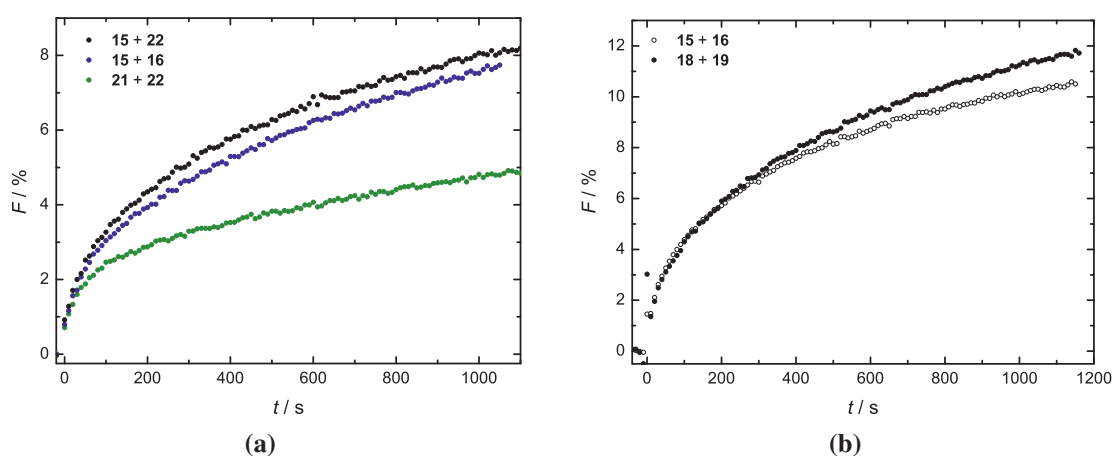


Figure 4.10. (a) Fusion curves resulting from assays with liposomes containing peptides of the “false” combination **15** + **22** (black). For comparison, the “correct” combinations **15** + **16** (blue) and **21** + **22** (green) are shown as well. (b) Influence of the C-terminal charge. Fusion curves resulting from assays with liposomes containing peptides **18** + **19** (●) and **15** + **16** (○). The P/L ratio in both cases in plot (b) is 1:200. All measurements were taken on the same day with the same liposomes.

It can be seen that this actually “false” combination is as efficient as the “correct” combination **15** + **16**. It shows that the additional N-terminally attached ala-PNA sequence is redundant and not necessary for efficient lipid mixing. If ala-PNA is attached to both interacting units (as in the combination **21** + **22**) this seems to disturb the recognition because less lipid mixing is detected compared to **15** + **16**. Note that in Figure 4.10a single measurements from the same day are presented. This is done to show the general finding that less fusion is observed for the combination **21** + **22**. This relative finding is significant, though the scatter of the data between several days leads to larger absolute errors (cf. Figure 4.9).



4. Fusion Assays

In addition, the fusogenicity of model peptides PNA3s-SxTMD-NH₂ (**18**) and PNA1s-SybTMD-NH₂ (**19**) was investigated (see Figure 4.10b). These peptides exhibit a pentameric aeg-PNA recognition unit and a neutral amide C-terminus instead of the negatively charged native carboxy terminus. The obtained fusion curves in assays with liposomes containing **18** + **19** are very similar to the fusion curves obtained in assays with liposomes containing **15** + **16**. In Figure 4.10b single measurements from the same day are compared. Further independently prepared assays yielded comparable results; even in the case when the peptide-to-lipid ratio was reduced to 1:1000. Thus, a dependence of the fusogenicity of the peptides on the C-terminal charge (negative or neutral) was not detected. These results are contradictory to results obtained from previous experiments which indicated that model peptides with an amide terminus show a superior fusogenicity compared to those with a carboxy terminus.^[19,117] The previous experiments were performed for model peptides containing a decameric aeg-PNA sequence. In this thesis, however, pentameric aeg-PNA recognition units were used. On top, a reduced overall lipid concentration was applied. These differences thus seem to be sufficient to equalize the fusogenicity of the model peptides and to compensate for the effect of the C-terminal charge.

It has been demonstrated before that base pairing of complementary strands containing both PNA types is possible (see also Section 3.1).^[176] Thus, it was expected that the additional ala-PNA stretch increases lipid mixing as the addition of extra base pairs should enhance the stability of the duplex and therefore might enhance fusogenicity accordingly. Especially, adding the ala-PNA part C-terminally to the aeg-PNA recognition unit was expected not only to enhance fusion but also to achieve an N→C-terminal zipper-like recognition as assumed for native SNAREs. Recently presented mechanistic concepts for SNARE assembly (see Section 2.4.3) propose that the force that is generated through the assembly of the recognition units directly acts on the linker and transmembrane domain.^[77,122] According to the initial hypothesis of this thesis, model peptides with a PNA hybrid recognition unit would start recognition in the aeg-PNA part and continue it to the ala-PNA stretch. Subsequent ala-PNA base pairing would generate extra force which—if transferable to the membrane—would enhance the extent of fusion. The finding that C-terminal addition of ala-PNA hindered fusion does not agree with this idea. Furthermore, the addition of an aeg-PNA stretch to an ala-PNA containing peptide impeded lipid mixing. The presented TLM assays therefore suggest that the expected zippering did not take place. Instead, five aeg-PNA monomers are sufficient and most efficient in lipid mixing.

Why is the extent of lipid mixing reduced when model peptides with a recognition unit exhibiting C-terminal ala-PNA are used? Figure 4.9 shows that the NBD emission signal is already stable after around 200 s when alanyl-PNA has been attached directly to the transmembrane domain. The interaction between the respective peptides and therefore liposome fusion seems to be less efficient compared with the species in which aeg-PNA is attached to the transmembrane domain. Also, the kinetic traces differ. This can be explained by the topological break between the different components. Alanyl-PNA exhibits a linear structure and thus differs from the helical aeg-PNA and the α -helical transmembrane domain. The transfer of mechanical force from the peptides to the membranes might not be possible anymore from alanyl-PNA to the α -helical peptide domain. Due to its high structural difference the ala-PNA tetramer acts as a spacer. This is why the extent of fusion is lower and also terminated earlier than if peptides with a C-terminal aeg-PNA sequence are used.

The relatively low lipid mixing efficiency of peptides with a pure ala-PNA recognition unit (**11 + 12**) is in accordance with observations made previously with ala-PNA oligomers.^[26] Due to sterical reasons, the formation of these oligomers is kinetically hindered and thus complementary strands meet less easily. Furthermore, it is possible that the ala-PNA nucleobases interact with the liposome surface which leads to a decreased availability for intended interaction with the complementary ala-PNA sequence. There are hints that there is an interaction between the ala-PNA sequence and the fluorophores which is discussed in more detail in Section 4.3.4. On top, it has to be noted that an increase in NBD emission is not only achieved when the lipids of labeled liposomes mix with those from unlabeled liposomes but also when aggregation or rupture of liposomes takes place. Both processes increase the donor–acceptor distance. Thus, another possible explanation for the low extent of lipid mixing of liposomes decorated with **11** and **12** is that these liposomes are less stable than the liposomes with peptides **15 + 16** or **21 + 22**. The difference might simply arise from discrepancies in the undesired background reactions. This is further discussed in Section 4.3.6 where the results of a quenching assay are used to explain the infinite increase in NBD emission as seen in the upper two fusion curve depicted in Figure 4.9. FCCS measurements, however, suggest that there is indeed a difference in the interaction behavior among the different PNA/peptide hybrids. This means that the observed differences in the TLM assays cannot be exclusively explained by the stability of the liposomes. The results of the FCCS measurements are presented and discussed in Section 4.5.

4.3.4. TLM Assays at High Concentrations of Peptides **11** + **12**

An interesting observation was made when TLM dequenching assays were performed for the peptide combination Ala2-SxTMD (**11**) and Ala1-SybTMD (**12**) at a high peptide-to-lipid ratio of 1:200. The resulting fusion curves are depicted in Figure 4.11.

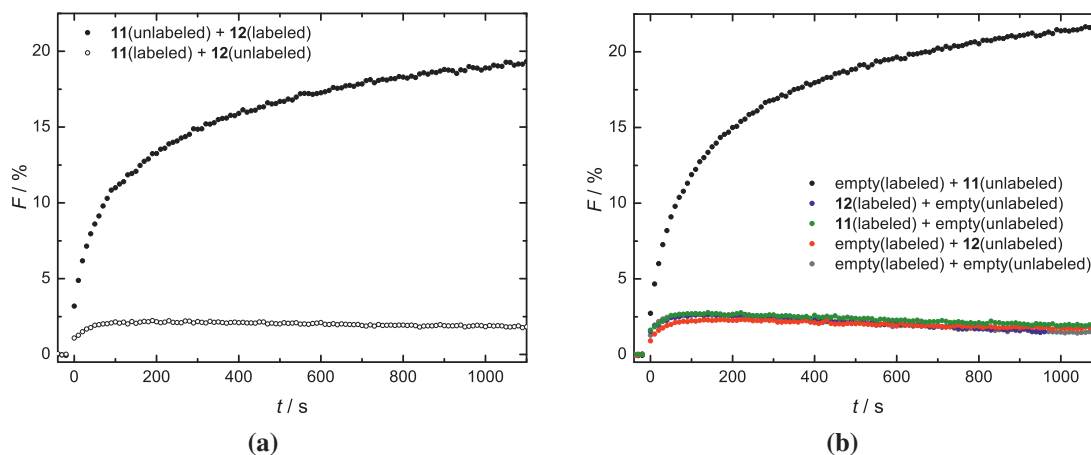


Figure 4.11. Results of TLM dequenching assays of liposomes containing **11** + **12** in a P/L ratio of 1:200. (a) Both liposome populations contain peptides; (b) control measurements in which either one or both liposome populations do not contain peptides. The respective combinations are indicated in the caption.

Contrary to the other peptide combinations, it did make an enormous difference which liposome population was labeled. If liposomes containing **12** were labeled, fusion curves showed the expected increase in donor emission. However, if liposomes containing **11** were labeled, an increase in the donor emission was not detected anymore (see Figure 4.11a). In the control measurements, in which the respective liposome population was mixed with an empty population, none of the possible combinations showed an increase, as expected. There was only one exception: Liposomes decorated with **11** showed a huge increase in NBD emission upon mixing with labeled empty liposomes (see Figure 4.11b). The extent of NBD emission did not differ much from the respective measurement with PNA/peptide hybrids in both liposome populations. The comparison of all control measurement curves suggests that there is an interaction between fluorophores on the one liposome population and PNA/peptide hybrids on the other population which led to the observed lipid mixing. The interaction must be specific for peptide **11** as the increase was not detected for peptide **12**. DLS measurements support this observation. The increase in size in assays with labeled liposomes lacking peptides and liposomes containing **11** was significantly higher than in assays without fluorophores (see Section 4.6). Similarly,



FCCS suggest a fluorophore–peptide interaction as well (see Section 4.5). The described effect was not visible at all at a low peptide-to-lipid ratio of 1:1000. Therefore, the fusion curve shown in Figure 4.9 (Section 4.3.3) can still be seen as the result of a specific interaction between the complementary PNA/peptide hybrids.

4.3.5. Control Experiments

Control experiments were routinely performed with liposomes lacking PNA/peptide hybrids. When added to labeled peptide-decorated liposomes, it was expected that NBD fluorescence does not increase, thus fusion does not occur because the interaction partner for the PNA/peptide hybrids is missing. Figure 4.12 depicts a summary of the results of all recorded control experiments. The combination of two liposome populations without any peptides is also shown.

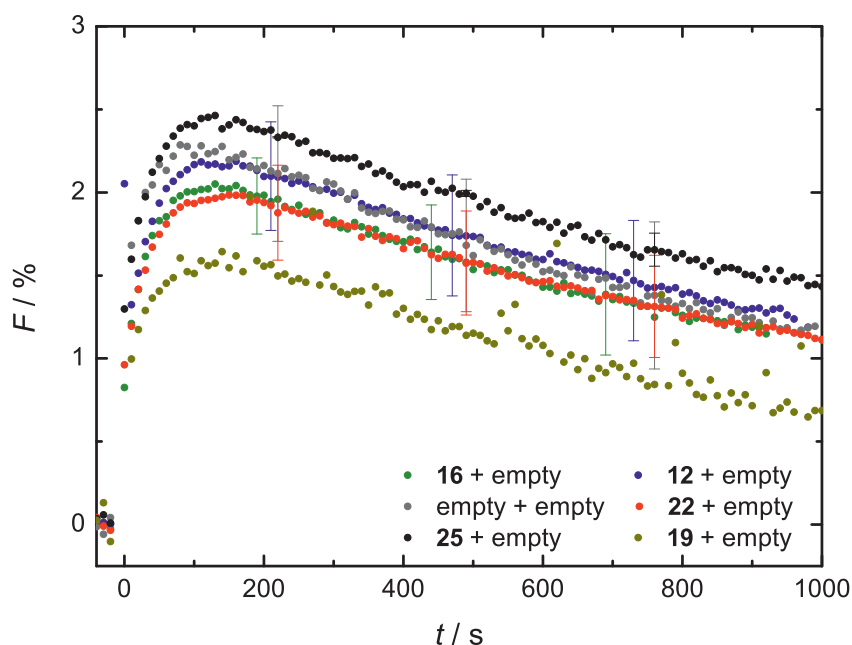


Figure 4.12. Fusion curves obtained from control experiments. Labeled liposomes containing the indicated peptide were mixed with unlabeled liposomes containing no peptide. The fusion curves that results when mixing liposomes without any peptides is also shown (filled grey circles). The P/L ratio was 1:1000 in all cases.

All fusion curves of the control measurements were very similar in their shape, independently of the incorporated peptides (see Figure 4.12). Changing the peptide-to-lipid ratio or changing the order of labeling (meaning that unlabeled liposomes contained peptides and were added to labeled liposomes lacking peptides) had no influence on the shape

4. Fusion Assays

of the fusion curve (data not shown). Surprisingly, all fusion curves of the control measurements of TLM dequenching assays reproducibly exhibit a slight increase in the first minutes of the TLM experiment. The expected decrease in NBD fluorescence due to sticking and photobleaching effects only became prevalent after approximately two minutes. The described initial increase was also observed when the labeled liposome population contain no PNA/peptide hybrids at all. This excludes an effect caused by unspecific interactions between peptides and membranes. It can probably be explained with the sensitivity of the NBD fluorophores to the polarity of their environment. Adding the second liposome population involves an overall decrease in polarity. Decreasing the polarity of the environment is known to result in an increase of NBD fluorescence intensity.^[198,199] Only small changes are sufficient to influence the emission of NBD, which is located in the water/membrane interface and which is thus easily susceptible for polarity changes due to its solvatochromic properties.^[200] This also explains why the initial increase is not detectable in ILM control experiments (see Figure 4.17 in Section 4.4). The emission of the NBD fluorophores on the inner leaflet is stable because the environment within the liposomal lumen remains unaffected. Thus, only fluorophores located on the outer leaflets are influenced by changes in the environment such as addition of further liposomes.

In addition, control measurements with liposomes containing peptides with non-complementary recognition units were performed. Figure 4.13 shows the results for the peptide combinations Ala1-SybTMD (**12**) and Ala1-SxTMD (**20**) as well as PNA1s-Ala1-SybTMD (**25**) and PNA1s-Ala1-SxTMD (**26**). The mean fusion curves of the assays with liposomes containing the complementary peptides as well as the mean control curve obtained from assays with liposomes lacking peptides are presented as well to better assess the results.

In case liposomes contained the non-complementary peptide combinations **12 + 20** and **25 + 26** higher values for the donor emission were detected than if no peptides were incorporated in the liposomes (compare open circles with filled grey circles in Figure 4.13). Thus, the presence of peptides alone has a slight influence on the extent of lipid mixing, probably due to unspecific interactions. The comparison of the results of the assays with liposomes containing complementary peptide combinations with the results of the control assays, in which liposomes contained non-complementary peptide combinations, can be used to evaluate if a specific interaction of complementary peptides leads to lipid mixing (compare filled black circles with open circles in Figure 4.13). In the case of **11 + 12**, the fusion curves are more or less significantly separated from each other to state that a specific interaction between **11** and **12** leads to a low lipid mixing. In the case of **24 + 25**,

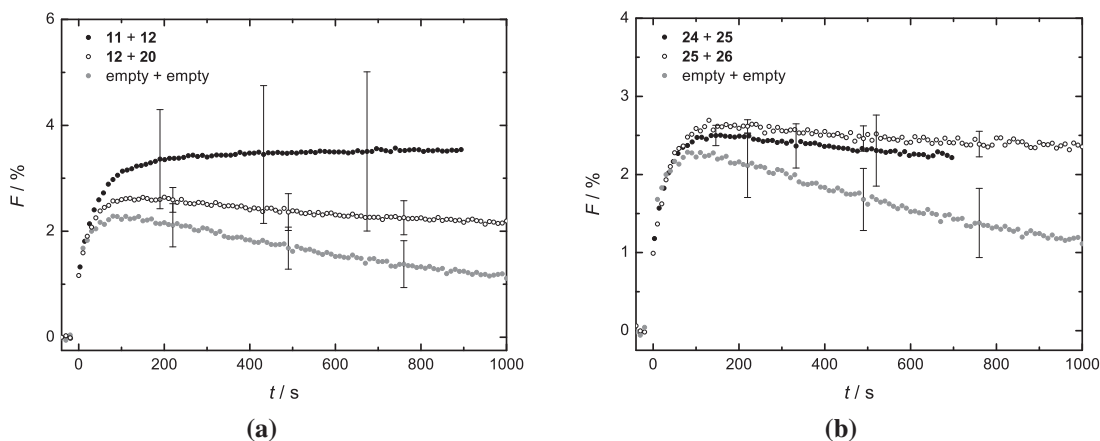


Figure 4.13. Control measurements with peptides containing non-complementary recognition units. (a) Controls for TLM assays with peptides **11 + 12**. Liposomes containing **12** were mixed with liposomes containing **20** (○). (b) Controls for TLM assays with peptides **24 + 25**. Liposomes containing **25** were mixed with liposomes containing **26** (○). For comparison, the mean fusion curves obtained from assays with the respective complementary peptides (●, identical to those in Figure 4.9 in Section 4.3.3) as well as those obtained from control measurements with liposomes lacking peptides (grey) are shown. The P/L ratio was 1:1000 in all cases.

the results of the assays with liposomes containing the complementary peptide combination and those of the assays with liposomes containing the non-complementary peptides, are equal. The extent of lipid mixing does not differ significantly from that of the control measurement with liposomes lacking peptides. Thus, by using peptides **24** and **25**, liposome fusion is completely inhibited.

4.3.6. Comparison of Quenching and Dequenching Assays

In TLM dequenching assays with liposomes containing peptides **15 + 16** and **21 + 22**, it was observed that the maximum extent of lipid mixing was not reached within the 20 minutes time frame of the experiments (see Figure 4.9 in Section 4.3.3). The change in NBD fluorescence was also monitored over a much longer period (180 min) but the NBD fluorescence never became saturated (data not shown). This observation indicates that the long-term increase is due to unspecific aggregation or rupture of the liposomes. Aggregated liposomes may exchange fluorophore-labeled lipids located on the outer leaflets as proposed by Pryor *et al.*^[201] This exchange would lead to an increase in NBD emission as it results in an immediate increase in the donor–acceptor distance. Destruction of the liposomes would cause an increase of the distance as well.

4. Fusion Assays

To assess this more closely, quenching assays were performed, which provide a useful alternative to dequenching assays. In these assays, one population is labeled with the donor fluorophore and the other population is labeled with the acceptor fluorophore. With this, lipid mixing can be detected by an increase in the acceptor emission. Fluorescence signals from lysed liposomes are not detected because these assays detect the specific FRET between donor and acceptor molecules which only takes place in case of lipid mixing between differently labeled liposomes.

In Figure 4.14, two representative fusion curves of a quenching and a dequenching assay are compared. The same experimental conditions were applied for both assays. For the obtained fusion curve of the quenching assay, the value for the acceptor fluorescence at $t = 0$ s (addition of the second liposome population) was subtracted from all data points. Note that—contrary to dequenching assays—it is not possible to obtain a value for F_{\max} in quenching assays. Thus, the fusion curve was scaled arbitrarily to be comparable to the dequenching fusion curve.

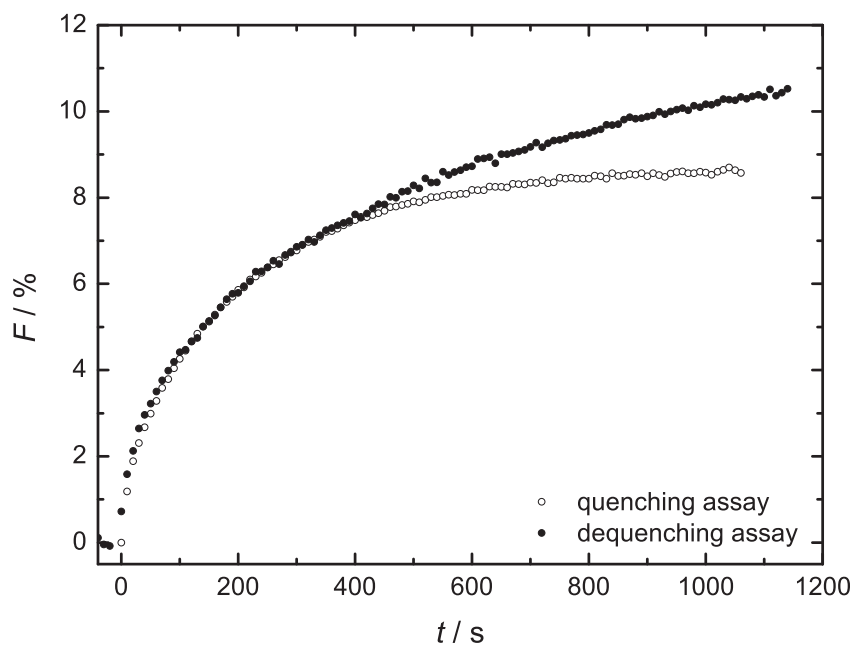


Figure 4.14. Comparison of the increase in fluorescence in the dequenching (●) and the quenching assay (○). The fusion curve of the dequenching assay was normalized as usual. The fusion curve obtained from the quenching assay was scaled arbitrarily. The liposomes used in both assays contained **15** and **16** in a P/L ratio of 1:200 with the fluorophores being NBD and Rh.

Comparing the fusion curves of both assays reveals a clear difference in the change of the fluorescence. After approx. 600 s, the acceptor fluorescence stays nearly constant in

the quenching assay. In the dequenching assay, however, the donor fluorescence keeps increasing almost linearly. Likely, this linear increase is not the result of liposome fusion due to specific interaction of the model peptides but rather the result of unspecific processes such as liposome aggregation or rupture. If specific liposome fusion had occurred after 600 s, a more pronounced increase in the fluorescence intensity would have been detected by the quenching assay. This disagreement shows that there has to be an additional contribution to the signal in dequenching assays. TLM quenching assays were also performed with liposomes containing **15** and **16** that were labeled with OG and TR instead of NBD and Rh (data not shown). As expected, the shape of the resulting fusion curve was identical to the fusion curve depicted in Figure 4.14. This indicates that the quenching assay with liposomes containing the mentioned peptides is not influenced by the type of fluorophores. The quenching assay provides more realistic information on the kinetic trace as far as the lipid mixing is concerned that happens due to specific interaction of peptide with complementary recognition units. Note, however, that there is evidence described in literature that with quenching assays it cannot be distinguished between liposome aggregation and true lipid mixing.^[193] The reason is that aggregation brings liposomes into a proximity that is close enough for FRET between the fluorophores of both liposomes.

The dequenching assay, in turn, is insensitive to an aggregation, which does not involve lipid mixing. Dequenching assays also allow the determination of F_{\max} , which is the theoretically achievable value of the donor fluorescence reflecting the situation of 100 % fusion. F_{\max} is not accessible with quenching assays. Thus, dequenching fusion curves can be normalized and expressed as percentage of the theoretically achievable fluorescence. With this, information on the amount of fused liposomes is available. For example, the stoichiometry of interacting liposomes can be roughly estimated which is described in Section 4.3.7.

In conclusion, both techniques are not devoid of artifacts and of the detection of signals arising from undesired processes. The combination of both techniques, though, will provide the most comprehensive information on total lipid mixing in bulk assays. Whereas quenching assays provide fusion curves with the correct shape, dequenching assays allow the estimation of the amount of interacting liposomes.

4.3.7. Estimated Stoichiometry of Liposome Interactions

In TLM dequenching assays, the labeled and unlabeled liposomes were always mixed in a 1:4 ratio. This was done in order to be able to compare the obtained results to

4. Fusion Assays

those from Lygina who investigated ratios between 1:1 and 1:4 but acquired most of the data at a ratio of 1:4. This ratio was found to yield the highest increase in NBD emission.^[167] The finding is reasonable because the rate of a reaction is increased when a higher concentration of the reactants is applied. If we assume that only one fusion process between two liposomes takes place, the reaction rate r is of a second-order type and given by Equation 4.1, with k being the rate coefficient and c_{labeled} and $c_{\text{unlabeled}}$ the concentrations of the labeled and unlabeled liposomes, respectively.

$$r = k \cdot c_{\text{labeled}} \cdot c_{\text{unlabeled}} \quad (4.1)$$

According to Equation 4.1, it should not make any difference whether the labeled and unlabeled liposomes are mixed in a 1:4 or in a 4:1 ratio, given that the overall concentration of liposomes is constant. The resulting fusion curves should show a comparable shape and height. Surprisingly, this could not be confirmed in the dequenching assays. Mixing the liposomes in a 4:1 ratio (labeled:unlabeled) resulted in a fusion curve that exhibits a much smaller increase in NBD fluorescence than the fusion curve that resulted if the liposomes had been mixed in a 1:4 ratio (see Figure 4.15).

It might be that the density of the fluorophore molecules in a liposome is so high that a 1:1 interaction with one unlabeled liposome is not sufficient to dequench the fluorophores completely. Then, the resulting increase in donor fluorescence is small. If we consider further fusion processes between liposomes that had already fused and unfused liposomes, the rate expression becomes more complicated. Assuming that k is constant for each fusion event regardless of the size of the fused liposomes, the rate becomes

$$r \sim c_{\text{labeled}}^i \cdot c_{\text{unlabeled}}^n \quad (4.2)$$

for a sequential process that results in a liposome consisting of i previously labeled and n previously unlabeled liposomes.

If we now assume that fluorophore dequenching only occurs if at least 2 unlabeled liposomes fuse with 1 labeled liposome and if we only take the processes with $i + n = 3$ into account (*i.e.* each liposome undergoes two fusion processes), then the rate for the fusion process contributing to the donor emission increase is

$$r_{\text{increase}} \sim c_{\text{labeled}} \cdot c_{\text{unlabeled}}^2 \quad (4.3)$$

For the two different concentration ratios that were experimentally probed, this model would yield

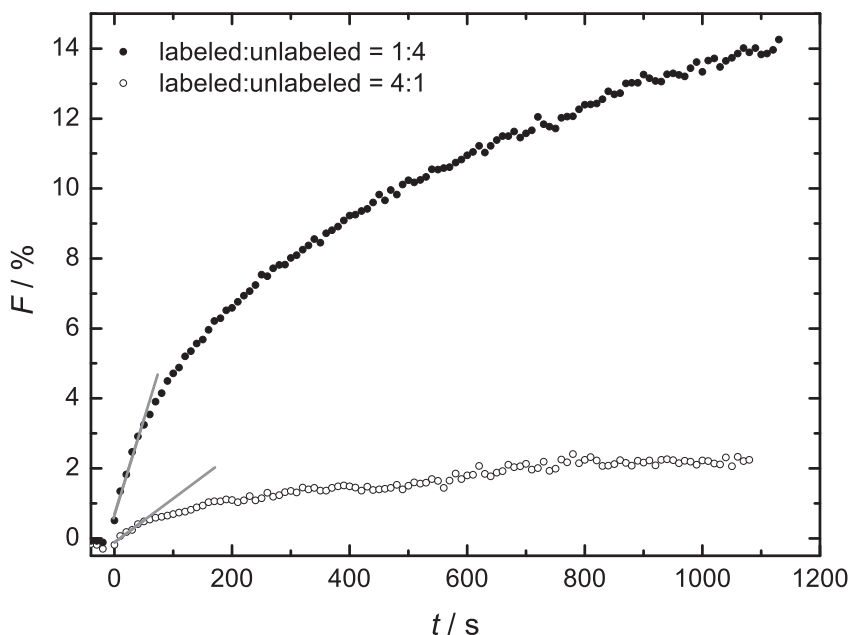


Figure 4.15. Comparison of fusion curves resulting from mixing labeled and unlabeled liposomes in a 1:4 ratio (●) and in a 4:1 ratio (○), respectively. The grey lines constitute the linear fit of the first six data points starting with the data point at $t = 0$ s. They are used as an aid to determine the initial slope of the fusion curves. Both assays were performed on the same day with liposomes containing **21** and **22** in a P/L ratio of 1:200. The amount of lipids in the lipid film was $2.5 \mu\text{mol}$.

$$\frac{r_{\text{increase},1:4}}{r_{\text{increase},4:1}} = \frac{c_{\text{labeled},1:4} \cdot c_{\text{unlabeled},1:4}^2}{c_{\text{labeled},4:1} \cdot c_{\text{unlabeled},4:1}^2} = \frac{1 \cdot 4^2}{4 \cdot 1^2} = \frac{4}{1}. \quad (4.4)$$

This resembles the experimentally found values. By comparing the initial slopes of both fusion curves (see indicated grey lines in Figure 4.15), we indeed find a ratio of around 4:1. However, the model presented above is certainly oversimplified since also processes with $i + n \neq 3$ will take place, the FRET depletion for processes with $i = 2$ and $n = 1$ is not zero, and the rate constant will depend on the liposomes' size. Nevertheless, a reasonable explanation for the observed concentration effects is that multiple fusion events per liposome likely take place. In addition, the analysis of the final diameter of fused liposomes as determined with DLS suggests that, in agreement with the conclusion discussed above, each liposome undergoes more than one fusion event (see Section 4.6).

4.4. Inner Lipid Mixing Assays

To investigate whether the inner leaflets are involved in the lipid mixing that was observed during TLM experiments, labeled liposomes were treated with a sodium dithionite solution, which reduces NBD molecules to non-fluorescent molecules (see Section 2.6.1 for a general description of ILM assays and Section 6.6.7 for experimental details). Dithionite does not cross the lipid membrane immediately, so that short-term exposure of liposomes to an excess of dithionite should keep the NBD fluorophores on the inner leaflets unimpaired. The distribution of NBD fluorophores between outer and inner leaflet has a ratio of roughly 60:40.^[19,202]

It was observed, however, that the decrease in NBD fluorescence upon dithionite addition did not stop at 60 % of its initial value but continued further. This was especially detected when the liposomes contained PNA/peptide hybrids. Peptides seem to make the liposomes permeable so that dithionite leaks into the liposomal lumen and reduces NBD fluorophores located on the inner leaflets as well. It was thus necessary to remove the dithionite as soon as all outer NBD fluorophores were reduced. It is likely that the membranes become leaky due to lipid reorganization during fusion.^[159] Reactive dithionite molecules would therefore penetrate into the liposomal lumen during fusion and falsify the experimental outcome. There are different methods described in literature for removing unreacted dithionite. One of the simplest is incubating the liposome sample with dithionite and waiting until the excess of dithionite is oxidized by ambient water and air, which is indicated to last at least 30 min.^[55,117] This is problematic, though, since within this time dithionite can penetrate through the membrane and reduce the inner NBD fluorophores as well. Another common method is the usage of a size exclusion column to separate dithionite from the liposomes.^[19,22,140] This was also tested in this thesis. A major drawback, however, was the loss of material as the vesicles run through the column. It was estimated via phosphate tests to be as high as 80 % for liposomes that were labeled, not reduced, contained peptides and were applied to the column as a concentrated solution with a small volume (100 μ L). In case liposomes did not carry any peptides the loss was lower. This observation suggests that the peptides on the surface let the vesicles stick to the column material preventing them from proper elution. If then only the dilution is considered but not the actual loss of lipid material on the column, far less liposomes are subjected to the subsequent ILM assay. This would clearly underestimate the extent of inner lipid mixing. Reduced liposomes were applied to the column in a higher volume (ca. 400 μ L). This was inevitable because it was necessary to monitor the reduction pro-

cess in a cuvette. Unfortunately, this led to highly diluted liposome fractions after the purification step. The phosphate test turned out to be insensitive if the phosphate content is very low. It was especially problematic when the sample was highly diluted with buffer as the conversion to inorganic phosphate was usually done with perchloric acid. The acid generated a suspension when added to diluted samples and a dark brown residue instead of a white residue resulted after the ashing process making the determination of the phosphate content impossible. An alternative phosphate assay,^[203] which uses sulfuric acid and hydrogen peroxide, was tested and found to be suitable for highly diluted samples. It was found to be less sensitive, though, so that it was not qualified to examine the low-concentrated samples that contained reduced liposomes either. Thus, as an alternative to the phosphate tests, liposome concentration was determined via the extent of the fluorescence of the Rh fluorophore upon excitation with $\lambda_{\text{ex}} = 573 \text{ nm}$. The fluorescence yield before the addition of dithionite and after the size exclusion chromatography was compared. In this way, a dilution factor can be calculated which is taken into account when setting the volume of labeled liposomes required for the ILM assays.

Removing dithionite via size exclusion chromatography is rather difficult and involves a high loss of liposome material. On top, additional errors result in the concentration determination. Therefore, another method was developed, which is fast and does not involve the size exclusion chromatography step. Dithionite was added to a small portion of labeled liposomes in the cuvette. The fluorescence decrease was monitored and as soon as it reached a value around 40 % of the starting value, oxygen was passed through the solution. This caused all remaining dithionite molecules to be oxidized within seconds. Afterwards, nitrogen was passed through the solution to outgas the sample in order to prevent unwanted oxidation of lipids. The liposomes treated in the way described above were then used in an ILM experiment. As the concentration of the liposomes does not change during this treatment, a reconfirmation of the concentration is not necessary.

As a validation of the described method, the following procedure according to Refs. [55] and [204] was used. Melittin⁴ was added to the partially reduced liposomes. It is known as a pore forming peptide, which makes membranes permeable for dithionite.^[205] Figure 4.16 shows two experiments.

In the first case, melittin is added to a sample of partially reduced liposomes without removing the residual dithionite (at point B as indicated in Figure 4.16). Here, a significant decrease in NBD fluorescence upon melittin addition was detected. This shows

⁴ The peptide melittin was synthesized using microwave assisted automated SPPS. A detailed description can be found in Sections 6.5.3 and 6.5.7.

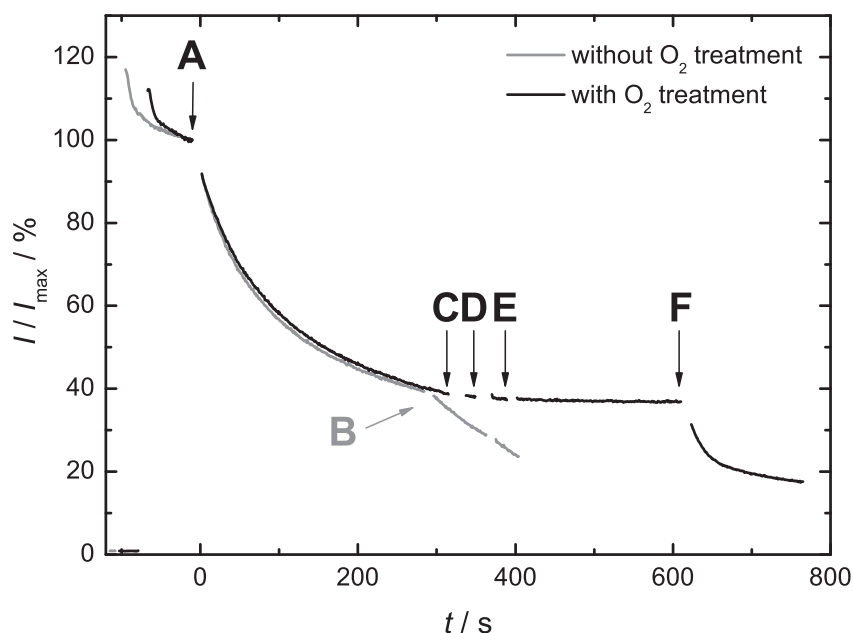


Figure 4.16. Melittin assay as a validation of the reduction process. The relative decrease in the intensity I of the NBD emission upon melittin addition in experiments without (grey) or with (black) treatment with oxygen is shown. The following substances were added: Dithionite (at points A and F), oxygen (C), nitrogen (D) and melittin (B+E). The experiments were performed with liposomes containing **16** in a P/L ratio of 1:200.

that the increased permeability of the liposomal membranes leads to a complete NBD reduction also on the inner leaflets. Hence, the amount of added dithionite is sufficient to reduce all NBD fluorophores on the outer leaflets. In a second experiment, melittin was added after the oxidation step (at point E). The fluorescence intensity did not drop, indicating dithionite had effectively been quenched. If then dithionite was added again, a significant decrease was visible confirming that melittin had formed pores and that now the fluorophores on the inner leaflets were reduced as well. Thus, stopping the dithionite treatment in point B enables quenching all outer leaflet fluorophores without reducing the NBD fluorophores in the inner leaflet.

The extent of mixing of the inner leaflets was investigated for liposomes containing PNA/peptide hybrids PNA3s-SxTMD (**15**) and PNA1s-SybTMD (**16**), PNA3s-SxTMD-NH₂ (**18**) and PNA1s-SybTMD-NH₂ (**19**), as well as Ala2-PNA3s-SxTMD (**21**) and Ala1-PNA1s-SybTMD (**22**). The peptide-to-lipid ratio needed to be increased to 1:200 for the ILM assays, as otherwise the obtained fluorescence yield was too small to be detected against the background. Unfortunately, the PNA/peptide hybrids containing ala-PNA in the C-terminal part of the recognition unit (**11 + 12** and **24 + 25**) could not be examined. The liposome stock solutions showed heavy precipitation directly after extrusion which



made it impossible to obtain reliable fusion curves. Figure 4.17 shows the determined inner lipid mixing fusion curves in comparison.

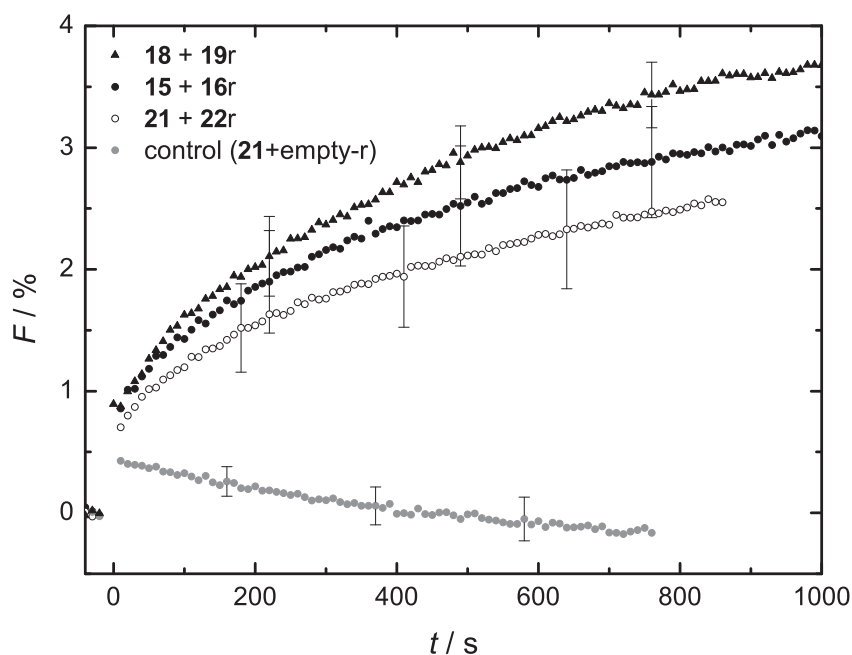


Figure 4.17. Mean fusion curves obtained from ILM assays with liposomes containing the peptide combinations **18 + 19** (\blacktriangle), **15 + 16** (\bullet), and **21 + 22** (\circ). The mean curve from the control measurement of **21 + 22** is shown as well (grey circles). Peptides that were incorporated in reduced liposomes are marked with an “r”. The peptide-to-lipid ratio was 1:200 in all cases.

For all tested peptide combinations, a significant increase in the NBD fluorescence was observed, which clearly differed from the results of the control measurements. Controls were performed with one liposome population lacking peptides. The fusion curves resulting from the control measurements were all very similar. As an example, the mean fusion curve of assays with unlabeled liposomes containing **21** and labeled liposomes lacking peptides is shown in Figure 4.17. Inner lipid mixing takes place with all investigated PNA/peptide hybrid combinations with the extent of inner lipid mixing being similar. The variation among fusion curves of single measurements is still quite high resulting in the large error bars shown in the plot. For liposomes bearing peptides with the additional ala-PNA recognition unit the extent of inner lipid mixing is tendentially lower. The curves thus show the same tendency as the TLM fusion curves (see Section 4.3.3). The ILM fusogenicity for the system containing **18 + 19**, which exhibit an amide terminus, is slightly higher compared to the systems with peptides containing a negatively charged carboxy terminus. Thus, the change of the C-terminus from acid to amide only has a



4. Fusion Assays

minimal influence on inner lipid mixing. This is contradictory to previous investigations on the influence of the C-terminus which showed a substantial enhancement of inner lipid mixing when peptides with an amide C-terminus were used.^[117]

When comparing the initial slope of the fusion curves it can be seen that the observed kinetics differ from previously reported data. Whereas Lygina *et al.*^[19] report a linear increase in lipid mixing, a saturation-curve-like increase can be seen in the plot of Figure 4.17 which is more similar to the fluorescence increase observed in the TLM experiments. It has to be noted that the PNA/peptide hybrids are different. In the case presented in this thesis, recognition units with five aeg-PNA monomers were used whereas Lygina *et al.* used decameric aeg-PNA sequences. The impact of this difference on total lipid mixing efficiency has already been discussed in Section 4.3.3. The impact on the ILM efficiency might be similar. In addition, the preparation procedure of reduced labeled liposomes was different. Lygina *et al.* employed the loss-making size exclusion chromatography step to remove excess dithionite.^[19] No information was given on the determination of the concentration of the liposomes after this step. Thus, it is conceivable that the concentration of labeled liposomes has not been properly adjusted resulting in a less pronounced increase in fluorescence intensity in the first minute of the ILM assays. A continuous linear increase in NBD emission was also discussed for the TLM assays described in Section 4.3. Accordingly, the linear increase in the ILM assays reported by Lygina *et al.* may also have a contribution from processes other than fusion events that lead to a dilution of the NBD fluorophore.

Summarizing, PNA/peptide hybrids with a pentameric aeg-PNA recognition unit were shown to be capable of outer and inner leaflet mixing. This is true regardless of an additional N-terminal ala-PNA in the recognition unit or different charge at the C-terminus. Compared with PNA/peptide hybrids containing a pentameric aeg-PNA sequence as the recognition unit, the extent of lipid mixing is slightly reduced when the recognition unit contains an additional ala-PNA sequence. Changing the C-terminus from negatively charged to neutral only slightly impacted the lipid mixing efficiency which is in contrast to observations made previously.^[19]

4.5. Fusion Monitored with Fluorescence Cross-Correlation Spectroscopy

The technique of fluorescence cross-correlation spectroscopy (FCCS) was employed as a further method to study the fusion of liposomes. With FCCS, a more detailed picture of liposome interaction can be obtained as it for example allows the quantitative determination of colocalized particles. Theoretical details were briefly described in Section 2.6.2. The following section depicts first experiments that were performed to explore the options of FCCS for studying model systems like those described in this thesis. FCCS measurements required one liposome population to be labeled with OG and another liposome population labeled with TR. The measurements were performed with LUVs, which were about 155 nm diameter in size (see Section 4.1). Most of the experiments were performed with liposomes containing peptides in a peptide-to-lipid ratio of 1:200. At this ratio, total lipid mixing quenching assays showed a significant increase in the acceptor emission (see Section 4.3.6).

The formation of large liposome aggregates was regularly observed in FCCS measurements. It resulted in very bright particles which caused the count rate detection of the avalanche photodiodes to exceed the upper limit. Thus, reliable information on cross-correlation or lifetime of these particles could not be obtained which is why the respective data points were not considered in the analysis.

The particle concentration was typically set to values around 0.5 particles at a time per focal volume. Compared to other applications of FCCS—for example the analysis of fusion of small unilamellar vesicles, which was performed with 5–30 particles per focal volume^[160]—this was a low value. It went along with an increased noise of the signal but it was necessary in order to prevent overload of the detectors.

Figure 4.18 shows the amount of cross-correlated particles, *i.e.* the cross-correlation, as a function of the time from an analysis of liposomes containing PNA3s-SxTMD (**15**) and PNA1s-SybTMD (**16**). Control measurements, in which either one or both liposome populations did not have any peptides incorporated, are shown as well. They were taken on the same day of the corresponding measurements using the same liposomes in order to ensure reliability and a good comparability of the data.

The cross-correlation when both liposome populations contain peptides (black curve in Figure 4.18a) was almost 100 % from the very beginning of the measurement. The time $t = 0$ s was the point at which mixing of the liposomes started. After around 15 s, data acquisition was initiated. Each data point is the average value of a 15 s measure-

4. Fusion Assays

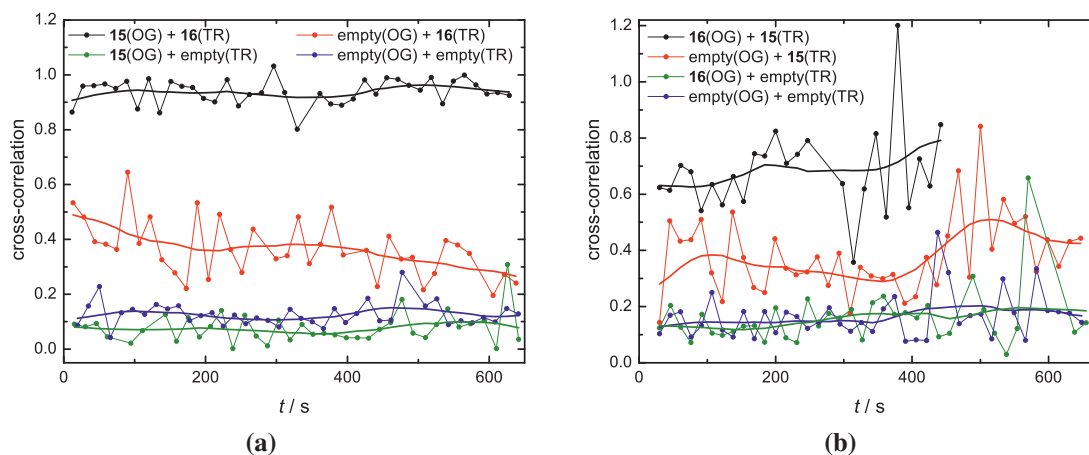


Figure 4.18. Time-dependent cross-correlation of liposomes containing **15** and **16**. (a) OG-labeled liposomes contained **15** and TR-labeled liposomes contained **16**; (b) OG-labeled liposomes contained **16** and TR-labeled liposomes contained **15**. Cross-correlation was measured for both liposome populations containing peptides (black); in the control measurements either none of the liposome populations (blue) or just one of the liposome populations contained peptides with either TR-labeled liposomes being without peptides (green) or the OG-labeled liposomes containing no peptides (red). For each data set, the weighted moving average was calculated (thick solid lines).

ment cycle and is showed at the end of the cycle resulting in the first data point to be displayed at around $t = 30$ s. The interaction between the liposomes thus happened in less than 30 s, which is too fast to be resolved. The control measurements showed a lower cross-correlation. When no peptides were present in both liposome populations, the cross-correlation was around 10 % indicating that no interaction takes place (green curve). The cross-correlation is not zero due to an unavoidable spectral cross-talk between the fluorophores. The same was true for the control measurement, in which only the OG-labeled liposomes contained peptides (blue curve). In the inversed case, when only TR-labeled liposomes contained peptides, the extent of cross-correlation was surprisingly high (averagely 40 %, red curve). A repetition of the assay with independently prepared liposomes samples yielded very similar results indicating that this unusually high extent of cross-correlation is significant. Possibly, peptide **16** interacts with the OG fluorophore leading to colocalized liposomes even if OG-labeled liposomes contained no peptides. When the labeling was reversed, meaning that OG-labeled liposomes contained **16** and TR-labeled liposomes contained **15**, the cross-correlation was not 100 % but rather 70 % on average (see Figure 4.18b). This reduced cross-correlation was confirmed with an independently prepared assay. It gives another hint that the OG fluorophore is involved in the liposome interaction. The cross-correlation of control measurements is only increased when the

4.5. Fusion Monitored with Fluorescence Cross-Correlation Spectroscopy

OG-labeled liposome population did not contain peptides. This shows that the incorporation of fluorophore-labeled lipids into membranes may disturb the liposome model system which has to be included in the interpretation of the FCCS measurements. Nevertheless, a comparison between the black and the red curves in Figure 4.18a and b shows that the specific interaction between the model peptides leads to a higher colocalization of liposomes than the interaction of the peptides with the fluorophore OG.

FCCS measurements were performed with liposomes containing the peptide combination **18** + **19** as well (see Figure 4.19a). These peptides have the same recognition unit as **15** + **16** but exhibit a neutral amide terminus instead of the negatively charged carboxy terminus. Previous studies showed a higher extent of lipid mixing for the amide terminus versions.^[117] The amount of cross-correlation was maximal from the beginning, and thus did not differ from experiments with **15** + **16** incorporated in the liposomes. All control measurements showed an average cross-correlation of 10–20 %. The measurement of OG-labeled liposomes lacking peptides and TR-labeled liposomes decorated with **19** was slightly increased compared to the other control measurements, thus showing the same tendency that was observed for the peptide combination **15** + **16** just described before.

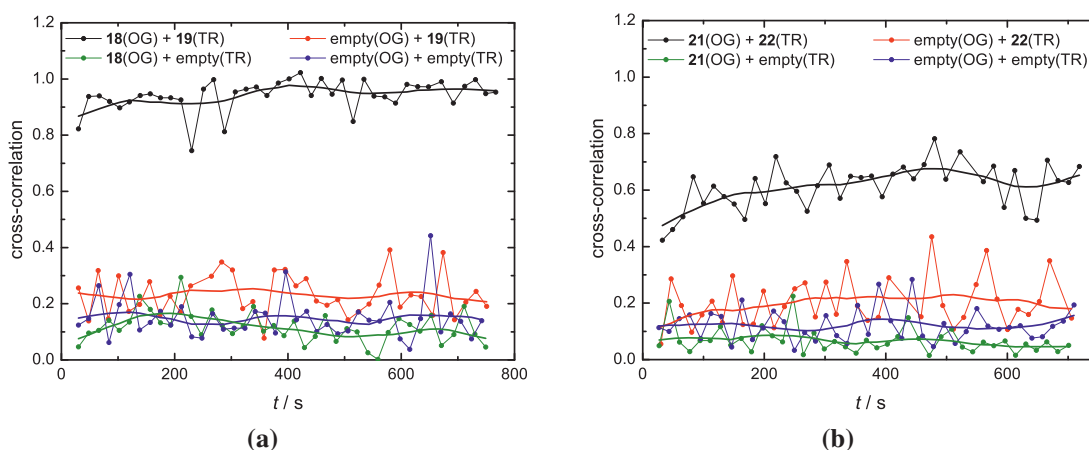


Figure 4.19. Time-dependent cross-correlation of liposomes containing **18** and **19** (a) or **21** and **22** (b). OG-labeled liposomes contained SxTMD-based peptides (**18** or **21**) and TR-labeled liposomes contained SybTMD-based peptides (**19** or **22**). The color code is the same as described in the caption of Figure 4.18.

Figure 4.19b shows the results of FCCS assays with liposomes containing Ala2-PNA3s-SxTMD (**21**) and Ala1-PNA1s-SybTMD (**22**). The cross-correlation was around 60 % and thus significantly lower compared to that of liposomes with **15** + **16** and **18** + **19**. The additional N-terminal ala-PNA part in the recognition unit of **21** + **22** seems to hinder

4. Fusion Assays

recognition and thus the colocalization of liposomes. The impeding influence of additional ala-PNA was also observed in TLM and ILM assays (see Sections 4.3.3 and 4.4). The lower extent of lipid mixing can therefore be explained by a lower extent of liposome interaction if ala-PNA is present in the recognition unit of the peptides.

The interaction of liposomes containing model peptides with a pure ala-PNA recognition unit was examined as well (see Figure 4.20a). The cross-correlation of OG-labeled liposomes with **12** and TR-labeled liposomes with **11** was approx. 70 % on average.

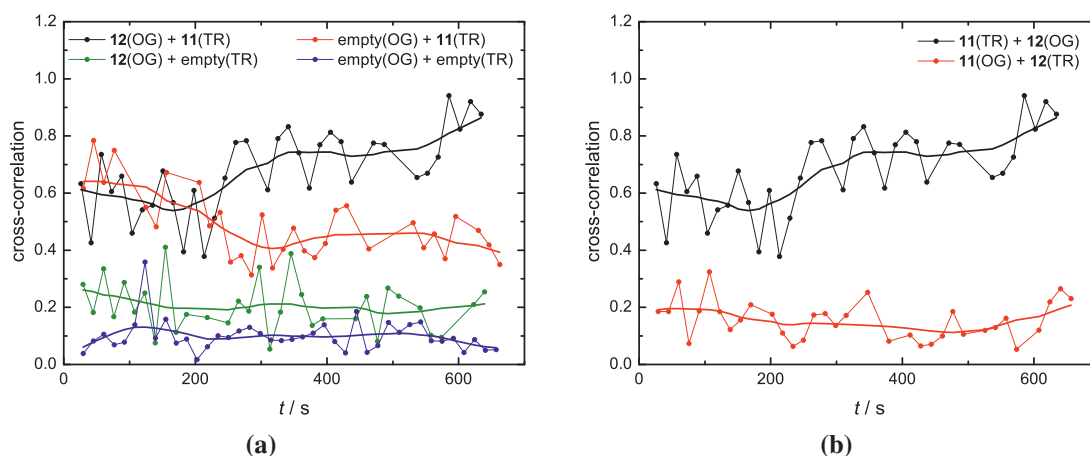


Figure 4.20. Time-dependent cross-correlation of liposomes containing **11** and **12**. (a) OG-labeled liposomes contained **12** and TR-labeled liposomes contained **11**. The color code is the same as described in the caption of Figure 4.18. (b) Changed order of labeling. OG-labeled liposomes contained **11** and TR-labeled liposomes contained **12** (red). For comparison, the results depicted in (a) in black are shown as well (black).

Is the liposome–liposome interaction in this case attributable to an exclusive interaction of the peptides? The results of two further measurements put this assumption into question. First, the control measurement of OG-labeled liposomes without peptides and TR-labeled liposomes containing **11** yielded an average cross-correlation of 50 % (red curve in Figure 4.20a). Despite of the fact that one liposome population contained no peptide and thus the binding partner of **11** was missing, interaction of the liposomes was very well detectable. Second, a measurement was performed in which the order of labeling in the liposomes was reversed meaning that OG-labeled liposomes contained **11** and TR-labeled liposomes were decorated with **12**. In this case, a low cross-correlation of averagely 15 % was observed (see red curve in Figure 4.20b). Considering that around 10 % cross-correlation is also observed when no interaction takes place due to cross-talk between the fluorophores, this is equatable to almost no interaction. Both measurements suggest an interaction of peptide **11** with the fluorophore OG. In the first case, this leads

4.5. Fusion Monitored with Fluorescence Cross-Correlation Spectroscopy

to liposome colocalization because **11** and OG are located on different liposome populations. In the second case, the interaction between the OG fluorophore and **11** would take place on the same liposome. Therefore, the amplitude of the cross-correlation is low because the fluorophore–peptide interaction might suppress the recognition between **11** and **12**.

A dependence on the fluorophore labeling of peptides **11** and **12** was also noted in TLM dequenching experiments in which the fluorophores NBD and Rh were used (see Section 4.3.4). When liposomes with **11** were mixed with labeled liposomes (NBD+Rh) lacking peptides, a dramatic increase in the donor emission was detected. Comparably, when mixing labeled (NBD+Rh) liposomes containing **11** with unlabeled liposomes containing **12**, no lipid mixing was observed suggesting that **11** rather interacts with one of the fluorophores than with the complementary recognition unit of peptide **12**. An interaction of **11** with the NBD or Rh fluorophore might explain why the kinetics observed in TLM experiments for peptides having a recognition unit with a C-terminal ala-PNA part differ from those with an N-terminal ala-PNA part (see Section 4.3.3). The above mentioned assumptions, however, need to be treated with caution and further experiments are necessary to confirm a possible fluorophore–peptide interaction.

Decreasing the peptide-to-lipid ratio went along with a reduction of the detectable cross-correlation and made it possible to detect the initial increase in liposome interaction. As an example, the results of a measurement of liposomes with peptides **15** and **16** are shown in Figure 4.21a. The cross-correlation increases up to a value of around 40 %. The scatter of the data points is quite high, but the difference to the control experiment (OG-labeled liposomes without peptides and TR-labeled liposomes with peptide **16**) is obvious. The peptide-to-lipid ratio therefore has a big influence on the extent of liposome interaction; the higher the peptide-to-lipid ratio the higher the extent of interaction. This is illustrated in Figure 4.21b in which the cross-correlation of liposomes containing **15** and **16** is compared at a high and a low peptide concentration.

In addition to the cross-correlation analysis, which provides information about the extent of interaction of the liposomes, the lifetime of the donor fluorophore OG was analyzed to obtain information about the type of interaction. In case of liposome fusion, FRET will take place expressed by a decrease of the donor fluorophore lifetime. Docking does not involve lipid mixing, but as the fluorophores are in close proximity at the docking site, the donor and acceptor fluorophore in this area can undergo FRET as well.^[206] As a consequence, there is a detectable FRET effect for docked vesicles. However, its intensity is lower compared to the intensity of FRET expected for fused liposomes.

4. Fusion Assays

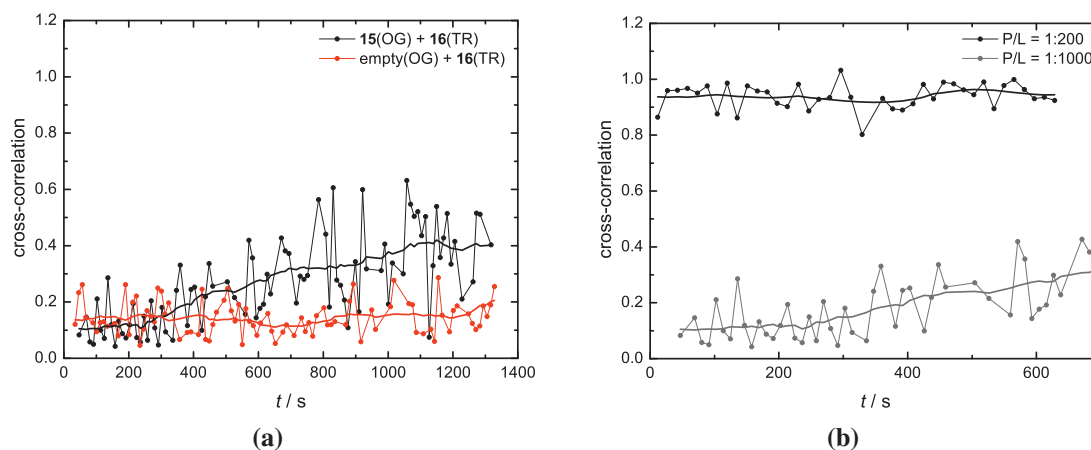


Figure 4.21. Influence of the peptide concentration on the cross-correlation. (a) Time-resolved cross-correlation of liposomes containing **15** and **16** in a P/L ratio of 1:1000. OG-labeled liposomes contained **15** and TR-labeled liposomes contained **16**. For comparison, a control measurement is shown as well (OG-labeled liposomes lacking peptides and TR-labeled liposomes containing **16**, red). (b) Comparison of the obtained cross-correlations for liposomes containing **15** and **16** at P/L ratios of 1:200 (black) and 1:1000 (grey).

As a test measurement, liposomes labeled with both OG (0.75 mol%) and TR (0.5 mol%) were examined. The usually applied molar ratio of the fluorophores was halved to reflect the concentrations in a liposome that arise out of the fusion of an OG-labeled liposome and a TR-labeled liposome. The lifetime of OG was determined to be 2.2 ns. The lifetime of OG in a liposome that was only labeled with OG was determined to be 3.9 ns which is in good accordance to values reported in literature.^[207] The lifetime of OG is thus significantly reduced in the doubly labeled liposome population confirming that FRET takes place.

Figure 4.22 shows the measured OG lifetimes in FCCS assays with liposomes containing **15** and **16**. The lifetime of OG decreases over time from (3.85 ± 0.06) ns to (3.71 ± 0.07) ns. This decrease is in contrast to the OG lifetimes obtained from all control measurements, which did not change in the monitored timespan.

The cross-correlation did not change but was maximal from the beginning (see Figure 4.18). Together with the fact that the OG lifetime did change, this suggests that docking, *i.e.* the colocalization of the liposomes, is fast and fusion, *i.e.* lipid mixing accompanied by FRET, is slower. The OG lifetime changes are small. In the limit of complete fusion, one might expect a more pronounced decrease as the lifetime of OG in liposomes containing the FRET pair was determined to be 2.2 ns. However, if the fusion is still incomplete, the lifetime decrease is expected to be small since only a small number of fluorophores in the

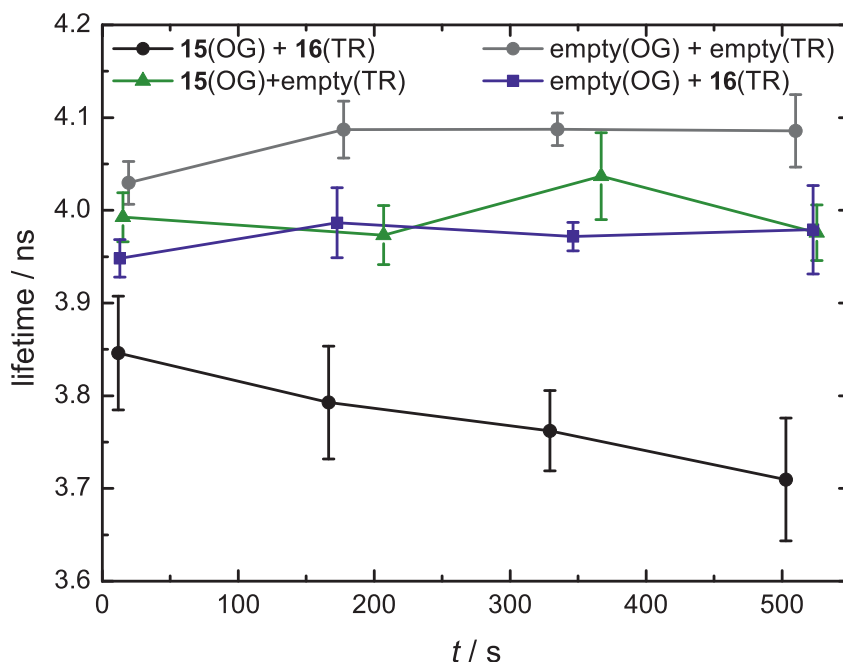


Figure 4.22. Measured OG lifetimes in the fusion reaction of liposomes containing **15** (OG-labeled) and **16** (TR-labeled) and in the respective control measurements. The P/L ratio was 1:200. All measurements were performed on the same day.

fused liposomes undergo FRET and an average lifetime of fused and not fused liposomes is obtained.

Summarizing, FCCS yields valuable information about the interaction of liposomes containing the model peptides. The extent of cross-correlation depends on the type of the recognition unit, thereby confirming the different extent of lipid mixing detected in TLM assays. The analysis of the OG lifetime gives first results about a possible fusion of the liposomes. Here, further studies are necessary to yield reliable data also on the effect of the other model peptides.

4.6. Fusion Monitored with Dynamic Light Scattering

Fusion of liposomes containing the PNA/peptide hybrids was also examined with dynamic light scattering (DLS). DLS allows monitoring the change in size and thus represents a complementary method to the above described lipid mixing assays, which cannot provide information on size change at all. In Section 2.6, the technique of DLS has been explained more detailedly.

4. Fusion Assays

DLS fusion assays were performed with the same liposome concentrations and ratios used for the lipid mixing assays (see Section 4.2) to ensure a good comparability between both assays. As it was technically not possible to stir the solution during the DLS measurements, the solution was stirred in between the measurements in a separate cuvette. Samples of 1 mL were taken from this cuvette at different points in time, measured and then transferred back as soon as the measurement was finished. The experimental procedure is detailedly described in Section 6.6.9.

Initially, it was checked whether the particle size changes within one population. After the liposomes had been extruded, DLS measurements were performed at different delays with respect to the extrusion. In Figure 4.23, the results are shown exemplarily for unlabeled liposomes containing Ala2-PNA3s-SxTMD (**21**).

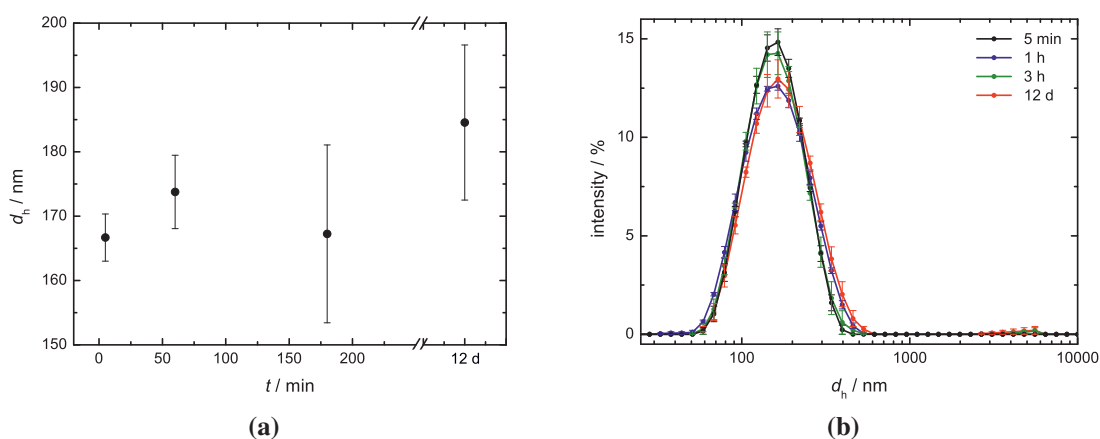


Figure 4.23. Change of the mean hydrodynamic diameter d_h of liposomes containing **21** at different delays with respect to the extrusion. Weighted mean average of the size distribution at 5 min, 1 hour, 3 hours and 12 days (a); plot of the appertaining mean size distributions (b). Liposomes were unlabeled and contained the peptide in a P/L of 1:200.

The mean diameter did not change significantly during the first three hours after extrusion. Only after several days a tendency towards higher diameters was visible, which is, however, a timespan irrelevant for fusion assays, which were always performed within an interval of minutes after extrusion of the liposomes. For labeled liposomes, the stability of the particle size was also checked and found to be similar to the described case (data not shown). This ensured that an increase in particle size after liposome mixing is not due to preceding unspecific aggregation within one population.

Monitoring the liposome fusion with DLS yielded reproducible data. The error bars shown in the plots in this section are based on measurements that were repeated two times with the identical sample. If independently prepared samples were used, however, the differences were only minor which confirms the reliability of this method. In Figure A.6

in the appendix, this is shown exemplarily for DLS assays with the peptide combinations PNA3s-SxTMD (**15**) and PNA1s-SybTMD (**16**) as well as PNA3s-SxTMD-NH₂ (**18**) and PNA1s-SybTMD-NH₂ (**19**).

In Figure 4.24, the results for mixing liposomes containing **18** and **19** are depicted. A significant increase in size was detected, which expectably differed from the respective control measurement in which the particle size stayed the same over time. This verified the validity of the control measurement, which was the same that was used in the lipid mixing assays monitored via fluorescence spectroscopy (see Section 4.2). The increase in size was large enough to be resolved by DLS which showed that DLS is a suitable method to monitor the fusion of liposomes decorated with the here investigated PNA/peptide hybrids.

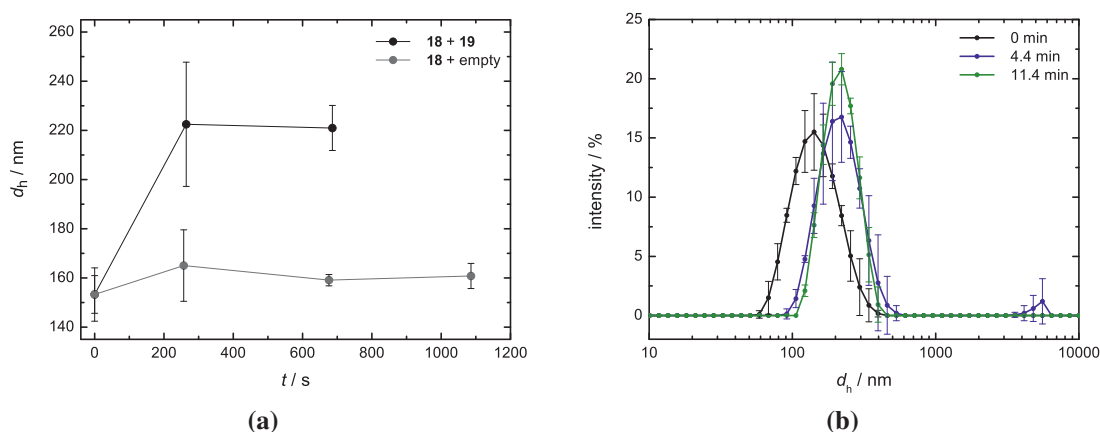


Figure 4.24. Fusion of liposomes containing **18 + 19** as monitored via DLS. (a) Mean hydrodynamic diameter of liposomes with **18** and **19** (●) and of the control measurement (grey circles). (b) The corresponding mean size distributions for **18 + 19** at the time points after mixing as indicated in the figure caption. The data points are connected via thin lines to guide the reader's eye. Liposomes were labeled with OG and TR and contained the peptides in a P/L ratio of 1:200.

A clear shift of the size distribution was observed as soon as **18** was added to **19** whereas in the control measurement, the size distribution is similar to the distribution shown in Figure 4.23 and constant over time (see Figure A.5 in the appendix). We see that the size distribution of the starting liposome population is narrow and monodisperse and that this did not change considerably when adding the second liposome population. The peak is rather shifted than broadened. This suggests that the starting material is consumed and largely converted to a monodispersely distributed target population. This interaction is too fast to be properly resolved by DLS and it is terminated after around 300 s as can be

4. Fusion Assays

seen in the size distribution measured at the third data point which barely differed from the data point before.

From Figure 4.24 it becomes clear that the fusion of liposomes with **18 + 19** leads to a mean diameter of around 220 nm. Assuming a spherical shape of the particles resulting from a complete liposome fusion, which is fair to assume on the basis of the total lipid mixing experiments of **18 + 19**, the number of liposomes that are combined to a larger particle can be estimated. The liposomal content is expressed by the volume of a sphere, $V = \frac{4}{3}\pi r^3$, and by comparing the volumes at radii of $r_{\text{start}} = 75$ nm and $r_{\text{end}} = 110$ nm one obtains that ≈ 3 liposomes fuse to one large liposome of the indicated final diameter. The number is in agreement with the estimated number of interacting liposomes containing peptides **21** and **22** made on the basis of TLM assays (see Section 4.3.7). Of course this interpretation has to be treated with caution since it is possible that liposomes in intermediate states are present in the sample as well. Those have a higher diameter than fused liposomes and thus lower the proportion of completely fused liposomes. On top, they do not exhibit a spherical shape and it is unclear whether DLS gives a reliable diameter for these particles.

In Figure 4.25 the peptide combination **18 + 19** is compared with the combination **15 + 16** at different peptide-to-lipid ratios. These combinations have the same recognition unit but differ in the C-terminus.

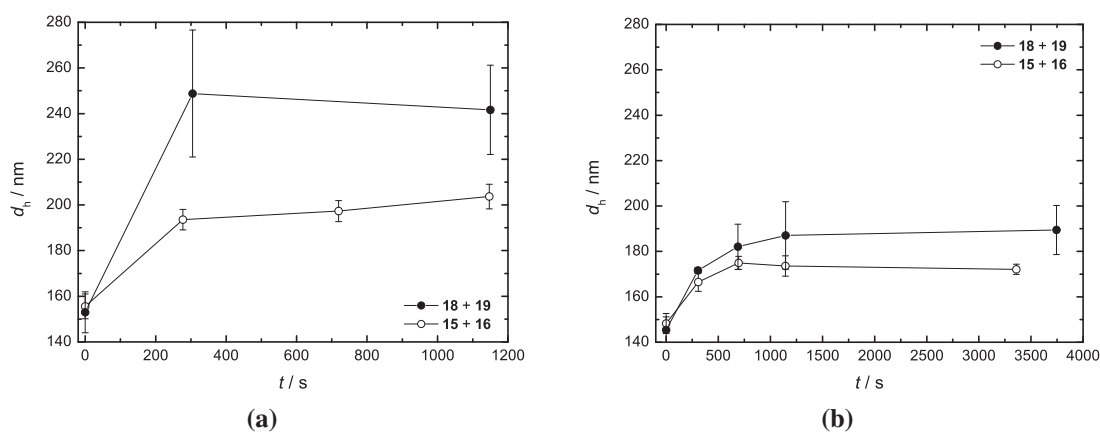


Figure 4.25. Change of the mean diameter in DLS assays with liposomes containing peptides **18 + 19** (●) and **15 + 16** (○) at P/L ratios of 1:200 (a) and 1:1000 (b). The data points are connected with thin lines to guide the reader's eye. Liposomes labeled with OG and TR were used.

From Figure 4.25a and 4.25b it can be seen that the combination **18 + 19** leads to larger particles compared to **15 + 16**. This is the case for high and low peptide-to-lipid ratios.

4.6. Fusion Monitored with Dynamic Light Scattering

However, the difference between the combinations is less pronounced at a P/L ratio of 1:1000. Also, it becomes clear that a high P/L ratio of 1:200 generally leads to larger particles than a low P/L ratio of 1:1000. This goes along with the observations made in TLM experiments, which showed that a higher P/L ratio achieved a higher extent of lipid mixing (see Section 4.3.1). The results are also consistent with the results obtained from the FCCS analysis. FCCS revealed that the amount of colocalized particles directly depends on the peptide concentration (see Figure 4.21 in Section 4.5)—the higher the P/L ratio, the higher the amount of interacting liposomes. Thus, DLS measurements allow the conclusion that in the case of the examined PNA/peptide hybrids a higher extent of lipid mixing and a higher amount of colocalized particles implies the generation of larger particles.

The plots nicely show that at a ratio of 1:200 the maximum size is achieved already at the second data point, so within the very first minutes after mixing. Due to the fact that the acquisition of one data point lasted about 230 s, it was not possible to lower the time resolution further, so that only a rough estimation can be made here. Liposomes with a peptide-to-lipid ratio of 1:1000, however, distinctly show a slower increase in size. Here, it lasts around 700 s until the maximal size is reached. This is likely a matter of concentration. The lesser the amount of interacting peptides the longer it takes until the reaction is finished. The resulting particles are larger if the liposomes contain a higher density of peptides which suggests that those liposomes fuse, or at least aggregate, more often.

In the TLM dequenching assays, a continual increase in NBD emission was visible, suggesting progressive lipid mixing. On the basis of these results, one would also expect a continuous increase in size, which is obviously not the case. The results obtained from DLS are more in line with results from TLM quenching assays and from FCCS analyses, which both suggest that the interaction of the liposomes is terminated after several minutes. They strengthen the hypothesis that the steady NBD emission increase is rather due to unspecific interactions than due to real fusion events.

The change in size was additionally monitored for a longer period than the usual 20 min. Figure 4.25b shows that the mean diameter almost did not change after the first 20 min after the liposomes had been mixed. This timespan thus is sufficient to detect all important features.

As already discussed in Section 4.3, TLM assays showed an unexpected behavior of liposomes containing the peptide combination Ala2-SxTMD (**11**) and Ala1-SybTMD (**12**) at a high peptide-to-lipid ratio. Mixing unlabeled liposomes containing **11** with labeled

4. Fusion Assays

liposomes lacking peptides led to a high increase of the donor emission, indicating a high extent of lipid mixing. To examine this more closely, DLS measurements were performed under the same conditions as applied in TLM assays. Figure 4.26 summarizes the changes in size when liposomes containing **11** were mixed with liposomes lacking peptides. The liposomes without peptides are either labeled or unlabeled. For comparison, the result of an experiment in which both of the liposome populations were without peptides is also plotted.

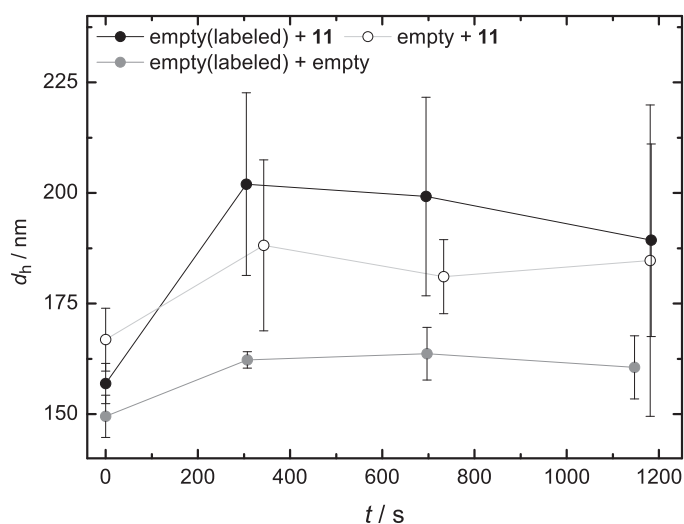


Figure 4.26. Change of the mean diameter in DLS assays when liposomes containing peptide **11** were mixed with liposomes lacking peptides. The liposomes without peptides were either labeled (●) or unlabeled (○). The result of a control measurement in which both liposome populations were without peptides is shown as well (grey circles). The P/L ratio in the liposomes was 1:200, labeled liposomes contained NBD and Rh.

The increase in size is highest in the case liposomes containing **11** were mixed with labeled liposomes lacking peptides (filled black circles). In the other two cases the increase is small and not as significant as in the first case. Thus, liposomes containing **11** seem to interact more strongly with labeled liposomes than with unlabeled liposomes (compare filled black circles with open circles in Figure 4.26). This leads to liposome aggregation resulting in a detectable increase in the particles' size. The observation made with the DLS assays allows drawing the same conclusion as from the results of TLM assays as well as FCCS assays, namely peptide **11** likely interacts with fluorophores.

5. Conclusions

In this thesis, SNARE-mimicking model peptides with artificial PNA hybrid recognition units were developed. The PNA hybrid recognition units are composed of alanyl (ala)-PNA and *N*-(2-aminoethyl)glycine (aeg)-PNA. The two PNA types exhibit different backbone structures due to which they feature different duplex topologies and thus different duplex formation rates. By combining both of them within one recognition unit, a directed duplex formation of the PNA hybrid recognition unit was intended to be achieved. With this, the SNARE analogues aimed at mimicking the assumed SNARE zippering which is thought to start at the N-termini of the SNARE motifs and to proceed in a zipper-like fashion towards the C-termini.

The model peptides were synthesized by using Fmoc-based solid-phase peptide synthesis. The synthesis started with assembling the native TMD sequence of either Synaptobrevin-2 or Syntaxin-1A, which were supposed to anchor the model peptides in the membrane of liposomes. Following this, the PNA monomers were attached step by step following an adjusted protocol. Purification of the model peptides was a challenging task. A variety of parameters in HPLC and SEC was tested but none of them was successful so that raw peptides were used for the fusion assays. In total, 20 model peptides were synthesized. Model peptides of the first generation featured a decameric aeg-PNA sequence, while the recognition unit of those of the second generation comprised a pentameric aeg-PNA sequence. Those model peptides of the second generation which were most intensively investigated are displayed in Figure 5.1.

First, the fusogenicity of the model peptides was comprehensively studied in total lipid mixing (TLM) and inner lipid mixing (ILM) assays. It was shown in this work that both quenching and dequenching assays are important to understand the fusion process and to provide complementary information. Quenching assays were more precise in indicating the peptide interaction kinetics; dequenching assays, in turn, offered a possibility to estimate the fraction of fused liposomes. A combination of the SNARE analogues **15** and **16** with pentameric aeg-PNA recognition units on opposite liposomes turned out to be the most fusogenic one. N-terminal elongation of the aeg-PNA pentamer with another

5. Conclusions

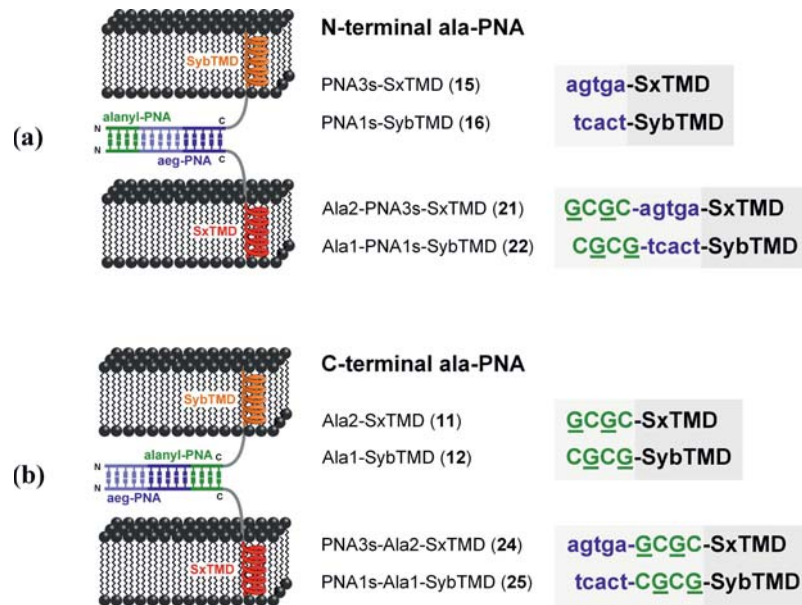


Figure 5.1. The model peptides designed and investigated in this thesis contain a PNA hybrid recognition unit attached to the TMDs of the neuronal SNAREs Syntaxin-1A (SxTMD) or Synaptobrevin-2 (SybTMD). The PNA hybrid recognition unit is made of aeg-PNA (blue) and ala-PNA (green) with the ala-PNA sequence being attached either N-terminally (a) or C-terminally (b) to the aeg-PNA part. The sequences of the principal model peptides of the second generation are given in detail.

five aeg-PNA monomers or an ala-PNA tetramer (as in peptides **21** and **22**) reduced the fusogenicity. ILM assays showed that **15** + **16** as well as **21** + **22** cause inner leaflet mixing as well. This observation as well as the observation that changing the C-terminal charge from negative to neutral did not have a large impact on the fusogenicity is in contradiction to previous observations made with peptides containing a decameric aeg-PNA sequence.^[19,117] Peptides **11** and **12** with a recognition unit made of an ala-PNA tetramer were significantly less fusogenic than those made of an aeg-PNA pentamer. Adding the aeg-PNA pentamer N-terminally to the ala-PNA recognition unit as in peptides **24** and **25** resulted in a complete loss in the fusogenicity of the respective peptides. TLM assays with liposomes containing peptides **11** and **12** indicated an interaction between peptide **11** and fluorophores. FCCS analyses came to the same conclusion. This shows that fluorophores as probes for the detection of fusion have to be used with care since they can disturb the system that is to be examined.

Selected peptide combinations were subjected to additional fusion assays in order to obtain a differentiated picture on the fusogenicity of the model peptides. Investigations with FCCS revealed that the degree of interaction between liposomes depended signifi-

cantly on the type of incorporated peptides. The cross-correlation, *i.e.* the colocalization of the liposomes, was high for liposomes containing peptides **15** and **16**, lower for liposomes containing **21** and **22** and very low for peptides **11** and **12**. Thus, the different lipid mixing efficiencies observed in the TLM assays are explainable by the different degrees of interaction of the liposomes. By analyzing fluorescence lifetimes, FCCS assays indicated that in liposomes decorated with peptides **15** and **16** fast docking of liposomes precedes lipid mixing.

DLS assays provided additional information on the size change of the liposomes during fusion. In agreement with FCCS assays, they revealed that the interaction between liposomes is fast because the maximum size change was achieved already within the first minutes of the experiments. Assuming full fusion, DLS results were used to estimate the stoichiometry of interacting liposomes. Like the results of the TLM dequenching assays, they suggested that liposomes containing peptides with a pentameric aeg-PNA recognition unit undergo more than one round of fusion.

Taken together, the techniques applied in this thesis provide a detailed picture on the fusogenicity of the investigated model peptides. The results obtained from the various fusion assays complement each other. Just applying one technique would not have been sufficient to fully characterize the fusion behavior of the model peptides. For instance, TLM assays were a reasonable starting point to obtain a general overview on the fusogenicity of the peptides. However, it was necessary to perform further assays to specify the results in greater detail. The fusion curves obtained from TLM dequenching assays did not describe the kinetics of liposome interaction properly. To this end, fusion curves obtained from TLM quenching assays were more accurate. With TLM assays it was not possible to gain information on the different intermediate states in liposome fusion. As a reasonable alternative, ILM assays and FCCS assays were performed, which provide information on whether liposomes decorated with the peptides of interest were in a docked, hemifused or fully fused state. As none of the techniques provided information on the size, liposomes were investigated by using dynamic light scattering (DLS). DLS is a valuable supplement to the techniques described above; however, it does not allow distinguishing between different fusion intermediates which is why the other techniques are needed as well.

The results of the different fusion assays show that the investigated SNARE model peptides are capable of membrane fusion. However, the model peptides do not provide the minimal structural requirements needed to mimic the SNARE zippering. In the preceding master thesis it was shown that duplex formation between the PNA hybrid oligomers



5. Conclusions

is possible and both PNA types contribute to it;^[176] however, the energy released from duplex formation may not be properly converted into a force acting on the TMDs and the membranes. Due to the high topological difference between linear ala-PNA and the helical transmembrane domain, ala-PNA may act as a spacer if it is attached C-terminally to aeg-PNA sequence in the recognition unit. In case it is attached N-terminally to the aeg-PNA sequence, it prevents fast recognition of aeg-PNA which is why peptides **20** and **21** show similar fusion kinetics compared to peptides **15** and **16** but a reduced fusogenicity.

The peptides with pentameric aeg-PNA recognition units were shown to exhibit a high fusogenicity. The effort to synthesize them is considerably reduced compared with peptides with a decameric PNA sequence. This is accompanied by a significant increase in the purity of the raw peptides. Therefore, peptides **15** and **16** constitute efficient alternatives to the previously presented model peptides based on a decameric aeg-PNA sequence.^[19,117] Up to now, the influence of the lipid composition of the membrane on the fusogenicity of the model peptides has not systematically been examined. The lipid composition, however, likely is an essential parameter that will affect the fusogenicity. In this thesis, it has been shown that the lipid DOPS has a substantial impact on the extent of lipid mixing. Lipids like PIP₂ or cholesterol are assumed to be involved in SNARE mediated membrane fusion as well.^[128,132] A systematic investigation will allow elucidating the role of the membrane environment and fine-tuning the fusion capacity of the SNARE analogues. It is also conceivable to apply them in purified synaptic vesicles which will allow studying the influence of a native membrane environment on the fusogenicity of the SNARE analogues. On top, as these peptides specifically interact via bioorthogonal recognition units they can be applied in native systems in which membrane fusion is desired without interfering with natively occurring processes.



6. Experimental Section

6.1. General Equipment and Methods

Solvents and Reagents. The solvents were of grade *pro analysi* (*p.a.*), those of technical grade were purified by means of distillation prior to use. Solvents for HPLC and spectroscopic measurements were of HPLC grade. To obtain ultrapure water (especially for HPLC applications and buffer solutions), demineralized water (supplied by an inhouse technique) was purified using either a *Simplicity* water purification system by *Merck Millipore* (Billerica, USA) or an *arium mini* lab water system by *Sartorius* (Göttingen, Germany). Commercially available reagents were purchased from different suppliers and corresponded to the highest purity available. PNA monomers were obtained from *ASM Research Chemicals* (Hannover, Germany). For solid-phase peptide synthesis, resins by *Novabiochem* (Merck KGaA, Darmstadt, Germany) were used. Amino acids were purchased from *GL Biochem(Shanghai) Ltd.* (Shanghai, China) or from *IRIS Biotech GmbH* (Marktredwitz, Germany). Lipids labeled with Oregon Green 488 and Texas Red were supplied by *molecular probes* (Eugene, USA). All other phospholipids were purchased from *Avanti Polar Lipids, Inc.* (Alabaster, USA).

Freeze-Drying. Aqueous samples were carefully frozen with liquid nitrogen and dried under reduced pressure (< 1 mbar) using an *Alpha-2-4-LD plus* benchtop freeze-dryer from *Christ* (Osterode am Harz, Germany). Small amounts (< 2 mL) were freeze-dried using a mounted *RVC 2-18* centrifuge by *Christ*.

Mass Spectrometry. Electrospray ionization (ESI) mass spectra were recorded at a *maXis* spectrometer by *Bruker Daltonik GmbH* (Bremen, Germany). Data was analyzed with the *Compass DataAnalysis* software (version 4.0) by *Bruker*. For sample preparation, PNA/peptide hybrids were dissolved in TFE and mixed with MeOH (HPLC grade) in a 1:1 ratio. Other peptides and compounds were dissolved in ultrapure water, acetonitrile (HPLC grade) or MeOH. 10 % formic acid was added in each case and the sample



6. Experimental Section

was injected to the mass spectrometer the same day. For each compound, the mass-to-charge (m/z) ratio is indicated, along with the relative intensity of the peak expressed as percentage. Deconvoluted ESI mass spectra as well as the measured ESI mass spectra are shown for selected peptides. All peaks attributable to the respective target peptide are labeled. For high-resolution mass spectrometry (HR-MS) results, the calculated (calc.) as well as the experimentally found peaks are indicated.

Matrix assisted laser desorption/ionization (MALDI) spectra were recorded with an *autoflex speed* MALDI-TOF spectrometer by *Bruker Daltonik GmbH* (Bremen, Germany). For sample preparation, approx. 0.5 mL of the sample to be analyzed was mixed with the same volume of the matrix directly on the MALDI target plate (polished steel, reusable). The matrix was a saturated solution of sinapinic acid in water. Measurements were taken within one hour after the solvent had evaporated.

Statistical Calculations. If measurements were performed repeatedly, usually the mean value was calculated and presented in the plots. Errors were calculated from the standard deviation of the mean multiplied by the respective t -value (from Student's t -distribution). The following Equation 6.1 was used to calculate the error f .

$$f = t_{95\%} \cdot \sqrt{\frac{1}{n-1} \sum_{i=1}^n (x_i - \bar{x})^2} \quad (6.1)$$

In this equation, n is the number of measurements, x_i is the data point of measurement i and \bar{x} is the mean. The t -values are based on a two-sided 95 % confidence interval and were included to compensate for the uncertainty of the measured value due to a low number of measurements. Data were plotted as $\bar{x} \pm f$.

Software. The software for acquisition of the data is indicated each time. For drawing chemical structures and calculation of molecular masses, *ChemBioDraw* (version 13) was used. Figures and schemes were created with *Inkscape* (version 0.84). The SNARE core complex in Figure 2.5 (Section 2.4.2) was created using the *UCSF Chimera* package (version 1.11.2). Chimera is developed by the Resource for Biocomputing, Visualization, and Informatics at the University of California, San Francisco (supported by NIGMS P41-GM103311).^[78] NMR spectra were analyzed with *MestReNova* (version 6). Graphs were plotted with *OriginPro* (version 8.5G).



6.2. Chromatographic Methods

Flash Chromatography. Flash silica gel with a grain size of 40–63 μm by *Merck KGaA* (Darmstadt, Germany) was used as the column material. The crude products were mixed with a small amount of silica gel (typically three times the weight of the sample) and an appropriate solvent, and the solvent was removed on a rotary evaporator. Afterwards, they were loaded as a dry powder onto the pre-packed silica column. The column was run at an overpressure of about 0.5 bar. The dimensions of the column are indicated for each synthesis.

Thin Layer Chromatography (TLC). For TLC, silica gel 60 F254 plates by *Merck KGaA* (Darmstadt, Germany) were used. The samples were detected via fluorescence deletion at 254 nm. Alternatively, the developed plate was immersed into an appropriate reagent and subsequently heated until spots became visible.

High Performance Liquid Chromatography (HPLC). For HPLC analysis, mainly an HPLC system by *JASCO* (Tokio, Japan) was used, equipped with an *MD-2010* diode array detector, two *PU-2085* semi-micro pumps, a *CO-2060* column thermostat and an *AS-2055* autosampler. Alternatively, HPLC runs were performed on an *ÄKTA basic 10* system by *Amersham Pharmacia Biotech* (Umeå, Sweden), equipped with a *P-900* pump module and a *UV-900* UV detection module. The peptides were detected at wavelengths of 215 nm, 260 nm and 280 nm if not otherwise indicated. The used solvents are listed below.

Solvent A	$\text{H}_2\text{O} + 0.1\% \text{ TFA}$
Solvent B	$\text{MeCN} + 0.1\% \text{ TFA}$
Solvent C	$\text{MeOH} + 0.1\% \text{ TFA}$
Solvent D	formic acid/ H_2O = 2:3
Solvent E	formic acid/1-propanol/TFE = 8:1:1

The employed analytical HPLC columns are listed below. Columns with Nucleodur and Nucleosil phases were from *Macherey-Nagel* (Düren, Germany), the column with a Jupiter phase was from *phenomenex* (Aschaffenburg, Germany) and the column with a Kromasil phase was from *AkzoNobel* (Amsterdam, Netherlands). In case compounds were purified on a large scale, semi-preparative columns were used with the identical column material.



6. Experimental Section

Column 1	Nucleodur, C-18ec, 250 x 4.6 mm, 100 Å, 5 µm
Column 2	Nucleosil, C-18, 250 x 4.0 mm, 100 Å, 10 µm
Column 3	Nucleosil, C-4, 250 x 4.6 mm, 120 Å, 5 µm
Column 4	Kromasil, C-8, 100 x 4.6 mm, 100 Å, 5 µm

The type and length of the applied gradient as well as the used column material are indicated in each case. The flow rates were 1 mL/min for analytical runs, and 3 mL/min for semi-preparative runs. If not otherwise stated, analyses were performed at room temperature.

Size Exclusion Chromatography (SEC). SEC was performed on the *ÄKTA basic 10* system equipped as described above. The column was a *Superose 12 10/300 GL* by *GE Healthcare* (Little Chalfont, UK). The eluent was a phosphate buffer (50 mM NaH₂PO₄, 50 mM Na₂HPO₄, 150 mM NaCl, pH = 7.0) with addition of 2 % SDS or 30 % MeCN. The sample was dissolved in the eluent. The separation was performed isocratically at a flow rate of 0.5 mL/min and a maximal pressure of 3 MPa. Prior to ESI-MS analysis, SDS was removed from the sample following a protocol described by Puchades *et al.* (chloroform/methanol/water extraction).^[185]

6.3. Spectroscopic Methods

Nuclear Magnetic Resonance (NMR) Spectroscopy. ¹H-NMR spectra were recorded at 300 MHz with a *Mercury-VX 300* or a *VNMRS-300* spectrometer by *Varian* (Palo Alto, California, USA). ¹³C-NMR spectra were recorded at 126 MHz with an *INOVA-500* spectrometer by *Varian*. The utilized deuterated solvents are indicated with each compound. The residual proton signals of the solvents served as an internal standard ($\delta = 2.50$ ppm (¹H-NMR) and $\delta = 39.5$ ppm (¹³C-NMR) for DMSO-*d*₆; $\delta = 7.26$ ppm (¹H-NMR) and $\delta = 77.16$ ppm (¹³C-NMR) for CDCl₃). The sample temperatures were 35 °C for DMSO-*d*₆ and 27 °C for CDCl₃. Chemical shifts δ are given in ppm, coupling constants *J* are given in Hertz (Hz). For description of the types of coupling, the following abbreviations are used: s (singlet), *s*_{br} (broad singlet), d (doublet), dd (doublet of doublets), t (triplet), m (multiplet).

UV Absorption Spectroscopy. UV absorption of a sample was measured with a *V-550* spectrometer from *JASCO* (Tokio, Japan) using the *Spectra Manager* software (version 1.54.03) provided by the manufacturer. Black quartz glass cuvettes from *Hellma Analytics*

(Müllheim, Germany) with 10 mm light path were used. The sample volume was 500 μL . To determine the concentration of a stock solution, 5 μL of this solution was mixed with 495 μL acetonitrile (HPLC grade). A blank sample with 5 μL of the solvent used for the stock solution was also prepared. The absorption was determined either at 260 nm (for sequences containing nucleobases) or at 280 nm (for purely peptidic sequences). The temperature was set to 25 $^{\circ}\text{C}$, the scanning speed was 200 nm/min with fast response and 2.0 nm bandwidth. Typically, the absorption was monitored over 30 s and the mean value was calculated. The concentration c was determined using the Beer–Lambert law (see following Equation 6.2).

$$c = \frac{A_{\text{sample}} - A_{\text{blank}}}{\epsilon \cdot d}, \quad (6.2)$$

with A_{sample} and A_{blank} being the measured mean absorption of the sample and the blank, respectively, ϵ being the molar extinction coefficient and d being the light path of the cuvette. The extinction coefficient was estimated from the sum of all contributing units in the respective molecule. In Table 6.1, the used values for ϵ are listed.

Table 6.1. The extinction coefficients ϵ of each contributing unit that were used to estimate the overall ϵ values of the peptides or PNA/peptide hybrids. Values marked with an asterisk (*) were estimated from the depicted plot in the indicated reference.

unit	$\epsilon / (\text{L} \cdot \text{mol}^{-1} \cdot \text{cm}^{-1})$	$\lambda_{\text{abs}} / \text{nm}$	Ref.
a	13700	260	[208]
c	6600	260	[208]
G	11700	260	[208]
t	8600	260	[208]
Trp	5500	280	[209]
	3300*	260	[210]
Tyr	1490	280	[209]
	600*	260	[210]
Phe	145*	260	[211]

The values for a, c and t have been determined directly for the aeg-PNA monomers; the indicated value for g is based on the determined value for the corresponding nucleotide.^[208] For the ala-PNA monomers C and G, the listed values for c and g were assumed.

Fluorescence Spectroscopy. Fluorescence spectroscopy was performed using an *FP-8200* fluorospectrometer from *JASCO* (Tokio, Japan). Quartz glass cuvettes from *Hellma*

6. Experimental Section

Analytics (Müllheim, Germany) were used, which had a light path of 10 x 4 mm (excitation: 10 mm, emission: 4 mm) and were equipped with a magnetic stirrer. The temperature was controlled with an *ETC-272T* peltier thermostat by *JASCO* connected to a *Thermo Haake WKL26* water recirculator by *Thermo Electron Corp.* (Waltham, USA). Data was acquired with the *Spectra Manager* software (version 1.54.03) provided by the manufacturer.

For lipid mixing experiments, the temperature was set to 25 °C and the stirring speed to ca. 900 rpm. Band widths of excitation and emission detection channels were both set to 5 nm. The sensitivity was set to “high” and data pitch was 1 nm. In case OG was used as the donor fluorophore in dequenching fusion assays, the sensitivity was set to “medium”. The scanning speed in the spectrum measurement mode was 125 nm/min with fast response. In the time course measurement mode, the response was set to 1 s and the recording time to 1200 s. The wavelengths for excitation and emission were adjusted to the respective used fluorophores. The following table summarizes excitation and emission wavelengths for the fluorophores used in this thesis.

Table 6.2. Excitation and emission wavelengths used in this thesis for the different FRET fluorophores.

type of fluorophore	λ_{ex}	λ_{em}
NBD	460 nm	530 nm
Rh	573 nm	585 nm
OG	501 nm	525 nm
TR	592 nm	607 nm

6.4. Synthesis of the Alanyl-PNA Building Blocks

The synthetic procedures of the building blocks described in this section are modifications of procedures described in the indicated references. Compared with Ref. [176], the syntheses were developed further and several additions were made. For instance, the determination of enantiomeric excess values was included. Though this section involves reproducing some protocols in the indicated references, a detailed description of the experimental procedures is given for the sake of completeness.

6.4.1. Determination of Enantiomeric Purity

Determination of the enantiomeric purity of the synthesized ala-PNA monomers was performed according to a protocol originally described by Manning and Moore^[212] and modified by Lohse^[213] for Boc-protected alanyl nucleic amino acids. The procedure for Fmoc-protected building blocks was developed on the basis of this protocol. Both methods are described in the following.

The Fmoc-protected building block (approx. 5 μmol , 1.00 eq) was weighted into a 5 mL round bottom flask. 500 μL of a solution of piperidine in DMF (20 % (v/v)) was added and the mixture was stirred for 30 min. Then, the solvent was removed *i. vac.* until the contents of the flask were completely dry. For Boc-protected alanyl nucleic amino acids, the building block (5 to 7 μmol , 1.00 eq) was dissolved in TFA (250 μL). After stirring the solution for 10 min, TFA was removed completely in a nitrogen stream.

The residue was subsequently suspended in 350 μL demineralized H_2O and 350 μL aqueous NaHCO_3 solution ($c = 1.2 \text{ M}$, $\text{pH} = 9$). Boc-L-Ala-OSu (6.00 eq) was dissolved in 700 μL THF and was added to the suspension. The resulting solution was stirred for at least 5 h at ambient temperature. After that, TFA (10 % in H_2O) was added to yield a pH of 2.5. The reaction mixture was filtrated and analyzed via HPLC (see Section 6.1 for technical details). For this, solvents A and B and column 1 (see Section 6.2) were used. The gradient was 10 \rightarrow 50 % solvent B in 30 min for guanine containing monomers and 10 \rightarrow 60 % solvent B in 30 min for cytosine containing monomers. A prerun of 1 min was slotted ahead of each gradient except for the Fmoc-D-AlaG-OH monomer. The peak areas of the absorption bands at 260 nm were used to calculate the enantiomeric excess (ee) according to the following Equation 6.3:

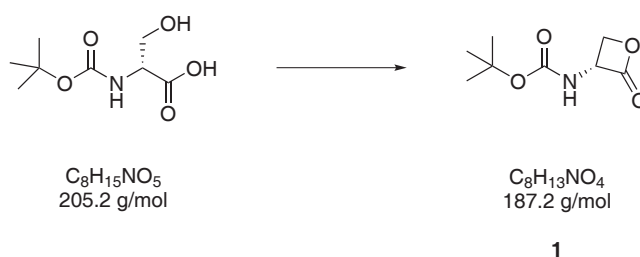
$$\text{ee} = \frac{|A_1 - A_2|}{A_1 + A_2} \quad (6.3)$$

6. Experimental Section

In this equation, A_1 is the area of the peak in the HPLC chromatogram belonging to the target compound and A_2 is the area of the peak belonging to its diastereomer. Assignment of the peaks was done by subjecting the other enantiomer of the alanyl-PNA building block to the procedure described above. For example, Fmoc-D-AlaC(Z)-OH was reacted with Boc-L-Ala-OSu to determine the retention time of Boc-L-Ala-D-AlaC(Z)-OH. Four HPLC chromatograms are shown as an example in the appendix (see Section A.1).

6.4.2. Detailed Synthetic Procedures

Boc-D-Serine β -Lactone (**1**)^[177]



Triphenylphosphine (6.46 g, 24.6 mmol, 1.01 eq) was dissolved in dry THF (100 mL) under an argon atmosphere. The solution was cooled to -70 °C. DEAD (3.98 mL, 24.6 mmol, 1.01 eq) was added dropwise within 10 min. The solution was stirred for another 10 min at -70 °C. Boc-D-serine (5.00 g, 24.4 mmol, 1.00 eq) was dissolved in dry THF (24 mL) and added dropwise within 25 min. The solution was stirred for 15 min at -30 °C and for 3 h at room temperature. The solvent was removed *in vacuo*. Purification was done via flash column chromatography ($l = 11$ cm, $d = 8$ cm, *n*-pentane/ethyl acetate = 3:1 \rightarrow 2:1). On a TLC plate, the product could be detected as a bright yellow spot on a blue background after staining with a solution of bromocresol green (0.04 % in ethanol). Compound **1** (2.47 g, 13.2 mmol, 54 %) was obtained as a white solid.

TLC (*n*-pentane/EtOAc = 2:1): $R_f = 0.45$.

$^1\text{H-NMR}$ (300 MHz, CDCl_3): δ (ppm) = 1.44 (s, 9 H, Boc- CH_3), 4.41-4.45 (m, 2 H, CH_2), 5.04-5.11 (m, 1 H, CH), 5.51-5.53 (m, 1 H, NH).

$^{13}\text{C-NMR}$ (126 MHz, CDCl_3): δ (ppm) = 28.3 (Boc- CH_3), 59.6 (CH), 66.7 (CH_2), 81.4 (Boc-C), 154.7 (OC(O)NH), 169.7 (Boc-CO).

MS (ESI): m/z (%) = 210.1 (39) $[\text{M}+\text{Na}]^+$, 397.2 (18) $[2\text{M}+\text{Na}]^+$, 562.2 (5) $[3\text{M}+\text{H}]^+$.

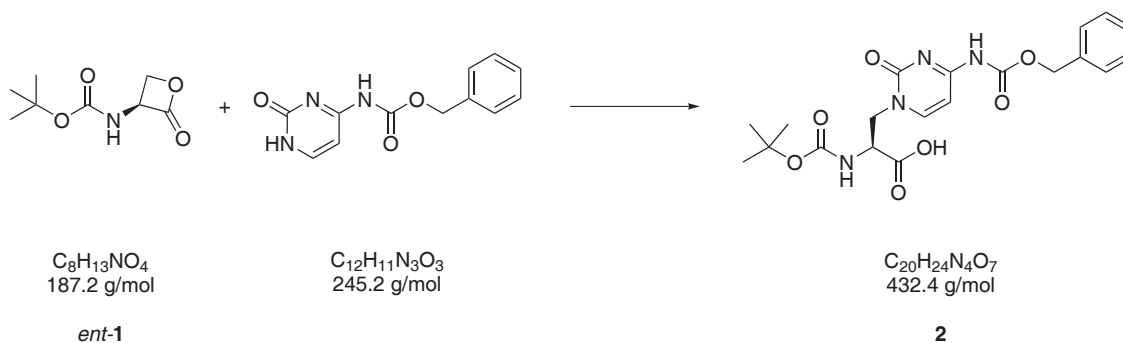
HR-MS (ESI): calc. for $\text{C}_8\text{H}_{13}\text{NO}_4$ ($[\text{M}+\text{Na}]^+$) 210.0737, found: 210.0739.



Boc-L-Serine β -Lactone (*ent*-1)^[177]

Boc-L-serine β -lactone (*ent*-1) was synthesized like compound **1**, starting however from Boc-L-serine. The synthesis yielded a white solid (1.60 g, 8.55 mmol, 35%). The recorded NMR spectrum and the recorded mass spectrum agree with the spectra recorded for the enantiomeric Boc-D-serine β -lactone (**1**, see Section 6.4.2).

Boc-L-AlaC(Z)-OH (**2**)^[26]



At room temperature, *N*4-Z-cytosine (4.19 g, 17.1 mmol, 2.00 eq) was suspended in dry DMSO (20 mL) under an argon atmosphere. DBU (1.91 mL, 12.8 mmol, 1.50 eq) was added dropwise. Afterwards, a solution of compound *ent*-1 (1.60 g, 8.55 mmol, 1.00 eq) was added dropwise as well. After stirring for 3.5 h, the reaction was terminated by the addition of glacial acetic acid (732 μL , 769 mg, 12.8 mmol, 1.50 eq). The solvent was coevaporated with DMF. The residue was suspended in MeOH (30 mL) and sonicated for 5 min. Unreacted *N*4-Z-cytosine was filtered off and washed with MeOH. The solvent was removed from the combined filtrates and the crude product was purified twice via flash column chromatography ($l = 23$ cm, $d = 5.5$ cm, ethyl acetate/MeOH = 4:1 with acetic acid gradient 0 \rightarrow 1 %). The product (3.14 g, 7.26 mmol, 85%, ee = 99%) was obtained as a white solid.

TLC (EtOAc/MeOH = 4:1, 0.5 % acetic acid): $R_f = 0.16$.

$^1\text{H-NMR}$ (300 MHz, DMSO- d_6): δ (ppm) = 1.23 (s, 9 H, Boc-CH₃), 4.04-4.12 (m, 2 H, β -CH₂), 4.45 (dd, $J = 12.9, 3.8$ Hz, 1 H, α -CH), 5.16 (s, 2 H, Z-CH₂), 6.05-6.16 (m, 1 H, Boc-NH), 6.86 (d, $J = 6.0$ Hz, 1 H, cytosine 5-H), 7.31-7.38 (m, 6 H, Z-CH), 7.85 (d, $J = 7.2$ Hz, 1 H, cytosine 6-H), 10.6 (s_{br} , 1 H, COOH).

$^{13}\text{C-NMR}$ (126 MHz, DMSO- d_6): δ (ppm) = 28.1 (Boc-CH₃), 52.9 (β -CH₂), 53.6 (α -CH), 66.4 (Z-CH₂), 77.8 (Boc-C), 93.5 (cytosine C-5), 127.3-128.4 (Z-CH₂), 136.0 (Z-

6. Experimental Section

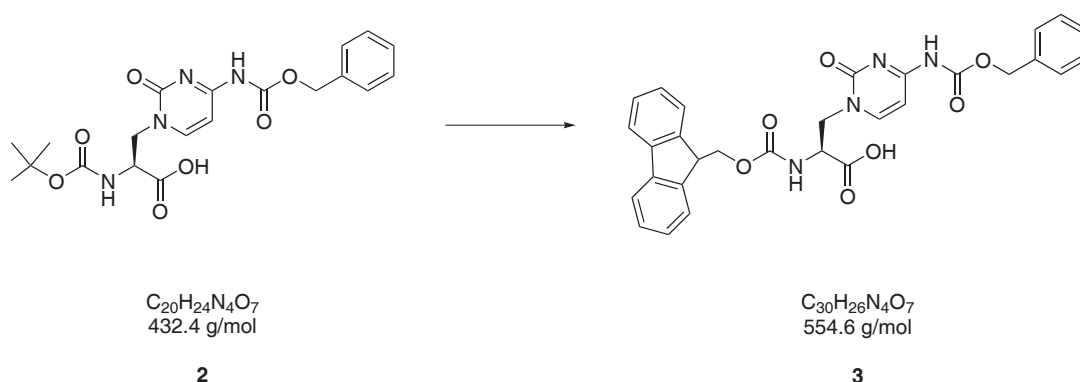
CH₂), 150.1 (cytosine C-6), 153.2 (Z-CO), 154.9 (cytosine C-2), 155.2 (Boc-CO), 162.4 (cytosine C-4), 171.6 (COOH).

MS (ESI): *m/z* (%) = 433.2 (69) [M+H]⁺, 455.2 (100) [M+Na]⁺, 865.3 (9) [2M+H]⁺, 887.3 (12) [2M+Na]⁺.

HR-MS (ESI): calc. for C₂₀H₂₅N₄O₇ ([M+H]⁺): 433.1718, found: 433.1722;

calc. for C₂₀H₂₄N₄O₇Na ([M+Na]⁺): 455.1537, found: 455.1540.

Fmoc-L-AlaC(Z)-OH (**3**)^[181]



Compound **2** (2.00 g, 4.62 mmol, 1.00 eq) was suspended in 1,4-dioxane (4 mL) and HCl (4 M in 1,4-dioxane, 12 mL, 4.80 mmol, 1.04 eq) was added. The mixture was stirred for 5 h and afterwards the solvent was removed *in vacuo*. Completeness of deprotection was confirmed via ESI-MS.

MS (ESI): *m/z* (%) = 333.1 (100) [M+H]⁺, 355.1 (41) [M+Na]⁺, 665.3 (21) [2M+H]⁺, 687.2 (15) [2M+Na]⁺.

HR-MS (ESI): calc. for C₁₅H₁₆N₄O₅ ([M+H]⁺): 333.1193, found: 333.1193;

calc. for C₁₅H₁₆N₄O₅: ([M+Na]⁺) 355.1013, found: 355.1000.

The residue was suspended in aqueous Na₂CO₃ solution (9% (w/v), 6 mL) and H₂O (14 mL) to yield a pH value of 9. The mixture was cooled to 0 °C and a solution of Fmoc-OSu (1.39 g, 4.11 mmol, 0.890 eq) in 1,4-dioxane (6 mL) was added. It was sonicated at 0 °C for 40 min and stirred at room temperature for 6 h. After lyophilization, purification was done via flash column chromatography (*l* = 12 cm, *d* = 7.5 cm, acetone/MeOH = 4:1, with H₂O gradient 0 → 7%). The desired product (1.57 g, 2.83 mmol, 61%, ee = 99%) was obtained as a white solid.

TLC (acetone/MeOH = 4:1, 4 % H₂O): $R_f = 0.51$.

HPLC (column 1, 20 → 100 % B in 30 min): $t_R = 13.0$ min.

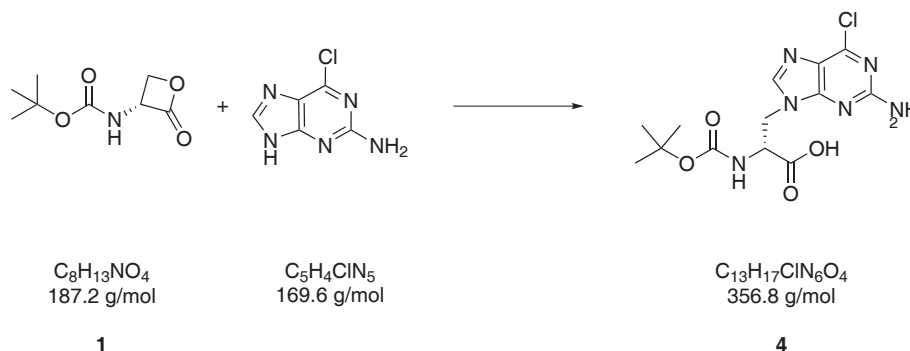
¹H-NMR (300 MHz, DMSO-*d*₆): δ (ppm) = 3.58-3.69 (m, 1 H, α -CH), 4.06-4.22 (m, 4 H, β -CH₂, Fmoc-CH₂, Fmoc-C_{sp³}H), 4.52 (dd, $J = 12.9$ Hz, 3.8 Hz, 1 H, β -CH₂), 5.13 (s, 2 H, Z-CH₂), 6.55 (*s_{br}*, 1 H, NH), 6.84 (d, $J = 7.1$ Hz, 1 H, cytosine 5-H), 6.99 (d, $J = 8.5$ Hz, 1 H, Fmoc-CH), 7.28-7.36 (m, 8 H, Fmoc-CH, Z-CH), 7.59-7.64 (m, 2 H, Fmoc-CH), 7.85 (d, $J = 7.2$ Hz, 2 H, Fmoc-CH), 7.96 (d, $J = 7.1$ Hz, 1 H, cytosine 6-H), 10.6 (*s_{br}*, 1 H, COOH).

¹³C-NMR (126 MHz, DMSO-*d*₆): δ (ppm) = 46.8 (Fmoc-C_{sp³}H), 52.3 (β -CH₂), 54.4 (α -CH), 66.5 (Z-CH₂), 66.6 (Fmoc-CH₂), 93.6 (cytosine C-5), 120.0 (2 Fmoc-CH), 127.0-128.9 (6 Fmoc-CH, 5 Z-CH), 135.8 (Z-C), 140.5 (cytosine C-6), 142.5 (2 Fmoc-C), 143.7 (2 Fmoc-C), 153.1 (Z-OC(O)NH), 155.1 (cytosine C-2), 155.7 (Fmoc-OC(O)NH), 162.5 (cytosine C-4), 171.9 (COOH).

MS (ESI): m/z (%) = 553.2 (100) [M-H]⁻.

HR-MS (ESI): calc. for C₃₀H₂₅N₄O₇ ([M-H]⁻): 553.1729, found: 553.1730.

Boc-D-Ala(2-amino-6-chloropurin-9-yl)-OH (**4**)^[26]



2-Amino-6-chloropurine (1.58 g, 9.33 mmol, 1.30 eq) was suspended in dry DMSO (6.6 mL) under an argon atmosphere at room temperature. DBU (1.17 mL, 1.19 g, 7.84 mmol, 1.10 eq) was added dropwise yielding a dark yellow solution. Stirring was continued for 10 min, then a solution of compound **1** (1.34 g, 7.16 mmol, 1.00 eq) in DMSO (5.5 mL) was added within 15 min. After stirring for 5.5 h, the reaction was stopped by the addition of glacial acetic acid (450 μ L, 473 mg, 7.87 mmol, 1.10 eq). The solvent was coevaporated with DMF. Purification was done via flash column chromatography ($l = 11$ cm, $d = 7.5$ cm, ethyl acetate/MeOH = 4:1 with acetic acid gradient 0 → 1.25 %) and yielded the product (1.14 g, 3.20 mmol, 45 %, ee = 96 %) as a white solid.

6. Experimental Section

TLC (EtOAc/MeOH = 4:1, 1 % acetic acid): $R_f = 0.24$.

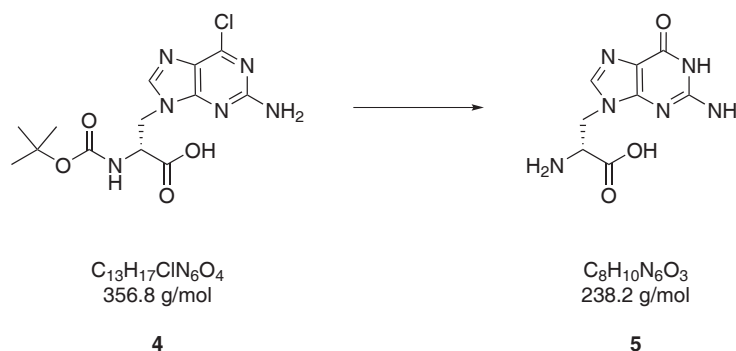
$^1\text{H-NMR}$ (300 MHz, DMSO- d_6): δ (ppm) = 1.03-1.25 (m, 9 H, Boc-CH₃), 4.12-4.32 (m, 2 H, β -CH₂), 4.51 (dd, $J = 13.5, 3.9$ Hz, 1 H, α -CH), 6.35 (*s_{br}*, 1 H, NH), 6.78-6.86 (m, 2 H, NH₂), 7.95 (s, 1 H, 8-H).

$^{13}\text{C-NMR}$ (126 MHz, DMSO- d_6): δ (ppm) = 28.0 (Boc-CH₃), 44.5 (β -CH₂), 53.6 (α -CH), 78.1 (Boc-C), 123.3 (guanine C-5), 143.5 (guanine C-8), 149.1 (guanine C-4), 154.3 (guanine C-2), 155.0 (OC(O)NH), 159.7 (guanine C-6), 171.7 (COOH).

MS (ESI): m/z (%) = 357.1 (99) [M+H]⁺, 379.1 (100) [M+Na]⁺, 713.2 (16) [2M+H]⁺, 735.2 (24) [2M+Na]⁺.

HR-MS (ESI): calc. for C₁₃H₁₈ClN₆O₄ ([M+H]⁺): 357.1073, found: 357.1068;
calc. for C₁₃H₁₇ClN₆O₄Na ([M+Na]⁺): 379.0892, found: 379.0882.

H₂N-D-AlaG-OH (5)



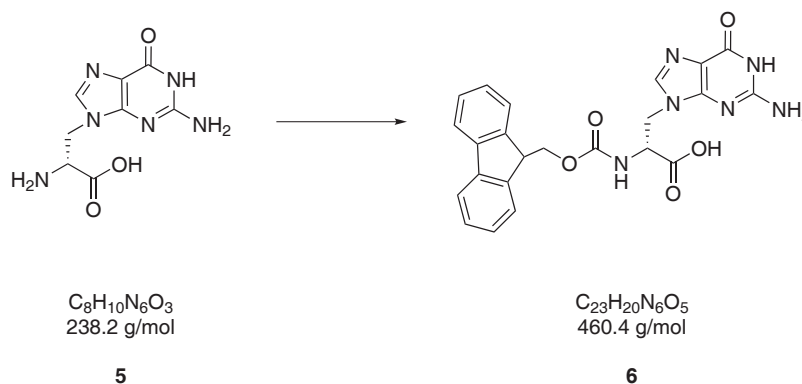
Method A.^[181] Compound **4** (1.14 g, 3.20 mmol, 1.00 eq) was dissolved in TFA/H₂O (3:1, 13 mL) and stirred for 4 days. The solvent was coevaporated with toluene. The mixture was suspended in H₂O and two times in HCl (1 M in H₂O) and the solvent was evaporated to dryness each time. The reaction proceeded quantitatively and the product was confirmed via ESI-MS. The crude product was used without further purification.

Method B. Compound **4** (1.00 g, 2.80 mmol, 1.00 eq) was mixed with an aqueous HCl solution (4 M, 30 mL) and stirred for 2 days at room temperature. The solvent was removed *in vacuo*. The reaction proceeded quantitatively and the product was confirmed via ESI-MS. The crude product was used without further purification.

MS (ESI): m/z (%) = 239.1 (100) [M+H]⁺, 261.1 (15) [M+Na]⁺, 477.2 (7) [2M+H]⁺, 499.2 (8) [2M+Na]⁺.

HR-MS (ESI): calc. for $C_8H_{11}N_6O_3$ ($[M+H]^+$): 239.0887, found: 239.0886.

Fmoc-D-AlaG-OH (6)^[181]



The reaction mixture of compound **5** (1.00 g, 2.80 mmol, 1.00 eq) was suspended in an aqueous solution of Na_2CO_3 (9 % (w/v), 5.5 mL) and H_2O (9 mL) to yield a pH value of pH = 9. The suspension was cooled to 0 °C and Fmoc-OSu (843 mg, 2.50 mmol, 0.893 eq) in 1,4-dioxane (3.6 mL) was added dropwise. The reaction mixture was sonicated for 10 min at 0 °C and then stirred at room temperature for 7 h. Afterwards, the suspension was lyophilized. Purification was performed via flash column chromatography ($l = 12$ cm, $d = 8$ cm, acetone/MeOH = 4:1, with H_2O gradient 0 → 8 %) and yielded the desired compound (336 mg, 0.730 mmol, 26 %, ee = 93 %) as a white solid.

TLC (acetone/EtOAc = 4:1, 4 % H_2O): $R_f = 0.42$.

HPLC (column 1, 30 → 50 % B in 30 min): $t_R = 11.7$ min.

1H -NMR (300 MHz, $DMSO-d_6$): δ (ppm) = 3.93-4.23 (m, 5 H, α -CH, β -CH₂, Fmoc-CH₂, Fmoc- $C_{sp^3}H$), 4.50 (d, $J = 10.6$ Hz, 1 H, β -CH₂), 6.80-8.87 (m, 3 H, NH₂, NH), 7.30 (t, $J = 7.3$ Hz, 2 H, Fmoc-CH), 7.39 (t, $J = 7.3$ Hz, 2 H, Fmoc-CH), 7.55 (s, 1 H, 8-H), 7.61-7.64 (m, 2 H, Fmoc-CH), 7.85 (d, $J = 7.4$ Hz, 2 H, Fmoc-CH), 11.4 (s, 1 H, COOH).

^{13}C -NMR (126 MHz, $DMSO-d_6$): δ (ppm) = 44.9 (β -CH₂), 46.6 (Fmoc- $C_{sp^3}H$), 55.9 (α -CH), 65.6 (Fmoc-CH₂), 109.8 (C-5), 120.0 (2 Fmoc-CH), 121.4 (2 Fmoc-CH), 127.6 (2 Fmoc-CH), 129.0 (2 Fmoc-CH), 140.6 (guanine C-8), 142.6 (2 Fmoc-C), 143.8 (2 Fmoc-C), 151.5 (guanine C-4), 153.9 (guanine C-2), 155.7 (Fmoc OC(O)NH), 157.2 (guanine C-6), 173.0 (COOH).

MS (ESI): m/z (%) = 459.2 (100) $[M-H]^-$.

HR-MS (ESI): calc. for $C_{23}H_{19}N_6O_5$ ($[M-H]^-$): 459.1422, found: 459.1422.



6.5. Peptide Synthesis

6.5.1. Loading of First Amino Acid

Loading a Rink Amide Resin. Rink amide resins were loaded employing standard peptide coupling methods as for example described in Ref. [214]. A portion of the unloaded Rink amide MBHA resin (0.38 mmol/g) was swollen in NMP. The Fmoc-protection group was removed with piperidine (20 % in NMP, *v/v*) by shaking the resin for 2 x 5 min at room temperature. The resin was washed (3 x NMP, 3 x DCM, 3 x NMP). Then, the Fmoc-protected amino acid (5.0 eq) was added to a solution of HOBt (4.9 eq) in NMP (750 μ L) and the mixture was dissolved with the help of a sonicator. DIC (4.9 eq) was added and the mixture was directly transferred to the resin. Coupling was performed under microwave irradiation (40 °C, 20 W, 10 min) by using a *Discover* microwave by *CEM* (Matthews, North Carolina, USA). The resin was washed (3 x NMP, 3 x DCM, 3 x NMP) and the coupling step was repeated. After further washing, the Kaiser test (see Section 6.5.2) was performed to confirm successful loading. In case of successful loading, a final capping step was carried out to eliminate possible residual free amino functionalities. The resin was shaken with $\text{Ac}_2\text{O}/2,6\text{-lutidine}/\text{NMP}$ (1:2:7, *v/v/v*) for 2 x 5 min, thoroughly washed afterwards, and dried in a desiccator.

Loading a Wang Resin (Loading Density < 0.2 mmol/g). The reaction was based upon the procedure described in Ref. [215] and modified to obtain the low loading density. The reaction was carried out at room temperature and in an argon atmosphere. The dry NovaPEG Wang resin (0.89 mmol/g) was swollen in dry DCM for 1 h in a dry flask. The Fmoc-protected amino acid (0.50 eq) was dissolved in dry DCM and a few drops of dry THF or dry DMF. 1-Methyl imidazole (0.38 eq) was added, followed by MSNT (0.50 eq). The dark yellow solution was transferred to the resin and the mixture was gently shaken for 90 min. Then, the resin was transferred into a *Discardit II* syringe (BD syringe) by *Becton Dickinson* (Heidelberg, Germany) and washed thoroughly with DMF and DCM. After washing with diethylether, the resin was dried in a desiccator. The loading density was determined according to the description in Section 6.5.2. Afterwards, a capping step was performed to cap free hydroxyl functionalities. For this, the resin was shaken with a solution of benzoic anhydride (5.0 eq) and pyridine (1.0 eq) in DMF for 50 min, washed subsequently with DMF, DCM and ether, and dried in a desiccator.



6.5.2. Determination of Resin Loading

The resin loading was determined qualitatively by employing the Kaiser test (for free amino groups) or the methyl red/diphenyldichlorosilane test (for free hydroxy groups) and quantitatively by measuring the UV absorption of dibenzofulvene, which is the Fmoc cleavage product.

Kaiser Test.^[216] For the colorimetric determination of free primary amino groups, a few resin beads were transferred into a small glass vial. The Kaiser test solutions consisted of ninhydrin in ethanol (0.05 g/mL), phenol in ethanol (4 g/mL) and 1 μ M aqueous KCN solution in pyridine (2:98, *v/v*). Three drops of each solution were added in the mentioned order to the resin beads. Mixing was achieved through gentle swivelling and the mixture was then heated to 120 °C for 5 min. Free primary amino groups were indicated by a blue solution whereas an orange-brownish solution indicated a negative testing.

Methyl Red/Diphenyldichlorosilane Test.^[217] For colorimetric determination of free hydroxyl groups, dry triethylamine (10 % in dry DMF, 200 μ L) was added to the dry resin (5 mg). Diphenyldichlorosilane (100 μ L) was added and the mixture was left to stand for 10 min. The solution was removed and the resin was washed several times with dry triethylamine (10 % in dry DMF). Subsequently, methyl red (0.75 % in DMF, 300 μ L) was added. After 10 min, the solution was removed and the resin was washed with DMF and DCM until the washing solution was colorless. A positive test was indicated by orange/red colored resin beads.

UV Absorption of Dibenzofulvene.^[218] The resin (ca. 5 mg) was weighted into a volumetric flask and 2 mL of a solution of DBU in DMF (2 %, *v/v*) was added. The flask was gently shaken for 30 min and afterwards filled to 10 mL with acetonitrile. This stock solution was then further diluted to the ratio of 1:12.5 by acetonitrile. A reference solution was prepared in the same manner without the resin. The absorption of both sample and reference was determined at 304 nm at room temperature (see Section 6.3 for details). The loading density ρ_{resin} was estimated on the basis of the Beer–Lambert law using the following equation:

$$\rho_{\text{resin}} = \frac{(A_{\text{sample}} - A_{\text{ref}}) \cdot V}{\epsilon \cdot d \cdot m_{\text{resin}}} \cdot f \quad (6.4)$$



6. Experimental Section

Here, A_{sample} and A_{ref} are the mean absorption values of the sample and the reference, respectively; V is the volume of the stock solution; f is the dilution factor; ϵ is the extinction coefficient of dibenzofulvene at 304 nm ($\epsilon = 7624 \text{ L mol}^{-1} \text{ cm}^{-1}$)^[218]; d is the light path through the cuvette and m_{resin} is the mass of the analyzed resin.

6.5.3. Automated Solid-Phase Peptide Synthesis

For the synthesis of peptidic sequences, a *Liberty Blue* peptide synthesizer by *CEM* (Matthews, North Carolina, USA) connected to a *Discover* microwave unit by *CEM* was used.

The following protected amino acids were used as 0.2 M solutions in DMF: Fmoc-Ala-OH, Fmoc-Arg(Pbf)-OH, Fmoc-Cys(Trt)-OH, Fmoc-Gln(Trt)-OH, Fmoc-Gly-OH, Fmoc-Ile-OH, Fmoc-Leu-OH, Fmoc-Lys(Boc)-OH, Fmoc-Met-OH, Fmoc-Phe-OH, Fmoc-Pro-OH, Fmoc-Ser(tBu)-OH, Fmoc-Trp(Boc)-OH, Fmoc-Tyr(tBu)-OH, Fmoc-Val-OH. For Fmoc-deprotection, a solution of piperidine in DMF (20 %, *v/v*) was used. Activation of the amino acid was accomplished with DIC (0.5 M in DMF) as the activator and Oxyma (1 M in DMF) as the activator base. The solutions of Oxyma and Fmoc-Phe-OH were filtered before usage. Proper mixing of the reaction mixture was ensured by bubbling nitrogen through the reaction vessel. A capping step was not performed.

The pre-loaded resin (0.10 mmol, 1.0 eq, loading density < 0.37 mmol/g) was swollen in DMF for at least 30 min. The deprotection solution was added (4 mL) and removal of the N-terminal Fmoc protection group was carried out in two cycles at elevated temperatures under microwave irradiation (1. 75 °C, 90 W, 15 s; 2. 90 °C, 20 W, 50 s). After washing with DMF (4 x 4 mL), the amino acid (5.0 eq) was transferred to the resin followed by DIC (5.0 eq) and Oxyma (5.0 eq). The coupling step (1. 75 °C, 170 W, 15 s; 2. 90 °C, 30 W, 110 s) was performed under microwave irradiation and was repeated once (double coupling). For the attachment of Fmoc-Arg(Pbf)-OH, the overall reaction temperature was reduced to 75 °C with the power of the microwave reduced accordingly and the reaction time was elongated. For Fmoc-Cys(Trt)-OH coupling, the temperature was further reduced to 50 °C.

After the synthesis, the resin was transferred into a BD syringe equipped with a polyethylene (PE) frit and washed several times with DCM. Afterwards, the resin was dried and stored in a desiccator.



6.5.4. Manual SPPS for Attachment of PNA Monomers

The SPPS of PNA monomers was performed at room temperature in BD syringes equipped with a PE frit, usually in a 5 μmol or 10 μmol scale. The following commercially available aeg-PNA monomers were used: Fmoc-a(Bhoc)-aeg-OH, Fmoc-c(Bhoc)-aeg-OH, Fmoc-g(Bhoc)-aeg-OH and Fmoc-t-aeg-OH. As ala-PNA monomers, Fmoc-L-AlaC(Z)-OH (**3**) and Fmoc-D-AlaG-OH (**6**) were used (for the synthesis see Section 6.4). Stock solutions of the coupling reagents in NMP were prepared each day. These were HATU (0.5 M), HOAt (2 M), DIPEA (2 M) and 2,6-lutidine (2 M). The indicated equivalents in this section are calculated on the basis of the molecular mass of the transmembrane domain including amino acid side chain protection groups.

The resin containing the peptidic transmembrane domain (1.0 eq) was swollen in NMP for 2 h. The SPPS cycle started with the deprotection of the N-terminal Fmoc group of the growing peptide chain, which was performed with piperidine in NMP (20 %, *v/v*). For this, the resin was shaken twice with 2 mL of the deprotection solution for 5 min. The aeg-PNA monomer (4.0 eq) was dissolved with the help of a sonicator in appropriate volumes of HATU and HOAt stock solutions to yield 3.9 eq of HATU and 4.0 eq of HOAt. Immediately before the coupling step, 2,6-lutidine (6.0 eq) and DIPEA (4.0 eq) were added to the solution, which was then transferred to the syringe containing the deprotected resin. The syringe was shaken for 1 h and the coupling step was repeated. Capping was performed by shaking the resin twice with 1.5 mL of a solution of Ac_2O /2,6-lutidine/NMP (1:2:7, *v/v/v*) for 5 min. A washing step (5 x NMP, 5 x DCM, 5 x NMP) was performed after each step except between two capping steps. After the second capping step, a special washing step (5 x DIPEA (5 % in NMP, *v/v*), 5 x DCM, 5 x NMP) was inserted, followed by a normal washing step. If a chaotropic salt was added to support deaggregation of the peptide chains, the resin was washed additionally with a solution of KSCN (0.4 M in NMP) or LiCl (0.4 M in NMP) prior to the coupling step. If the synthesis was continued on the next day, the resin was stored overnight in NMP at $-20\text{ }^\circ\text{C}$. The cycle was repeated until the desired length of the sequence was reached. Then, the resin was washed (10 x DCM) and dried and stored in a desiccator.

A similar procedure was followed for attaching an ala-PNA monomer. The following changes were made: The concentration of the HOAt stock solution was 1 M and the ala-PNA monomer (5.0 eq) was mixed with HATU (4.5 eq) and HOAt (5.0 eq). The time for the coupling step was elongated to 2 h. The capping step was omitted. It was also omitted when aeg-PNA monomers were attached to a sequences that already contained ala-PNA. If PyBOP was used as the activator, the ala-PNA building block **6** (6.0 eq) was mixed

6. Experimental Section

with PyBOP (6 eq) and DIPEA (18 eq). If DMSO was used as the solvent, the resin was washed with dry DMSO and shaken in dry DMSO (7 min) prior to the coupling step. All reagents were dissolved in dry DMSO, except for DIPEA and piperidine. DIPEA was added to the reaction mixture without mixing it with DMSO beforehand because it is not soluble in DMSO. The deprotection step with piperidine was performed in NMP. In case of microwave-assisted coupling of the ala-PNA monomers, a *Discover* microwave unit by CEM (Matthews, North Carolina, USA) was used. The highest yields were achieved if the coupling step was performed at 60 °C ($\Delta T = 5$ °C) for 3 min at a power of 20 W and if it was performed twice. All other steps were carried out as described above.

6.5.5. Cleavage from Resin and Work-Up

Cleavage of the peptide sequences from the resin was performed in a 2 mL BD syringe equipped with a PE frit. The resin was shaken at room temperature for at least 2 h (peptide hybrids that contained the alanyl-PNA unit AlaC(Z): at least 3 h) in an appropriate cleavage mixture. The following mixtures were applied depending on the sequence of the peptide (the indicated numbers are ratios based on volume).

Mix A	TFA / H ₂ O / TIS (95 : 2.5 : 2.5)
Mix B	TFA / H ₂ O / EDT / TIS (94 : 2.5 : 2.5 : 1)
Mix C	TFA / <i>m</i> -cresol / EDT / TIS (87.5 : 5 : 5 : 2.5)
Mix D	TFA / thioanisole / <i>m</i> -cresol / EDT / TIS (63 : 15 : 14.5 : 5 : 2.5)

Mix A and B were used for purely peptidic sequences without and with Cys present, respectively; Mix C was used for peptide hybrids containing aeg-PNA sequences only, and Mix D was used for peptide hybrids containing both alanyl-PNA and aeg-PNA sequences. After treatment with the respective cleavage cocktail, the cleavage solution was filtered from the resin beads, collected in an *Eppendorf* tube and concentrated in a nitrogen stream. Subsequently, the peptide was precipitated with icecold ether (either diethylether or methyl *tert*-butyl ether). The peptide pellet was washed at least four times with the icecold ether and was dried afterwards in a desiccator.

6.5.6. Attempts for Purification of Model Peptides

Purification of the target peptides was tested via HPLC. The utilized HPLC equipment including columns and solvents is described in Section 6.2. The following Table 6.3 provides an overview of the conditions that were applied in order to find a suitable purification method for the target PNA/peptide hybrids. The chromatogram with the best resolved

peaks was obtained from peptide **10** with the conditions listed in Table 6.3 (marked with an asterisk). It is shown in Figure A.2b in the appendix.

Table 6.3. Applied HPLC purification methods for selected PNA/peptide hybrids. *The chromatogram of peptide **10** obtained from HPLC applying the indicated conditions is shown in the appendix.

Peptide	Peptide dissolved in	Column	Solvents
10	MeOH/FA (20:1)	Column 2	A+C
10*	MeOH/TFE/FA (10:1:0.8)	Column 2	A+C
10	MeCN/FA (5:1)	Column 3	A+B
8	MeCN/FA (5:1)	Column 3	A+B, 60 °C
9	DCM/HFIP/pyridine (4:1:0.25)	Column 3	D+E
9	FA/H ₂ O (2:3)	Column 3	D+E
9	MeCN/H ₂ O (3:1)	Column 3	A+B
10	MeCN/FA (5:1)	Column 4	A+B

Purification of the model peptides was also tested with size exclusion chromatography (see Section 6.2 for the equipment). Selected chromatograms are shown in Figure 3.10 (Section 3.4) and in Figure A.3 in the appendix.

6.5.7. Synthesized Model Peptide Sequences

In the following, structural details and analytical data for all synthesized peptides and PNA/peptide hybrid sequences are listed. The indicated molecular mass below each structure is the relative molecular mass. Syntheses were performed according to the general instructions given in Sections 6.5.1–6.5.5. Deviating conditions and procedures are indicated.

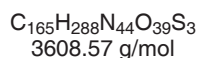
Syntaxin-1A (256-288)

The transmembrane domain of Syntaxin-1A (256-288) from *Rattus norvegicus* was synthesized automatically according to the description in Section 6.5.3. As solid support, low loaded resins were used preloaded with the amino acid Fmoc-Gly-OH. To obtain a C-terminus with a carboxylic acid functionality, a Wang resin was used. To yield the C-terminal amide, a NovaPEG Rink amide resin was applied. Cleavage from the resin was performed with Mix B as described in Section 6.5.5.



6. Experimental Section

SxTMD-COOH

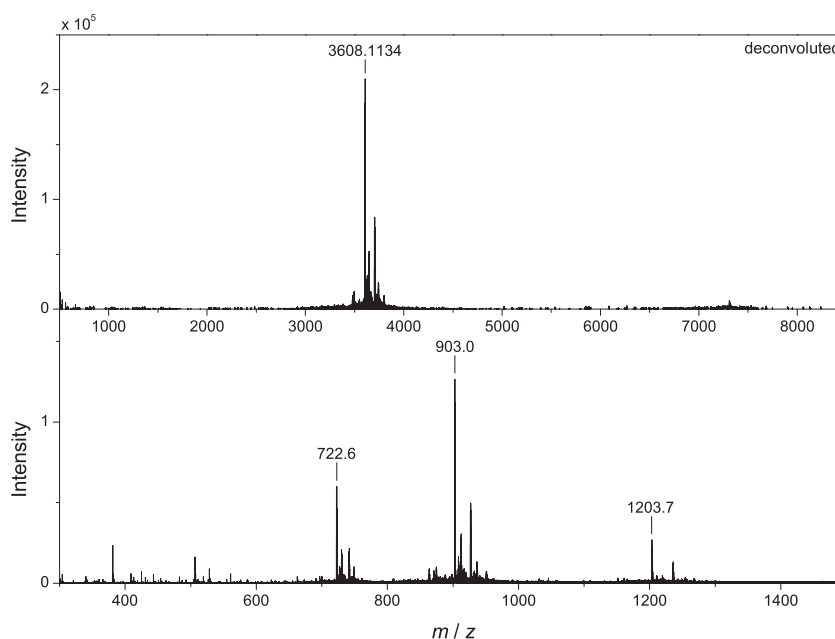


MS (ESI): m/z (%) = 722.6 (47) $[\text{M}+5\text{H}]^{5+}$, 903.0 (100) $[\text{M}+4\text{H}]^{4+}$, 1203.7 (21) $[\text{M}+3\text{H}]^{3+}$.

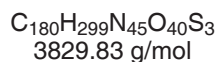
HR-MS (ESI): calc. for $\text{C}_{165}\text{H}_{293}\text{N}_{44}\text{O}_{39}\text{S}_3$ ($[\text{M}+5\text{H}]^{5+}$): 722.6299, found: 722.6296;

calc. for $\text{C}_{165}\text{H}_{292}\text{N}_{44}\text{O}_{39}\text{S}_3$ ($[\text{M}+4\text{H}]^{4+}$): 903.0355, found: 903.0359;

calc. for $\text{C}_{165}\text{H}_{291}\text{N}_{44}\text{O}_{39}\text{S}_3$ ($[\text{M}+3\text{H}]^{3+}$): 1203.7116, found: 1203.7111.



Fmoc-SxTMD-NH₂



MS (ESI): m/z (%) = 958.3 (100) $[\text{M}+4\text{H}]^{4+}$, 1277.4 (85) $[\text{M}+3\text{H}]^{3+}$.

HR-MS (ESI): calc. for $\text{C}_{180}\text{H}_{303}\text{N}_{45}\text{O}_{40}\text{S}_3$ ($[\text{M}+4\text{H}]^{4+}$): 958.3063, found: 958.3059;

calc. for $\text{C}_{180}\text{H}_{302}\text{N}_{45}\text{O}_{40}\text{S}_3$ ($[\text{M}+3\text{H}]^{3+}$): 1277.4059, found: 1277.4053.

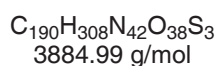
MS (MALDI, reflectron mode): m/z = 3831.8411 ($[\text{M}+\text{H}]^+$).

Synaptobrevin-2 (85-116)

The transmembrane domain of Synaptobrevin-2 (85-116) from *Rattus norvegicus* was synthesized automatically according to the description in Section 6.5.3. As solid support, low loaded resins were used preloaded with the amino acid Fmoc-Thr(tBu)-OH. To obtain a C-terminus with a carboxylic acid functionality, a Wang resin was used. To yield the C-terminal amide, a NovaPEG Rink amide resin was applied. Cleavage from the resin was performed with Mix B as described in Section 6.5.5.

SybTMD-COOH

H-KRKYWWKNLKMMIILGVICAILIIIIIVYFST-OH

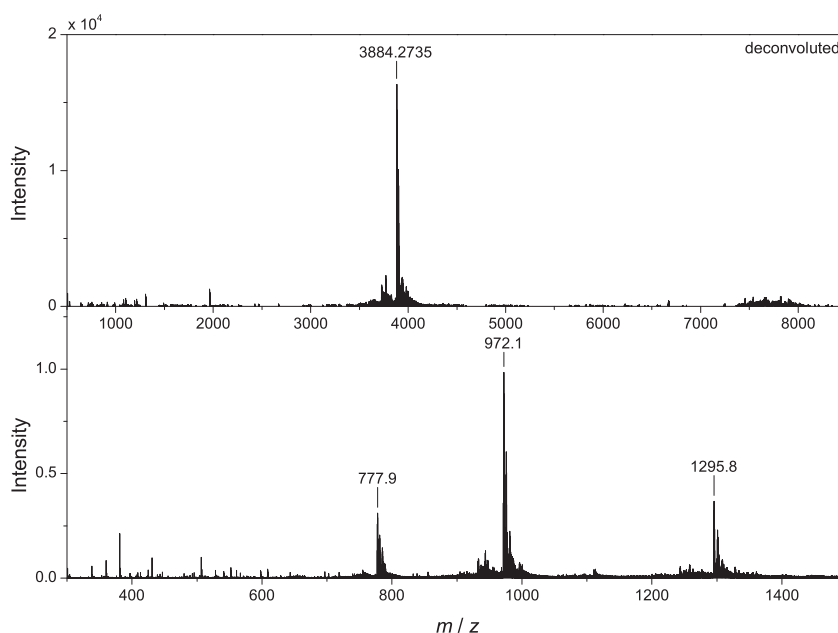


MS (ESI): m/z (%) = 777.9 (31) $[\text{M}+5\text{H}]^{5+}$, 972.1 (100) $[\text{M}+4\text{H}]^{4+}$, 1295.8 (37) $[\text{M}+3\text{H}]^{3+}$.

HR-MS (ESI): calc. for $\text{C}_{190}\text{H}_{313}\text{N}_{42}\text{O}_{38}\text{S}_3$ ($[\text{M}+5\text{H}]^{5+}$): 777.8608, found: 777.8601;

calc. for $\text{C}_{190}\text{H}_{312}\text{N}_{42}\text{O}_{38}\text{S}_3$ ($[\text{M}+4\text{H}]^{4+}$): 972.0742, found: 972.0743;

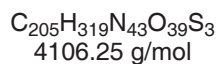
calc. for $\text{C}_{190}\text{H}_{311}\text{N}_{42}\text{O}_{38}\text{S}_3$ ($[\text{M}+3\text{H}]^{3+}$): 1295.7631, found: 1295.7624.





6. Experimental Section

Fmoc-SybTMD-NH₂

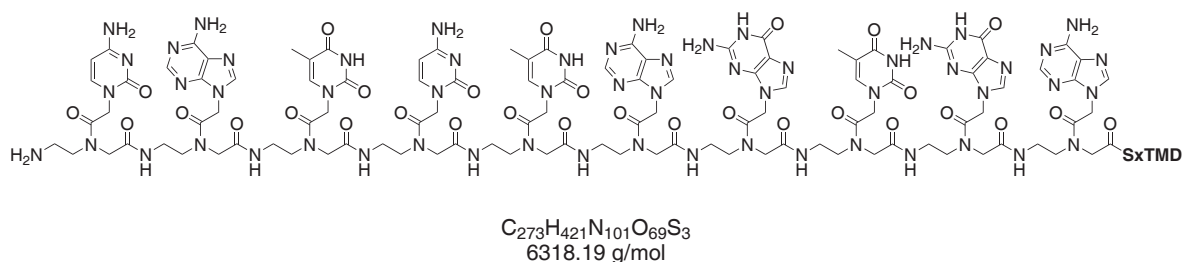


MS (ESI): m/z (%) = 1027.3 (100) [M+4H]⁴⁺, 1369.8 (67) [M+3H]³⁺.

HR-MS (ESI): calc. for C₂₀₅H₃₂₃N₄₃O₃₉S₃ ([M+4H]⁴⁺): 1027.3452, found: 1027.3443;

calc. for C₂₀₅H₃₂₂N₄₃O₃₉S₃ ([M+3H]³⁺): 1369.7919, found: 1369.7907.

MS (MALDI, reflectron mode): m/z = 4107.8687 ([M+H]⁺).

PNA3-SxTMD (7)


7

The synthesis was performed via manual SPPS as described in Section 6.5.4 on a Wang resin that contained the Syntaxin-1A transmembrane domain. Cleavage from the resin was performed with Mix C as described in Section 6.5.5.

MS (ESI): m/z (%) = 790.7 (18) $[M+8H]^{8+}$, 903.5 (45) $[M+7H]^{7+}$, 1053.9 (100) $[M+6H]^{6+}$, 1264.4 (79) $[M+5H]^{5+}$, 1580.3 (17) $[M+4H]^{4+}$.

HR-MS (ESI): calc. for $C_{273}H_{429}N_{101}O_{69}S_3$ ($[M+8H]^{8+}$): 790.6545, found: 790.6562;

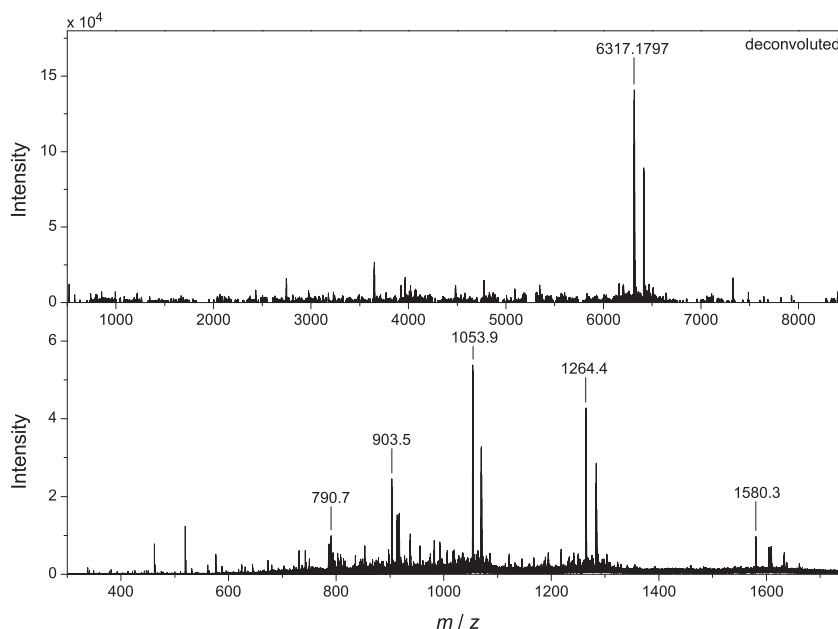
calc. for $C_{273}H_{428}N_{101}O_{69}S_3$ ($[M+7H]^{7+}$): 903.4612, found: 903.4629;

calc. for $C_{273}H_{427}N_{101}O_{69}S_3$ ($[M+6H]^{6+}$): 1053.8702, found: 1053.8705;

calc. for $C_{273}H_{426}N_{101}O_{69}S_3$ ($[M+5H]^{5+}$): 1264.4428, found: 1264.4440;

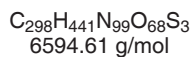
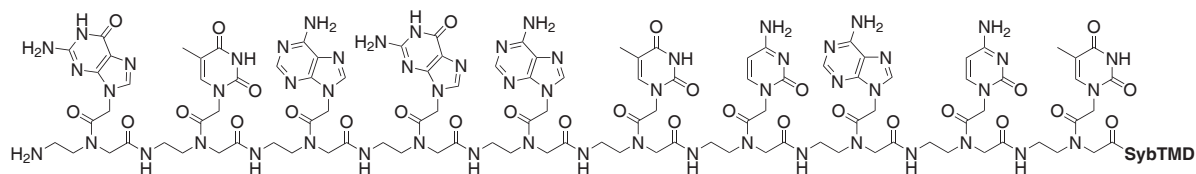
calc. for $C_{273}H_{425}N_{101}O_{69}S_3$ ($[M+4H]^{4+}$): 1580.3017, found: 1580.3014.

MS (MALDI, linear mode): m/z = 6310.120.



6. Experimental Section

PNA1-SybTMD (8)



8

The synthesis was performed via manual SPPS as described in Section 6.5.4 on a Wang resin that contained the Synaptobrevin-2 transmembrane domain. Cleavage from the resin was performed with Mix C as described in Section 6.5.5.

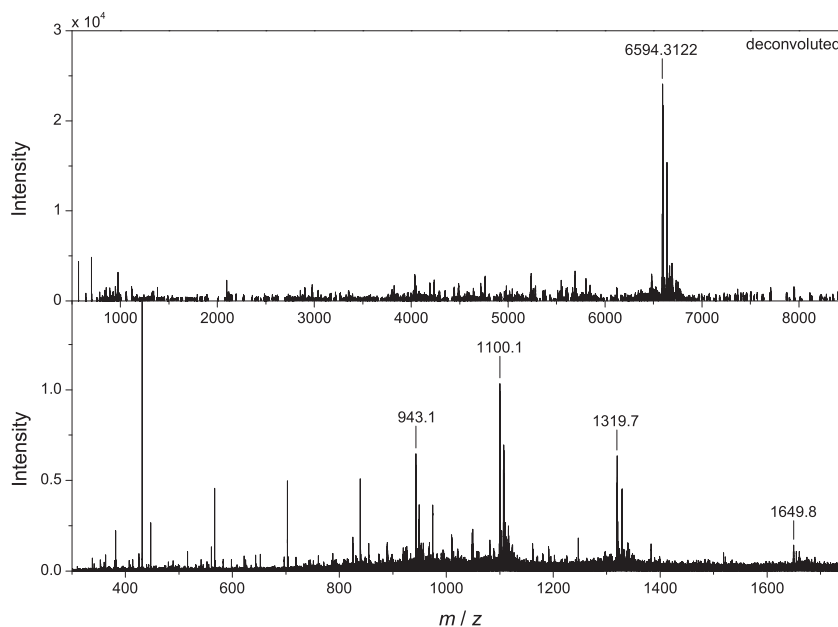
MS (ESI): m/z (%) = 943.1 (12) $[\text{M}+7\text{H}]^{7+}$, 1100.1 (43) $[\text{M}+6\text{H}]^{6+}$, 1319.7 (100) $[\text{M}+5\text{H}]^{5+}$, 1649.8 (18) $[\text{M}+4\text{H}]^{4+}$.

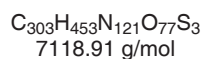
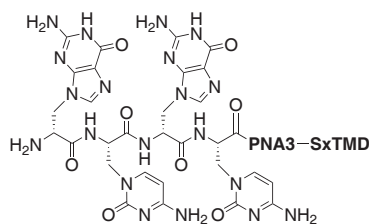
HR-MS (ESI): calc. for $\text{C}_{298}\text{H}_{448}\text{N}_{99}\text{O}_{68}\text{S}_3$ ($[\text{M}+7\text{H}]^{7+}$): 943.0552, found: 943.0557;

calc. for $\text{C}_{298}\text{H}_{447}\text{N}_{99}\text{O}_{68}\text{S}_3$ ($[\text{M}+6\text{H}]^{6+}$): 1100.0632, found: 1100.0645;

calc. for $\text{C}_{298}\text{H}_{446}\text{N}_{99}\text{O}_{68}\text{S}_3$ ($[\text{M}+5\text{H}]^{5+}$): 1319.8744, found: 1319.8763;

calc. for $\text{C}_{298}\text{H}_{445}\text{N}_{99}\text{O}_{68}\text{S}_3$ ($[\text{M}+4\text{H}]^{4+}$): 1649.5912, found: 1649.5849.



Ala2-PNA3-SxTMD (9)

9

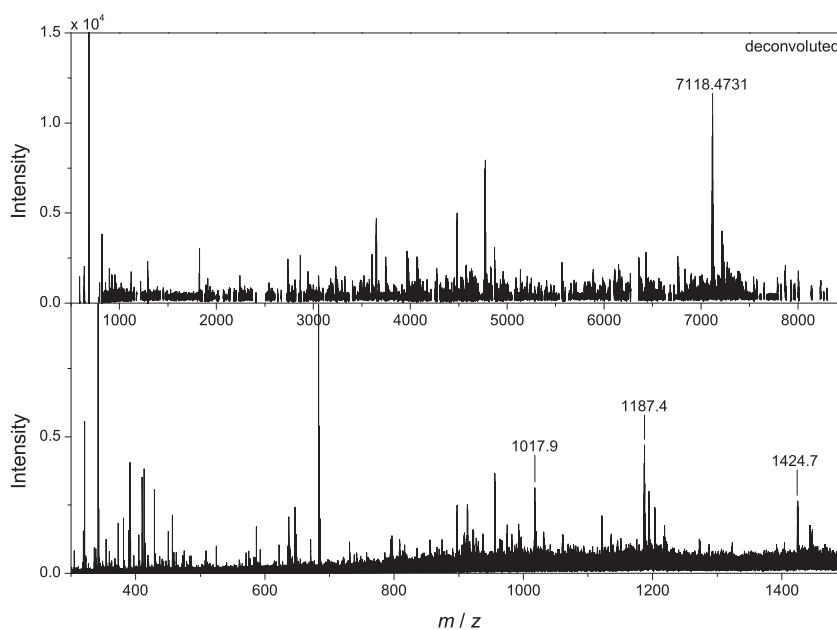
The synthesis was performed via manual SPPS as described in Section 6.5.4 on a Wang resin that contained the Syntaxin-1A transmembrane domain and the PNA3 sequence. Cleavage from the resin was performed with Mix D as described in Section 6.5.5.

MS (ESI): m/z (%) = 1017.9 [M+7H]⁷⁺, 1187.4 [M+6H]⁶⁺, 1424.7 [M+5H]⁵⁺.

HR-MS (ESI): calc. for $\text{C}_{303}\text{H}_{460}\text{N}_{121}\text{O}_{77}\text{S}_3$ ([M+7H]⁷⁺): 1017.9288, found: 1017.9290;

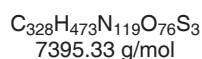
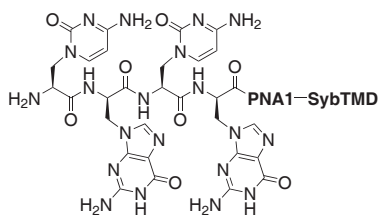
calc. for $\text{C}_{303}\text{H}_{459}\text{N}_{121}\text{O}_{77}\text{S}_3$ ([M+6H]⁶⁺): 1187.4158, found: 1187.4117;

calc. for $\text{C}_{303}\text{H}_{458}\text{N}_{121}\text{O}_{77}\text{S}_3$ ([M+5H]⁵⁺): 1424.6975, found: 1424.7014.



6. Experimental Section

Ala1-PNA1-SybTMD (10)



10

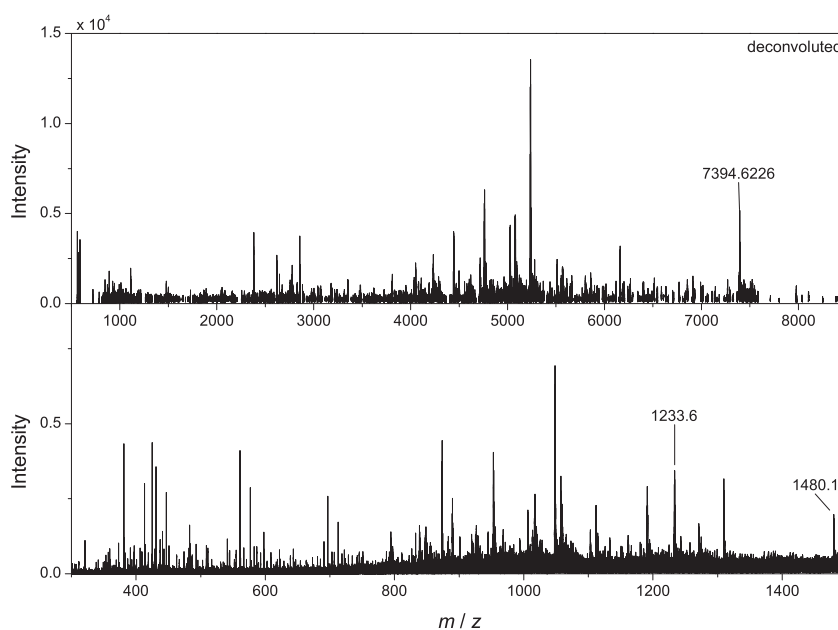
The synthesis was performed via manual SPPS as described in Section 6.5.4 on a Wang resin that contained the Synaptobrevin-2 transmembrane domain and the PNA1 sequence. Cleavage from the resin was performed with Mix D as described in Section 6.5.5.

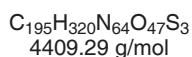
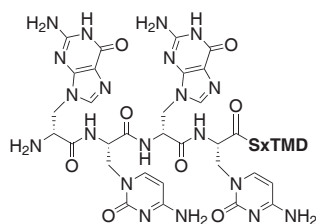
MS (ESI): m/z (%) = 1233.6 [M+6H]⁶⁺, 1480.1 [M+5H]⁵⁺.

HR-MS (ESI): calc. for $\text{C}_{328}\text{H}_{480}\text{N}_{119}\text{O}_{76}\text{S}_3$ ([M+7H]⁷⁺): 1057.3797, found: 1057.3761;

calc. for $\text{C}_{328}\text{H}_{479}\text{N}_{119}\text{O}_{76}\text{S}_3$ ([M+6H]⁶⁺): 1233.4417, found: 1233.4410;

calc. for $\text{C}_{328}\text{H}_{478}\text{N}_{119}\text{O}_{76}\text{S}_3$ ([M+5H]⁵⁺): 1479.9286, found: 1479.9283.



Ala2-SxTMD (11)

11

The synthesis was performed via manual SPPS as described in Section 6.5.4 on a Wang resin that contained the Syntaxin-1A transmembrane domain. Cleavage from the resin was performed with Mix D as described in Section 6.5.5.

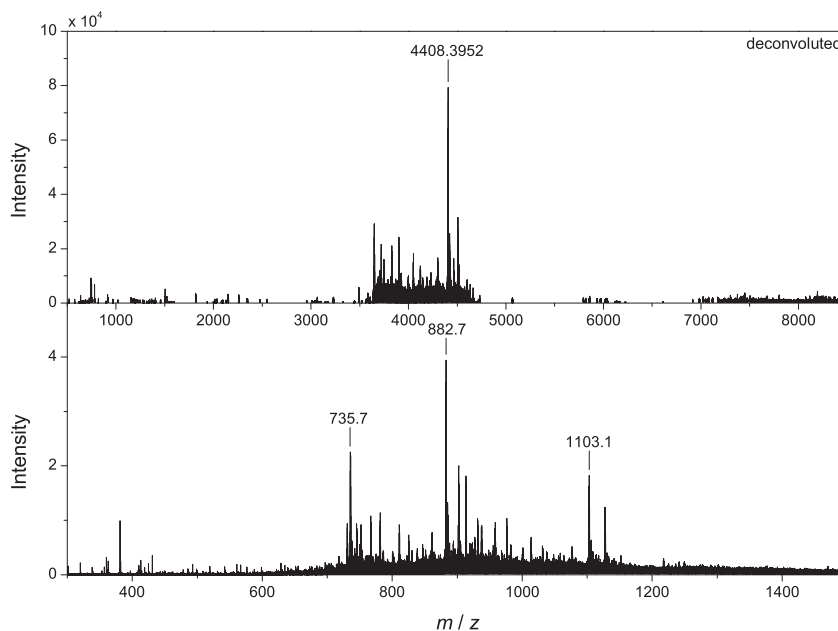
MS (ESI): m/z (%) = 735.7 (57) $[\text{M}+6\text{H}]^{6+}$, 882.7 (100) $[\text{M}+5\text{H}]^{5+}$, 1103.1 (46) $[\text{M}+4\text{H}]^{4+}$.

HR-MS (ESI): calc. for $\text{C}_{195}\text{H}_{326}\text{N}_{64}\text{O}_{47}\text{S}_3$ ($[\text{M}+6\text{H}]^{6+}$): 735.7378, found: 735.7379;

calc. for $\text{C}_{195}\text{H}_{325}\text{N}_{64}\text{O}_{47}\text{S}_3$ ($[\text{M}+5\text{H}]^{5+}$): 882.6839, found: 882.6848;

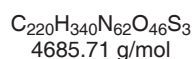
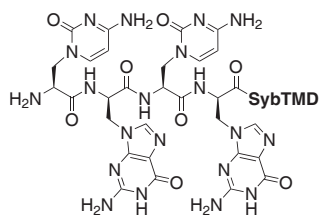
calc. for $\text{C}_{195}\text{H}_{324}\text{N}_{64}\text{O}_{47}\text{S}_3$ ($[\text{M}+4\text{H}]^{4+}$): 1103.1030, found: 1103.1034.

MS (MALDI, reflectron mode): m/z = 4406.994.



6. Experimental Section

Ala1-SybTMD (12)



12

The synthesis was performed via manual SPPS as described in Section 6.5.4 on a Wang resin that contained the Synaptobrevin-2 transmembrane domain. Cleavage from the resin was performed with Mix D as described in Section 6.5.5.

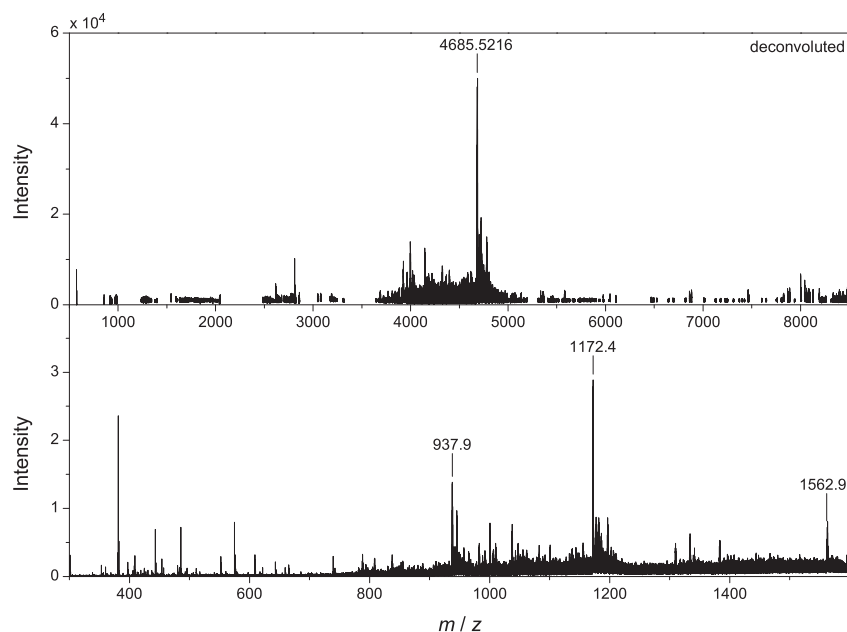
MS (ESI): m/z (%) = 937.9 (48) $[\text{M}+5\text{H}]^{5+}$, 1172.4 (100) $[\text{M}+4\text{H}]^{4+}$, 1562.9 (26) $[\text{M}+3\text{H}]^{3+}$.

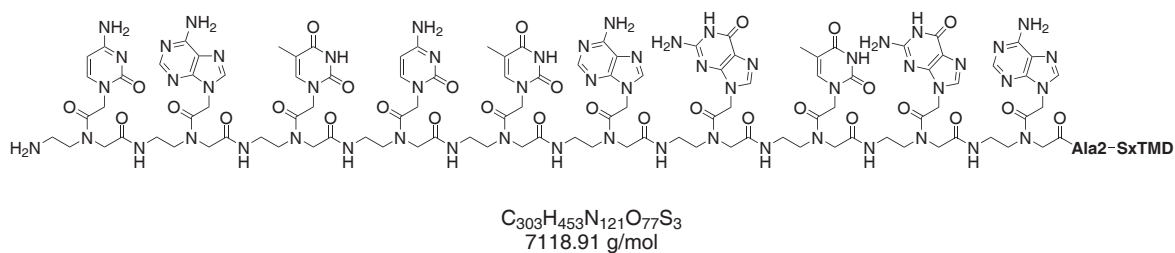
HR-MS (ESI): calc. for $\text{C}_{220}\text{H}_{345}\text{N}_{62}\text{O}_{46}\text{S}_3$ ($[\text{M}+5\text{H}]^{5+}$): 937.9150, found: 937.9137;

calc. for $\text{C}_{220}\text{H}_{344}\text{N}_{62}\text{O}_{46}\text{S}_3$ ($[\text{M}+4\text{H}]^{4+}$): 1172.3930, found: 1172.3911;

calc. for $\text{C}_{220}\text{H}_{343}\text{N}_{62}\text{O}_{46}\text{S}_3$ ($[\text{M}+3\text{H}]^{3+}$): 1562.8549, found: 1562.8517.

MS (MALDI, reflectron mode): m/z = 4682.691.



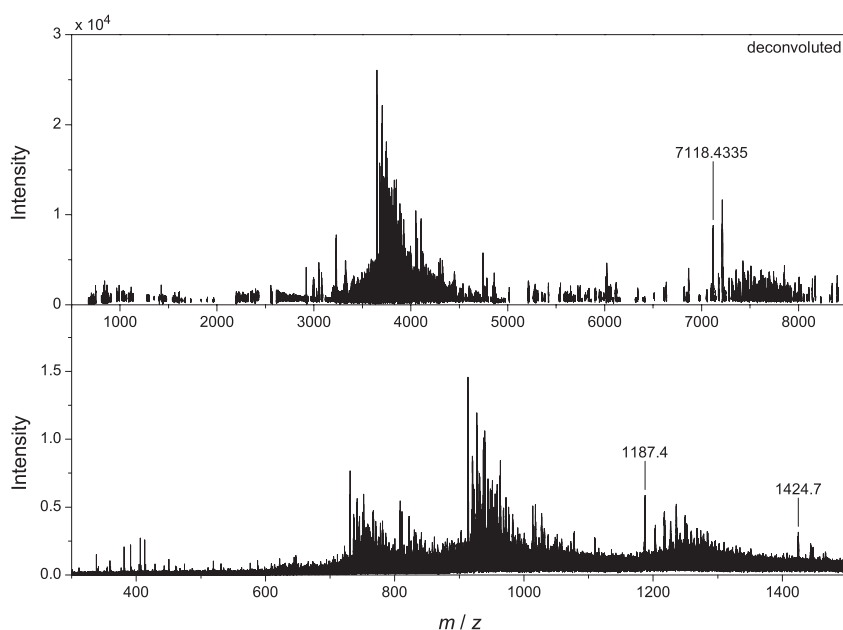
PNA3-Ala2-SxTMD (13)

13

The synthesis was performed via manual SPPS as described in Section 6.5.4 on a Wang resin that contained the Syntaxin-1A transmembrane domain and the Ala2 sequence. Cleavage from the resin was performed with Mix D as described in Section 6.5.5.

MS (ESI): m/z (%) = 1187.4 (100) $[M+6H]^{6+}$, 1424.7 (55) $[M+5H]^{5+}$.

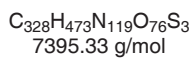
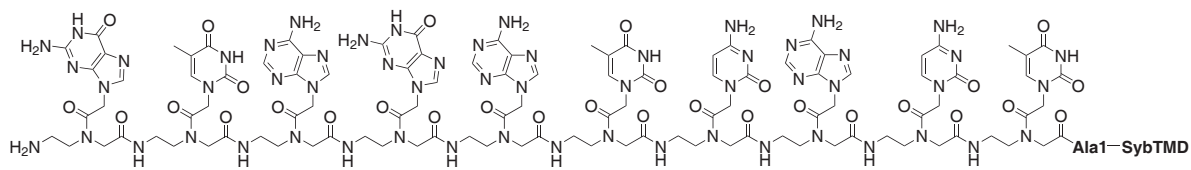
HR-MS (ESI): calc. for $C_{303}H_{459}N_{121}O_{77}S_3$ ($[M+6H]^{6+}$): 1187.4158, found: 1187.4094;

calc. for $C_{303}H_{458}N_{121}O_{77}S_3$ ($[M+5H]^{5+}$): 1424.6975, found: 1424.7050.



6. Experimental Section

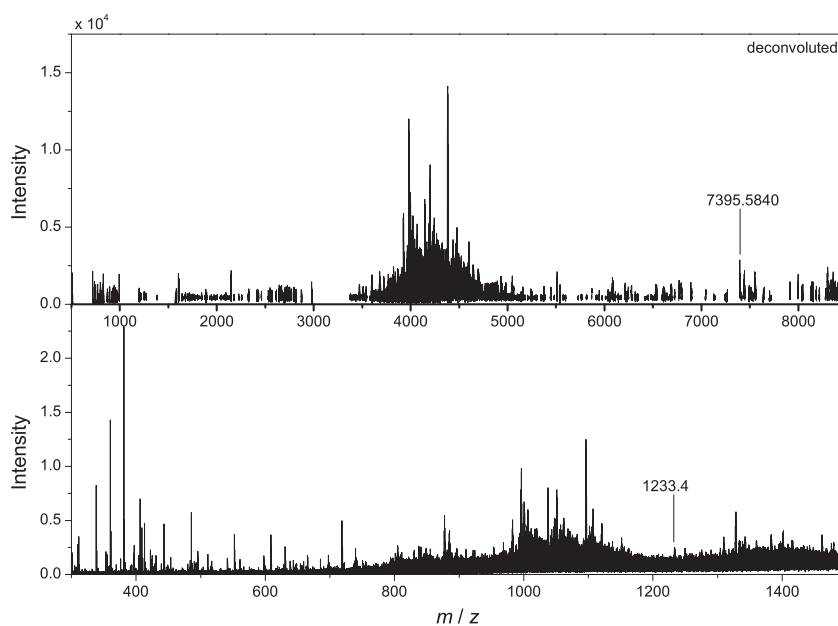
PNA1-Ala1-SybTMD (14)

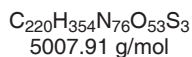
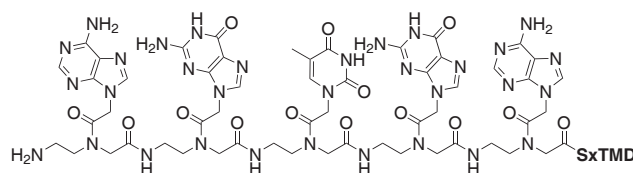


14

The synthesis was performed via manual SPPS as described in Section 6.5.4 on a Wang resin that contained the Synaptobrevin-2 transmembrane domain and the Ala1 sequence. Cleavage from the resin was performed with Mix D as described in Section 6.5.5.

MS (ESI): m/z (%) = 1233.3 $[\text{M}+6\text{H}]^{6+}$.



PNA3s-SxTMD (15)

15

The synthesis was performed via manual SPPS as described in Section 6.5.4 on a Wang resin that contained the Syntaxin-1A transmembrane domain. Cleavage from the resin was performed with Mix C as described in Section 6.5.5.

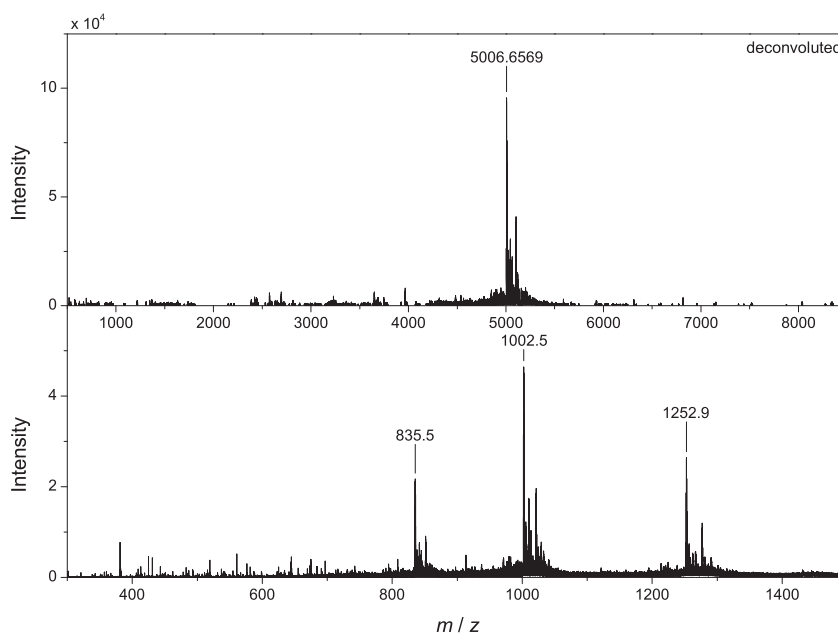
MS (ESI): m/z (%) = 835.5 (46) $[\text{M}+6\text{H}]^{6+}$, 1002.5 (100) $[\text{M}+5\text{H}]^{5+}$, 1252.9 (56) $[\text{M}+4\text{H}]^{4+}$.

HR-MS (ESI): calc. for $\text{C}_{220}\text{H}_{360}\text{N}_{76}\text{O}_{53}\text{S}_3$ ($[\text{M}+6\text{H}]^{6+}$): 835.4499, found: 835.4525;

calc. for $\text{C}_{220}\text{H}_{359}\text{N}_{76}\text{O}_{53}\text{S}_3$ ($[\text{M}+5\text{H}]^{5+}$): 1002.5393, found: 1002.5409;

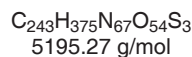
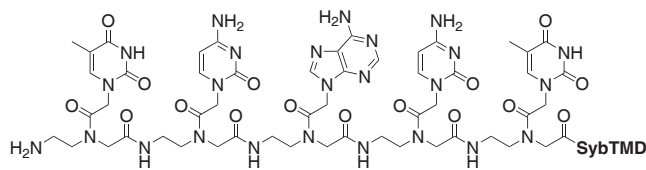
calc. for $\text{C}_{220}\text{H}_{358}\text{N}_{76}\text{O}_{53}\text{S}_3$ ($[\text{M}+4\text{H}]^{4+}$): 1252.9222, found: 1252.9232.

MS (MALDI, linear mode): m/z = 5004.0415.



6. Experimental Section

PNA1s-SybTMD (16)



16

The synthesis was performed via manual SPPS as described in Section 6.5.4 on a Wang resin that contained the Synaptobrevin-2 transmembrane domain. Cleavage from the resin was performed with Mix C as described in Section 6.5.5.

MS (ESI): m/z (%) = 743.1 (13) $[\text{M}+7\text{H}]^{7+}$, 867.0 (59) $[\text{M}+6\text{H}]^{6+}$, 1040.0 (100) $[\text{M}+5\text{H}]^{5+}$, 1299.7 (49) $[\text{M}+4\text{H}]^{4+}$.

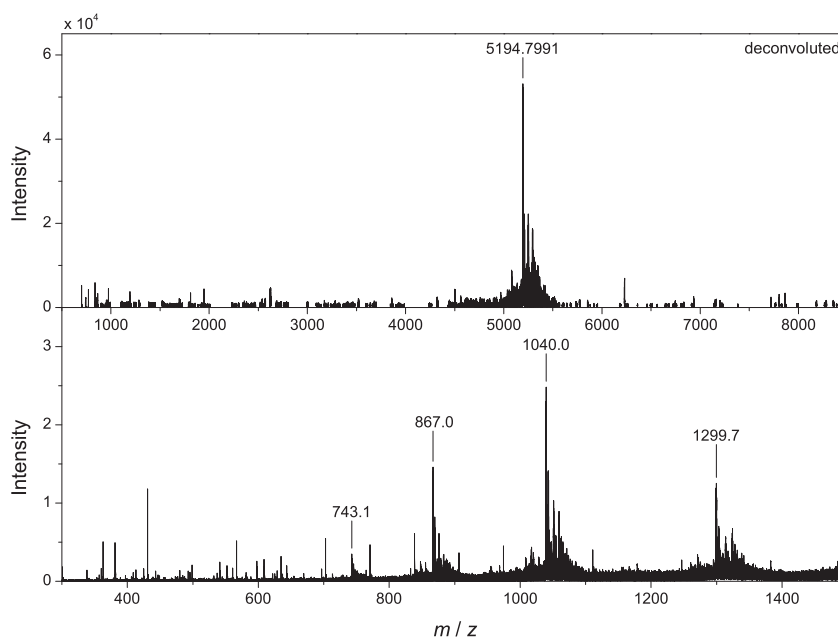
HR-MS (ESI): calc. for $\text{C}_{243}\text{H}_{382}\text{N}_{67}\text{O}_{54}\text{S}_3$ ($[\text{M}+7\text{H}]^{7+}$): 743.1204, found: 743.1190;

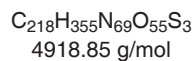
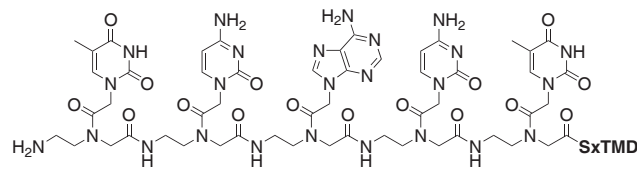
calc. for $\text{C}_{243}\text{H}_{381}\text{N}_{67}\text{O}_{54}\text{S}_3$ ($[\text{M}+6\text{H}]^{6+}$): 866.9731, found: 866.9736;

calc. for $\text{C}_{243}\text{H}_{380}\text{N}_{67}\text{O}_{54}\text{S}_3$ ($[\text{M}+5\text{H}]^{5+}$): 1039.9656, found: 1039.9660;

calc. for $\text{C}_{243}\text{H}_{379}\text{N}_{67}\text{O}_{54}\text{S}_3$ ($[\text{M}+4\text{H}]^{4+}$): 1299.7052, found: 1299.7067.

MS (MALDI, linear mode): m/z = 5192.1519.



PNA1s-SxTMD (17)


17

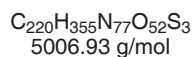
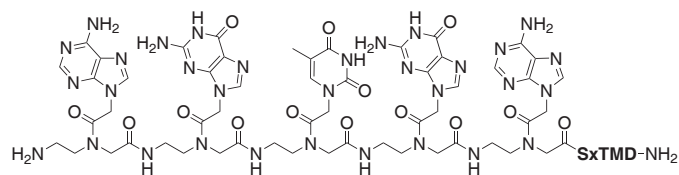
The synthesis was performed via manual SPPS as described in Section 6.5.4 on a Wang resin that contained the Syntaxin-1A transmembrane domain. Cleavage from the resin was performed with Mix C as described in Section 6.5.5.

MS (ESI): m/z (%) = 984.7 (44) $[\text{M}+5\text{H}]^{5+}$, 1230.7 (100) $[\text{M}+4\text{H}]^{4+}$.

HR-MS (ESI): calc. for $\text{C}_{218}\text{H}_{360}\text{N}_{69}\text{O}_{55}\text{S}_3$ ($[\text{M}+5\text{H}]^{5+}$): 984.7340, found: 984.7329;
 calc. for $\text{C}_{218}\text{H}_{359}\text{N}_{69}\text{O}_{55}\text{S}_3$ ($[\text{M}+4\text{H}]^{4+}$): 1230.6657, found: 1230.6646.

6. Experimental Section

PNA3s-SxTMD-NH₂ (18)



18

The synthesis was performed via manual SPPS as described in Section 6.5.4 on a NovaPEG Rink amide resin that contained the Syntaxin-1A transmembrane domain. Cleavage from the resin was performed with Mix C as described in Section 6.5.5.

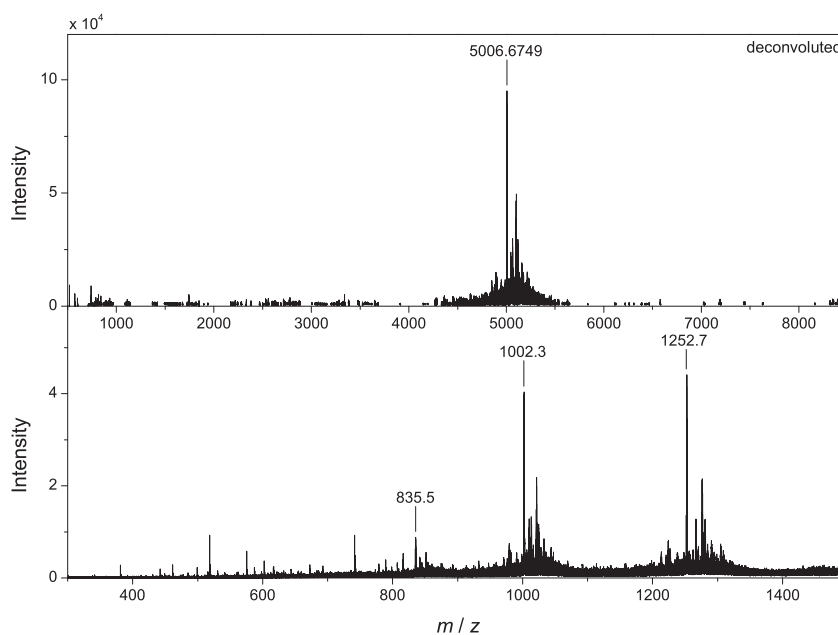
MS (ESI): m/z (%) = 835.5 (19) $[\text{M}+6\text{H}]^{6+}$, 1002.3 (91) $[\text{M}+5\text{H}]^{5+}$, 1252.7 (100) $[\text{M}+4\text{H}]^{4+}$.

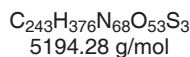
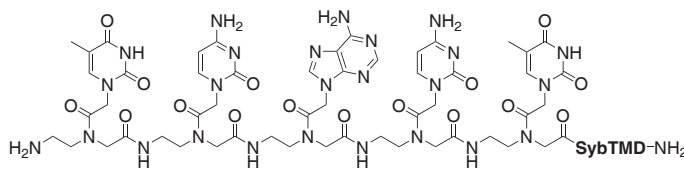
HR-MS (ESI): calc. for $\text{C}_{220}\text{H}_{361}\text{N}_{77}\text{O}_{52}\text{S}_3$ ($[\text{M}+6\text{H}]^{6+}$): 835.4533, found: 835.4546;

calc. for $\text{C}_{220}\text{H}_{360}\text{N}_{77}\text{O}_{52}\text{S}_3$ ($[\text{M}+5\text{H}]^{5+}$): 1002.3425, found: 1002.3407;

calc. for $\text{C}_{220}\text{H}_{359}\text{N}_{77}\text{O}_{52}\text{S}_3$ ($[\text{M}+4\text{H}]^{4+}$): 1252.6762, found: 1252.6759.

MS (MALDI, reflectron mode): m/z = 5004.300.



PNA1s-SybTMD-NH₂ (19)

19

The synthesis was performed via manual SPPS as described in Section 6.5.4 on a NovaPEG Rink amide resin that contained the Synaptobrevin-2 transmembrane domain. Cleavage from the resin was performed with Mix C as described in Section 6.5.5.

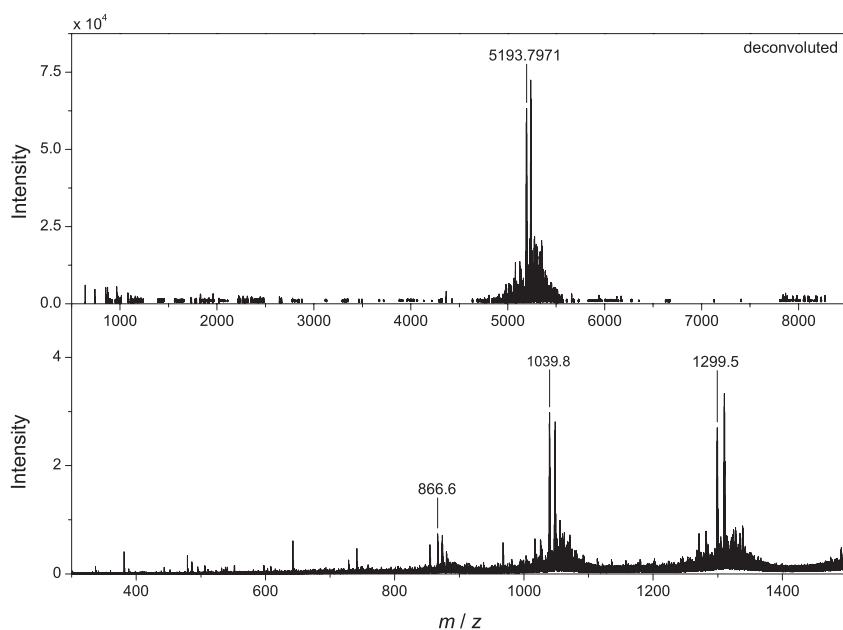
MS (ESI): m/z (%) = 866.6 (24) $[\text{M}+6\text{H}]^{6+}$, 1039.8 (100) $[\text{M}+5\text{H}]^{5+}$, 1299.5 (90) $[\text{M}+4\text{H}]^{4+}$.

HR-MS (ESI): calc. for $\text{C}_{243}\text{H}_{382}\text{N}_{68}\text{O}_{53}\text{S}_3$ ($[\text{M}+6\text{H}]^{6+}$): 866.6419, found: 866.6417;

calc. for $\text{C}_{243}\text{H}_{381}\text{N}_{68}\text{O}_{53}\text{S}_3$ ($[\text{M}+5\text{H}]^{5+}$): 1039.7688, found: 1039.7684;

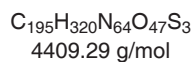
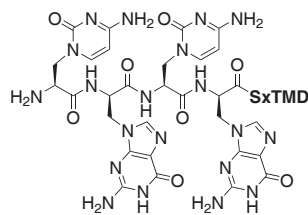
calc. for $\text{C}_{243}\text{H}_{380}\text{N}_{68}\text{O}_{53}\text{S}_3$ ($[\text{M}+4\text{H}]^{4+}$): 1299.4592, found: 1299.4583.

MS (MALDI, reflectron mode): m/z = 5190.624.



6. Experimental Section

Ala1-SxTMD (20)

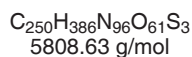
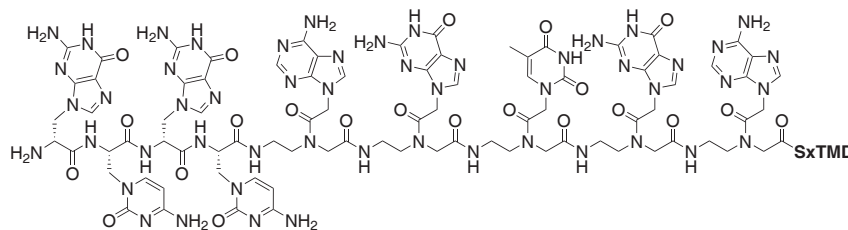


20

The synthesis was performed via manual SPPS as described in Section 6.5.4 on a Wang resin that contained the Syntaxin-1A transmembrane domain. Cleavage from the resin was performed with Mix D as described in Section 6.5.5.

MS (ESI): m/z (%) = 882.7 (15) $[\text{M}+5\text{H}]^{5+}$, 1103.1 (100) $[\text{M}+4\text{H}]^{4+}$.

HR-MS (ESI): calc. for $\text{C}_{195}\text{H}_{325}\text{N}_{64}\text{O}_{47}\text{S}_3$ ($[\text{M}+5\text{H}]^{5+}$): 882.6839, found: 882.6829;
calc. for $\text{C}_{195}\text{H}_{324}\text{N}_{64}\text{O}_{47}\text{S}_3$ ($[\text{M}+4\text{H}]^{4+}$): 1103.1030, found: 1103.1024.

Ala2-PNA3s-SxTMD (21)

21

The synthesis was performed via manual SPPS as described in Section 6.5.4 on a Wang resin that contained the Syntaxin-1A transmembrane domain and the aeg-PNA part of the recognition unit. Cleavage from the resin was performed with Mix D as described in Section 6.5.5.

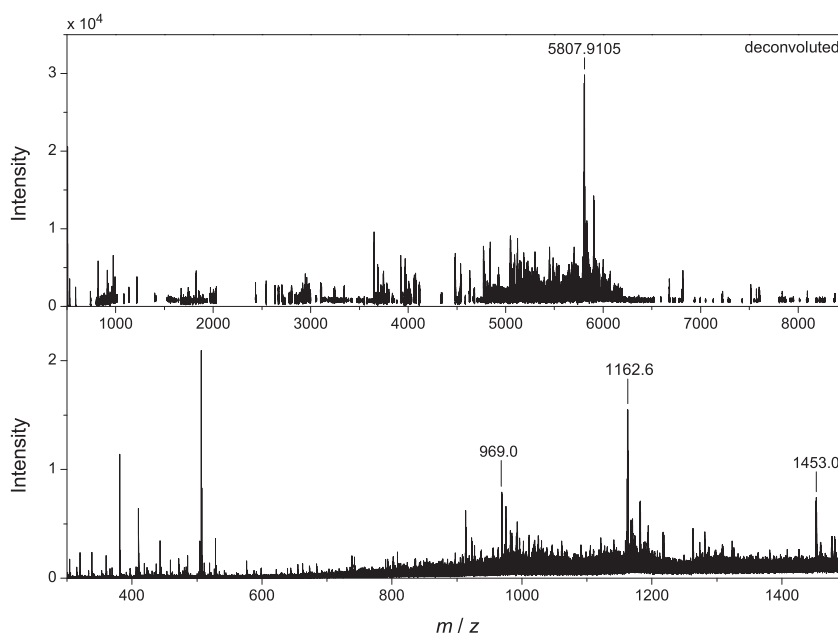
MS (ESI): m/z (%) = 969.0 (49) $[\text{M}+6\text{H}]^{6+}$, 1162.6 (100) $[\text{M}+5\text{H}]^{5+}$, 1453.0 (45) $[\text{M}+4\text{H}]^{4+}$.

HR-MS (ESI): calc. for $\text{C}_{250}\text{H}_{392}\text{N}_{96}\text{O}_{61}\text{S}_3$ ($[\text{M}+6\text{H}]^{6+}$): 968.9954, found: 968.9952;

calc. for $\text{C}_{250}\text{H}_{391}\text{N}_{96}\text{O}_{61}\text{S}_3$ ($[\text{M}+5\text{H}]^{5+}$): 1162.5930, found: 1162.5950;

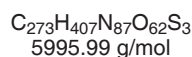
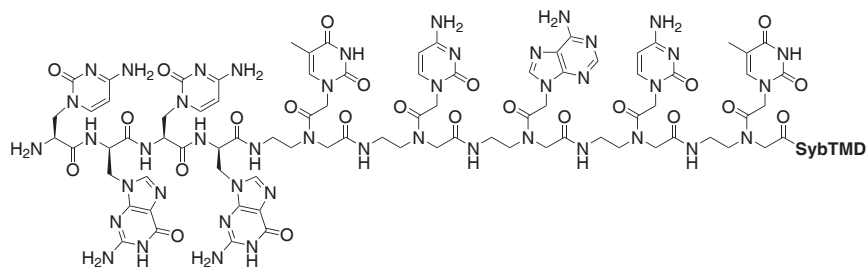
calc. for $\text{C}_{250}\text{H}_{390}\text{N}_{96}\text{O}_{61}\text{S}_3$ ($[\text{M}+4\text{H}]^{4+}$): 1452.9895, found: 1452.9866.

MS (MALDI, linear mode): m/z = 5805.7065.



6. Experimental Section

Ala1-PNA1s-SybTMD (22)



22

The synthesis was performed via manual SPPS as described in Section 6.5.4 on a Wang resin that contained the Synaptobrevin-2 transmembrane domain and the aeg-PNA part of the recognition unit. Cleavage from the resin was performed with Mix D as described in Section 6.5.5.

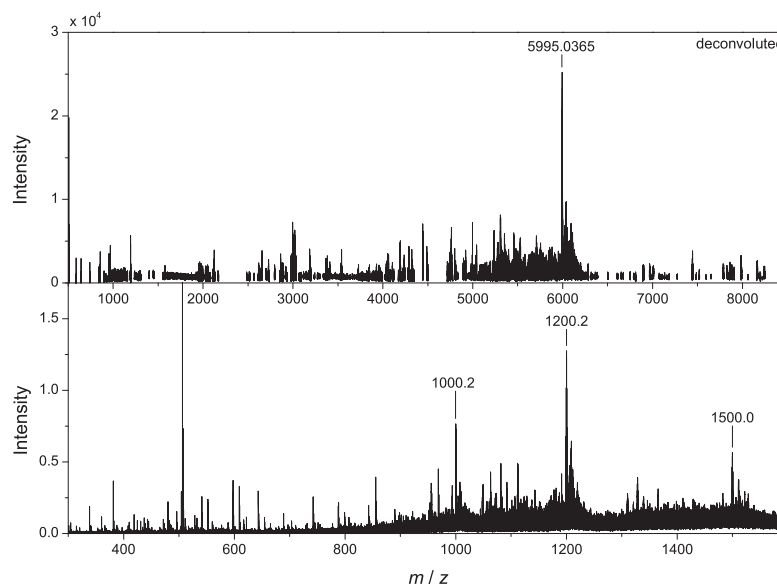
MS (ESI): m/z (%) = 1000.2 (60) $[\text{M}+6\text{H}]^{6+}$, 1200.2 (100) $[\text{M}+5\text{H}]^{5+}$, 1500.0 (42) $[\text{M}+4\text{H}]^{4+}$.

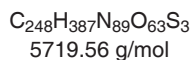
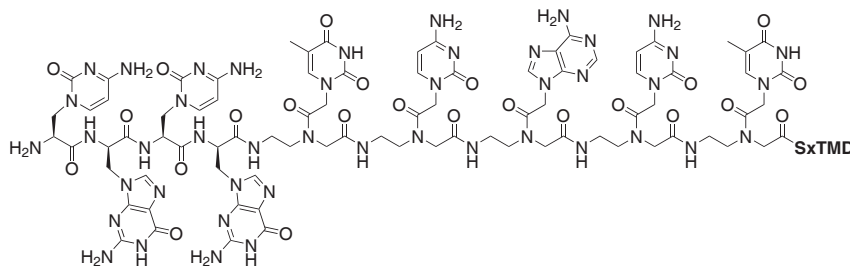
HR-MS (ESI): calc. for $\text{C}_{273}\text{H}_{413}\text{N}_{87}\text{O}_{62}\text{S}_3$ ($[\text{M}+6\text{H}]^{6+}$): 1000.1841, found: 1000.1828;

calc. for $\text{C}_{273}\text{H}_{412}\text{N}_{87}\text{O}_{62}\text{S}_3$ ($[\text{M}+5\text{H}]^{5+}$): 1200.2199, found: 1200.2181;

calc. for $\text{C}_{273}\text{H}_{411}\text{N}_{87}\text{O}_{62}\text{S}_3$ ($[\text{M}+4\text{H}]^{4+}$): 1500.0230, found: 1500.0225.

MS (MALDI, linear mode): m/z = 5992.0376.



Ala1-PNA1s-SxTMD (23)


23

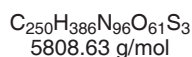
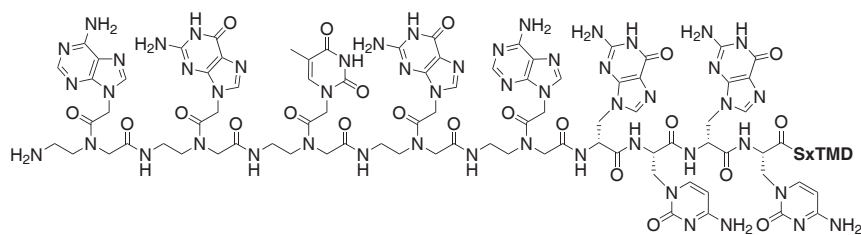
The synthesis was performed via manual SPPS as described in Section 6.5.4 on a Wang resin that contained the Syntaxin-1A transmembrane domain and the aeg-PNA part of the recognition unit. Cleavage from the resin was performed with Mix D as described in Section 6.5.5.

MS (ESI): m/z (%) = 1144.8 (100) $[\text{M}+5\text{H}]^{5+}$, 1431.0 (37) $[\text{M}+4\text{H}]^{4+}$.

HR-MS (ESI): calc. for $\text{C}_{248}\text{H}_{392}\text{N}_{89}\text{O}_{63}\text{S}_3$ ($[\text{M}+5\text{H}]^{5+}$): 1144.7883, found: 1144.7886;
 calc. for $\text{C}_{248}\text{H}_{391}\text{N}_{89}\text{O}_{63}\text{S}_3$ ($[\text{M}+4\text{H}]^{4+}$): 1430.7335, found: 1430.7346.

6. Experimental Section

PNA3s-Ala2-SxTMD (24)



24

The synthesis was performed via manual SPPS as described in Section 6.5.4 on a Wang resin that contained the Syntaxin-1A transmembrane domain and the ala-PNA part of the recognition unit. Cleavage from the resin was performed with Mix D as described in Section 6.5.5.

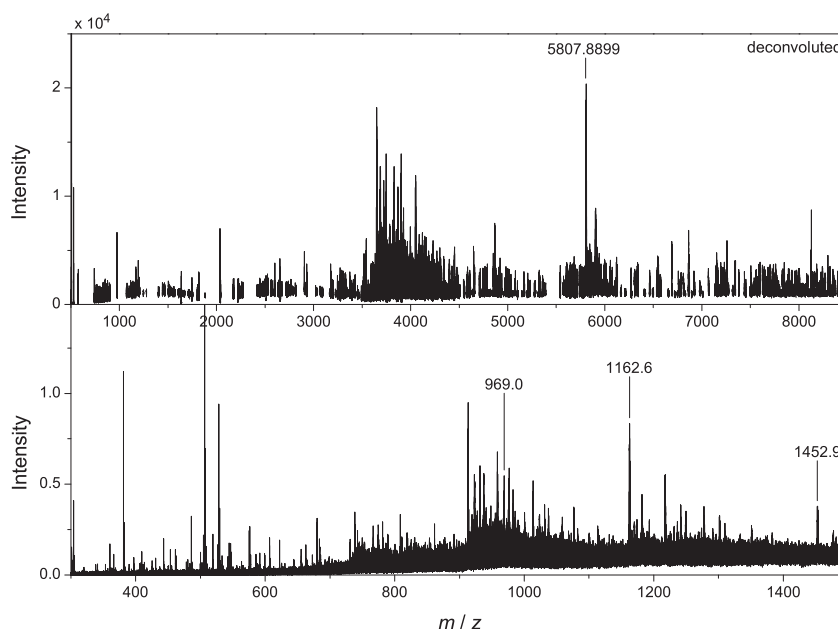
MS (ESI): m/z (%) = 969.0 (63) $[\text{M}+6\text{H}]^{6+}$, 1162.6 (100) $[\text{M}+5\text{H}]^{5+}$, 1452.9 (40) $[\text{M}+4\text{H}]^{4+}$.

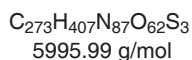
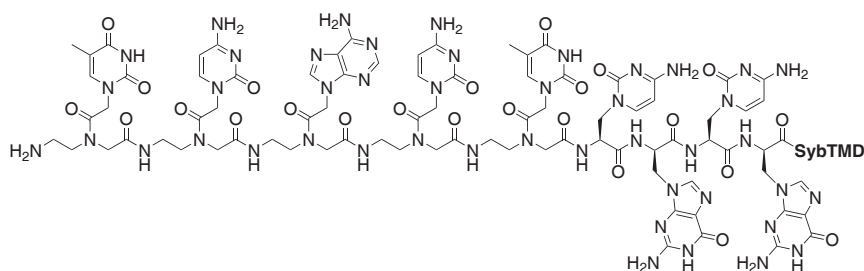
HR-MS (ESI): calc. for $\text{C}_{250}\text{H}_{392}\text{N}_{96}\text{O}_{61}\text{S}_3$ ($[\text{M}+6\text{H}]^{6+}$): 968.9954, found: 969.0087;

calc. for $\text{C}_{250}\text{H}_{391}\text{N}_{96}\text{O}_{61}\text{S}_3$ ($[\text{M}+5\text{H}]^{5+}$): 1162.5930, found: 1162.5956;

calc. for $\text{C}_{250}\text{H}_{390}\text{N}_{96}\text{O}_{61}\text{S}_3$ ($[\text{M}+4\text{H}]^{4+}$): 1452.9895, found: 1452.9881.

MS (MALDI, linear mode): m/z = 5806.3081.



PNA1s-Ala1-SybTMD (25)

25

The synthesis was performed via manual SPPS as described in Section 6.5.4 on a Wang resin that contained the Synaptobrevin-2 transmembrane domain and the ala-PNA part of the recognition unit. Cleavage from the resin was performed with Mix D as described in Section 6.5.5.

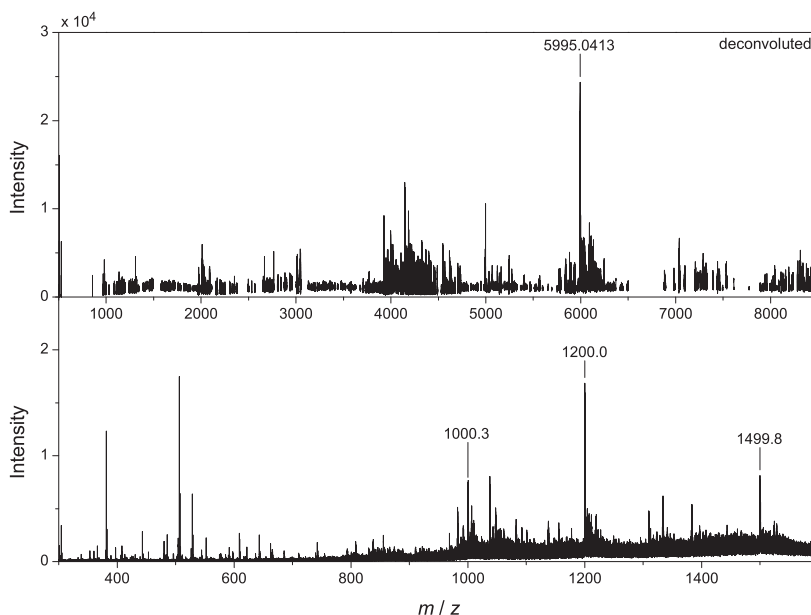
MS (ESI): m/z (%) = 1000.3 (45) $[\text{M}+6\text{H}]^{6+}$, 1200.0 (100) $[\text{M}+5\text{H}]^{5+}$, 1499.8 (45) $[\text{M}+4\text{H}]^{4+}$.

HR-MS (ESI): calc. for $\text{C}_{273}\text{H}_{413}\text{N}_{87}\text{O}_{62}\text{S}_3$ ($[\text{M}+6\text{H}]^{6+}$): 1000.1841, found: 1000.1822;

calc. for $\text{C}_{273}\text{H}_{412}\text{N}_{87}\text{O}_{62}\text{S}_3$ ($[\text{M}+5\text{H}]^{5+}$): 1200.0194, found: 1200.0186;

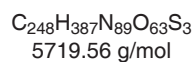
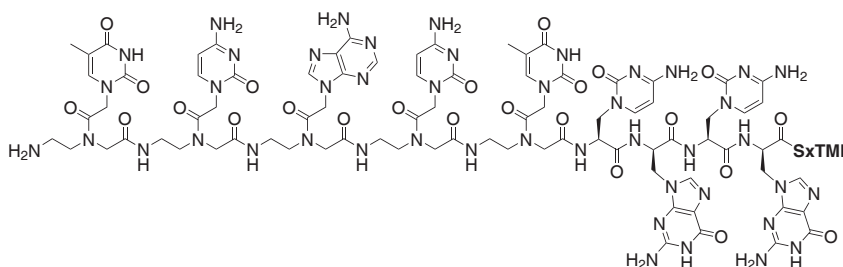
calc. for $\text{C}_{273}\text{H}_{411}\text{N}_{87}\text{O}_{62}\text{S}_3$ ($[\text{M}+4\text{H}]^{4+}$): 1499.7725, found: 1499.7747.

MS (MALDI, reflectron mode): m/z = 5992.



6. Experimental Section

PNA1s-Ala1-SxTMD (26)



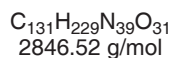
26

The synthesis was performed via manual SPPS as described in Section 6.5.4 on a Wang resin that contained the Syntaxin-1A transmembrane domain and the ala-PNA part of the recognition unit. Cleavage from the resin was performed with Mix D as described in Section 6.5.5.

MS (ESI): m/z (%) = 1144.8 (70) $[\text{M}+5\text{H}]^{5+}$.

HR-MS (ESI): calc. for $\text{C}_{248}\text{H}_{392}\text{N}_{89}\text{O}_{63}\text{S}_3$ ($[\text{M}+5\text{H}]^{5+}$): 1144.7883, found: 1144.7890;
 calc. for $\text{C}_{248}\text{H}_{391}\text{N}_{89}\text{O}_{63}\text{S}_3$ ($[\text{M}+4\text{H}]^{4+}$): 1430.7335, found: 1430.7308.

Melittin



Melittin (1-26) from *Apis mellifera* was synthesized automatically according to the description in Section 6.5.3. A low loaded Rink amide MBHA resin was used, which was preloaded with Fmoc-Gln(Trt)-OH as described in Section 6.5.1. Cleavage from the resin was performed with Mix A as indicated in Section 6.5.5. Purification was done via HPLC as described in Section 6.2.

HPLC (column 3, 20 → 80 % B in 30 min): $t_R = 19.1$ min.

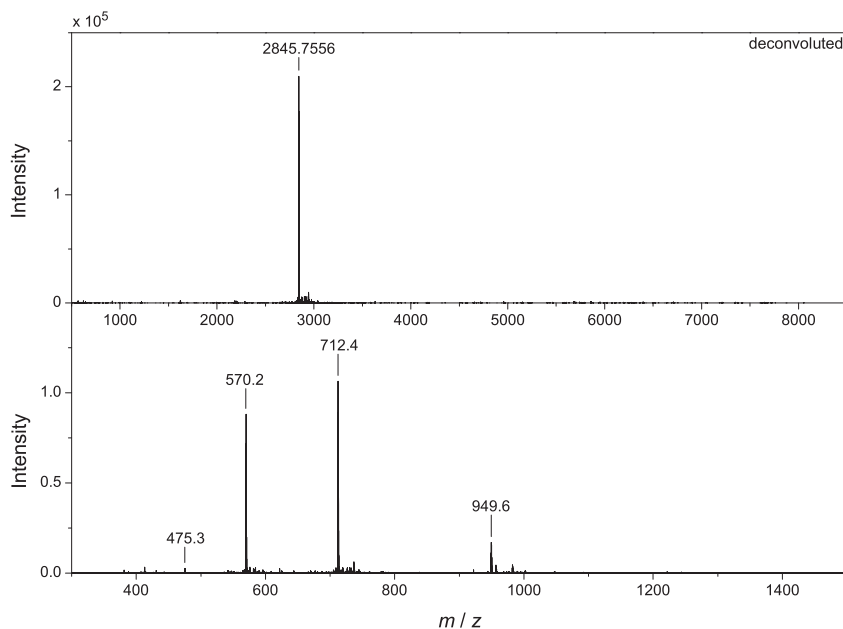
MS (ESI): m/z (%) = 475.3 (2) $[\text{M}+6\text{H}]^{6+}$, 570.2 (82) $[\text{M}+5\text{H}]^{5+}$, 712.4 (100) $[\text{M}+4\text{H}]^{4+}$, 949.6 (16) $[\text{M}+3\text{H}]^{3+}$.

HR-MS (ESI): calc. for $\text{C}_{131}\text{H}_{235}\text{N}_{39}\text{O}_{31}$ ($[\text{M}+6\text{H}]^{6+}$): 475.3001, found: 475.2995;

calc. for $\text{C}_{131}\text{H}_{234}\text{N}_{39}\text{O}_{31}$ ($[\text{M}+5\text{H}]^{5+}$): 570.1587, found: 570.1595;

calc. for $\text{C}_{131}\text{H}_{233}\text{N}_{39}\text{O}_{31}$ ($[\text{M}+4\text{H}]^{4+}$): 712.4465, found: 712.4474;

calc. for $\text{C}_{131}\text{H}_{232}\text{N}_{39}\text{O}_{31}$ ($[\text{M}+3\text{H}]^{3+}$): 949.5929, found: 949.5936.





6.6. Fusion Assays

6.6.1. General Remarks

Buffer. All fusion assays were carried out in HEPES buffer (20 mM HEPES, 100 mM KCl, 1 mM EDTA, 1 mM DTT, pH = 7.4). The buffer was prepared freshly each day. For this, a 10-fold stock solution consisting of HEPES, KCl and EDTA was diluted with ultrapure water. DTT was added, and the pH value was adjusted using 1 M KOH. The buffer was filtered through a *Chromafil* syringe filter (regenerated cellulose, 0.45 μ m pore size) by *Macherey-Nagel GmbH & Co. KG* (Düren, Germany).

Lipid Stock Solutions. Solid phospholipids were stored at -20 °C. Stock solutions were prepared in chloroform and stored at -20 °C in brown glass vials. The concentration of 1,2-dioleoyl-*sn*-glycero-3-phosphocholine (18:1, Δ 9-*cis*, DOPC), 1,2-dioleoyl-*sn*-glycero-3-phosphoethanolamine (18:1, Δ 9-*cis*, DOPE) and cholesterol stock solutions was 20 mg/mL, that of NBD-DOPE, NBD-DOPS and Rh-DOPE stock solutions was 2 mg/mL and stock solutions of OG-DHPE and TR-DHPE had a concentration of 1 mg/mL.

Peptide Stock Solutions. Peptides were dissolved in TFE and the solution was filtered. The concentration of the stock solutions was determined via UV absorption at 260 nm as described in Section 6.3. The stock solutions were stored in *Eppendorf* tubes at -20 °C.

Extruder. For extrusion of the lipid solutions, a *LiposoFast-Basic* extruder by *Avestin* (Ottawa, Canada) was used. Before assembling, all parts were thoroughly washed with ethanol, ultrapure water and buffer (in this order). A polycarbonate membrane with a pore diameter of 100 nm by *Avestin* was used together with *Whatman* polyester drain discs by *GE Healthcare* (Little Chalfont, UK) located before and behind the membrane. It was made sure that every part was mounted tightly and that no air bubbles were inside the extruder.

6.6.2. Preparation of Lipid Films via Direct Mixing

Lipid films were prepared in small glass test tubes. The preparation was performed on ice to prevent evaporation of the solvents. The total volume in the test tube was 500 μ L, of that 250 μ L chloroform and 250 μ L TFE. First, chloroform was added, followed by appropriate amounts of lipid stock solutions according to the desired lipid composition.



Table 6.4 provides an overview of the lipid compositions of the liposomes used in this thesis.

Table 6.4. Lipid composition of liposomes used in this thesis.

Type of liposome	Lipid composition (molar ratio)
unlabeled	DOPC/DOPE/Chol = 50:25:25
unlabeled	DOPC/DOPE/DOPS/Chol = 50:20:20:10
labeled (NBD+Rh)	DOPC/DOPE/Chol/NBD-DOPE/Rh-DOPE = 50:22:25:1.5:1.5
labeled (NBD+Rh)	DOPC/DOPE/DOPS/Chol/NBD-DOPE/Rh-DOPE = 50:17:20:10:1.5:1.5
NBD-labeled	DOPC/DOPE/Chol/NBD-DOPE = 50:23.5:25:1.5
Rh-labeled	DOPC/DOPE/Chol/Rh-DOPE = 50:23.5:25:1.5
labeled (OG+TR)	DOPC/DOPE/Chol/OG-DHPE/TR-DHPE = 50:22.5:25:1.5:1
OG-labeled	DOPC/DOPE/Chol/OG-DHPE = 50:23.5:25:1.5
TR-labeled	DOPC/DOPE/Chol/TR-DHPE = 50:24:25:1

After that, TFE was added, followed by the respective peptide stock solution according to the desired peptide-to-lipid ratio. The solution was allowed to warm up to room temperature and then vortexed for 5 s. The solution was warmed up to 50 °C and again vortexed for 5 s. Subsequently, solvents were removed in a slight N₂ stream at 50 °C which produced a clear lipid film on the wall of the test tubes. Test tubes containing labeled lipids were wrapped with aluminum foil to protect the samples from light. To ensure complete solvent removal, the lipid films were stored overnight at 50 °C in a vacuum oven. If the lipid films were not used for the preparation of liposomes on the next day, the test tubes were filled with argon, closed with *Parafilm M* and stored at –20 °C.

6.6.3. Preparation of Lipid Films via Detergent Removal

The following procedure was adapted from a procedure described for SNARE protein reconstitution into liposomes.^[219] A lipid film containing lipids only (2.5 μmol) was produced as described in Section 6.6.2. *n*-Octyl-β-D-glucoside (nOG) was dissolved in HEPES buffer (0.1 M) and was added (18.2 μmol nOG). The mixture was incubated on ice for 20 min, vortexed (3 x 30 s) and incubated for further 10 min. Then, the peptide stock solution was added to yield a peptide-to-lipid ratio of 1:200, and the mixture was incubated for another 50 min. Afterwards, the detergent was removed via an *illustra NAP10* size exclusion column by *GE Healthcare* (Little Chalfont, UK) equilibrated with buffer. The combined fractions containing lipids were concentrated in a lyophilizer centrifuge. The concentrate was subjected to another size exclusion column equilibrated with ultra-pure water to remove the buffer salts. The collected fractions were concentrated again,



6. Experimental Section

transferred to a small glass flask and dried overnight over a saturated NaCl solution under reduced pressure to yield a clear lipid film.

6.6.4. Preparation of Liposomes via Extrusion

The principle of preparing liposomes via extrusion was first described by Hope *et al.*^[220]

The appropriate amount of buffer was added to the test tubes containing the lipid film. Three glass beads ($\varnothing = 2$ mm) were added to support detaching the lipid film from the wall. The test tube was then sealed with *Parafilm M* and incubated at 40 °C with gentle shaking (ca. 150 rpm) on a *Unimax 1010* platform shaker by *Heidolph* (Schwabach, Germany) equipped with an *Incubator 1000* for at least 2 h. After incubation, the lipid film was treated in an ultrasonic bath. As soon as a homogeneous emulsion was formed (typically after several seconds) the mixture was filled into the syringe of the prepared extruder (see Section 6.6.1) and was extruded 31 times. The resulting liposome solution was put into *Eppendorf* tubes and stored at room temperature until utilized. Tubes containing labeled liposomes were wrapped with aluminum foil. Long term storage was done in the refrigerator at 4 °C.

6.6.5. Phosphate Test for Quantification of Phospholipids

The phosphate test is based on a procedure originally described by Rouser *et al.*^[221]

For determination of the total amount of phosphorus, a small volume of the solution of vesicles to be analyzed (typically 20 μL of a 1.25 μM solution) was placed in a small screw-capped glass vial. 200 μL of perchloric acid (70 % in H_2O) was added and mixed with the vesicles by short gentle shaking. A calibration curve was obtained by applying the test to different dilutions of the sodium dihydrogenphosphate standard solution ($c = 0.089$ g/L). For this, five different vials were prepared containing a total mass of phosphorus in the range from 0 μg to 1 μg and each vial was filled up with ultrapure water to make a total volume of 100 μL . All vials (standard and vesicle samples) were prepared in duplicate. After that, all vials were incubated without a cap at 220 °C for at least 20 min until the strong fume development had declined and the vial contents were completely dry. The vials were cooled to ambient temperature. After that, 700 μL of Reagent A (0.45 % $(\text{NH}_4)_6\text{Mo}_7\text{O}_{24} \cdot 4\text{H}_2\text{O}$ and 12.6 % HClO_4 in H_2O) and 700 μL of Reagent B (1.7 % ascorbic acid in H_2O) were added, thoroughly mixed and the vials were capped with a screw-cap. The reagents were made freshly each day. Immediately after this, the vials were incubated in a water bath at 80 °C for 7.5 min. Directly after cooling down

for a few minutes, the vials were shaken to redissolve condensed water from the walls. 200 μL of each sample was transferred onto a microtiter plate (polystyrene, F-bottom) by *Greiner Bio-One GmbH* (Kremsmünster, Austria) and the absorbance at 820 nm was read out with a *CLARIOstar* plate reader by *BMG LABTECH* (Ortenberg, Germany). Alternatively, 1 mL of each sample was transferred to disposable polystyrene cuvettes by *Brand GmbH* (Wertheim, Germany) and the absorbance was determined at 820 nm for 30 s at a *JASCO* spectrofluorometer (see Section 6.3). The calibration curve was obtained by a linear fit of the absorbance values found for the standard measurements. By using the calibration curve, the phosphorus content of the samples could then be determined.

6.6.6. Examination of Liposome Fusion with TLM Assays

Lipid mixing was monitored using a *JASCO* spectrofluorometer (see Section 6.3 for setting details). In dequenching lipid mixing assays, the donor fluorophore was excited and the donor emission was recorded. In quenching assays, the donor fluorophore was excited and the acceptor emission was monitored. The wavelengths applied for excitation and emission can be found in Table 6.2 in Section 6.3. A typical dequenching lipid mixing assay consisted of the following steps. First, a spectrum of the buffer was recorded, followed by monitoring the emission at a fixed wavelength (donor excitation) over time to obtain a mean value of the buffer for background subtraction. The labeled liposomes were added (final concentration in the cuvette: $9.3 \mu\text{M}^1$) and a spectrum was recorded to check for the quality of the liposomes. Subsequently, the emission at a fixed excitation wavelength over time was recorded, and after around 40 s, the unlabeled liposomes ($37 \mu\text{M}$) were added within 10 s. After around 20 min, TX-100 was added (2.5 % in buffer (v/v), $0.68 \mu\text{M}$). After stabilization of the signal, the signal was recorded for further 60 seconds. Lastly, a spectrum was recorded to check if the vesicles were completely destroyed by the detergent (*i.e.* if no FRET signal could be detected anymore). Typically, the buffer volume in the cuvette was 1310 μL and 10 μL of labeled liposomes, 40 μL of unlabeled liposomes and 25 μL of TX-100 were added. The buffer-only measurements were used as a reference for all lipid mixing measurements that were conducted at the same day.

The acquired data was analyzed according to the following: Equation 6.5 was used to calculate F , which was plotted as a function of the time t to obtain the fusion curve.

¹ Note that the indicated values for the final concentration of the liposomes were calculated on the basis of the amount of lipids in the lipid film (typically $0.625 \mu\text{mol}$). The real concentration were lower as the loss of material during extrusion was not considered.

6. Experimental Section

$$F = \frac{F_t - F_0}{F_{\text{total}} - F_0} \quad (6.5)$$

F_t is the recorded fluorescence at the time t , F_0 is the fluorescence recorded before the addition of the second vesicle population and is calculated as the mean value from the last 30 data points before the addition. F_{total} is the fluorescence recorded after the addition of the detergent and is calculated as the mean value from 50 data points after the signal had stabilized. The time $t = 0$ s is set to the first data point after closing the lid of the spectrometer. The fusion curves shown in this thesis are not corrected for the fluorescence quenching or fluorescence enhancing effect of the added detergent.

Quenching experiments followed the steps mentioned above. Detergent, however, was not added. Furthermore, liposomes were added in a 1:1 ratio. Typically, the buffer volume in the cuvette was 1270 μL and 40 μL of each liposome population was added (final concentration of each liposome population: 37 μM). The raw data was corrected for the background. For this, the value for the acceptor emission at $t = 0$ s (addition of the second liposome population) was subtracted from all data points. Fusion curves were then scaled arbitrarily in order to compare their shape to those from dequenching assays.

If not otherwise stated the fusion curves obtained from bulk lipid mixing assays shown in this thesis are the results of TLM dequenching assays with liposomes meeting the following criteria: no DOPS present, total amount of lipids in the lipid film: 0.625 μmol , peptide-to-lipid ratio: 1:1000, preparation via extrusion of lipid films that had been prepared by direct lipid mixing, liposomes labeled with NBD and Rh, Syb-based peptides in labeled liposomes (for dequenching assays) or in liposomes labeled with the acceptor fluorophore (for quenching assays). Fusion curves shown with error bars are mean fusion curves calculated from the data of several independent measurements, those without error bars are single measurements.

6.6.7. Examination of Liposome Fusion with ILM Assays

In order to monitor inner lipid mixing, the labeled vesicles were first treated with $\text{S}_2\text{O}_4^{2-}$ ions to inactivate NBD fluorophores on the outer leaflets. For this, labeled vesicles (typically 40 μL) were diluted with buffer (typically 1250 μL , final concentration of liposomes in the cuvette: 39 μM). The residual NBD fluorescence upon NBD excitation was monitored ($\lambda_{\text{ex}} = 460$ nm, $\lambda_{\text{em}} = 530$ nm) and then a sodium dithionite solution (50 mM) was added (typically 20 μL , yielding a final $\text{S}_2\text{O}_4^{2-}$ concentration in the cuvette of ~ 760 μM). For the sodium dithionite solution, solid $\text{Na}_2\text{S}_2\text{O}_4$ was dissolved in liposome buffer im-

mediately before use. NBD fluorescence was monitored until the fluorescence reached 40 % of its initial value. Then, O₂ was bubbled through the cuvette for 10 s to oxidize excess dithionite ions, following by N₂ for 10 s to remove excess oxygen from the solution. A quarter of the mixture with the reduced labeled vesicles was diluted with buffer to a volume of 1310 μL in a fresh cuvette and inner lipid mixing was then monitored in the same way as described for total lipid mixing (see Section 6.6.6).

For the tests with melittin, a melittin stock solution was prepared in ultrapure water and the concentration was determined via UV absorption as described in Section 6.3. The solution was prepared freshly each day. It was added at distinct times to examine the reduction process. The final concentration of melittin in the cuvette was 1.8 μM.

ILM assays were performed with liposomes that contained the model peptides in a peptide-to-lipid ratio of 1:200. Other than that, liposomes met the same criteria as liposomes used for TLM assays (see Section 6.6.6).

6.6.8. Examination of Liposome Fusion with FCCS

For the FCCS measurements a setup similar to that described in Ref. [222] was used with the following modifications. A *Chameleon* titanium-sapphire laser (90 MHz, 800 nm) by *Coherent* (Santa Clara, USA) was used to simultaneously excite the two different fluorophores with an excitation energy of around 22 mW. The laser beam was directed via a lens system through an *FEL0750* long pass filter by *ThorLabs* (Newton, USA) and the first dichroic mirror to the objective, which pointed onto a coverslip on which the sample droplet was located. The emission was collected by the same objective, passed the first dichroic mirror, and was split via a second dichroic mirror (and filtered by band pass filters) to allow individual detection of the fluorescence intensities in the green (detection of OG-labeled particles) and the red channel (detection of TR-labeled particles). Detection was performed with avalanche photodiodes. Analysis of the detector signals was accomplished using constant fraction discriminator inputs of a *DPC-230* 16-channel photon correlator by *Becker&Hickl* (Berlin, Germany). The acquired data was processed using a homemade software.

First, the particle concentration of each liposome population was monitored and adjusted to 0.3–0.7 particles at a time per focal volume by appropriate dilution with buffer. This corresponded to a lipid concentration of roughly 40 μM per liposome population. It was made sure that those liposome solutions that were to be mixed, exhibited the same particle concentration. OG- and TR-labeled liposomes were then mixed in a 1:1 ratio (40 μL each) by short pipetting. 40 μL of the mixture was transferred to the coverslip

6. Experimental Section

and the measurement was started immediately. The time $t = 0$ s was set to the point at which the liposomes had been mixed. A typical measurement took 10 min. Data was acquired at room temperature during 15 s measuring cycles, which were repeated 40 times to cover a monitored timespan of 10 min. Data that had been acquired when the detected count rate exceeded the limit of the detectors was not considered in the analysis. Control measurements were performed on the same day as the corresponding measurements using the same liposomes. If not indicated otherwise, the P/L ratio in the liposomes was 1:200. For the fluorescence lifetime analysis only measurements taken on the same day were compared to ensure identical conditions such as the same age of the fluorophores.

The plotted mean lifetime values were calculated from 8–10 data points (corresponding to 8–10 measuring cycles). The cross-correlation was plotted as the ratio of cross-correlated particles, $\frac{1}{2}(\frac{N_x}{N_G} + \frac{N_x}{N_R})$, considering the numbers of particles in the red channel (N_R), in the green channel (N_G) and the number of cross-correlated particles (N_x). Each plotted data point corresponds to the mean value resulting from one cycle. For each data set, the weighted moving average was calculated (points of window: 10, boundary condition: repeat) and is depicted as a solid line.

6.6.9. Examination of Liposome Fusion with DLS

The size distribution of liposomes and its change during liposome fusion were monitored on a *Zetasizer Nano S* light scattering system by *Malvern Instruments* (Malvern, UK), equipped with a 4 mW laser of 633 nm wavelength, which probed the samples at a scattering angle of 173° . Data was acquired with the software provided by the manufacturer. The temperature during measurement was 25°C . The sample volume was 1 mL and it was measured in disposable cuvettes. For measuring individual liposome samples, one measurement consisted of 10 runs at 10 s and was repeated twice. For measuring the size change during liposome fusion, the liposomes were mixed in a separate cuvette and samples were then taken every few minutes. If not indicated otherwise, the liposome concentrations in the DLS cuvette were the same as in the cuvette during dequenching lipid mixing experiments (see Section 6.6.6). Between the measurements, the liposome mixture was stirred continuously. Each plotted data point represents the results of a measurement that comprised 6 runs at 10 s, which was repeated twice. Including an optimizing procedure at the beginning, the acquisition time thus was around 230 s for a measurement. Each plotted data point is the weighted arithmetic mean calculated from the intensity size distribution. In plots of time-dependent analyses, the indicated time points refer to the time points at the end of the measurement cycle.

A. Appendix

A.1. Additional Chromatograms Obtained From HPLC and SEC

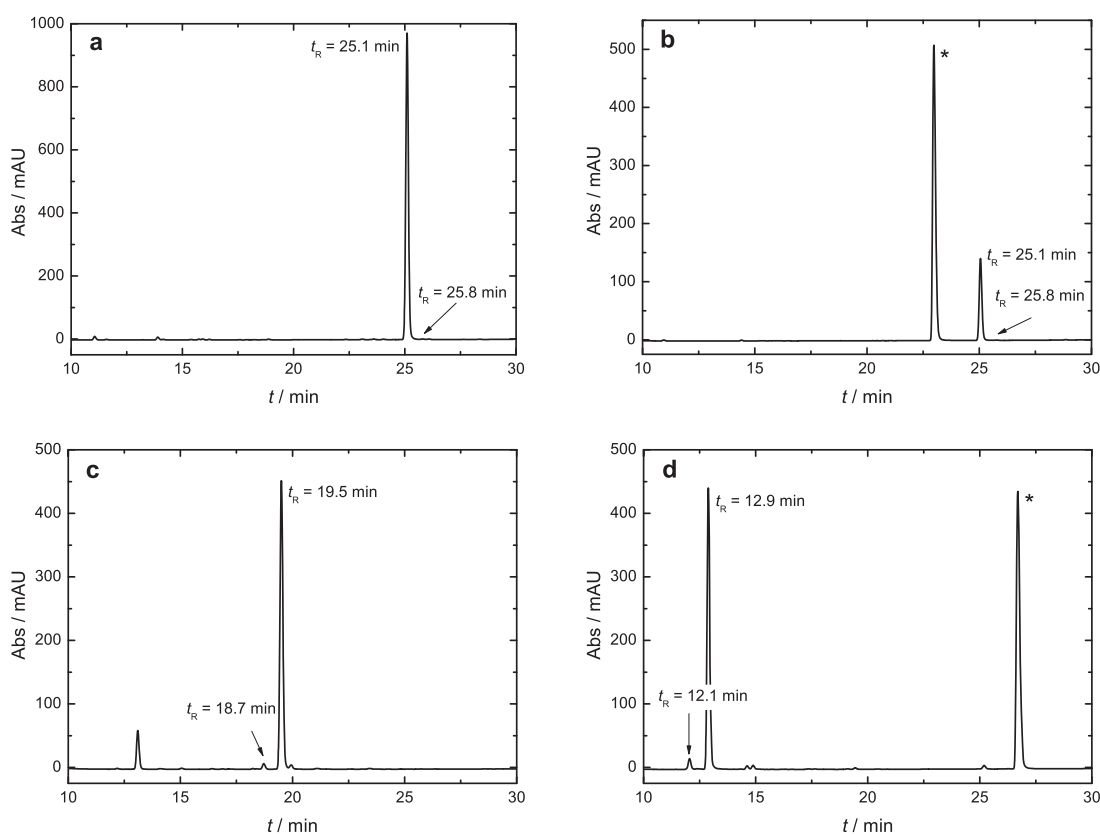


Figure A.1. Determination of the enantiomeric excess (see also Section 3.2). Building blocks were converted to the respective diastereomers and the reaction mixture was analyzed via HPLC. Peaks labeled with retention times were integrated and compared to calculate the ee values. Peaks marked with an asterisk arise from the cleaved Fmoc protection group. See Section 6.4.1 for details about HPLC conditions. (a) Boc-L-AlaC(Z)-OH, (b) Fmoc-L-AlaC(Z)-OH, (c) Boc-D-Ala(2-amino-6-chloropurin-9-yl)-OH, (d) Fmoc-D-AlaG-OH.

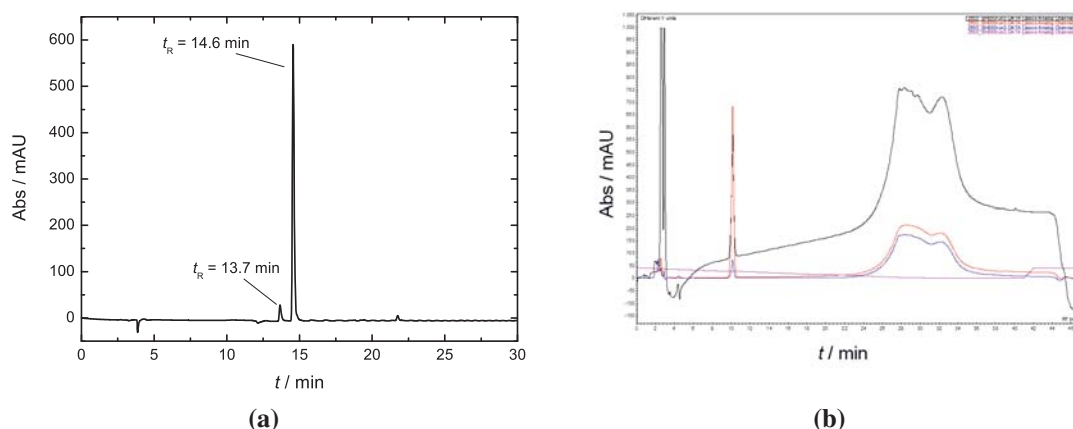


Figure A.2. (a) Chromatogram obtained from HPLC of the test tripeptide Boc-L-Ala-D-Ala-Gly-OH, which was synthesized to elucidate if the stereochemical information is maintained during coupling (column 1, 0 → 20 % B in 30 min). The absorption was recorded at 260 nm. ESI-MS confirmed that both peaks can be assigned to the tripeptide (ee = 88 %). See Section 3.3. (b) Chromatogram obtained from HPLC of Ala1-PNA1-SybTMD (**10**) on column 2, 60 → 100 % solvent C in 30 min. It represents one of the chromatograms with the best resolved peaks during purification of the model peptides. The sample was dissolved in MeOH/TFE/FA (10:1:0.8) prior to injection. The absorption was recorded at 215 nm (black line), 254 nm (red) and 280 nm (blue). See Section 3.4.

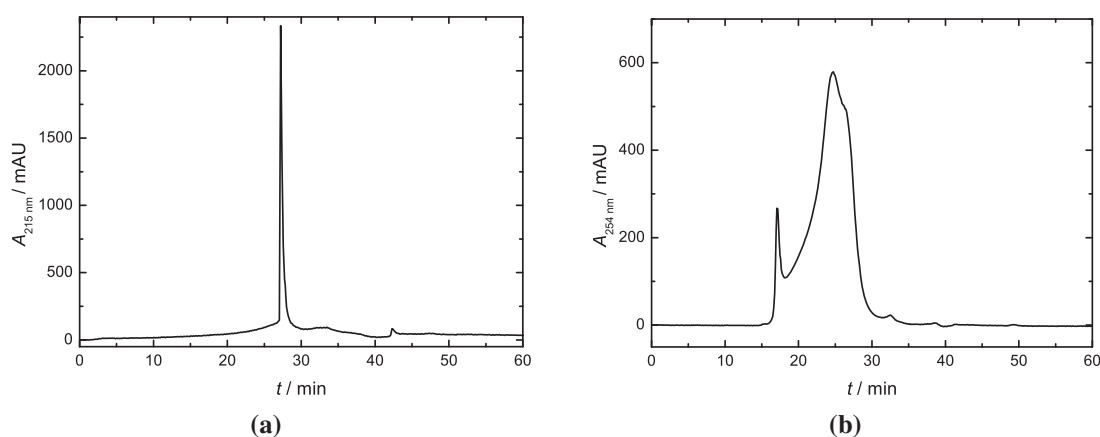


Figure A.3. Chromatograms obtained from SEC of PNA1-SybTMD (**8**) (a) and Ala1-PNA1-SybTMD (**10**) (b) on a Superose column. The solvent was a phosphate buffer with 2 % SDS added; the SEC was performed isocratically at a flow rate of 0.5 mL/min. The sample was dissolved in MeCN and H₂O (**8**) or in the eluent (**10**) prior to injection. The absorption was recorded at 215 nm (a) and 254 nm (b), respectively. See Section 3.4.



A.2. Individual Fusion Curves From TLM Dequenching Assays

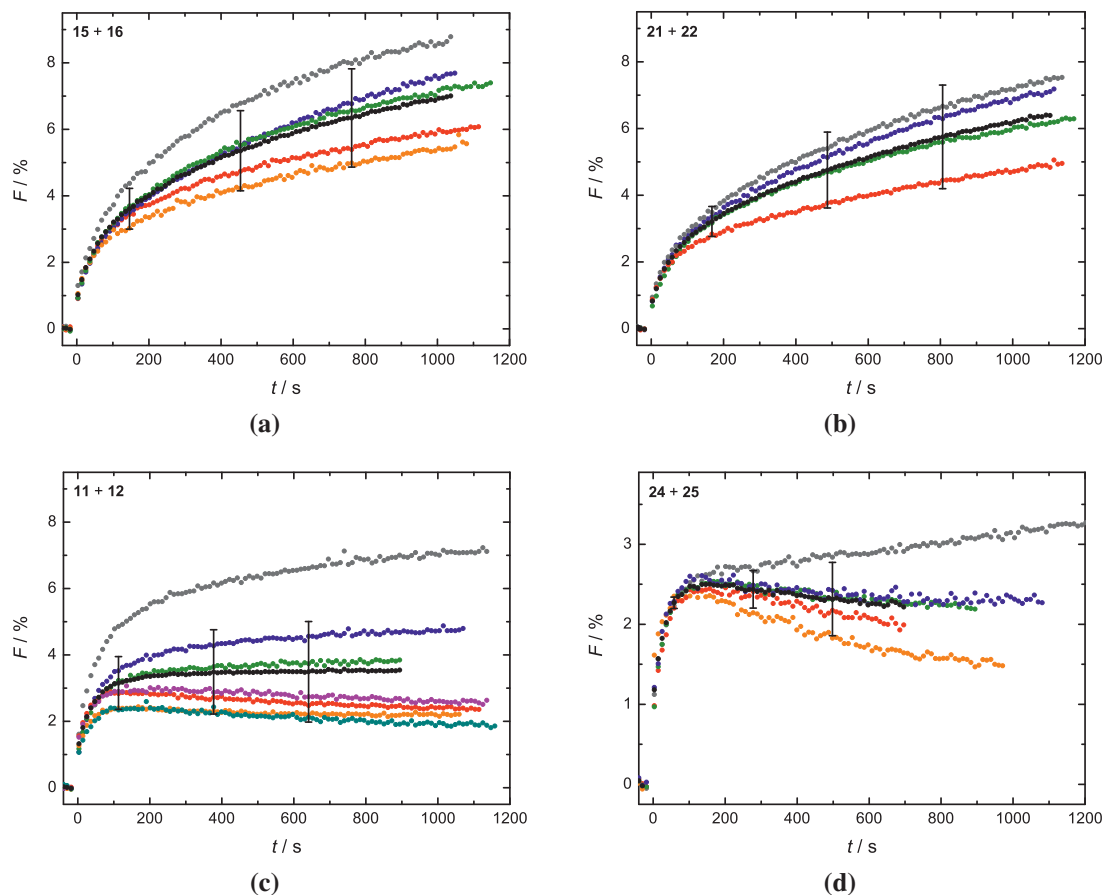


Figure A.4. Overview of individual fusion curves obtained from TLM dequenching assays of **15 + 16** (a), **21 + 22** (b), **11 + 12** (c) and **24 + 25** (d), which were used to calculate the mean fusion curves. The mean fusion curves including error bars are depicted black. They are identical to those shown in Figure 4.9 (Section 4.3.3). All fusion curves represent the experimental outcome of assays with independently prepared liposome samples and with the same experimental conditions being applied. Details can be found in Section 6.6.6.

A.3. Additional DLS Data

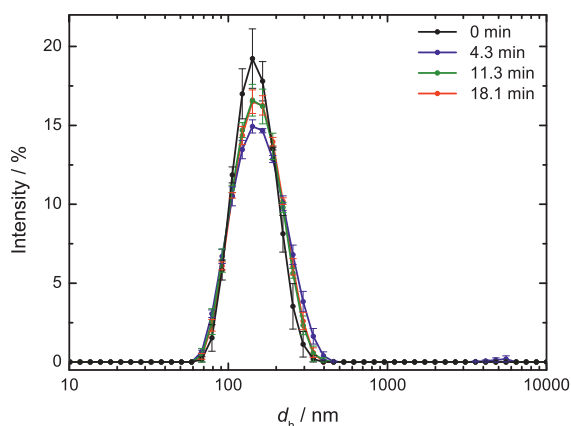


Figure A.5. Mean size distribution as determined by DLS of the control measurement, in which empty liposomes were added to liposomes containing **19**. The mean size distribution obtained from the corresponding experiment in which both liposome populations contained peptides is shown in Figure 4.24 (Section 4.6). Liposomes labeled with OG and TR were used and the P/L ratio was 1:200.

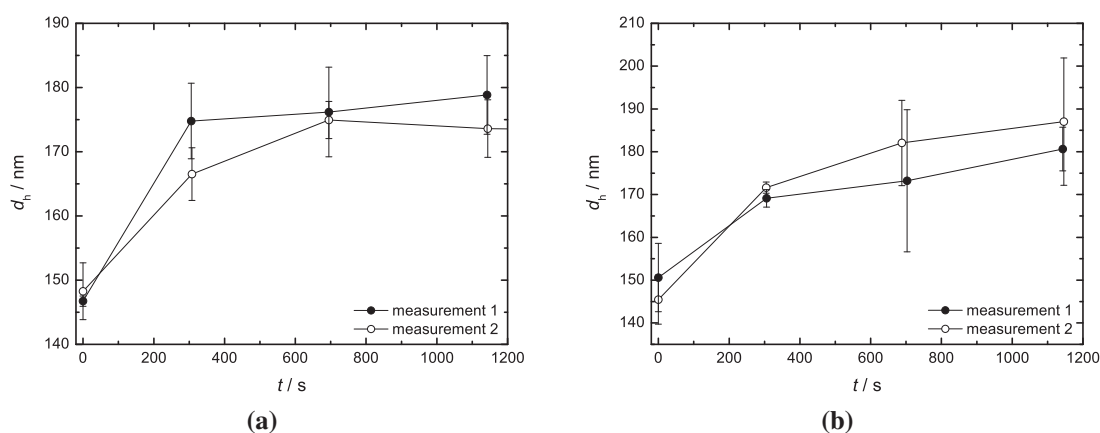


Figure A.6. The reproducibility of the DLS measurements is exemplarily shown for assays with liposomes containing **15 + 16** (a) and **18 + 19** (b) at P/L = 1:1000. The measurements were performed on different days with independently prepared liposomes samples. Liposomes labeled with NBD and Rh as in TLM dequenching assays were used. The data points are connected via thin lines to guide the reader's eye.

A.4. Estimating the Number of Lipids and Model Peptides per Liposome

By assuming the liposome as a uniform sphere with the radius r , its surface S is calculated by

$$S = 4\pi r^2. \quad (\text{A.1})$$

Considering that the lipid bilayer of the liposome has a thickness h and consists of an inner and an outer leaflet, which both comprise lipids, and that each lipid covers an area that corresponds to the lipid headgroup area a , one obtains for the amount of lipids per liposome:

$$N_{\text{Lipids}} = \frac{4\pi(r^2 + (r-h)^2)}{a} \quad (\text{A.2})$$

The following values are needed to calculate N_{Lipids} and can be found in the indicated references. As the radius r of the liposomes, the mean value from the DLS measurements (see Section 4.1) is taken.

h	5 nm ^[223]
a_{PE}	0.54 nm ² ^[224]
a_{PC}	0.57 nm ² ^[225]
a_{Chol}	0.24 nm ² ^[225]
r	75 nm

Considering the lipid composition of the liposomes (50 mol% DOPC, 25 mol% DOPE, 25 mol% Chol), this yields an estimated rounded number of lipids per liposomes of 275,000. The number of PNA/peptide hybrids is then easily calculated from the peptide-to-lipid ratio $R_{\text{P/L}}$ according to the following equation:

$$N_{\text{Peptides}} = N_{\text{Lipids}} \cdot R_{\text{P/L}} \quad (\text{A.3})$$

The number of PNA/peptide hybrids per liposome is thus ≈ 1400 or ≈ 275 for peptide-to-lipid ratios of 1:200 or 1:1000, respectively.





List of Abbreviations

General. Standard α -amino acids are abbreviated using the common one- or three-letter-code. Nucleobases in aeg-PNA sequences are abbreviated with small letters (a,c,g,t), those in ala-PNA sequences are written in capitals (C, G, the D-configured building block is underlined).

A	absorption intensity
aeg-PNA	<i>N</i> -(2-aminoethyl)glycine-PNA
ala-PNA	alanyl-PNA
ATP	adenosine triphosphate
AU	absorption unit
BD syringe	syringe by <i>Becton Dickinson</i>
Bhoc	benzhydryloxycarbonyl protection group
Boc	butyloxycarbonyl protection group
calc.	calculated
CHAPS	3-[(3-cholamidopropyl)dimethylammonio]-1-propane-sulfonate
Chol	cholesterol
δ	chemical shift (NMR)
DBU	1,8-diazabicyclo[5.4.0]undec-7-ene
DCM	dichloromethane
DEAD	diethyl azodicarboxylate
DHPE	1,2-dihexadecanoyl- <i>sn</i> -glycero-3-phosphoethanolamine
DIC	<i>N,N'</i> -diisopropylcarbodiimide
DIPEA	<i>N,N</i> -diisopropylethylamine
d_h	hydrodynamic diameter
DLS	dynamic light scattering
DMF	dimethylformamide



List of Abbreviations

DMSO	dimethylsulfoxide
DNA	deoxyribonucleic acid
DOPC	1,2-dioleoyl- <i>sn</i> -glycero-3-phosphocholine
DOPE	1,2-dioleoyl- <i>sn</i> -glycero-3-phosphoethanolamine
DOPS	1,2-dioleoyl- <i>sn</i> -glycero-3-phospho-L-serine
DTT	dithiothreitol
ϵ	extinction coefficient
EDT	1,2-ethanedithiole
EDTA	ethylenediaminetetraacetic acid
ee	enantiomeric excess
ent	enantiomer
eq	equivalents
ESI-MS	electrospray ionisation mass spectrometry
F	normalized fluorescence intensity (according to Equation 6.5)
FA	formic acid
FCCS	fluorescence cross-correlation spectroscopy
Fmoc	9-fluorenylmethoxycarbonyl protection group
FRET	Förster resonance energy transfer
HATU	1-(bis(dimethylamino)methylene)-1 <i>H</i> -1,2,3-triazolo[4,5- <i>b</i>]- pyridinium 3-oxide hexafluorophosphate
HEPES	4-(2-hydroxyethyl)-1-piperazineethanesulfonic acid
HOAt	1-hydroxy-7-azabenzotriazole
HPLC	high performance liquid chromatography
HR-MS	high resolution mass spectrometry
J	coupling constant
LPC	lysophosphatidylcholine
LUV	large unilamellar vesicle
MALDI	matrix-assisted laser desorption/ionization
MBHA	methylbenzhydramine
MeCN	acetonitrile
MeOH	methanol
MLV	multilamellar vesicles
MSNT	1-(mesitylene-2-sulfonyl)-3-nitro-1,2,4-triazole
Munc18	mammalian uncoordinated-18
m/z	mass-to-charge ratio



NBD	7-nitro-2-1,3-benzoxadiazole
NMP	<i>N</i> -methylpyrrolidone
NMR	nuclear magnetic resonance
NSF	<i>N</i> -ethylmaleimide sensitive factor
OG	Oregon Green 488
Oxyma	ethyl cyanohydroxyiminoacetate
Pbf	2,2,4,6,7-pentamethyldihydrobenzofuran-5-sulfonyl protection group
PE	phosphatidylethanolamine
PEG	polyethylene glycol
PIP ₂	phosphatidylinositol 4,5-bisphosphate
P/L ratio	peptide-to-lipid ratio
PNA	peptide nucleic acid
ppm	parts per million
PS	phosphatidylserine
PyBOP	benzotriazol-1-yl-oxytripyrrolidinophosphonium hexafluorophosphate
<i>R_f</i>	retention factor
Rh	Lissamine Rhodamine B
RP	reversed phase
rpm	rotations per minute
rt	room temperature
SDS	sodium dodecylsulfate
SEC	size exclusion chromatography
SM	Sec1/Munc18-like
SNAP	soluble NSF attachment protein
SNAP-25	25-kDa synaptosome-associated protein
SNARE	soluble <i>N</i> -ethylmaleimide-sensitive factor attachment protein receptor
SPPS	solid-phase peptide synthesis
Sx	Syntaxin-1A
SxTMD	Syntaxin-1A (256-288)
Syb	Synaptobrevin-2
SybTMD	Synaptobrevin-2 (85-116)
tBu	<i>tert</i> -butyl protection group



List of Abbreviations

TFA	trifluoroacetic acid
TFE	trifluoroethanol
TIS	triisopropylsilane
THF	tetrahydrofuran
TLC	thin layer chromatography
TMD	transmembrane domain
TR	Texas Red
t_R	retention time
Trt	trityl protection group
TX-100	Triton X-100
UV	ultraviolet
v/v	volume/volume ratio
w/v	weight/volume ratio
Z	carboxybenzyl protection group



Bibliography

- [1] T. C. Südhof, Neurotransmitter release: the last millisecond in the life of a synaptic vesicle, *Neuron* **2013**, *80*, 675–690.
- [2] R. W. Baker, F. M. Hughson, Chaperoning SNARE assembly and disassembly, *Nat. Rev. Mol. Cell Biol.* **2016**, *17*, 465–479.
- [3] R. Jahn, D. Fasshauer, Molecular machines governing exocytosis of synaptic vesicles, *Nature* **2012**, *490*, 201–207.
- [4] J. Rizo, T. C. Südhof, The membrane fusion enigma: SNAREs, Sec1/Munc18 proteins, and their accomplices—guilty as charged?, *Annu. Rev. Cell Dev. Biol.* **2012**, *28*, 279–308.
- [5] X. Lou, Y.-K. Shin, SNARE zippering, *Biosci. Rep.* **2016**, *36*.
- [6] Y. Gao, S. Zorman, G. Gundersen, Z. Xi, L. Ma, G. Sirinakis, J. E. Rothman, Y. Zhang, Single reconstituted neuronal SNARE complexes zipper in three distinct stages, *Science* **2012**, *337*, 1340–1343.
- [7] F. Li, D. Kümmel, J. Coleman, K. M. Reinisch, J. E. Rothman, F. Pincet, A half-zipped SNARE complex represents a functional intermediate in membrane fusion, *J. Am. Chem. Soc.* **2014**, *136*, 3456–3464.
- [8] A. V. Pobbati, A. Stein, D. Fasshauer, N- to C-terminal SNARE complex assembly promotes rapid membrane fusion, *Science* **2006**, *313*, 673–676.
- [9] W. Hong, SNAREs and traffic, *Biochim. Biophys. Acta, Mol. Cell Res.* **2005**, *1744*, 120–144.
- [10] W. S. Trimble, D. M. Cowan, R. H. Scheller, VAMP-1: A synaptic vesicle associated integral membrane protein, *Proc. Natl. Acad. Sci. U.S.A.* **1988**, *85*, 4538–4542.



Bibliography

- [11] M. K. Bennett, N. Calakos, R. H. Scheller, Syntaxin: A Synaptic Protein Implicated in Docking of Synaptic Vesicles at Presynaptic Active Zones, *Science* **1992**, 257, 255–259.
- [12] J. Han, K. Pluhackova, R. A. Böckmann, The Multifaceted Role of SNARE Proteins in Membrane Fusion, *Front. Physiol.* **2017**, 8, 5.
- [13] P. Kumar, S. Guha, U. Diederichsen, SNARE protein analog-mediated membrane fusion, *J. Pept. Sci.* **2015**, 21, 621–629.
- [14] H. R. Marsden, I. Tomatsu, A. Kros, Model systems for membrane fusion, *Chem. Soc. Rev.* **2011**, 40, 1572–1585.
- [15] K. Meyenberg, A. S. Lygina, G. van den Bogaart, R. Jahn, U. Diederichsen, SNARE derived peptide mimic inducing membrane fusion, *Chem. Commun.* **2011**, 47, 9405–9407.
- [16] H. R. Marsden, N. A. Elbers, P. H. H. Bomans, N. A. J. M. Sommerdijk, A. Kros, A reduced SNARE model for membrane fusion, *Angew. Chem. Int. Ed.* **2009**, 48, 2330–2333.
- [17] Y.-H. M. Chan, B. van Lengerich, S. G. Boxer, Lipid-anchored DNA mediates vesicle fusion as observed by lipid and content mixing, *Biointerphases* **2008**, 3, FA17.
- [18] G. Stengel, R. Zahn, F. Höök, DNA-induced programmable fusion of phospholipid vesicles, *J. Am. Chem. Soc.* **2007**, 129, 9584–9585.
- [19] A. S. Lygina, K. Meyenberg, R. Jahn, U. Diederichsen, Transmembrane domain peptide/peptide nucleic acid hybrid as a model of a SNARE protein in vesicle fusion, *Angew. Chem. Int. Ed.* **2011**, 50, 8597–8601.
- [20] A. Rabe, P. M. G. Löffler, O. Ries, S. Vogel, Programmable fusion of liposomes mediated by lipidated PNA, *Chem. Commun.* **2017**, 53, 11921–11924.
- [21] S. A. Whitehead, C. D. McNitt, S. I. Mattern-Schain, A. J. Carr, S. Alam, V. V. Popik, M. D. Best, Artificial Membrane Fusion Triggered by Strain-Promoted Alkyne-Azide Cycloaddition, *Bioconjugate Chem.* **2017**, 28, 923–932.



- [22] A. Kashiwada, M. Tsuboi, T. Mizuno, T. Nagasaki, K. Matsuda, Target-selective vesicle fusion system with pH-selectivity and responsiveness, *Soft Matter* **2009**, *5*, 4719–4725.
- [23] M. Ma, A. Paredes, D. Bong, Intra- and intermembrane pairwise molecular recognition between synthetic hydrogen-bonding phospholipids, *J. Am. Chem. Soc.* **2008**, *130*, 14456–14458.
- [24] P. E. Nielsen, M. Egholm, R. H. Berg, O. Buchardt, Sequence-Selective Recognition of DNA by Strand Displacement with a Thymine-Substituted Polyamide, *Science* **1991**, *254*, 1497–1500.
- [25] P. Wittung, P. E. Nielsen, O. Buchardt, M. Egholm, B. Nordén, DNA-like double helix formed by peptide nucleic acid, *Nature* **1994**, *368*, 561–563.
- [26] U. Diederichsen, Alanyl-PNA: Evidence for Linear Band Structures Based on Guanine-Cytosine Base Pairs, *Angew. Chem. Int. Ed.* **1997**, *36*, 1886–1889.
- [27] D. Langosch, M. Hofmann, C. Ungermann, The role of transmembrane domains in membrane fusion, *Cell Mol. Life Sci.* **2007**, *64*, 850–864.
- [28] J. C. McIntyre, R. G. Sleight, Fluorescence Assay for Phospholipid Membrane Asymmetry, *Biochemistry* **1991**, *30*, 11819–11827.
- [29] J. Nikolaus, M. Stöckl, D. Langosch, R. Volkmer, A. Herrmann, Direct visualization of large and protein-free hemifusion diaphragms, *Biophys. J.* **2010**, *98*, 1192–1199.
- [30] L. V. Chernomordik, M. M. Kozlov, Mechanics of membrane fusion, *Nat. Struct. Mol. Biol.* **2008**, *15*, 675–683.
- [31] R. Lipowsky, The conformation of membranes, *Nature* **1991**, *349*, 475–481.
- [32] M. S. Bretscher, M. C. Raff, Mammalian plasma membranes, *Nature* **1975**, *258*, 43–49.
- [33] G. van Meer, D. R. Voelker, G. W. Feigenson, Membrane lipids: where they are and how they behave, *Nat. Rev. Mol. Cell Biol.* **2008**, *9*, 112–124.
- [34] E. Sezgin, I. Levental, S. Mayor, C. Eggeling, The mystery of membrane organization: composition, regulation and roles of lipid rafts, *Nat. Rev. Mol. Cell Biol.* **2017**, *18*, 361–374.



Bibliography

- [35] W. Dowhan, Molecular Basis for Membrane Phospholipid Diversity: Why Are There So Many Lipids?, *Annu. Rev. Biochem.* **1997**, *66*, 199–232.
- [36] Z. Cournia, T. W. Allen, I. Andricioaei, B. Antony, D. Baum, G. Brannigan, N.-V. Buchete, J. T. Deckman, L. Delemotte, C. Del Val, R. Friedman, P. Gkeka, H.-C. Hege, J. Hénin, M. A. Kasimova, A. Kolocouris, M. L. Klein, S. Khalid, M. J. Lemieux, N. Lindow, M. Roy, J. Selent, M. Tarek, F. Tofoleanu, S. Vanni, S. Urban, D. J. Wales, J. C. Smith, A.-N. Bondar, Membrane Protein Structure, Function, and Dynamics: A Perspective from Experiments and Theory, *J. Membr. Biol.* **2015**, *248*, 611–640.
- [37] J.-L. Popot, D. M. Engelman, Helical Membrane Protein Folding, Stability, and Evolution, *Annu. Rev. Biochem.* **2000**, *69*, 881–922.
- [38] J. W. Fairman, N. Noinaj, S. K. Buchanan, The structural biology of β -barrel membrane proteins: a summary of recent reports, *Curr. Opin. Struct. Biol.* **2011**, *21*, 523–531.
- [39] S. J. Singer, G. L. Nicolson, The Fluid Mosaic Model of the Structure of Cell Membranes, *Science* **1972**, *175*, 720–731.
- [40] K. Simons, M. J. Gerl, Revitalizing membrane rafts: new tools and insights, *Nat. Rev. Mol. Cell Biol.* **2010**, *11*, 688–699.
- [41] L. J. Pike, Rafts defined: a report on the Keystone symposium on lipid rafts and cell function, *J. Lipid Res.* **2006**, *47*, 1597–1598.
- [42] K. Simons, E. Ikonen, Functional rafts in cell membranes, *Nature* **1997**, *387*, 569–572.
- [43] S. Munro, Lipid Rafts: Elusive or Illusive?, *Cell* **2003**, *115*, 377–388.
- [44] M. L. Kraft, Plasma membrane organization and function: moving past lipid rafts, *Mol. Biol. Cell* **2013**, *24*, 2765–2768.
- [45] T. Yeung, G. E. Gilbert, J. Shi, J. Silvius, A. Kapus, S. Grinstein, Membrane Phosphatidylserine Regulates Surface Charge and Protein Localization, *Science* **2008**, *319*, 210–213.
- [46] R. G. W. Anderson, K. Jacobson, A role for lipid shells in targeting proteins to caveolae, rafts, and other lipid domains, *Science* **2002**, *296*, 1821–1825.

- [47] E. Sevcsik, G. J. Schütz, With or without rafts? Alternative views on cell membranes, *BioEssays* **2016**, *38*, 129–139.
- [48] G. E. Palade, R. R. Bruns, Structural Modulations of Plasmalemmal Vesicles, *J. Cell Biol.* **1968**, *37*, 633–649.
- [49] L. V. Chernomordik, M. M. Kozlov, Membrane hemifusion: crossing a chasm in two leaps, *Cell* **2005**, *123*, 375–382.
- [50] M. B. Jackson, E. R. Chapman, The fusion pores of Ca²⁺-triggered exocytosis, *Nat. Struct. Mol. Biol.* **2008**, *15*, 684–689.
- [51] M. Lindau, W. Almers, Structure and function of fusion pores in exocytosis and ectoplasmic membrane fusion, *Curr. Opin. Cell Biol.* **1995**, *7*, 509–517.
- [52] M. M. Kozlov, V. S. Markin, [Possible mechanism of membrane fusion (in Russian)], *Biofizika* **1983**, *28*, 242–247.
- [53] V. S. Markin, J. P. Albanesi, Membrane Fusion: Stalk Model Revisited, *Biophys. J.* **2002**, *82*, 693–712.
- [54] Y. Kozlovsky, M. M. Kozlov, Stalk Model of Membrane Fusion: Solution of Energy Crisis, *Biophys. J.* **2002**, *82*, 882–895.
- [55] J. M. Hernandez, A. Stein, E. Behrmann, D. Riedel, A. Cypionka, Z. Farsi, P. J. Walla, S. Raunser, R. Jahn, Membrane fusion intermediates via directional and full assembly of the SNARE complex, *Science* **2012**, *336*, 1581–1584.
- [56] R. J. Ryham, T. S. Klotz, L. Yao, F. S. Cohen, Calculating Transition Energy Barriers and Characterizing Activation States for Steps of Fusion, *Biophys. J.* **2016**, *110*, 1110–1124.
- [57] H. J. Risselada, Y. Smirnova, H. Grubmüller, Free energy landscape of rim-pore expansion in membrane fusion, *Biophys. J.* **2014**, *107*, 2287–2295.
- [58] H. J. Risselada, H. Grubmüller, How SNARE molecules mediate membrane fusion: recent insights from molecular simulations, *Curr. Opin. Struct. Biol.* **2012**, *22*, 187–196.
- [59] J. M. Seddon, Structure of the inverted hexagonal (H_{II}) phase, and non-lamellar phase transitions of lipids, *Biochim. Biophys. Acta, Rev. Biomembr.* **1990**, *1031*, 1–69.



Bibliography

- [60] B. Katz, R. Miledi, The timing of calcium action during neuromuscular transmission, *J. Physiol.* **1967**, *189*, 535–544.
- [61] Q. Jarosz, “Neuron Hand-tuned”, https://commons.wikimedia.org/wiki/File:Neuron_Hand-tuned.svg, retrieved from English Wikipedia on **August 11, 2017**.
- [62] P. S. Kaeser, W. G. Regehr, Molecular mechanisms for synchronous, asynchronous, and spontaneous neurotransmitter release, *Annu. Rev. Physiol.* **2014**, *76*, 333–363.
- [63] J. S. Bonifacino, B. S. Glick, The Mechanisms of Vesicle Budding and Fusion, *Cell* **2004**, *116*, 153–166.
- [64] P. S. Kaeser, W. G. Regehr, The readily releasable pool of synaptic vesicles, *Curr. Opin. Neurobiol.* **2017**, *43*, 63–70.
- [65] T. C. Südhof, The synaptic vesicle cycle, *Annu. Rev. Neurosci.* **2004**, *27*, 509–547.
- [66] S. C. Harrison, Viral membrane fusion, *Nat. Struct. Mol. Biol.* **2008**, *15*, 690–698.
- [67] T. J. Moss, A. Daga, J. A. McNew, Fusing a lasting relationship between ER tubules, *Trends Cell Biol.* **2011**, *21*, 416–423.
- [68] T. Y. Liu, X. Bian, F. B. Romano, T. Shemesh, T. A. Rapoport, J. Hu, Cis and trans interactions between atlastin molecules during membrane fusion, *Proc. Natl. Acad. Sci. U.S.A.* **2015**, *112*, E1851–60.
- [69] R. Jahn, R. H. Scheller, SNAREs—engines for membrane fusion, *Nat. Rev. Mol. Cell Biol.* **2006**, *7*, 631–643.
- [70] K. G. Hales, M. T. Fuller, Developmentally Regulated Mitochondrial Fusion Mediated by a Conserved, Novel, Predicted GTPase, *Cell* **1997**, *90*, 121–129.
- [71] B. Westermann, Mitochondrial fusion and fission in cell life and death, *Nat. Rev. Mol. Cell Biol.* **2010**, *11*, 872–884.
- [72] A. M. van der Bliek, Q. Shen, S. Kawajiri, Mechanisms of mitochondrial fission and fusion, *Cold Spring Harb. Perspect. Biol.* **2013**, *5*, 1–16.
- [73] P. S. Aguilar, M. K. Baylies, A. Fleissner, L. Helming, N. Inoue, B. Podbilewicz, H. Wang, M. Wong, Genetic basis of cell–cell fusion mechanisms, *Trends Genet.* **2013**, *29*, 427–437.

- [74] J. Pérez-Vargas, T. Krey, C. Valansi, O. Avinoam, A. Haouz, M. Jamin, H. Raveh-Barak, B. Podbilewicz, F. A. Rey, Structural basis of eukaryotic cell–cell fusion, *Cell* **2014**, *157*, 407–419.
- [75] J. C. Lerman, J. Robblee, R. Fairman, F. M. Hughson, Structural Analysis of the Neuronal SNARE Protein Syntaxin-1A, *Biochemistry* **2000**, *39*, 8470–8479.
- [76] S.-H. Hu, C. F. Latham, C. L. Gee, D. E. James, J. L. Martin, Structure of the Munc18c/Syntaxin4 N-peptide complex defines universal features of the N-peptide binding mode of Sec1/Munc18 proteins, *Proc. Natl. Acad. Sci. U.S.A.* **2007**, *104*, 8773–8778.
- [77] A. Stein, G. Weber, M. C. Wahl, R. Jahn, Helical extension of the neuronal SNARE complex into the membrane, *Nature* **2009**, *460*, 525–528.
- [78] E. F. Pettersen, T. D. Goddard, C. C. Huang, G. S. Couch, D. M. Greenblatt, E. C. Meng, T. E. Ferrin, UCSF Chimera—a visualization system for exploratory research and analysis, *J. Comput. Chem.* **2004**, *25*, 1605–1612.
- [79] R. B. Sutton, D. Fasshauer, R. Jahn, A. T. Brunger, Crystal structure of a SNARE complex involved in synaptic exocytosis at 2.4 Å resolution, *Nature* **1998**, *395*, 347–353.
- [80] M. Bowen, A. T. Brunger, Conformation of the synaptobrevin transmembrane domain, *Proc. Natl. Acad. Sci. U.S.A.* **2006**, *103*, 8378–8383.
- [81] D. Fasshauer, R. B. Sutton, A. T. Brunger, R. Jahn, Conserved structural features of the synaptic fusion complex: SNARE proteins reclassified as Q- and R-SNAREs, *Proc. Natl. Acad. Sci. U.S.A.* **1998**, *95*, 15781–15786.
- [82] D. Fasshauer, W. Antonin, V. Subramaniam, R. Jahn, SNARE assembly and disassembly exhibit a pronounced hysteresis, *Nat. Struct. Biol.* **2002**, *9*, 144–151.
- [83] J.-K. Ryu, R. Jahn, T.-Y. Yoon, Progresses in understanding N-ethylmaleimide sensitive factor (NSF) mediated disassembly of SNARE complexes, *Biopolymers* **2016**, *105*, 518–531.
- [84] L. E. P. Dietrich, C. Boeddinghaus, T. J. LaGrassa, C. Ungermann, Control of eukaryotic membrane fusion by N-terminal domains of SNARE proteins, *Biochim. Biophys. Acta, Mol. Cell Res.* **2003**, *1641*, 111–119.



Bibliography

- [85] M. Margittai, J. Widengren, E. Schweinberger, G. F. Schröder, S. Felekyan, E. Haustein, M. König, D. Fasshauer, H. Grubmüller, R. Jahn, C. A. M. Seidel, Single-molecule fluorescence resonance energy transfer reveals a dynamic equilibrium between closed and open conformations of syntaxin 1, *Proc. Natl. Acad. Sci. U.S.A.* **2003**, *100*, 15516–15521.
- [86] P. Zhou, Z. P. Pang, X. Yang, Y. Zhang, C. Rosenmund, T. Bacaj, T. C. Südhof, Syntaxin-1 N-peptide and H_{abc}-domain perform distinct essential functions in synaptic vesicle fusion, *EMBO J.* **2013**, *32*, 159–171.
- [87] D. Fasshauer, H. Otto, W. K. Eliason, R. Jahn, A. T. Brünger, Structural Changes Are Associated with Soluble N-Ethylmaleimide-sensitive Fusion Protein Attachment Protein Receptor Complex Formation, *J. Biol. Chem.* **1997**, *272*, 28036–28041.
- [88] J. F. Ellena, B. Liang, M. Wiktor, A. Stein, D. S. Cafiso, R. Jahn, L. K. Tamm, Dynamic structure of lipid-bound synaptobrevin suggests a nucleation-propagation mechanism for trans-SNARE complex formation, *Proc. Natl. Acad. Sci. U.S.A.* **2009**, *106*, 20306–20311.
- [89] B. Liang, V. Kiessling, L. K. Tamm, Prefusion structure of syntaxin-1A suggests pathway for folding into neuronal trans-SNARE complex fusion intermediate, *Proc. Natl. Acad. Sci. U.S.A.* **2013**, *110*, 19384–19389.
- [90] A. T. Brunger, D. J. Cipriano, J. Diao, Towards reconstitution of membrane fusion mediated by SNAREs and other synaptic proteins, *Crit. Rev. Biochem. Mol. Biol.* **2014**, *50*, 231–241.
- [91] J. Shin, X. Lou, D.-H. Kweon, Y.-K. Shin, Multiple conformations of a single SNAREpin between two nanodisc membranes reveal diverse pre-fusion states, *Biochem. J.* **2014**, *459*, 95–102.
- [92] F. Li, N. Tiwari, J. E. Rothman, F. Pincet, Kinetic barriers to SNAREpin assembly in the regulation of membrane docking/priming and fusion, *Proc. Natl. Acad. Sci. U.S.A.* **2016**, *113*, 10536–10541.
- [93] S. Zorman, A. A. Rebane, L. Ma, G. Yang, M. A. Molski, J. Coleman, F. Pincet, J. E. Rothman, Y. Zhang, Common intermediates and kinetics, but different energetics, in the assembly of SNARE proteins, *eLife* **2014**, e03348.

- [94] A. Witkowska, R. Jahn, Rapid SNARE-mediated Fusion of Liposomes and Chromaffin Granules with Giant Unilamellar Vesicles, *Biophys. J.* **2017**, *113*, 1251–1259.
- [95] C. M. Carr, J. Rizo, At the junction of SNARE and SM protein function, *Curr. Opin. Cell Biol.* **2010**, *22*, 488–495.
- [96] T. C. Südhof, J. E. Rothman, Membrane fusion: grappling with SNARE and SM proteins, *Science* **2009**, *323*, 474–477.
- [97] J. E. Gerst, SNARE regulators: Matchmakers and matchbreakers, *Biochim. Biophys. Acta, Mol. Cell Res.* **2003**, *1641*, 99–110.
- [98] T. C. Südhof, A molecular machine for neurotransmitter release: Synaptotagmin and beyond, *Nat. Med.* **2013**, *19*, 1227–1231.
- [99] K. M. S. Misura, R. H. Scheller, W. I. Weis, Three-dimensional structure of the neuronal-Sec1-syntaxin 1a complex, *Nature* **2000**, *404*, 355–362.
- [100] J. Rizo, J. Xu, The Synaptic Vesicle Release Machinery, *Annu. Rev. Biophys.* **2015**, *44*, 339–367.
- [101] M. Verhage, A. S. Maia, J. J. Plomp, A. B. Brussaard, J. H. Heeroma, H. Vermeer, R. F. Toonen, R. E. Hammer, T. K. van den Berg, M. Missler, H. J. Geuze, T. C. Südhof, Synaptic Assembly of the Brain in the Absence of Neurotransmitter Secretion, *Science* **2000**, *287*, 864–869.
- [102] C. Ma, L. Su, A. B. Seven, Y. Xu, J. Rizo, Reconstitution of the vital functions of Munc18 and Munc13 in neurotransmitter release, *Science* **2013**, *339*, 421–425.
- [103] C. Ma, W. Li, Y. Xu, J. Rizo, Munc13 mediates the transition from the closed syntaxin-Munc18 complex to the SNARE complex, *Nat. Struct. Mol. Biol.* **2011**, *18*, 542–549.
- [104] X. Yang, S. Wang, Y. Sheng, M. Zhang, W. Zou, L. Wu, L. Kang, J. Rizo, R. Zhang, T. Xu, C. Ma, Syntaxin opening by the MUN domain underlies the function of Munc13 in synaptic-vesicle priming, *Nat. Struct. Mol. Biol.* **2015**, *22*, 547–554.
- [105] W. Li, C. Ma, R. Guan, Y. Xu, D. R. Tomchick, J. Rizo, The crystal structure of a Munc13 C-terminal module exhibits a remarkable similarity to vesicle tethering factors, *Structure* **2011**, *19*, 1443–1455.



Bibliography

- [106] Y. Park, J. B. Seo, A. Fraind, A. Pérez-Lara, H. Yavuz, K. Han, S.-R. Jung, I. Kattan, P. J. Walla, M. Choi, D. S. Cafiso, D.-S. Koh, R. Jahn, Synaptotagmin-1 binds to PIP₂-containing membrane but not to SNAREs at physiological ionic strength, *Nat. Struct. Mol. Biol.* **2015**, *22*, 815–823.
- [107] P. Cao, X. Yang, T. C. Südhof, Complexin activates exocytosis of distinct secretory vesicles controlled by different synaptotagmins, *J. Neurosci.* **2013**, *33*, 1714–1727.
- [108] S. Pabst, J. W. Hazzard, W. Antonin, T. C. Südhof, R. Jahn, J. Rizo, D. Fasshauer, Selective interaction of complexin with the neuronal SNARE complex. Determination of the binding regions, *J. Biol. Chem.* **2000**, *275*, 19808–19818.
- [109] X. Chen, D. Tomchick, E. Kovrigin, D. Araç, M. Machius, T. C. Südhof, J. Rizo, Three-dimensional structure of the complexin/SNARE complex, *Neuron* **2002**, *33*, 397–409.
- [110] M. Xue, K. Reim, X. Chen, H.-T. Chao, H. Deng, J. Rizo, N. Brose, C. Rosenmund, Distinct domains of complexin I differentially regulate neurotransmitter release, *Nat. Struct. Mol. Biol.* **2007**, *14*, 949–958.
- [111] T. Trimbuch, J. Xu, D. Flaherty, D. R. Tomchick, J. Rizo, C. Rosenmund, Re-examining how complexin inhibits neurotransmitter release, *eLife* **2014**, *3*:e02391.
- [112] R. Zdanowicz, A. Kreutzberger, B. Liang, V. Kiessling, L. K. Tamm, D. S. Cafiso, Complexin Binding to Membranes and Acceptor t-SNAREs Explains Its Clamping Effect on Fusion, *Biophys. J.* **2017**, *113*, 1235–1250.
- [113] J. P. Erzberger, J. M. Berger, Evolutionary relationships and structural mechanisms of AAA+ proteins, *Annu. Rev. Biophys. Biomol. Struct.* **2006**, *35*, 93–114.
- [114] M. Zhao, S. Wu, Q. Zhou, S. Vivona, D. J. Cipriano, Y. Cheng, A. T. Brunger, Mechanistic insights into the recycling machine of the SNARE complex, *Nature* **2015**, *518*, 61–67.
- [115] J.-K. Ryu, D. Min, S.-H. Rah, S. J. Kim, Y. Park, H. Kim, C. Hyeon, H. M. Kim, R. Jahn, T.-Y. Yoon, Spring-loaded unraveling of a single SNARE complex by NSF in one round of ATP turnover, *Science* **2015**, *347*, 1485–1489.
- [116] J. Rizo, J. Xu, Synaptic vesicle fusion without SNARE transmembrane regions, *Dev. Cell* **2013**, *27*, 124–126.

- [117] J.-D. Wehland, A. S. Lygina, P. Kumar, S. Guha, B. E. Hubrich, R. Jahn, U. Diederichsen, Role of the transmembrane domain in SNARE protein mediated membrane fusion: peptide nucleic acid/peptide model systems, *Mol. Biosyst.* **2016**, *12*, 2770–2776.
- [118] Y. Xu, F. Zhang, Z. Su, J. A. McNew, Y.-K. Shin, Hemifusion in SNARE-mediated membrane fusion, *Nat. Struct. Mol. Biol.* **2005**, *12*, 417–422.
- [119] P. Zhou, T. Bacaj, X. Yang, Z. P. Pang, T. C. Südhof, Lipid-Anchored SNAREs Lacking Transmembrane Regions Fully Support Membrane Fusion during Neurotransmitter Release, *Neuron* **2013**, *80*, 470–483.
- [120] J. A. McNew, T. Weber, F. Parlati, R. J. Johnston, T. J. Melia, T. H. Söllner, J. E. Rothman, Close Is Not Enough: SNARE-dependent Membrane Fusion Requires an Active Mechanism that Transduces Force to Membrane Anchors, *J. Cell Biol.* **2000**, *150*, 105–117.
- [121] M. Pieren, Y. Desfougères, L. Michailat, A. Schmidt, A. Mayer, Vacuolar SNARE protein transmembrane domains serve as nonspecific membrane anchors with unequal roles in lipid mixing, *J. Biol. Chem.* **2015**, *290*, 12821–12832.
- [122] A. N. Ngatchou, K. Kisler, Q. Fang, A. M. Walter, Y. Zhao, D. Bruns, J. B. Sørensen, M. Lindau, Role of the synaptobrevin C terminus in fusion pore formation, *Proc. Natl. Acad. Sci. U.S.A.* **2010**, *107*, 18463–18468.
- [123] M. D’Agostino, H. J. Risselada, A. Mayer, Steric hindrance of SNARE transmembrane domain organization impairs the hemifusion-to-fusion transition, *EMBO Rep.* **2016**, *17*, 1590–1608.
- [124] H. J. Risselada, G. Bubnis, H. Grubmüller, Expansion of the fusion stalk and its implication for biological membrane fusion, *Proc. Natl. Acad. Sci. U.S.A.* **2014**, *111*, 11043–11048.
- [125] D. Milovanovic, A. Honigmann, S. Koike, F. Göttfert, G. Pähler, M. Junius, S. Müller, U. Diederichsen, A. Janshoff, H. Grubmüller, H. J. Risselada, C. Eggeling, S. W. Hell, G. van den Bogaart, R. Jahn, Hydrophobic mismatch sorts SNARE proteins into distinct membrane domains, *Nat. Commun.* **2015**, *6*, 5984.



Bibliography

- [126] R. A. Böckmann, H. Grubmüller, Multistep binding of divalent cations to phospholipid bilayers: A molecular dynamics study, *Angew. Chem. Int. Ed.* **2004**, *43*, 1021–1024.
- [127] T. F. J. Martin, Role of PI(4,5)P₂ in vesicle exocytosis and membrane fusion, in *Phosphoinositides II: The Diverse Biological Functions*, edited by T. Balla, M. Wymann, J. D. York, Springer Netherlands, Dordrecht, Subcellular Biochemistry, **2012**, pp. 111–130.
- [128] G. van den Bogaart, K. Meyenberg, H. J. Risselada, H. Amin, K. I. Willig, B. E. Hubrich, M. Dier, S. W. Hell, H. Grubmüller, U. Diederichsen, R. Jahn, Membrane protein sequestering by ionic protein-lipid interactions, *Nature* **2011**, *479*, 552–555.
- [129] M. R. Ammar, N. Kassas, S. Chasserot-Golaz, M.-F. Bader, N. Vitale, Lipids in regulated exocytosis: what are they doing?, *Front. Endocrinol.* **2013**, *4*, 125.
- [130] D. Milovanovic, M. Platen, M. Junius, U. Diederichsen, I. A. T. Schaap, A. Honigmann, R. Jahn, G. van den Bogaart, Calcium Promotes the Formation of Syntaxin 1 Mesoscale Domains through Phosphatidylinositol 4,5-Bisphosphate, *J. Biol. Chem.* **2016**, *291*, 7868–7876.
- [131] G. van den Bogaart, K. Meyenberg, U. Diederichsen, R. Jahn, Phosphatidylinositol 4,5-bisphosphate increases Ca²⁺ affinity of synaptotagmin-1 by 40-fold, *J. Biol. Chem.* **2012**, *287*, 16447–16453.
- [132] S.-T. Yang, A. J. B. Kreuzberger, J. Lee, V. Kiessling, L. K. Tamm, The role of cholesterol in membrane fusion, *Chem. Phys. Lipids* **2016**, *199*, 136–143.
- [133] B. S. Stratton, J. M. Warner, Z. Wu, J. Nikolaus, G. Wei, E. Wagnon, D. Baddeley, E. Karatekin, B. O’Shaughnessy, Cholesterol Increases the Openness of SNARE-Mediated Flickering Fusion Pores, *Biophys. J.* **2016**, *110*, 1538–1550.
- [134] T. Weber, B. V. Zemelman, J. A. McNew, B. Westermann, M. Gmachl, F. Parlati, T. H. Söllner, J. E. Rothman, SNAREpins: Minimal Machinery for Membrane Fusion, *Cell* **1998**, *92*, 759–772.
- [135] X. Chen, D. Araç, T.-M. Wang, C. J. Gilpin, J. Zimmerberg, J. Rizo, SNARE-Mediated Lipid Mixing Depends on the Physical State of the Vesicles, *Biophys. J.* **2006**, *90*, 2062–2074.



- [136] B. L. Sabatini, W. G. Regehr, Timing of neurotransmission at fast synapses in the mammalian brain, *Nature* **1996**, *384*, 170–172.
- [137] M. K. Domanska, V. Kiessling, A. Stein, D. Fasshauer, L. K. Tamm, Single vesicle millisecond fusion kinetics reveals number of SNARE complexes optimal for fast SNARE-mediated membrane fusion, *J. Biol. Chem.* **2009**, *284*, 32158–32166.
- [138] J. Diao, Z. Su, Y. Ishitsuka, B. Lu, K. S. Lee, Y. Lai, Y.-K. Shin, T. Ha, A single-vesicle content mixing assay for SNARE-mediated membrane fusion, *Nat. Commun.* **2010**, *1*, 54.
- [139] A. Kashiwada, M. Tsuboi, K. Matsuda, Target-selective vesicle fusion induced by molecular recognition on lipid bilayers, *Chem. Commun.* **2009**, 695–697.
- [140] G. Stengel, L. Simonsson, R. A. Campbell, F. Höök, Determinants for membrane fusion induced by cholesterol-modified DNA zippers, *J. Phys. Chem. B* **2008**, *112*, 8264–8274.
- [141] Y. Gong, Y. Luo, D. Bong, Membrane activation: selective vesicle fusion via small molecule recognition, *J. Am. Chem. Soc.* **2006**, *128*, 14430–14431.
- [142] J. R. Litowski, R. S. Hodges, Designing heterodimeric two-stranded α -helical coiled-coils. Effects of hydrophobicity and α -helical propensity on protein folding, stability, and specificity, *J. Biol. Chem.* **2002**, *277*, 37272–37279.
- [143] T. Zheng, J. Voskuhl, F. Versluis, H. R. Zope, I. Tomatsu, H. R. Marsden, A. Kros, Controlling the rate of coiled coil driven membrane fusion, *Chem. Commun.* **2013**, *49*, 3649–3651.
- [144] F. Versluis, J. Dominguez, J. Voskuhl, A. Kros, Coiled-coil driven membrane fusion: Zipper-like vs. non-zipper-like peptide orientation, *Faraday Discuss.* **2013**, *166*, 349–359.
- [145] T. Zheng, M. Bulacu, G. Daudey, F. Versluis, J. Voskuhl, G. Martelli, J. Raap, G. J. A. Sevink, A. Kros, A. L. Boyle, A non-zipper-like tetrameric coiled coil promotes membrane fusion, *RSC Adv.* **2016**, *6*, 7990–7998.
- [146] G. Pähler, C. Panse, U. Diederichsen, A. Janshoff, Coiled-coil formation on lipid bilayers—implications for docking and fusion efficiency, *Biophys. J.* **2012**, *103*, 2295–2303.



Bibliography

- [147] F. Versluis, J. Voskuhl, B. van Kolck, H. Zope, M. Bremmer, T. Albregtse, A. Kros, In situ modification of plain liposomes with lipidated coiled coil forming peptides induces membrane fusion, *J. Am. Chem. Soc.* **2013**, *135*, 8057–8062.
- [148] K. M. Flavier, S. G. Boxer, Vesicle Fusion Mediated by Solanesol-Anchored DNA, *Biophys. J.* **2017**, *113*, 1260–1268.
- [149] M. Sadek, D. Berndt, D. Milovanovic, R. Jahn, U. Diederichsen, Distance Regulated Vesicle Fusion and Docking Mediated by β -Peptide Nucleic Acid SNARE Protein Analogues, *ChemBioChem* **2016**, *17*, 479–485.
- [150] V. Trivedi, C. Yu, B. Veeramuthu, S. Francis, D. Chang, Fusion induced aggregation of model vesicles studied by dynamic and static light scattering, *Chem. Phys. Lipids* **2000**, *107*, 99–106.
- [151] D. K. Struck, D. Hoekstra, R. E. Pagano, Use of Resonance Energy Transfer To Monitor Membrane Fusion, *Biochemistry* **1981**, *20*, 4093–4099.
- [152] N. Hildebrandt, How to Apply FRET: From Experimental Design to Data Analysis, in *FRET-Förster Resonance Energy Transfer-From Theory to Applications*, edited by I. Medintz, N. Hildebrandt, Wiley-VCH, Weinheim, **2014**, pp. 105–163.
- [153] L. M. S. Loura, M. Prieto, FRET in Membrane Biophysics: An Overview, *Front. Physiol.* **2011**, *2*, 82.
- [154] G. van den Bogaart, M. G. Holt, G. Bunt, D. Riedel, F. S. Wouters, R. Jahn, One SNARE complex is sufficient for membrane fusion, *Nat. Struct. Mol. Biol.* **2010**, *17*, 358–364.
- [155] D. Hoekstra, T. de Boer, K. Klappe, J. Wilschut, Fluorescence method for measuring the kinetics of fusion between biological membranes, *Biochemistry* **1984**, *23*, 5675–5681.
- [156] H.-J. Galla, W. Hartmann, Excimer-forming lipids in membrane research, *Chem. Phys. Lipids* **1980**, *27*, 199–219.
- [157] C. R. Wasmuth, C. Edwards, R. Hutcherson, Participation of the SO_2^- Radical Ion in the Reduction of *p*-Nitrophenol by Sodium Dithionite, *J. Phys. Chem.* **1964**, *68*, 423–425.



- [158] J. Wilschut, N. Düzgüneş, R. Fraley, D. Papahadjopoulos, Studies on the mechanism of membrane fusion: kinetics of calcium ion induced fusion of phosphatidylserine vesicles followed by a new assay for mixing of aqueous vesicle contents, *Biochemistry* **1980**, *19*, 6011–6021.
- [159] P. C. Zucchi, M. Zick, Membrane fusion catalyzed by a Rab, SNAREs, and SNARE chaperones is accompanied by enhanced permeability to small molecules and by lysis, *Mol. Biol. Cell* **2011**, *22*, 4635–4646.
- [160] A. Cypionka, A. Stein, J. M. Hernandez, H. Hippchen, R. Jahn, P. J. Walla, Discrimination between docking and fusion of liposomes reconstituted with neuronal SNARE-proteins using FCS, *Proc. Natl. Acad. Sci. U.S.A.* **2009**, *106*, 18575–18580.
- [161] J. Ries, P. Schwille, Fluorescence correlation spectroscopy, *BioEssays* **2012**, *34*, 361–368.
- [162] P. J. Walla, *Modern Biophysical Chemistry: Detection and Analysis of Biomolecules*, 2 ed., Wiley-VCH, Weinheim, **2014**.
- [163] E. P. Day, J. T. Ho, R. K. Kunze, S. T. Sun, Dynamic light scattering study of calcium-induced fusion in phospholipid vesicles, *Biochim. Biophys. Acta, Biomembr.* **1977**, *470*, 503–508.
- [164] Y. Yang, P. Heo, B. Kong, J.-B. Park, Y.-H. Jung, J. Shin, C. Jeong, D.-H. Kweon, Dynamic light scattering analysis of SNARE-driven membrane fusion and the effects of SNARE-binding flavonoids, *Biochem. Biophys. Res. Commun.* **2015**, *465*, 864–870.
- [165] W. Schärtl, *Dynamic Light Scattering: With Applications to Chemistry, Biology, and Physics*, Springer Berlin Heidelberg, **2007**.
- [166] D. E. Koppel, Analysis of Macromolecular Polydispersity in Intensity Correlation Spectroscopy: The Method of Cumulants, *J. Chem. Phys.* **1972**, *57*, 4814–4820.
- [167] A. S. Lygina, Design, Synthesis and Fusion Activity of PNA/Peptide Hybrids As SNARE Protein Models, PhD thesis, University of Göttingen, Göttingen, **2011**.
- [168] B. Hyrup, P. E. Nielsen, Peptide Nucleic Acids (PNA): Synthesis, Properties and Potential Applications, *Bioorg. Med. Chem.* **1996**, *4*, 5–23.



Bibliography

- [169] U. Diederichsen, Pairing Properties of Alanyl Peptide Nucleic Acids Containing an Amino Acid Backbone with Alternating Configuration, *Angew. Chem. Int. Ed.* **1996**, *35*, 445–448.
- [170] O. Berger, L. Adler-Abramovich, M. Levy-Sakin, A. Grunwald, Y. Liebes-Peer, M. Bachar, L. Buzhansky, E. Mossou, V. T. Forsyth, T. Schwartz, Y. Ebenstein, F. Frolow, L. J. W. Shimon, F. Patolsky, E. Gazit, Light-emitting self-assembled peptide nucleic acids exhibit both stacking interactions and Watson-Crick base pairing, *Nat. Nanotechnol.* **2015**, *10*, 353–360.
- [171] J. M. Berg, J. L. Tymoczko, L. Stryer, *Biochemistry*, 7 ed., W. H. Freeman and Company, Basingstoke, USA, **2012**, p. 118.
- [172] J. Hunziker, H.-J. Roth, M. Böhringer, A. Giger, U. Diederichsen, M. Göbel, R. Krishnan, B. Jaun, C. Leumann, A. Eschenmoser, Warum Pentose- und nicht Hexose-Nucleinsäuren? Teil III. Oligo(2',3'-dideoxy- β -D-glucopyranosyl) nucleotide ('homo-DNS'): Paarungseigenschaften, *Helv. Chim. Acta* **1993**, *76*, 259–352.
- [173] H. Rasmussen, J. Sandholm Kastrup, J. N. Nielsen, J. M. Nielsen, P. E. Nielsen, Crystal structure of a peptide nucleic acid (PNA) duplex at 1.7 Å resolution, *Nat. Struct. Biol.* **1997**, *4*, 98–101.
- [174] M. F. H. Hoffmann, A. M. Brückner, T. Hupp, B. Engels, U. Diederichsen, Specific Purine-Purine Base Pairing in Linear Alanyl-Peptide Nucleic Acids, *Helv. Chim. Acta* **2000**, *83*, 2580–2593.
- [175] U. Diederichsen, Oligomers with Intercalating Cytosine–Cytosine⁺ Base Pairs and Peptide Backbone: DNA i-Motif Analogues, *Angew. Chem. Int. Ed.* **1998**, *37*, 2273–2276.
- [176] B. E. Hubrich, Synthese von Hybrid-Oligomeren aus Alanyl-PNA und N-(2-Aminoethyl)glycin-PNA zur Verwendung in Modellsystemen für die SNARE-vermittelte Membranfusion, Master thesis, University of Göttingen, Göttingen, **2013**.
- [177] L. D. Arnold, T. H. Kalantar, J. C. Vederas, Conversion of Serine to Stereochemically Pure β -Substituted α -Amino Acids via β -Lactones, *J. Am. Chem. Soc.* **1985**, *107*, 7105–7109.

- [178] S. V. Pansare, L. D. Arnold, J. C. Vederas, N-tert-Butoxycarbonyl-L-serine β -lactone and (S)-3-amino-2-oxetanone p-toluenesulfonic acid salt, *Org. Synth.* **1992**, *70*, 10.
- [179] M. Peifer, F. De Giacomo, M. Schandl, A. Vasella, Oligonucleotide Analogues with Integrated Bases and Backbone–Hydrazide and Amide-Linked Analogues. 1. Design and Synthesis of Monomeric Building Blocks, *Helv. Chim. Acta* **2009**, *92*, 1134–1166.
- [180] J. Kjellberg, N. G. Johansson, Studies on the Alkylation of Derivatives of Guanines, *Nucleosides Nucleotides* **1989**, *8*, 225–256.
- [181] S. Stoller, Synthese und Anwendung eines neuen Spinlabels und Untersuchung der Assoziation von Nukleobasen-funktionalisierten Transmembranpeptiden in Lipid-doppelschichten, PhD thesis, University of Göttingen, Göttingen, **2010**.
- [182] R. Casale, I. S. Jensen, M. Egholm, Synthesis of PNA Oligomers by Fmoc Chemistry, in *Peptide Nucleic Acids – Protocols and Applications*, edited by P. E. Nielsen, Horizon Bioscience, Wymondham, Norfolk, UK, **2004**, pp. 61–76.
- [183] F. García-Martín, M. Quintanar-Audelo, Y. García-Ramos, L. J. Cruz, C. Gravel, R. Furic, S. Côté, J. Tulla-Puche, F. Albericio, ChemMatrix, a poly(ethylene glycol)-based support for the solid-phase synthesis of complex peptides, *J. Comb. Chem.* **2006**, *8*, 213–220.
- [184] T. Hara, Y. Huang, A. Ito, T. Kawakami, H. Hojo, M. Murata, Trifluoroethanol-containing RP-HPLC mobile phases for the separation of transmembrane peptides human glycoporphin-A, integrin alpha-1, and p24: Analysis and prevention of potential side reactions due to formic acid, *J. Pept. Sci.* **2015**, *21*, 61–70.
- [185] M. Puchades, A. Westman, K. Blennow, P. Davidsson, Removal of sodium dodecyl sulfate from protein samples prior to matrix-assisted laser desorption/ionization mass spectrometry, *Rapid Commun. Mass Spectrom.* **1999**, *13*, 344–349.
- [186] F. Cornelius, Functional reconstitution of the sodium pump. Kinetics of exchange reactions performed by reconstituted Na/K-ATPase, *Biochim. Biophys. Acta, Rev. Biomembr.* **1991**, *1071*, 19–66.



Bibliography

- [187] R. Schubert, Liposome Preparation by Detergent Removal, in *Liposomes, Part A*, vol. 367 of *Methods in Enzymology*, edited by N. Düzgüneş, Elsevier, **2003**, pp. 46–70.
- [188] J. R. Lakowicz, *Principles of Fluorescence Spectroscopy*, 3 ed., Springer Science+Business Media LLC, New York, **2006**.
- [189] N. Düzgüneş, L. A. Bagatolli, P. Meers, Y.-K. Oh, R. M. Straubinger, Fluorescence methods in liposome research, in *Liposomes*, edited by V. P. Torchilin, V. Weissig, Oxford University Press, Oxford, The Practical Approach Series, **2003**, pp. 105–147.
- [190] S. L. Roth, G. R. Whittaker, Promotion of vesicular stomatitis virus fusion by the endosome-specific phospholipid bis(monoacylglycero)phosphate (BMP), *FEBS Lett.* **2011**, 585, 865–869.
- [191] X. Lu, F. Zhang, J. A. McNew, Y.-K. Shin, Membrane fusion induced by neuronal SNAREs transits through hemifusion, *J. Biol. Chem.* **2005**, 280, 30538–30541.
- [192] J. W. Holland, C. Hui, P. R. Cullis, T. D. Madden, Poly(ethylene glycol)–lipid conjugates regulate the calcium-induced fusion of liposomes composed of phosphatidylethanolamine and phosphatidylserine, *Biochemistry* **1996**, 35, 2618–2624.
- [193] N. Düzgüneş, T. M. Allen, J. Fedor, D. Papahadjopoulos, Lipid Mixing during Membrane Aggregation and Fusion: Why Fusion Assays Disagree, *Biochemistry* **1987**, 26, 8435–8442.
- [194] J. Lasch, V. Weissig, M. Brandl, Preparation of liposomes, in *Liposomes*, vol. 264 of *The Practical Approach Series*, edited by V. P. Torchilin, V. Weissig, Oxford University Press, Oxford, **2003**.
- [195] S. Takamori, M. Holt, K. Stenius, E. A. Lemke, M. Grønborg, D. Riedel, H. Urlaub, S. Schenck, B. Brügger, P. Ringler, S. A. Müller, B. Rammner, F. Gräter, J. S. Hub, B. L. de Groot, G. Mieskes, Y. Moriyama, J. Klingauf, H. Grubmüller, J. Heuser, F. Wieland, R. Jahn, Molecular anatomy of a trafficking organelle, *Cell* **2006**, 127, 831–846.
- [196] M. K. Domanska, V. Kiessling, L. K. Tamm, Docking and fast fusion of synaptobrevin vesicles depends on the lipid compositions of the vesicle and the acceptor SNARE complex-containing target membrane, *Biophys. J.* **2010**, 99, 2936–2946.

- [197] M. E. Haque, T. J. McIntosh, B. R. Lentz, Influence of Lipid Composition on Physical Properties and PEG-Mediated Fusion of Curved and Uncurved Model Membrane Vesicles: “Nature’s Own” Fusogenic Lipid Bilayer, *Biochemistry* **2001**, *40*, 4340–4348.
- [198] A. Chattopadhyay, Chemistry and biology of *N*-(7-nitrobenz-2-oxa-1,3-diazol-4-yl)-labeled lipids: fluorescent probes of biological and model membranes, *Chem. Phys. Lipids* **1990**, *53*, 1–15.
- [199] S. Fery-Forgues, J.-P. Fayet, A. Lopez, Drastic changes in the fluorescence properties of NBD probes with the polarity of the medium: involvement of a TICT state?, *J. Photochem. Photobiol. A* **1993**, *70*, 229–243.
- [200] S. Mazères, V. Schram, J.-F. Tocanne, A. Lopez, 7-Nitrobenz-2-oxa-1,3-diazole-4-yl-labeled phospholipids in lipid membranes: differences in fluorescence behavior, *Biophys. J.* **1996**, *71*, 327–335.
- [201] C. Pryor, M. Bridge, L. M. Loew, Aggregation, lipid exchange, and metastable phases of dimyristoylphosphatidylethanolamine vesicles, *Biochemistry* **1985**, *24*, 2203–2209.
- [202] D. Marquardt, B. Geier, G. Pabst, Asymmetric lipid membranes: towards more realistic model systems, *Membranes* **2015**, *5*, 180–196.
- [203] P. S. Chen, T. Y. Toribara, H. Warner, Microdetermination of Phosphorus, *Anal. Chem.* **1956**, *28*, 1756–1758.
- [204] A. Bhalla, M. C. Chicka, W. C. Tucker, E. R. Chapman, Ca²⁺-synaptotagmin directly regulates t-SNARE function during reconstituted membrane fusion, *Nat. Struct. Mol. Biol.* **2006**, *13*, 323–330.
- [205] C. E. Dempsey, The actions of melittin on membranes, *Biochim. Biophys. Acta, Rev. Biomembr.* **1990**, *1031*, 143–161.
- [206] C.-C. Lin, J. Seikowski, A. Pérez-Lara, R. Jahn, C. Höbartner, P. J. Walla, Control of membrane gaps by synaptotagmin-Ca²⁺ measured with a novel membrane distance ruler, *Nat. Commun.* **2014**, *5*, 5859.
- [207] E. Rusinova, V. Tretyachenko-Ladokhina, O. E. Vele, D. F. Seneor, A. J. B. Ross, Alexa and Oregon Green dyes as fluorescence anisotropy probes for measuring



Bibliography

- protein–protein and protein–nucleic acid interactions, *Anal. Biochem.* **2002**, *308*, 18–25.
- [208] P. E. Nielsen, Appendix, in *Peptide Nucleic Acids – Protocols and Applications*, edited by P. E. Nielsen, Horizon Bioscience, Wymondham, Norfolk, UK, **2004**, pp. 305–313.
- [209] N. C. Pace, F. Vajdos, L. Fee, G. Grimsley, T. Gray, How to measure and predict the molar absorption coefficient of a protein, *Protein Sci.* **1995**, *4*, 2411–2432.
- [210] H. Edelhoch, Spectroscopic Determination of Tryptophan and Tyrosine in Proteins, *Biochemistry* **1967**, *6*, 1948–1954.
- [211] D. B. Wetlaufer, Ultraviolet Spectra of Proteins and Amino Acids, in *Advances in Protein Chemistry*, vol. 17 of *Advances in Protein Chemistry*, edited by C. B. Anfinsen, M. L. Anson, K. Bailey, J. T. Edsall, Academic Press, Inc., London, **1962**, pp. 303–390.
- [212] J. M. Manning, S. Moore, Determination of D- and L-Amino Acids by Ion Exchange Chromatography as L-D and L-L Dipeptides, *J. Biol. Chem.* **1968**, *243*, 5591–5597.
- [213] P. Lohse, B. Oberhauser, B. Oberhauser-Hofbauer, G. Baschang, A. Eschenmoser, Chemie von α -Aminonitrilen. XVII. Oligo(nukleodipeptamidinium)-Salze, *Croat. Chim. Acta* **1996**, *69*, 535–562.
- [214] W. C. Chan, P. D. White, Basic Procedures, in *Fmoc Solid Phase Peptide Synthesis – A Practical Approach*, Oxford University Press, Oxford, **2000**, pp. 41–76.
- [215] B. Blankenmeyer-Menge, M. Nimtz, R. Frank, An efficient method for anchoring Fmoc-amino acids to hydroxyl-functionalised solid supports, *Tetrahedron Lett.* **1990**, *31*, 1701–1704.
- [216] E. Kaiser, R. L. Colescott, C. D. Bossinger, P. I. Cook, Color Test for Detection of Free Terminal Amino Groups in the Solid-Phase Synthesis of Peptides, *Anal. Biochem.* **1970**, *34*, 595–598.
- [217] B. A. Burkett, R. C. Brown, M. M. Meloni, A simple colorimetric test for the detection of polymer-supported tertiary alcohols, *Tetrahedron Lett.* **2001**, *42*, 5773–5775.

- [218] M. Gude, J. Ryf, P. D. White, An accurate method for the quantitation of Fmoc-derivatized solid phase supports, *Lett. Pept. Sci.* **2002**, 9, 203–206.
- [219] L. L. G. Schwenen, R. Hubrich, D. Milovanovic, B. Geil, J. Yang, A. Kros, R. Jahn, C. Steinem, Resolving single membrane fusion events on planar pore-spanning membranes, *Sci. Rep.* **2015**, 5, 12006.
- [220] M. J. Hope, M. B. Bally, G. Webb, P. R. Cullis, Production of large unilamellar vesicles by a rapid extrusion procedure. Characterization of size distribution, trapped volume and ability to maintain a membrane potential, *Biochim. Biophys. Acta, Biomembr.* **1985**, 812, 55–65.
- [221] G. Rouser, S. Fleischer, A. Yamamoto, Two dimensional thin layer chromatographic separation of polar lipids and determination of phospholipids by phosphorus analysis of spots, *Lipids* **1970**, 5, 494–496.
- [222] W. Vennekate, S. Schröder, C.-C. Lin, G. van den Bogaart, M. Grunwald, R. Jahn, P. J. Walla, Cis- and trans-membrane interactions of synaptotagmin-1, *Proc. Natl. Acad. Sci. U.S.A.* **2012**, 109, 11037–11042.
- [223] N. Kučerka, S. Tristram-Nagle, J. F. Nagle, Structure of fully hydrated fluid phase lipid bilayers with monounsaturated chains, *J. Membr. Biol.* **2005**, 208, 193–202.
- [224] J. Zanghellini, D. Ruckerbauer, F. Wodlei, H.-H. von Grünberg, C. Jungreuthmayer, Phospholipid Demixing, in *Advances in Planar Lipid Bilayers and Liposomes*, vol. 11 of *Advances in Planar Lipid Bilayers and Liposomes*, edited by A. Iglic, Elsevier, **2010**, pp. 1–28.
- [225] M. Alwarawrah, J. Dai, J. Huang, A molecular view of the cholesterol condensing effect in DOPC lipid bilayers, *J. Phys. Chem. B* **2010**, 114, 7516–7523.





Acknowledgements

I would like to thank my supervisor Prof. Dr. Ulf Diederichsen for giving me the opportunity to contribute to a highly interesting and fascinating project at the interface of chemistry and biology. I thank him for his great support and confidence by giving me a lot of freedom in my research. Moreover, I would like to thank Prof. Dr. Reinhard Jahn and Prof. Dr. Claudia Steinem for being part of my thesis committee. Thesis committee meetings always left me highly motivated thanks to the helpful discussions and countless ideas they brought along. I also thank Prof. Dr. Kai Tittmann, Prof. Dr. Silvio Rizzoli and Dr. Sebastian Kruss for their readiness to be members of the examination board.

I am really grateful for the possibility to carry out my PhD thesis within the Göttingen Graduate School for Biophysics, Neurosciences and Molecular Biosciences (GGNB). It was a great opportunity to meet and network with people from various research fields and to learn a lot in the methods and soft skills courses. I thank Antje Erdmann, Tina Trost and Frauke Bergmann from the IMPRS PBCS office for their great organization and always very fast response whenever I had questions.

I am indebted to Prof. Dr. Peter Jomo Walla who gave me the opportunity to work in his lab and to use the FCCS setup. A special debt is owed to Dr. Matthias Grunwald, Dr. Nour Hafi and Tobias Grothe who familiarized me with the technique of FCCS. Thank you for your great commitment and your patience to sit for endless hours in a dark lab to analyze liposome interactions. I appreciate the generous help by Christian Roßner and Wentao Peng from Prof. Dr. Philipp Vana's lab as well as by Dr. Julia Preobraschenski and Dr. Angel Pérez-Lara from Prof. Dr. Reinhard Jahn's lab who willingly provided their DLS machines and helped me with the measurements.

I'd like to say thank you to the whole Diederichsen group for the really nice time I had, especially to those with whom I shared the Lab 102 during the last four years—Brigitte Worbs, Julia Graf, Jan-Dirk Wehland, Dina Zanbot, Mike Groth and Viktoria Mrđen Debono—for the nice and cooperative working atmosphere and our common opinion that only a tidy lab is a good one to work in; to Daniel Frank and Meike Junius with whom I shared the responsibility to keep our various HPLC systems running; to those I worked



together in the SFB B5 project—Jan-Dirk Wehland, Dr. Samit Guha, Dr. Pawan Kumar, Dr. Matthias Körling, Muheeb Sadek, Anastasiya Schirmacher, and Mike Groth—for inspiring and fruitful discussions, our shared fight against the unpurifiable peptides and that the team spirit always outweighed the competitiveness; and to Aoife Neville and Angela Heinemann from the office who kindly took on all administrative things straightforwardly.

I thank “my” Bachelor students Mike Groth, Jacqueline Küch and Hermann Neitz whose high commitment, support and excellent work I very much appreciated. I really enjoyed teaching you and giving you an understanding about our research fields.

I’d like to say thank you to the NMR service facility run by Dr. Michael John and his team for the acquisition of NMR spectra and especially to the Central Analytics team of Dr. Holm Frauendorf for their constant advice and commitment to measure countless mass spectra for me.

A big thank you goes to the proofreaders of this thesis, Bastian Krüger, Mike Groth, and Marie Bergner who put the finishing touches on this work.

Last but not least I would like to thank my parents, my sisters, my brother and Bastian as well as my friends outside the lab for their continuous support and their sincere faith in me in all situations. I am glad about you standing always by my side.



Curriculum Vitae

Barbara Elisabeth Hubrich

Born September 5, 1989 in Bonn, Germany

Education

- 2014–2017 **PhD thesis** with Prof. Dr. Ulf Diederichsen, University of Göttingen
“Synthesis of Model Systems for SNARE Mediated Membrane Fusion Based on PNA/PNA Base Pair Recognition”
– Member of the Collaborative Research Center 803 “Functionality Controlled by Organization In and Between Membranes”
– Member of the Göttingen Graduate School for Neurosciences, Biophysics and Moleculare Biosciences (GGNB, program: IMPRS-PBCS)
- 2011–2013 **M. Sc. Chemistry**, University of Göttingen
overall grade: very good (1.3) with distinction
Master thesis (04–10/2013) with Prof. Dr. Ulf Diederichsen
“Synthese von Hybrid-Oligomeren aus Alanyl-PNA und *N*-(2-Aminoethyl)glycin-PNA zur Verwendung in Modellsystemen für die SNARE-vermittelte Membranfusion”
- 2008–2011 **B. Sc. Chemistry**, University of Göttingen
overall grade: very good (1.4)
Bachelor thesis (03–06/2011) with Prof. Dr. Ulf Diederichsen
“Synthese von Transmembranpeptiden zur Untersuchung von Peptid-Lipid-Interaktionen”
- 2008 Remedial course in Physics, University of Bonn
- 2008 High-school diploma “Abitur”, Erzb. St.-Joseph-Gymnasium Rheinbach, intensive courses: Chemistry, Biology
overall grade: good (1.6)



Scientific Contributions

Selected Oral Presentations

- 2016 International SFB Symposium, Grimma, Germany. Construction of novel hybrid biooligomers as artificial SNAREs.
- 2015 XII. German Peptide Symposium, Darmstadt, Germany. Novel PNA hybrid oligomers as artificial recognition units for SNARE mimetics. Short talk to the presented poster.
- 2014 5th SFB803 Winter School, Volkenroda, Germany. Development of novel hybrid biooligomers as model systems for the SNARE mediated membrane fusion.

Selected Poster Presentations

- 2016 European Peptide Symposium, Leipzig, Germany. Development of Hybrid Biooligomers with PNA Recognition Units to Mimic the Action of SNARE Proteins.
- 2015 XII. German Peptide Symposium, Darmstadt, Germany. Novel PNA hybrid oligomers as artificial recognition units for SNARE mimetics.
- 2014 3rd SFB803 Symposium, Göttingen, Germany. Artificial SNARE protein analogues for the investigation of the SNARE mediated membrane fusion.

Peer-Reviewed Publications

J.-D. Wehland, A. S. Lygina, P. Kumar, S. Guha, B. E. Hubrich, R. Jahn, U. Diederichsen, *Mol. Biosyst.* **2016**, *12*, 2770–2776.

G. v. d. Bogaart, K. Meyenberg, H. J. Risselada, H. Amin, K. I. Willig, B. E. Hubrich, M. Dier, S. W. Hell, H. Grubmüller, U. Diederichsen, R. Jahn, *Nature* **2011**, *479*, 552–555.

Awards

- 2015 Poster Presentation Award at XII. German Peptide Symposium
- 2008 GDCh Award for the best high-school graduate in Chemistry



Teaching Experience

- 2014–2016 Teaching assistant, supervision of undergraduate students in the basic and the advanced practical course in organic chemistry
- 2014–2015 Chief teaching assistant in the lecture “Introduction to Organic Chemistry” for undergraduate students
- 2014–2015 Supervision of three bachelor theses and one student internship
- 2010–2012 Student assistant, supervision of undergraduate students in the courses “Introduction to Organic Chemistry”, “Chemistry for Medical Students” and “Introduction to General and Inorganic Chemistry”

Work Experience Outside Academia

- 2012–2013 Four-month internship at Lanxess AG (Dormagen, Germany), Department of High Performance Elastomers
- 2011 Working student at Merck KGaA (Darmstadt, Germany) for 10 weeks, Department of Pigments & Coatings - Coatings - Global Application Technology





